

**INTEGRATED ASSESSMENT OF MULTI-SENSOR GRIDDED
DATA PRODUCTS FOR AGRICULTURAL AND
HYDROLOGICAL APPLICATIONS**

A Dissertation
Presented to
The Academic Faculty

by

Husayn El Sharif

In Partial Fulfillment
of the Requirements for the Degree
Doctor of Philosophy in the
School of Civil and Environmental Engineering

Georgia Institute of Technology
May 2019

COPYRIGHT © 2019 BY HUSAYN EL SHARIF

**INTEGRATED ASSESSMENT OF MULTI-SENSOR GRIDDED
DATA PRODUCTS FOR AGRICULTURAL AND
HYDROLOGICAL APPLICATIONS**

Approved by:

Dr. Aris Georgakakos, Advisor
School of Civil and Environmental
Engineering
Georgia Institute of Technology

Dr. Grey Nearing
Department of Geological Sciences
University of Alabama

Dr. Jingfeng Wang, Advisor
School of Civil and Environmental
Engineering
Georgia Institute of Technology

Dr. Emanuele Di Lorenzo
School of Earth and Atmospheric
Sciences
Georgia Institute of Technology

Dr. Rafael Bras
School of Civil and Environmental
Engineering
Georgia Institute of Technology

Date Approved: March 28, 2019

ACKNOWLEDGEMENTS

Completing my doctorate studies at Georgia Institute of Technology has been an incredible and fulfilling experience, far exceeding what I could have ever expected or hoped. From the first day on campus to the last page of this dissertation, my time at Georgia Tech challenged me in a positive way, pushing me towards greater achievement and accomplishment. I thank my advisor Dr. Aris Georgakakos, for his guidance and enthusiastic pursuit of perfection during the course of my studies. Likewise I thank Dr. Wang for his thought provoking discussions, advices, and support. I also express gratitude to my committee members, Dr. Rafael Bras, Dr. Emanuele Di Lorenzo, and Dr. Grey Nearing for their time, comments, and instruction. A special thanks also goes to the doctorate students of Dr. Georgakakos and Dr. Wang, including Shih-Yu Huang, Yao Tang, Irfan Abid, among others whose examples inspired me to remain steadfast in completing this doctorate. I also thank Dr. Ramesh Teegavarapu, my Master's thesis advisor from Florida Atlantic University, whose efforts and encouragement were instrumental to me in deciding on and getting accepted to Georgia Tech. Lastly I thank my parents, especially my mother, for their patience, understanding, and loving support throughout the way.

TABLE OF CONTENTS

ACKNOWLEDGEMENTS	iii
LIST OF TABLES	x
LIST OF FIGURES	xii
SUMMARY	xx
CHAPTER 1 INTRODUCTION	1
1.1 Objectives and Scope	3
1.2 Thesis Organization	4
CHAPTER 2 LITERATURE REVIEW	6
2.1 Crop yield and irrigation demand models and data assimilation	6
2.2 Sacramento Soil Moisture Accounting Model for Streamflow prediction	11
2.3 NASA SMAP L3 Enhanced (surface soil moisture)	14
2.4 NASA GPM IMERG Precipitation	15
2.5 JAXA GSMaP and GSMaP-Gauge Precipitation	16
2.6 GRIDMET Surface Meteorological Data	17
2.7 Daymet Surface Meteorological Data	18
2.8 HarvestChoice Global high-resolution soil profile database (HC-GHRSPD)	19
2.9 USDA NASS Cropscape – Cropland Data Layer	20
2.10 LOCA Downscaled CMIP5 Climate Projections	22
CHAPTER 3 ERROR ANALYSIS OF REMOTE SENSING PRECIPITATION AND AGRI-HYDROLOGICAL MODEL SENSITIVITIES TO GRIDDED INPUT DATA	24

3.1	Comparison of Near Real Time NASA GPM IMERG and JAXA GSMP products over the continental US	24
3.1.1	Annual Assessments	25
3.1.2	Seasonal Assessments	30
3.1.3	Assessment of Empirical Probability Density Functions of Daily Precipitation and Summary Statistics	41
3.2	Bias assessment of remote sensing precipitation and surface soil moisture with respect to in-situ measurements	47
3.3	Correlation of errors in remote sensing retrievals of precipitation and remote sensing retrievals of surface soil moisture	49
3.4	Spatial correlation in errors in GPM IMERG and GSMP-Gauge precipitation products	58
3.5	Impact of spatial averaging of high-resolution gridded meteorological and soil data on DSSAT crop model output	63
3.6	Summary	77
CHAPTER 4 HINDCASTING AND NEAR-REAL-TIME PREDICTION OF CROP YIELD, IRRIGATION DEMAND, DROUGHT, AND HYDROLOGICAL FLOWS		80
4.1	Preliminary Study: Modeling regional crop yield and irrigation demand using SMAP type of soil moisture data (El Sharif, et al. 2015)	80
4.1.1	Abstract	80
4.1.2	Capsule	81
4.1.3	Section 1: Introduction	81
4.1.4	Section 2: Methodology and Data	88

4.1.5	Section 3: Data	93
4.1.6	Section 4: Results	96
4.1.7	Section 5: Conclusions and on-going research	98
4.1.8	Acknowledgments	99
4.1.9	References	100
4.1.10	Tables	104
4.1.11	Figures	106
4.2	Incorporation of remote sensing SMAP L3 Enhanced surface soil moisture data in DSSAT-CSM rainfed crop simulations	109
4.3	Incorporation of remote sensing GPM IMERG daily precipitation in DSSAT- CSM crop simulations	113
4.4	Incorporation of remote sensing JAXA GSMaP daily precipitation products in DSSAT-CSM crop simulations	121
4.5	Historical Climate Variability and Crop Yield / Irrigation Assessment: Case Study in the Apalachicola-Chattahoochee-Flint (ACF) River Basin	126
4.5.1	DSSAT-CSM Calibration	128
4.5.2	ACF Assessment Methodology	130
4.5.3	ACF Assessment Results: Corn	132
4.5.4	ACF Assessment Results: Peanut	138
4.5.5	ACF Assessment Results: Cotton	143
4.5.6	ACF Assessment Results: Soybean	149
4.5.7	ACF Assessment Results: Summary Statistics	154
4.5.8	ACF Assessment Results: Monthly Irrigation Volumes	160

4.5.9	ACF Monthly Irrigation Volumes: Upper Chattahoochee	162
4.5.10	ACF Monthly Irrigation Volumes: Middle Chattahoochee and Upper Flint	162
4.5.11	ACF Monthly Irrigation Volumes: Middle and Lower Flint and Lower Chattahoochee	166
4.5.12	ACF Monthly Irrigation Volumes: Apalachicola	172
4.5.13	ACF Agricultural and Irrigation Demand Assessments: Summary	174
4.6	Hindcasting of natural streamflows using GPM IMERG daily precipitation retrievals	175
4.6.1	East Fork White River at Columbus, Indiana	176
4.6.2	Grand River at Lansing, Michigan	179
4.6.3	North Fork John Day River at Monument, Oregon	181
4.6.4	Greens Bayou near Houston, Texas	183
4.6.5	French Broad River at Asheville, North Carolina	185
4.6.6	Sacramento R.A. Delta, California	187
4.6.7	North Fork of Clearwater River near Canyon Ranger Station, Montana	189
4.7	Hindcasting of natural streamflows using JAXA GSMaP daily precipitation retrievals	191
4.7.1	East Fork White River at Columbus, Indiana	191
4.7.2	Grand River at Lansing, Michigan	193
4.7.3	North Fork John Day River at Monument, Oregon	195
4.7.4	Greens Bayou near Houston, Texas	197

4.7.5	French Broad River at Asheville, North Carolina	199
4.7.6	Sacramento R.A. Delta, California	201
4.7.7	North Fork of Clearwater River near Canyon Ranger Station, Montana	203
4.8	SAC-SMA calibration using recent remote sensing precipitation retrievals	205
4.9	Summary	214
CHAPTER 5 SEASONAL AGRICULTURAL FORECASTS AND CLIMATE CHANGE ASSESSMENTS		216
5.1	Depth-averaged soil moisture-based historical analog for crop yield and irrigation forecasting – synthetic experiments	216
5.1.1	Methodology	216
5.1.2	Results	217
5.2	Comparing DSSAT surface soil moisture to SMAP retrievals	226
5.3	GRIDMET-based historical analog for rainfed and irrigated crop yield forecasting	229
5.3.1	Methodology	229
5.3.2	Results	230
5.4	Assessment of local climate change impacts on crop production and irrigation demand using bias-corrected and downscaled Global Circulation Model (GCM) output	235
5.4.1	Generating climate change forecasts of daily solar radiation	236
5.4.2	Results	240
5.5	Summary	244

CHAPTER 6 CONCLUSIONS	246
6.1 Summary and contributions	246
6.1.1 Quality Assessment of remote sensing retrievals of precipitation over the continental U.S.	247
6.1.2 Leveraging SMAP surface soil moisture retrievals to improve accuracy of remote sensing precipitation retrievals	248
6.1.3 Impact of spatial averaging of high-resolution gridded meteorological data on DSSAT-CSM crop model output	248
6.1.4 Hindcasting and near-real-time prediction of crop yield, irrigation demand, and agricultural drought	249
6.1.5 Incorporation of remote sensing retrievals of precipitation for near-real-time monitoring of hydrological flows	250
6.1.6 Use of modern multi-sensor data for seasonal prediction of and climate-change impacts on local crop yield and irrigation demand	250
6.2 Recommendations for future work	252
REFERENCES	255

LIST OF TABLES

Table 2-1: Minimum data sets for operation of DSSAT-CSM, from (Jones et al. 2003)...	8
Table 2-2: Description of DSSAT-CSM modules and sub-modules, from (Jones et al. 2003)	9
Table 2-3: Parameters of the Sacramento Soil Moisture Accounting Model (SAC-SMA) in the Hydromad modeling package, from (Andrews 2013).	14
Table 2-4: Performance metrics of SMAP Passive Enhanced Surface Soil Moisture data product at various cropland in-situ core validation sites (CVS) over the April 2015 to October 2016 period, from (Chan et al. 2018).....	15
Table 2-5: Soil profile parameters provided by the HC-GHRSPD data set, from (Han et al. 2015).	20
Table 3-1: Summary performance statistics for remote sensing retrievals of daily precipitation over the 2015-2016 period.....	46
Table 3-2: Locations of select SMAP core validation sites and neighboring GHCN rain gauges	48
Table 3-3: Biases in SMAP L3 Enhanced surface soil moisture retrievals paired with percent biases in neighboring daily precipitation retrievals from GRIDMET, GPM, GSMaP-Standard, and GSMaP-Gauge for the April 2015 to October 2016 period.	49
Table 3-4: Input parameters for DSSAT-CSM year 2005-2016 maize simulations.....	66
Table 4-1: Calibrated input parameters for rainfed county-level DSSAT-CSM maize simulations.	110
Table 4-2: Calibrated input parameters for rainfed and irrigated county-level DSSAT-CSM maize simulations.....	115
Table 4-3: Calibrated DSSAT-CSM input parameters for automatic-irrigation of maize	115
Table 4-4: Quantity of 30 x 30 m ² single-planting corn, peanut, cotton, and soybean field pixels identified in the 2016 USDA-NASS Cropland Data Layer for each ACF sub-basin.	128
Table 4-5: DSSAT-CSM input parameters for the rainfed and irrigated corn, peanut, cotton, and soybean simulations in the ACF basin.	129

Table 4-6: Summary statistics for corn crop yield and irrigation demand for the 1980-1997 and 1998-2015 periods and characterization of the change going from the former period to the latter.	156
Table 4-7: Summary statistics for peanut crop yield and irrigation demand for the 1980-1997 and 1998-2015 periods and characterization of the change going from the former period to the latter.	157
Table 4-8: Summary statistics for cotton crop yield and irrigation demand for the 1980-1997 and 1998-2015 periods and characterization of the change going from the former period to the latter.	158
Table 4-9: Summary statistics for soybean crop yield and irrigation demand for the 1980-1997 and 1998-2015 periods and characterization of the change going from the former period to the latter.	159
Table 4-10: Fraction of acreage that is irrigated ($F_{i,c}$) for corn, peanut, cotton, and soybean fields in each ACF sub-basin, estimated from year 2014-2016 county-level crop acreage data provided by the USDA Farm Service Agency.	161
Table 4-11: Case study locations for assessing SAC-SMA performance with incorporation of remote sensing precipitation retrievals	175
Table 4-12: SAC-SMA calibrated water storage parameters (in mm depth units) for the East Fork White River at Columbus, Indiana case study.....	213
Table 4-13: SAC-SMA calibrated water storage parameters (in mm depth units) for the Sacramento R.A. Delta, California case study.....	213
Table 5-1: DSSAT-CSM input parameters for crop yield prediction via depth-averaged soil moisture-based historical analog method.....	217
Table 5-2: Calibrated input parameters for LOCA CMIP5 data driven DSSAT-CSM maize simulations.	235
Table 5-3: Performance of Artificial Neural Network (ANN) model for estimation of surface solar radiation compared to seasonally calibrated Bristow & Campbell (1984) model. Green highlights indicate best performance for the specified metric.	239

LIST OF FIGURES

Figure 2-1: Schematic of runoff components and moisture reservoirs of the Sacramento Soil Moisture Accounting Model (SAC-SMA), from (World Bank 2016).	13
Figure 2-2: Year 2009 Cropscape Map with major land cover categories, from (Han et al. 2012)	21
Figure 3-1: Nine climate regions for assessment of remote sensing precipitation products over the continental United States. From (NCDC 2017).	25
Figure 3-2: Assessment of year 2015 cumulative precipitation from GPM IMERG, GSMaP-Standard, and GSMaP-Gauge data products.....	27
Figure 3-3: Assessment of year 2016 cumulative precipitation from GPM IMERG, GSMaP-Standard, and GSMaP-Gauge data products.....	28
Figure 3-4: Assessment of year 2015 regional cumulative precipitation from GPM IMERG, GSMaP-Standard, and GSMaP-Gauge data products.....	29
Figure 3-5: Assessment of year 2016 regional cumulative precipitation from GPM IMERG, GSMaP-Standard, and GSMaP-Gauge data products.....	30
Figure 3-6: Seasonal assessment of year 2015 cumulative precipitation from GPM IMERG, GSMaP-Standard, and GSMaP-Gauge data products for the Continental US	31
Figure 3-7: Seasonal assessment of year 2016 cumulative precipitation from GPM IMERG, GSMaP-Standard, and GSMaP-Gauge data products for the Continental US	32
Figure 3-8: Assessment of year 2015 regional winter cumulative precipitation from GPM IMERG, GSMaP-Standard, and GSMaP-Gauge data products.....	34
Figure 3-9: Assessment of year 2016 regional winter cumulative precipitation from GPM IMERG, GSMaP-Standard, and GSMaP-Gauge data products.....	35
Figure 3-10: Assessment of year 2015 regional spring cumulative precipitation from GPM IMERG, GSMaP-Standard, and GSMaP-Gauge data products.....	36
Figure 3-11: Assessment of year 2016 regional spring cumulative precipitation from GPM IMERG, GSMaP-Standard, and GSMaP-Gauge data products.....	37
Figure 3-12: Assessment of year 2015 regional summer cumulative precipitation from GPM IMERG, GSMaP-Standard, and GSMaP-Gauge data products.	38

Figure 3-13: Assessment of year 2016 regional summer cumulative precipitation from GPM IMERG, GSMaP-Standard, and GSMaP-Gauge data products.	39
Figure 3-14: Assessment of year 2015 regional fall cumulative precipitation from GPM IMERG, GSMaP-Standard, and GSMaP-Gauge data products.	40
Figure 3-15: Assessment of year 2016 regional fall cumulative precipitation from GPM IMERG, GSMaP-Standard, and GSMaP-Gauge data products.	41
Figure 3-16: Empirical probability (PDF) and cumulative density functions (CDF) for daily precipitation over the 2015-2016 period for the continental United States	42
Figure 3-17: Seasonal empirical probability density functions and cumulative probabilities for daily precipitation over the 2015-2016 period for the continental United States.	43
Figure 3-18: Empirical probability density functions for daily precipitation over the 2015-2016 period for nine climate regions of the continental United States.	44
Figure 3-19: Cumulative probabilities for daily precipitation over the 2015-2016 period for nine climate regions of the continental United States.	45
Figure 3-20: Correlation between errors in retrievals of regional mean daily precipitation from GPM IMERG (Version 5, Late Release) and SMAP Enhanced Level 3 regional mean surface soil moisture estimates for year 2016.	52
Figure 3-21: Correlation between errors in retrievals of regional mean daily precipitation from GSMaP-Gauge (Version 7) and SMAP Enhanced Level 3 regional mean surface soil moisture estimates for year 2016.	53
Figure 3-22: Correlation between errors in retrievals of regional mean daily precipitation from GPM IMERG (Version 5 Late Release), GSMaP-Gauge (Version 7), and SMAP Enhanced Level 3 regional mean surface soil moisture estimates for each season during the 2015-2016 period.	54
Figure 3-23: Correlation between errors in retrievals of regional mean daily precipitation from GPM IMERG (Version 5, Late Release) and one-day change in SMAP Enhanced Level 3 regional mean surface soil moisture estimates during year 2016.	56
Figure 3-24: Correlation between errors in retrievals of regional mean daily precipitation from GSMaP-Gauge (Version 7) and one-day change in SMAP Enhanced Level 3 regional mean surface soil moisture estimates during year 2016.	57
Figure 3-25: 15 sub-regions within a sample transect in the southeastern United States for assessment of spatial correlations in errors of remote sensing retrievals of daily precipitation.	59
Figure 3-26: Spatial correlations of remote sensing precipitation errors as a function of latitude distance for regions 1 and 8 during the year 2015-2016 period.	60

Figure 3-27: Spatial correlations of remote sensing precipitation errors as a function of latitude distance and season for region 1 during the year 2015-2016 period.	62
Figure 3-28: Schematic of domain for DSSAT simulations driven by multi-scale weather and soil data products.....	64
Figure 3-29: Schematic of domain for DSSAT simulations driven by 10km weather and soil data products. One 10km grid cell (red) is randomly selected in each of the 25 40km by 40km subdomains.	65
Figure 3-30: Comparison of year 2005-2016 Daymet daily precipitation at 1km and 40km spatial aggregation scales. The subplots each represent a 40km x 40km domain for different U.S. climate regions.	68
Figure 3-31: DSSAT summarized crop production metrics for year 2007 simulated rainfed corn using (a) 1km and (b) 40km soil and meteorological input data. Midwest case study region.	69
Figure 3-32: Comparison of mean rainfed corn yield, irrigated corn yield, and corn irrigation amount with meteorological forcing and soil input data with spatial resolutions ranging from 1km to 40km. The standard error of the mean is indicated by the shaded region. Southeast case study region.	72
Figure 3-33: Comparison of mean of irrigated corn yield and corn irrigation amount with meteorological forcing and soil input data with spatial resolutions ranging from 1km to 10km. The standard error of the mean is indicated by the shaded region. West case study region.	73
Figure 3-34: Comparison of mean rainfed corn yield, irrigated corn yield, and corn irrigation amount with meteorological forcing and soil input data with spatial resolutions ranging from 1km to 40km. The standard error of the mean is indicated by the shaded region. South case study region.	74
Figure 3-35: Comparison of mean rainfed corn yield with meteorological forcing and soil input data with spatial resolutions ranging from 1km to 40km. The standard error of the mean is indicated by the shaded region. Midwest case study region.....	75
Figure 3-36: Box plots of mean precipitation during the growing season for case studies in the southeast, west, south, and midwest regions as a function of scale of spatial aggregation of GRIDMET precipitation data.	76
Figure 4-1: Box plots of simulated year 2015 and 2016 county-level rain-fed maize yield without SMAP data incorporation (DSSAT control) and with SMAP data incorporation (DSSAT+SMAP).....	112
Figure 4-2: Comparison of DSSAT simulated and SMAP estimated surface soil moisture for the rain-fed maize case study locations.....	113

Figure 4-3: Box plots of simulated year 2015 and 2016 county-level maize yield and irrigation amount without GPM IMERG data incorporation (DSSAT Control) and with GPM IMERG data incorporation. Box plots of growing season cumulative precipitation and consecutive dry days derived from GRIDMET (DSSAT Control) and GPM IMERG are also provided for reference.	120
Figure 4-4: Box plots of simulated year 2015 and 2016 county-level maize yield and irrigation amount without JAXA GSMaP-Gauge data incorporation (DSSAT Control) and with GSMaP-Gauge data incorporation. Box plots of growing season cumulative precipitation and consecutive dry days derived from GRIDMET (DSSAT Control) and GSMaP-Gauge are also provided for reference.	125
Figure 4-5: A map of the ACF basin and its 14 sub-basins.	127
Figure 4-6: an example posterior Student t-distribution for the regression slope determined using Bayesian Linear Regression. Probability statements (with concise abbreviations) describe the certainty regarding the slope's sign (i.e. positive or negative).	131
Figure 4-7: Simulated ACF mean <i>rainfed</i> corn yield for 1980–2016 and present-day corn fields.	133
Figure 4-8: Simulated ACF mean irrigated corn yield for historical meteorology and present-day corn fields.	136
Figure 4-9: Simulated ACF mean irrigation amount for historical meteorology and present-day corn fields.	137
Figure 4-10: Simulated ACF mean <i>rainfed</i> peanut yield for 1980–2016 and present-day peanut fields.	139
Figure 4-11: Simulated ACF mean irrigated peanut yield for historical meteorology and present-day peanut fields.	141
Figure 4-12: Simulated ACF mean irrigation amount for historical meteorology and present-day peanut fields.	142
Figure 4-13: Simulated ACF mean <i>rainfed</i> cotton yield for 1980–2016 and present-day cotton fields.	144
Figure 4-14: Simulated ACF mean irrigated cotton yield for historical meteorology and present-day cotton fields.	147
Figure 4-15: Simulated ACF mean irrigation amount for historical meteorology and present-day cotton fields.	148
Figure 4-16: Simulated ACF mean <i>rainfed</i> soybean yield for 1980–2016 and present-day soybean fields.	150

Figure 4-17: Simulated ACF mean irrigated soybean yield for historical meteorology and present-day soybean fields.....	152
Figure 4-18: Simulated ACF mean irrigation amount for historical meteorology and present-day soybean fields.....	153
Figure 4-19: Probability statements describing the change in a summary statistic going from the 1980-1997 period to the 1998-2015 period.....	154
Figure 4-20: Monthly irrigation volumes for ACF Sub-basin 5	163
Figure 4-21: Monthly irrigation volumes for ACF Sub-basin 7	164
Figure 4-22: Monthly irrigation volumes for ACF Sub-basin 8	165
Figure 4-23: Monthly irrigation volumes for ACF Sub-basin 9	167
Figure 4-24: Monthly irrigation volumes for ACF Sub-basin 10	168
Figure 4-25: Monthly irrigation volumes for ACF Sub-basin 11	169
Figure 4-26: Monthly irrigation volumes for ACF Sub-basin 12	170
Figure 4-27: Monthly irrigation volumes for ACF Sub-basin 13	171
Figure 4-28: Monthly irrigation volumes for ACF Sub-basin 14.....	173
Figure 4-29: Year 2015-2016 SAC-SMA performance at East Fork White River at Columbus, Indiana site with incorporation of GPM IMERG daily precipitation retrievals. (a) Streamflow time series during the calibration (1980-2000) and validation (2015-2016) period. (b) Time series during 2015-2016 period (c) Year 2015-2016 scatter plot (d) Summary performance metrics during the 2015-2016 period	178
Figure 4-30: Year 2015-2016 SAC-SMA performance at Grand River at Lansing, Michigan site with incorporation of GPM IMERG daily precipitation retrievals	180
Figure 4-31: Year 2015-2016 SAC-SMA performance at North Fork John Day River at Monument, Oregon site with incorporation of GPM IMERG daily precipitation retrievals	182
Figure 4-32: Year 2015-2016 SAC-SMA performance at Greens Bayou near Houston, Texas site with incorporation of GPM IMERG daily precipitation retrievals.....	184
Figure 4-33: Year 2015-2016 SAC-SMA performance at French Broad River at Asheville, North Carolina site with incorporation of GPM IMERG daily precipitation retrievals .	186
Figure 4-34: Year 2015-2016 SAC-SMA performance at Sacramento R.A. Delta, California site with incorporation of GPM IMERG daily precipitation retrievals	188

Figure 4-35: Year 2015-2016 SAC-SMA performance at North Fork of Clearwater River near Canyon Ranger Station, Montana site with incorporation of GPM IMERG daily precipitation retrievals	190
Figure 4-36: Year 2015-2016 SAC-SMA performance at East Fork White River at Columbus, Indiana site with incorporation of JAXA GSMaP-Gauge daily precipitation retrievals. (a) Streamflow time series during the calibration (1980-2000) and validation (2015-2016) period. (b) Time series during 2015-2016 period (c) Year 2015-2016 scatter plot (d) Summary performance metrics during the 2015-2016 period	192
Figure 4-37: Year 2015-2016 SAC-SMA performance at Grand River at Lansing, Michigan site with incorporation of JAXA GSMaP-Gauge daily precipitation retrievals	194
Figure 4-38: Year 2015-2016 SAC-SMA performance at North Fork John Day River at Monument, Oregon site with incorporation of JAXA GSMaP-Gauge daily precipitation retrievals.....	196
Figure 4-39: Year 2015-2016 SAC-SMA performance at Greens Bayou near Houston, Texas site with incorporation of JAXA GSMaP-Gauge daily precipitation retrievals...	198
Figure 4-40: Year 2015-2016 SAC-SMA performance at French Broad River at Asheville, North Carolina site with incorporation of JAXA GSMaP-Gauge daily precipitation retrievals.....	200
Figure 4-41: Year 2015-2016 SAC-SMA performance at Sacramento R.A. Delta, California site with incorporation of JAXA GSMaP-Gauge daily precipitation retrievals	202
Figure 4-42: Year 2015-2016 SAC-SMA performance at North Fork of Clearwater River near Canyon Ranger Station, Montana site with incorporation of JAXA GSMaP-Gauge daily precipitation retrievals	204
Figure 4-43: Year 2017-2018 SAC-SMA performance at East Fork White River at Columbus, Indiana site with model calibration using daily remote sensing precipitation retrievals. (a) Precipitation time series including snow melt (b) Streamflow time series during 2017-2018 period (c) SAC-SMA normalized upper zone water content (d) Year 2017-2018 scatter plot (e) Performance metrics during the 2017-2018 period.	208
Figure 4-44: Year 2017-2018 SAC-SMA performance at Grand River at Lansing, Michigan site with model calibration using daily remote sensing precipitation retrievals. (a) Precipitation time series including snow melt (b) Streamflow time series during 2017-2018 period (c) SAC-SMA normalized upper zone water content (d) Year 2017-2018 scatter plot (e) Performance metrics during the 2017-2018 period.	209
Figure 4-45: Year 2017-2018 SAC-SMA performance at Greens Bayou near Houston, Texas site with model calibration using daily remote sensing precipitation retrievals. (a) Precipitation time series including snow melt (b) Streamflow time series during 2017-2018	

period (c) SAC-SMA normalized upper zone water content (d) Year 2017-2018 scatter plot (e) Performance metrics during the 2017-2018 period. 210

Figure 4-46: Year 2017-2018 SAC-SMA performance at French Broad River at Asheville, North Carolina site with model calibration using daily remote sensing precipitation retrievals. (a) Precipitation time series including snow melt (b) Streamflow time series during 2017-2018 period (c) SAC-SMA normalized upper zone water content (d) Year 2017-2018 scatter plot (e) Performance metrics during the 2017-2018 period. 211

Figure 4-47: Year 2017-2018 SAC-SMA performance at Sacramento R.A. Delta, California site with model calibration using daily remote sensing precipitation retrievals. (a) Precipitation time series including snow melt (b) Streamflow time series during 2017-2018 period (c) SAC-SMA normalized upper zone water content (d) Year 2017-2018 scatter plot (e) Performance metrics during the 2017-2018 period. 212

Figure 5-1: Schematic comparing the empirical probability distributions of historical analog-based estimates of a target quantity. The red probability distribution, resultant from the best historical analog based estimates, has reduced bias and reduced spread compared to the control scenario (in blue), while still capturing the target value..... 218

Figure 5-2: Analysis of bias and reliability of soil moisture based historical analog forecasts of July – December cumulative precipitation. Iowa case study site. 221

Figure 5-3: Analysis of bias and reliability of soil moisture based historical analog forecasts of July – December cumulative precipitation. Georgia case study site. 222

Figure 5-4: Analysis of bias and reliability of soil moisture based historical analog forecasts of July – December cumulative precipitation. California case study site. 222

Figure 5-5: Analysis of bias and reliability of soil moisture based historical analog forecasts of rainfed crop yield. Iowa case study site. 223

Figure 5-6: Analysis of bias and reliability of soil moisture based historical analog forecasts of rainfed crop yield, irrigated crop yield, and irrigation amount. Georgia case study site. 224

Figure 5-7: Analysis of bias and reliability of soil moisture based historical analog forecasts of irrigated crop yield and irrigation amount. California case study site. 225

Figure 5-8: Comparison of year 2016 DSSAT surface soil moisture (top 5cm) for major rainfed and irrigated crops in ACF Subbasin #11 and SMAP L3 Enhanced surface soil moisture retrievals..... 227

Figure 5-9: Year 2016 USDA Crop Land Layer for ACF Sub-basin #11 228

Figure 5-10: Year 2016 USDA Crop Land Data Layer land surface area designations for ACF Sub-basin #11 228

Figure 5-11: Analysis of bias and reliability of monthly precipitation based historical analog forecasts of July – December cumulative precipitation. Iowa case study site. ...	231
Figure 5-12: Analysis of bias and reliability of monthly precipitation based historical analog forecasts of July – December cumulative precipitation. Georgia case study site.	232
Figure 5-13: Analysis of bias and reliability of monthly precipitation based historical analog forecasts of rainfed crop yield. Iowa case study site.....	233
Figure 5-14: Analysis of bias and reliability of monthly precipitation based historical analog forecasts of rainfed crop yield, irrigated crop yield, and irrigation amount. Georgia case study site.	234
Figure 5-15: Performance of calibrated artificial neural networks (ANN) for estimation of daily surface solar radiation at case study locations during years 2001-2016.....	237
Figure 5-16: Time series of GRIDMET and Artificial Neural Network (ANN) estimated daily surface solar radiation at the Mitchell County, Georgia case study site during years 2001-2016.	238
Figure 5-17: Time series of GRIDMET and Artificial Neural Network (ANN) estimated daily surface solar radiation at the San Joaquin County, California case study site during years 2001-2016.....	238
Figure 5-18: Comparison of DSSAT modeled corn yield and irrigation amount at the Mitchell County, Georgia and San Joaquin County, California case study sites given GRIDMET reference and ANN modeled surface solar radiation forcing data.	240
Figure 5-19: Year 2000 – 2095 Mitchell County, Georgia corn crop yield and irrigation demand forecasts from DSSAT model simulations driven by LOCA CMIP5 downscaled data.	242
Figure 5-20: Year 2000 – 2095 San Joaquin County, California corn crop yield and irrigation demand forecasts from DSSAT model simulations driven by LOCA CMIP5 downscaled data.	244

SUMMARY

New remote sensing and gridded reanalysis data products from sources including the NASA Soil Moisture Active Passive (SMAP) Mission, Global Precipitation Measurement (GPM) Mission, North American Land Data Assimilation System (NLDAS), Parameter-elevation Relationships on Independent Slopes Model (PRISM), and others provide unprecedented fine resolution characterization of near-surface atmospheric variables (e.g. air temperature, precipitation, downwelling solar radiation, etc.) and surface-to-root-zone hydrologic variables (e.g. soil moisture, hydraulic conductivity, soil composition, etc.) with national to global coverage. When integrated with state-of-the-science process models, these novel data products have the potential to provide useful information for applications in agriculture management, drought assessment, irrigation planning, and hydrological (e.g. streamflow) assessments. This study investigates the value of integrating these new multi-sensor gridded data products for hindcasting and prediction of regional-scale crop yield, irrigation demand, monitoring of agricultural drought, and hydrological flows.

CHAPTER 1

INTRODUCTION

New multi-sensor data products such as those from sources including the NASA Soil Moisture Active Passive (SMAP) Mission, Global Precipitation Measurement (GPM) Mission, North American Land Data Assimilation System (NLDAS), Parameter-elevation Relationships on Independent Slopes Model (PRISM), and others provide useful information with national to global coverage and with potentially valuable applications in agriculture management, drought monitoring, irrigation planning, and streamflow modeling.

Gridded data plays an increasingly important role in the development of crop yield and crop water-stress models used to predict and monitor the physical availability of food, the critical “supply-side” dimension of food security. Such data and models may also guide regional water resources management as more accurate modelling and forecasting of water demand for crop production would lead to a more efficient allocation of limited water supplies. Careful monitoring and provision of water resources for agricultural use is critical as agriculture demands a large fraction of total water use in the United States and the world. In 2005, irrigation in the United States consumed 128 billion gallons per day, accounting for 37 percent of all freshwater withdrawals and 62 percent of all freshwater withdrawals excluding thermoelectric withdrawals (Kenny et al. 2009). The Water Resources chapter of the 2014 National Climate Assessment (Georgakakos et al. 2014) indicates that under

the A2 emissions scenario (which assumes continued global emissions of greenhouse gases), U.S. water demand will increase by 34 percent over the year 2005 to 2060 period, and increase to 82 percent over 2005 levels by year 2090. As consumptive water use is currently and projected to be by far dominated by agricultural irrigation (81 percent of consumptive water use is consumed by agriculture), new multi-sensor gridded data products, coupled with models that can accurately estimate irrigation demand, would play a vital role in planning for future risks and addressing vulnerabilities in water supplies.

Also According to the 2014 National Climate Assessment annual precipitation and river-flow increases are now being observed in the midwestern and northwestern United States. Nationally, intense precipitation events have increased and are also projected to increase in all regions. Flooding may intensify nationally, even in regions where total precipitation is expected to decline. These findings highlight the importance of modeling streamflow-runoff phenomena in order to understand, monitor, and predict hydrological flows. As mentioned previously with regard to modeling agricultural yield and irrigation demand, modern gridded data products, especially remote sensing of precipitation, may be uniquely leveraged to improve streamflow models.

This study explores how new multi-sensor gridded data products can shed light on the hydrologic processes and variables that are vital to crop growth and development, thereby improving regional scale assessments of crop yield, agricultural drought, and irrigation. Likewise, this study tests how these data products can be used to monitor hydrologic processes such as streamflow. Benefits derived from this research may not only assist water resources managers and related stake-holders who strive to efficiently and equitably allocate limited water resources, but also provide guidance on what kinds of improvements

to data products and models may be necessary for more accurate agricultural and hydrological assessments.

1.1 Objectives and Scope

This study explores how new multi-sensor gridded data products can shed light on the hydrologic processes and variables that are vital to crop growth and development, thereby improving regional scale assessments of crop yield, agricultural drought, and irrigation. Likewise, this study tests how these data products can be used to monitor hydrologic processes such as streamflow. The science question to be answered by this research is:

Can prediction of crop yield, assessment of irrigation demand, and monitoring of agricultural drought and hydrological flows be improved by integrating multiple gridded data sets with agricultural and hydrological models?

The research objectives as scope are as follows:

- To provide a quality/accuracy assessment of new remote sensing data products of surface soil moisture (i.e. from the SMAP mission) and their impacts on crop yield prediction.
- To provide a quality/accuracy assessment of new remote sensing data products of daily precipitation (i.e. from the GPM mission) and their impacts on crop yield prediction, irrigation planning, and streamflow modeling.
- Development of an operational framework to incorporate multi-sensor gridded data products for hindcasting and prediction applications in crop yield modeling, drought monitoring, irrigation planning, and streamflow modeling.
- To provide recommendations for improvements in multi-sensor gridded data products necessary for more accurate agricultural and hydrologic modeling.

Benefits derived from this research may not only assist water resources managers and related stake-holders who strive to efficiently and equitably allocate limited water resources, but also provide guidance on what kinds of improvements to data products and models may be necessary for more accurate agricultural and hydrological assessments.

1.2 Thesis Organization

This dissertation comprises six chapters and is organized as follows:

Chapter 2 reviews previous studies on incorporating remote sensing and reanalysis data into agricultural and hydrological models, as well as providing a description of the new multi-sensor gridded data products and models used in this research.

Chapter 3 investigates the accuracy of remote sensing daily precipitation retrievals in comparison to gauge-based gridded precipitation estimates over the continental United States (CONUS). Remote sensing data of soil moisture is explored as a tool to improve accuracy of the remote sensing precipitation retrievals. Finally, the sensitivity of crop model performance to spatial averaging of gridded meteorological and soil input data is assessed.

Chapter 4 explores multiple case studies in which multi-sensor gridded data products are incorporated into crop and streamflow models for hindcasting and near-real-time monitoring of crop yield, irrigation demand, drought, and hydrological flows.

Chapter 5 explores multiple case studies in which multi-sensor gridded estimates of soil moisture and precipitation are used for near-future (seasonal) forecasting of crop yield and irrigation demand via a historical analog approach. Additionally, finely downscaled and

biased-corrected global circulation model (GCM) outputs are integrated with other agriculture-relevant data products into a crop model to assess long-term climate change impacts on localized crop production and irrigation demand.

Chapter 6 summarizes the dissertation and provides recommendations to guide the future development of gridded data products for agricultural and hydrologic modeling.

CHAPTER 2

LITERATURE REVIEW

2.1 Crop yield and irrigation demand models and data assimilation

Crop models were born out of a necessity to test hypotheses related to crop production under various scenarios without resorting exclusively to costly, time-consuming field experiments. Agriculture scientists dating back to 19th century proposed the “law of the minimum”, stating that plant development would be impeded by environmental “limiting factors” (El-Sharkawy 2011). In early singular scale crop models, crop production was estimated based on empirical relationships between depth of applied water and crop yield per unit area (Hexem and Heady 1978; Brumelow and Georgakakos 2007). With the development of biophysical sciences and computational technology, physiologically-based crop models could overcome some of the limitations of these empiricisms. The first comprehensive physiological crop model was formulated based on the dynamics of the growth of specific crop tissues and the influence of environmental factors on photosynthesis and various forms of crop stress (Brumelow 2001). Combined with relevant field data, it was feasible to calibrate such models to local crop genetic characteristics and soil-water-atmospheric environmental conditions. However, field data for calibration of crop models can be a prohibitively expensive, time consuming endeavor, and minimum data requirements for the operation of dynamic biophysical crop model can often times be unavailable at appropriate spatial and temporal resolutions, especially in data scarce regions of the developing world.

Table 2-1 lists the minimum data sets for operation of a popular field scale cropping systems model used in this study, the Decision Support System for Agrotechnology Transfer – Cropping Systems Model (DSSAT-CSM) (Jones et al. 2003). Table 2-2 lists and describes the major modules and sub-modules of the program. Early crop models were developed for single plot or field scale studies in agrotechnology transfer, but modelling focus has since been expanded to address regional-scale simulation of different crops, management practices, climate change impacts, and food security risks (Ewert et al. 2014) at spatiotemporal resolutions that are in-line with recent gridded multi-sensor data products.

Table 2-1: Minimum data sets for operation of DSSAT-CSM, from (Jones et al. 2003)

Category	Minimum Required Data
Site	Latitude and longitude, elevation; average annual temperature; average annual amplitude in temperature; slope and aspect; major obstruction to the sun (e.g. nearby mountain); drainage (type, spacing and depth); surface stones (coverage and size)
Weather	Daily global solar radiation; maximum and minimum air temperatures; precipitation
Soil	Classification using the local system and (to family level) the USDA-NRCS taxonomic system; Basic profile characteristics by soil layer: in-situ water release curve characteristics (saturated drained upper limit, lower limit); bulk density, organic carbon; pH; root growth factor; drainage coefficient
Initial Conditions	Previous crop, root, and nodule amounts; numbers and effectiveness of rhizobia (nodulating crop); Water, ammonium and nitrate by soil layer
Management	Cultivar name and type; planting date, depth and method; row spacing and direction; plant population; irrigation and water management, dates, methods and amounts or depths; fertilizer (inorganic) and inoculant applications; residue (organic fertilizer) applications (material, depth of incorporation, amount and nutrient concentrations); Tillage; Environment (aerial) adjustments; Harvest schedule

Table 2-2: Description of DSSAT-CSM modules and sub-modules, from (Jones et al. 2003)

Modules	Sub modules	Behavior
Main program (DSSAT-CSM)		Controls time loops, determines which modules to call based on user input switches, controls print timing for all modules.
Land unit		Provides a single interface between cropping system behavior and applications that control the use of the cropping system. It serves as a collection point for all components that interact on a homogenous area of land.
Weather		Reads or generates daily weather parameters used by the model. Adjusts daily values if required, and computes hourly values.
Soil	Soil dynamics	Computes soil structure characteristics by layer. This module currently reads values from a file, but future versions can modify soil properties in response to tillage, etc.
	Soil temperature module	Computes soil temperature by layer.
	Soil water module	Computes soil water processes including snow accumulation and melt, runoff, infiltration, saturated flow and water table depth. Volumetric soil water content is updated daily for all soil layers. Tipping bucket approach is used.
	Soil nitrogen and carbon module	Computes soil nitrogen and carbon processes, including organic and inorganic fertilizer and residue placement, decomposition rates, nutrient fluxes between various pools and soil layers. Soil nitrate and ammonium concentrations are updated on a daily basis for each layer.
SPAM		Resolves competition for resources in soil-plant-atmosphere system. Current version computes partitioning of energy and resolves energy balance processes for soil evaporation, transpiration, and root water extraction.
CROPGRO Crop Template module		Computes crop growth processes including phenology, photosynthesis, plant nitrogen and carbon demand, growth partitioning, and pest and disease damage for crops modeled using the CROPGRO model Crop Template (soybean, peanut, dry bean, chickpea, cowpea, faba bean, tomato, Macuna, Brachiaria, Bahiagrass).
Individual plant growth modules	CERES-Maize; CERES-Wheat; CERES-Rice; SubStor-Potato; Other plant models	Modules that simulate growth and yield for individual species. Each is a separate module that simulates phenology, daily growth and partitioning, plant nitrogen and carbon demands, senescence of plant material, etc.
Management operations module	Planting	Determines planting date based on read-in value or simulated using an input planting window and soil, weather conditions.
	Harvesting	Determines harvest date, based on maturity, read-in value or on a harvesting window along with soil, weather conditions.
	Irrigation	Determines daily irrigation, based on read-in values or automatic applications based on monitoring of dates, crop growth stage, soil water depletion, and/or modeled potential evapotranspiration.
	Fertilizer	Determines fertilizer additions, based on read-in values or automatic conditions.
	Residue	Application of residues and other organic material (plant, animal) as read-in values or simulated in crop rotations.

Improving agricultural models by incorporating remote-sensing and reanalysis data as model input has become a growing field of study. The advantage of such data products are that they may allow for the quantification of critical state variables of a crop at a given time instant; this information can then be used to force, recalibrate, or update modeled crop states (Maas 1988). Furthermore, remote-sensing data can provide relatively accurate information on critical variables (such as of rainfall, temperature, soil moisture, etc.) for large regions with relatively high spatial and temporal resolutions. The availability of this information makes possible the application of field-scale crop models at regional scales, and also allows for the models to be useful in ungauged locales (e.g. such as in many places in the developing world). Maas (1988) explored four techniques for incorporating remotely-sensed data into in a uniform white-maize monoculture at a USDA Research Farm in the state of Texas. Direct input of remotely-sensed data was the simplest method of data assimilation; however, the method required frequent observations not available at the time of the study. Moulin et al. (1998) addressed challenges in incorporating coarse resolution remote-sensing data to estimate regional crop yields using a similar approach. Delécolle et al. (1992) also explored remotely-sensed data assimilation techniques in relation to different categories of crop models. Mo et al. (2005) used remotely-sensed retrievals of Leaf Area Index (LAI) with a process-based soil-vegetation-atmosphere transfer (SVAT) model to predict crop yield, water consumption, and water use efficiency for a sub-region of the North China Plain. Ines et al. (2013) utilized an Ensemble Kalman Filter to assimilate remotely-sensed AMSR-E soil moisture and MODIS Leaf Area Index (LAI) data products into DSSAT-CSM to model year 2003 – 2009 maize yields in Story County, Iowa. Data assimilation improved the correlation between modeled and observed

crop yield from 0.47 (no data assimilation) to 0.65 (with combined assimilation of soil moisture and LAI data). Nearing et al. (2012) investigated using the Ensemble Kalman Filter and a Sequential Importance Resampling Filter (SIRF) through an observing system simulation experiment for assimilating surface soil moisture and LAI. The study highlighted the importance of having more than just remote sensing surface soil moisture data for improving agricultural yield estimates, as crop state is understandably more connected to root zone soil moisture state than just surface soil water condition alone. This finding provides an opening for remote sensing soil moisture to be used in tandem with precipitation data to improve agricultural modeling. Incorporating remote-sensing data into crop system models such as DSSAT-CSM has the potential to improve the accuracy of crop yield simulations related to regional irrigation forecasting and water resources management.

2.2 Sacramento Soil Moisture Accounting Model for Streamflow prediction

Moradkhani and Sorooshian (2008) conducted an introductory review of the history of rainfall-runoff modeling. In it, the authors mention the variety of rainfall-runoff models including deterministic, stochastic, physically-based, empirical (e.g. “black box”), lumped models, and distributed models. Owing to its relatively simple conceptualization and development, the lumped modeling approach characterizes a river basin as a single unit and disregards spatial variability. In such models, the main focus is to relate forcing data (i.e. precipitation input) to streamflow without having to resolve the finest details of the spatial processes, patterns, and characteristics that govern streamflow generation. One such lumped model that found widespread use by the US National Weather Service (NWS) for flood forecasting is the Sacramento Soil Moisture Accounting Modeling (SAC-SMA)

(Burnash et al. 1973; Burnash 1995). SAC-SMA divides relatively large watersheds into lower and upper subsurface zones and defines the distribution and transport of two types of water components within these zones: tension water (moisture transported by way of evapotranspiration and diffusion) and free water (driven by gravity). By way of about 13 parameters (with values determined by manual analysis of historical streamflow and precipitation records or by automated optimization approaches), SAC-SMA converts input of daily precipitation and potential evapotranspiration to streamflow. The computed streamflow consists of five basic forms including direct runoff from impervious areas; surface runoff due to precipitation occurring at a faster rate than percolation and interflow when upper zone moisture storage reservoirs are full; interflow resulting from lateral drainage of a temporary free water storage; supplemental base flow; and primary base flow (Burnash 1995). For scenarios in which precipitation data includes snowfall, then the snowfall data needs to be converted to liquid water available for streamflow generation by way of a snowpack/snowmelt model. One such snowmelt discharge model also adopted by the NWS is the SNOW-17 model (Anderson 1973) which only requires input of daily precipitation and air temperature. Figure 2-1 illustrates the main processes, runoff components, and moisture reservoirs included in SAC-SMA, and Table 2-3 lists the parameters of the model. In this research, the open-source Hydromad software package (Andrews et al. 2011; Andrews 2013), which includes a SAC-SMA module as well as data-fitting optimization tools for estimating SAC-SMA input parameters, is utilized for estimating streamflow and for quantifying the impact of using both gridded meteorological forcing data (i.e. GRIDMET) and remote sensing precipitation data (i.e. GPM IMERG and JAXA GSMap products) on model performance.

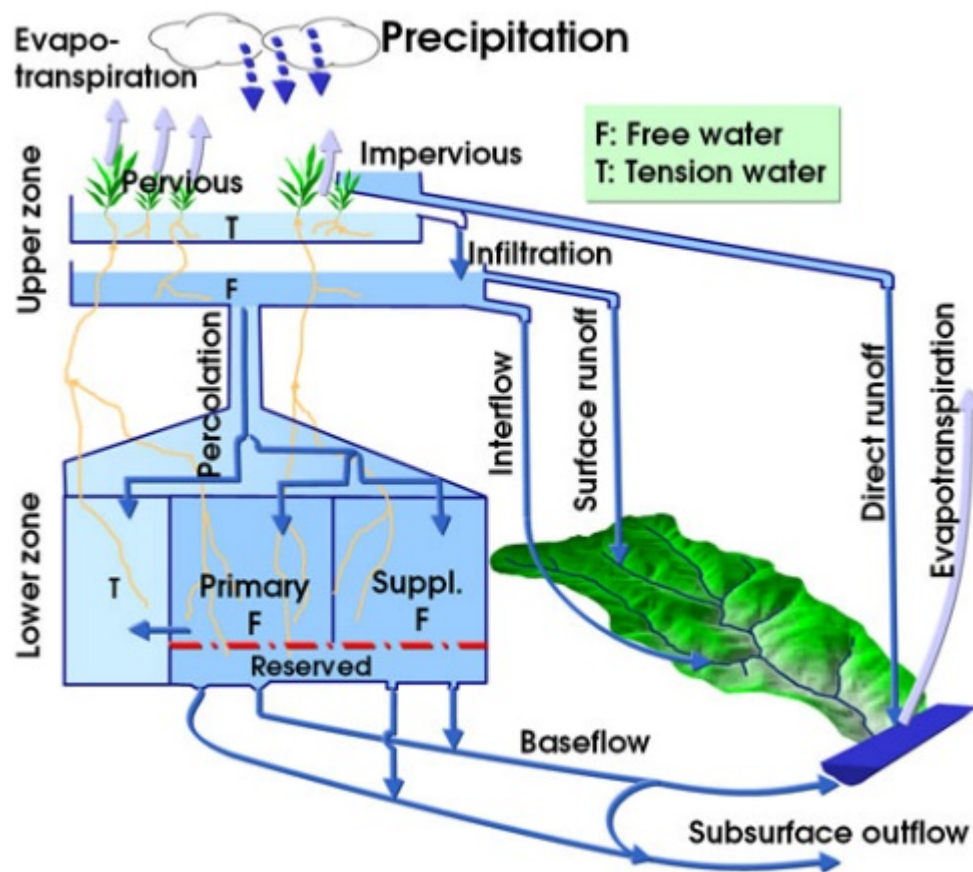


Figure 2-1: Schematic of runoff components and moisture reservoirs of the Sacramento Soil Moisture Accounting Model (SAC-SMA), from (World Bank 2016).

Table 2-3: Parameters of the Sacramento Soil Moisture Accounting Model (SAC-SMA) in the Hydromad modeling package, from (Andrews 2013).

SAC-SMA Parameter	Description
UZWWM	Upper zone tension water maximum capacity (mm).
UZFWM	Upper zone free water maximum capacity (mm).
UZK	Lateral drainage rate of upper zone free water expressed as a fraction of contents per day.
PCTIM	The fraction of the catchment which produces impervious runoff during low flow conditions.
ADIMP	The additional fraction of the catchment which exhibits impervious characteristics when the catchment's tension water requirements are met.
ZPERC	Maximum percolation (from upper zone free water into the lower zone) rate coefficient.
REXP	An exponent determining the rate of change of the percolation rate with changing lower zone water contents.
LZWWM	Lower zone tension water maximum capacity (mm).
LZFSM	Lower zone supplemental free water maximum capacity (mm).
LZFPM	Lower zone primary free water maximum capacity (mm).
LZSK	Lateral drainage rate of lower zone supplemental free water expressed as a fraction of contents per day.
LZPK	Lateral drainage rate of lower zone primary free water expressed as a fraction of contents per day.
PFREE	Direct percolation fraction from upper to lower zone free water (the percentage of percolated water which is available to the lower zone free water aquifers before all lower zone tension water deficiencies are satisfied).

2.3 NASA SMAP L3 Enhanced (surface soil moisture)

The launch of NASA Soil Moisture Active Passive (SMAP) satellite on 31 January 2015 offers an opportunity to improve the observed soil moisture record with high spatial and temporal resolution data products with global coverage. SMAP data has the potential to reduce the uncertainty in food-security essential estimates of crop yield, water-stress, and irrigation demand when incorporated in agricultural models, and can also serve as vital input for parameterizations of soil water infiltration and crop transpiration. The Level 3 Enhanced SMAP data product (SMAP_L3_SMPE) provides 36 km (posted to a 9km grid)

and 2-3 daily top 5 cm layer soil moisture (Entekhabi et al. 2010b). The mission requires the product's unbiased root-mean-squared-error (ubRMSE), the RMSE between satellite retrieved and upscaled in-situ soil moisture estimates after the temporal mean has been removed from both data streams (Entekhabi et al. 2010a), not exceed $0.04 \text{ cm}^3 \text{ cm}^{-3}$ (Entekhabi et al. 2014). Chan et al. (2018) investigated the performance of the SMAP enhanced passive surface soil moisture data product over a collection of core validation sites with distinct climates. Table 2-4 summarizes the performance metrics at various cropland sites. In general the SMAP data is well-correlated with in-situ data; however, the combined impact of the ubRMSE and bias may drive soil moisture estimates to deviate from in-situ estimates by over $0.1 \text{ cm}^3/\text{cm}^3$ which may adversely impact crop yield and irrigation demand simulations if this data is incorporated into a cropping systems model.

Table 2-4: Performance metrics of SMAP Passive Enhanced Surface Soil Moisture data product at various cropland in-situ core validation sites (CVS) over the April 2015 to October 2016 period, from (Chan et al. 2018).

Cropland CVS Name	Location	Climate	ubRMSE (m^3/m^3)	Bias (m^3/m^3)	RMSE (m^3/m^3)	Correlation
South Fork	Iowa, USA	Cold	0.054	- 0.062	0.082	0.646
Little River	Georgia, USA	Temperate	0.028	0.087	0.092	0.887
Kenaston	Canada	Cold	0.022	- 0.040	0.046	0.854
Monte Buey	Argentina	Arid	0.051	- 0.020	0.055	0.840
REMEDIHUS	Spain	Temperate	0.042	- 0.007	0.042	0.872
Twente	Netherlands	Temperate	0.056	0.013	0.057	0.885
Yanco	Australia	Arid	0.043	0.020	0.048	0.964

2.4 NASA GPM IMERG Precipitation

The NASA Global Precipitation Measurement (GPM) mission with its core satellite launched on 27 February 2014 combines the measurements from a constellation of satellites to provide precipitation measurements with global coverage (between the Arctic

and Antarctic Circles) at sub-daily temporal resolutions (NASA 2012). The Late release Level 3 data product from the GPM's Integrated Multi-Satellite Retrievals (IMERG) provides gridded rainfall intensity data at 0.1° spatial and half-hourly resolution with 18 hour latency (NASA 2015). The availability of the GPM rainfall observations together with the SMAP soil moisture data and hydrologic and agricultural models allows continuous and more accurate assessment of soil moisture state from surface to root zone at global scale. These data are expected to significantly reduce the uncertainty in the forecast of crop production and drought monitoring not only over the United States but also for the data scarce (ungauged) regions in the developing world.

2.5 JAXA GSMaP and GSMaP-Gauge Precipitation

The Global Satellite Mapping of Precipitation (GSMaP) Project is a research project started in 2002 sponsored by the Core Research for Evolutional Science and Technology (CREST) of the Japan Science and Technology Corporation (JST) and promoted by the Japan Aerospace Exploration Agency (JAXA) Precipitation Measuring Mission (PMM) Science Team (Okamoto et al. 2005; JAXA/EORC 2018). GSMaP's objective is to produce high precision, high resolution global maps of precipitation using satellite data. The finest resolution data available from GSMaP is 0.1° spatial and hourly resolution. The latest versions of GSMaP data incorporates rain rate retrievals from the GPM mission. In this research, two daily aggregated precipitation products from GSMaP are utilized, the first: GSMaP-Standard product, which integrates passive microwave radiometer data with infrared radiometer data into a Kalman filter to produce fine resolution precipitation maps, while the GSMaP-Gauge product calibrates the Standard product with global rain gauge

analysis (CPC Unified Gauge-Based Analysis of Global Daily Precipitation) supplied by United States' National Oceanic and Atmospheric Administration (NOAA) (JAXA/EORC 2017). Tian et al. (2009) evaluated the performance of GSMaP precipitation estimates over the contiguous United States and found that GSMaP does well in capturing spatial patterns of precipitation, particularly in the summer, with better performance over the eastern United States than the western region. Summertime overestimates were attributed to overestimation of strong precipitation events. It is important to note however that this analysis was completed before retrievals from the GPM mission were available. Before incorporating daily GSMaP data into agricultural and streamflow models, it is of interest to re-evaluate the performance of this data (both GSMaP-Standard and GSMaP-Gauge) over the contiguous United States.

2.6 GRIDMET Surface Meteorological Data

GRIDMET is a recently developed, publicly available data set of high spatial resolution (~4 km) gridded daily surface meteorological data covering the contiguous United States from 1979 to present (Abatzoglou 2011). GRIDMET combines the fine resolution spatial attributes of gridded climate data from Parameter Regression on Independent Slopes Model (PRISM) (Daly et al. 1994) with the fine temporal resolution of NLDAS-2 (Mitchell et al. 2004) reanalysis data. Primary and derived climate variables in this data set include daily maximum and minimum air temperature, precipitation, downwelling surface shortwave-radiation, reference evapotranspiration, 10-day Palmer Drought Severity Index, mean vapor pressure deficit, and other variables. Behnke et al. (2016) evaluated the performance of multiple gridded temperature and precipitation data products, including GRIDMET,

over the contiguous United States. They found that at the national level, GRIDMET's (as well as other data sets') temperature data was highly correlated (greater than 0.9) and shared nearly identical temporal variability with weather station records. However for precipitation evaluated at the national scale, the correlation was considerably weaker (between 0.5 and 0.6) with annual wet biases in the Great Basin, Northern Rockies, and Pacific Northwest regions, and mean annual absolute errors of greater than 3 mm in the Southeast and Deep South regions. GRIDMET data has been incorporated in cropping systems models (e.g. (Karimi et al. 2018)) and streamflow models (e.g. (Ficklin et al. 2016)). Despite some discrepancies in precipitation data, GRIDMET, due to its derivation from products strongly linked to a wide range of monitoring networks, arguably represents one of the finest resolution data products with low latency mimicking "ground truth". It is of interest in this study to assess the performance of remote sensing data products of precipitation (i.e. GPM and GSMaP products) in relation to the GRIDMET data set.

2.7 Daymet Surface Meteorological Data

Similar to GRIDMET, Daymet is a data set providing fine resolution gridded model estimates of daily weather variables for North America based on daily meteorological observations (Thornton et al. 1997; Thornton and Running 1999; Thornton et al. 2000; Thornton et al. 2014). The spatial resolution is 1 km x 1 km with temporal coverage beginning from 1980, but unlike GRIDMET which includes up to near present-day estimates, the most recent Daymet data is from the previous calendar year. Daily variables available from this data set include daylight length (seconds), daily precipitation (converted to water-equivalent), incident shortwave radiation, and maximum and minimum air temperature (2 meters above surface). Daymet is archived and distributed through the Oak

Ridge National Laboratory Distributed Active Archive Center for Biogeochemical Dynamics (ORNL DAAC), and is supported by NASA Earth Science Data and Information System (ESDIS) and the Terrestrial Ecosystem Program. Because of its fine spatial resolution (1 km x 1 km), Daymet data lends itself to a useful analysis of how the spatial coarsening of daily meteorological inputs impacts crop yield and irrigation estimates from cropping systems models such as DSSAT-CSM which were originally developed for point-scale (e.g. single farm field scale) modeling. For example, how much do crop model predictions change when daily meteorological input data is coarsened (by spatial averaging of 1 km pixels) from 1 km resolution to 30 km resolution? What is the coarsest spatial resolution of meteorological input data that is acceptable for crop modeling applications? This study explores these questions by way of this data set.

2.8 HarvestChoice Global high-resolution soil profile database (HC-GHRSPD)

The HarvestChoice Global high-resolution soil profile database for crop modeling applications (hereafter referred to as HC-GHRSPD) is a relatively new (released in 2015) data set providing estimates of soil composition, hydraulic properties, and other soil properties that are critical inputs to cropping systems models, particularly DSSAT-CSM (Han et al. 2015). HC-GHRSPD provides DSSAT-CSM compatible surface-to-root-zone soil profiles at the 5 arc-minute (~10km) spatial resolution with global coverage (with a global crop mask applied). Table 2-1 lists the parameters provided by the data set with their associated units.

Table 2-5: Soil profile parameters provided by the HC-GHRSPD data set, from (Han et al. 2015).

Variable name	Definition
SCOM	Color, moist, Munsell hue
SALB	Albedo, fraction
SLU1	Evaporation limit, mm
SLDR	Drainage rate, fraction day ⁻¹
SLRO	Runoff curve no. (Soil Conservation Service)
SLNF	Mineralization factor, 0 to 1 scale
SLPF	Photosynthesis factor, 0 to 1 scale
SMHB	pH in buffer determination method, code
SMPX	Phosphorus determination code
SMKE	Potassium determination method, code
SLLL	lower limit, or wilting point, cm ³ cm ⁻³
SDUL	drained upper limit, or field capacity, cm ³ cm ⁻³
SSAT	Upper limit, saturated, cm ³ cm ⁻³
SRGF	Root growth factor, soil only, 0.0 to 1.0
SSKS	Sat. hydraulic conductivity, cm h ⁻¹
SBDM	Bulk density, g cm ⁻³
SLOC	Organic carbon, %
SLCL	Clay (<0.002 mm), %
SLSI	Silt (0.05 to 0.002 mm), %
SLNI	Total nitrogen, %
SLHW	pH in water
SCEC	Cation exchange capacity, cmol kg ⁻¹

2.9 USDA NASS Cropscape – Cropland Data Layer

The USDA National Agricultural Statistics Service (USDA-NASS) Cropland Data Layer (Han et al. 2012; USDA NASS 2015), referred to as Cropscape, contains crop and other land cover classifications derived from remote sensing of the contiguous United States and has been publicly accessible through a web service based application since year 2011. With regard to data relevant to agricultural decision support, the Cropscape data product, produced yearly, provides geo-referenced, high accuracy thematic maps of crop acreages by crop type (e.g. Corn, Cotton, Soybeans, Potatoes, Grassland/Pasture, etc.) at spatial resolution as fine as 30 meters. Data sources used to develop the product include satellite imagery from the Advanced Wide Field Sensor (AWiFS), Landsat, USDA Farm

Service Agency (USDA-FSA), USDA National Agricultural Statistics Service (USDA-NASS) June Agricultural Survey data, and the US Geological Survey (USGS) National Land Cover Datasets (NLCD) (Han et al. 2012). A sample thematic map is presented in Figure 2-2. The Cropscape data product has found many applications such as agricultural land cover monitoring, crop acreage and yield estimation, disaster assessment, bioenergy crop inventory, carbon accounting, among other studies (West et al. 2010; Han et al. 2012; Kutz et al. 2012; Green et al. 2018).

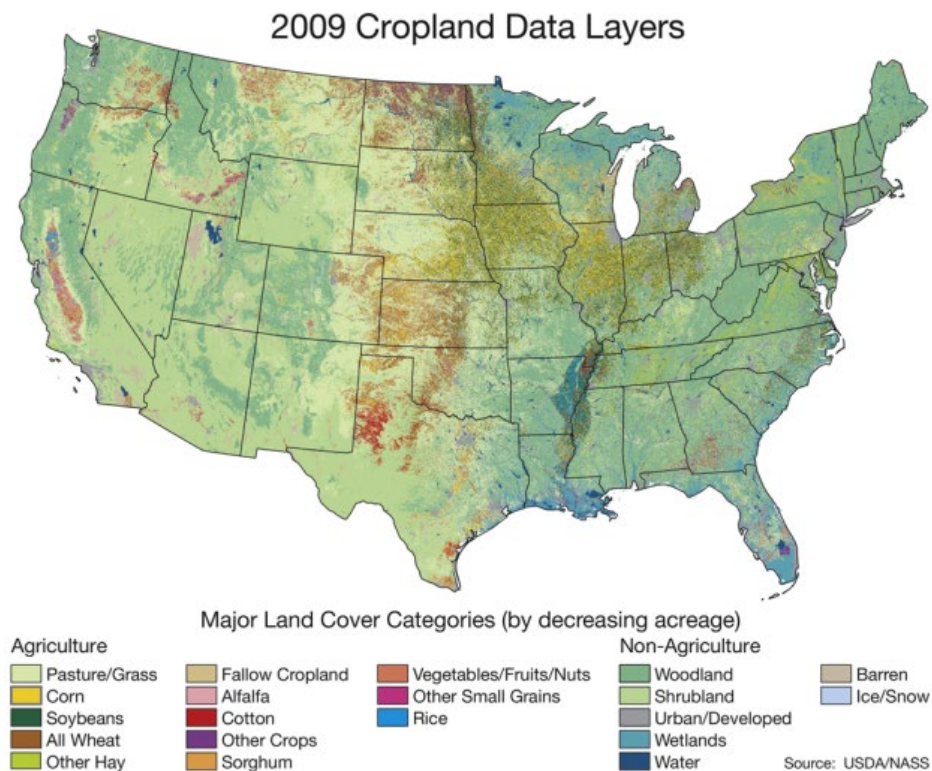


Figure 2-2: Year 2009 Cropscape Map with major land cover categories, from (Han et al. 2012)

One innovative use of this data product to be explored in this research includes estimation of regional-scale crop irrigation volumes. While there are data products that provide local (e.g. U.S. county-level) insight on what percentage of a specific crop type's

acreage are irrigated, the actual irrigation amount or irrigation volume, in many cases is neither reported nor monitored (sometimes due to privacy concerns). Gridded Cropscape data can be integrated with local information on irrigated acreage to more precisely determine how much land area of a given crop is either irrigated or rainfed. From there crop systems models, such as DSSAT-CSM, driven by high resolution gridded meteorological data (e.g. GRIDMET) and soil information (e.g. HC-GHRSPD) can be leveraged to determine crop specific irrigation volumes. The results of such an investigation could prove invaluable to drought monitoring, food security studies, and guide irrigation withdrawal planning and permitting.

2.10 LOCA Downscaled CMIP5 Climate Projections

The Coupled Model Intercomparison Project phase 5 (CMIP5) recently released downscaled climate projections based on the relatively new Localized Constructed Analogs (LOCA) method (Pierce et al. 2014). Constructed Analog methods spatially downscale GCM output by searching for a set of observed days, from a spatially coarsened observational data set, that are most similar to the coarse grid GCM data. Then the fine-resolution observations from the analog days are combined to create the final spatially downscaled field (Hidalgo et al. 2008; Bracken 2016). LOCA improves on commonly used constructed analog approaches by selecting analog days based on an analysis within a synoptic-scale (approximately 1000 km) region instead of the entire downscaling domain; and by selecting a single analog day from a set of 30 candidates based on local (approximately 100 km about the point being downscaled) matching between the downscaled model and fine observational grid instead of using a weighted average of

candidate analog days (Bracken 2016). While the LOCA downscaling method requires more computational power than previous methods, performance tests showed LOCA downscaled variable fields (maximum and minimum air temperature and precipitation) provide better estimates of extreme days, more realistically preserve spatial coherence of the downscaled variables, and avoid the problem of producing light-precipitation artifacts (Pierce et al. 2014). Furthermore, the novel bias-correction procedure adopted for this data set is an improvement over conventional methods with regard to preserving the GCMs' climate change signal as well as the frequency-dependent variance of climate variables (Pierce et al. 2015). It is also important to note that the LOCA procedure also involves treatment for future climate anomalies (in precipitation and temperature) that are outside the bounds of historical observations (Pierce et al. 2014). LOCA-CMIP5 downscaled estimates of maximum and minimum air temperature and precipitation for two CO₂ emission path scenarios (RCP 4.5 and RCP 8.5) from 32 different GCM models are publicly available at <https://gdo-dcp.ucllnl.org/>. The coverage is the continental U.S. from year 1950 – 2099 and the resolution is 1/16th degree (~6 km x 6 km grid cells) at the daily time step. With its aforementioned spatial, temporal, and statistical features, the LOCA-CMIP5 product is uniquely suited for use with agricultural models. Review of recent literature showed that this modern data set has yet to be incorporated into a crop systems model for assessment of local climate change impacts on agricultural production and irrigation demand.

CHAPTER 3

ERROR ANALYSIS OF REMOTE SENSING PRECIPITATION AND AGRI-HYDROLOGICAL MODEL SENSITIVITIES TO GRIDDED INPUT DATA

3.1 Comparison of Near Real Time NASA GPM IMERG and JAXA GSMaP products over the continental US

As mentioned in Chapter 2, recent remote sensing precipitation missions such as NASA GPM and JAXA GSMaP provide a unique opportunity to monitor precipitation, a vital input to agricultural and streamflow models, in near real time. However, before these data are incorporated into hydrological models it is important to understand how accurate (or inaccurate) these data are. In this study, low-latency (e.g. available to the public within three days or less from the satellite retrieval time) gridded retrievals of daily rainfall from NASA GPM IMERG (Version 5, Level 3, Late Release), JAXA GSMaP (Version 7), and JAXA GSMaP-Gauge (Version 7) are compared to the GRIDMET rainfall product over the years 2015-2016 for various regions of the continental United States. While the GRIDMET product is a reanalysis estimate of precipitation, precipitation estimates from this product are driven by a wide range of “ground-truth” monitoring networks.

Figure 3-1 presents a map of the nine climate regions of the continental United States used for assessing the quality of the remote sensing precipitation data products. These nine regions were identified as being climatically consistent by the U.S. National Centers for

Environmental Information (NCEI) and useful for understanding current climate anomalies (Karl and Koss 1984).

U.S. Climate Regions

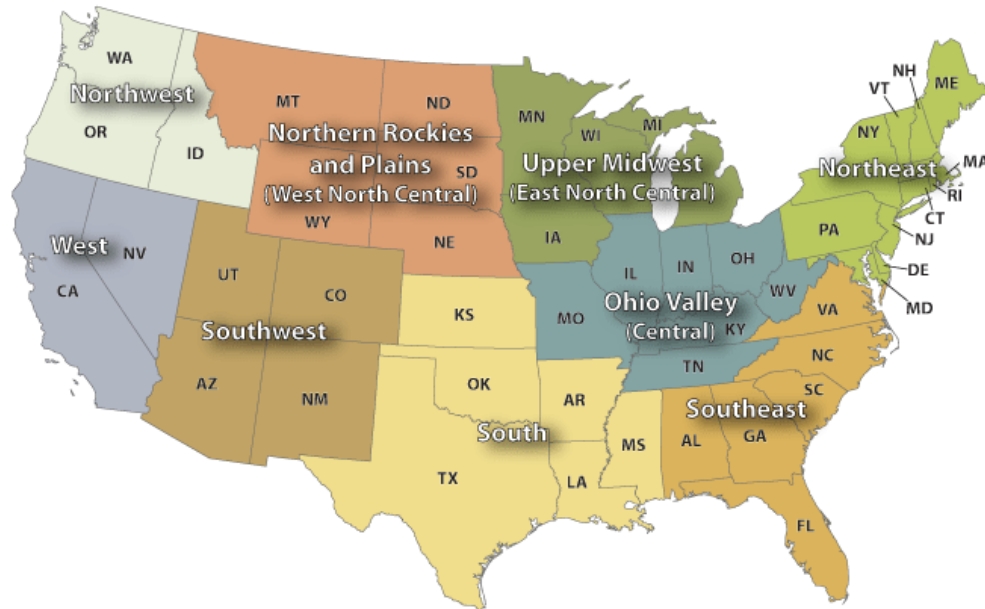


Figure 3-1: Nine climate regions for assessment of remote sensing precipitation products over the continental United States. From (NCDC 2017).

3.1.1 Annual Assessments

Figure 3-2 and Figure 3-3 illustrate the performance of the remote sensing precipitation data products in estimating annual accumulated precipitation over the continental U.S. during years 2015 and 2016 respectively. In 2015, The GRIDMET product estimated the annual precipitation as 878 mm while the remote sensing retrievals were 1017 mm, 1246 mm, and 877 mm for GPM IMERG, GSMaP-Standard, and GSMaP-Gauge respectively. In 2016, The GRIDMET product estimated the annual precipitation as 823 mm. All of the remote sensing products had higher estimates of 901 mm, 1321 mm, and 831 mm for GPM IMERG, GSMaP-Standard, and GSMaP-Gauge respectively. The discrepancy between the GSMaP-Standard and the GSMaP-Gauge product (in both years) highlights the impact and

importance of the rain-gauge correction for ensuring the accuracy of remote sensing precipitation retrievals.

Figure 3-4 and Figure 3-5 highlight how the performance of the remote sensing precipitation retrievals vary by climate region. For all climate regions of the continental U.S., the JAXA GSMP-Standard product greatly overestimates precipitation in comparison to the rain-gauge derived GRIDMET data product. The rain-gauge correction introduced in the GSMP-Gauge product is essential for producing more accurate retrievals. The GPM IMERG product typically overestimates precipitation (relative to GRIDMET), except for West in year 2015 and West and Northwest climate regions in year 2016 where the GPM IMERG product appears to have a considerable dry bias. The best performance of the GPM IMERG product is in the Southeast, Southwest, and West North Central for both years as the deviation (usually overestimation) from the GRIDMET product is less than 100 mm. In year 2015, the West and Northwest regions are also in good agreement with GRIDMET, and in year 2016, the South region agrees well with GRIDMET.

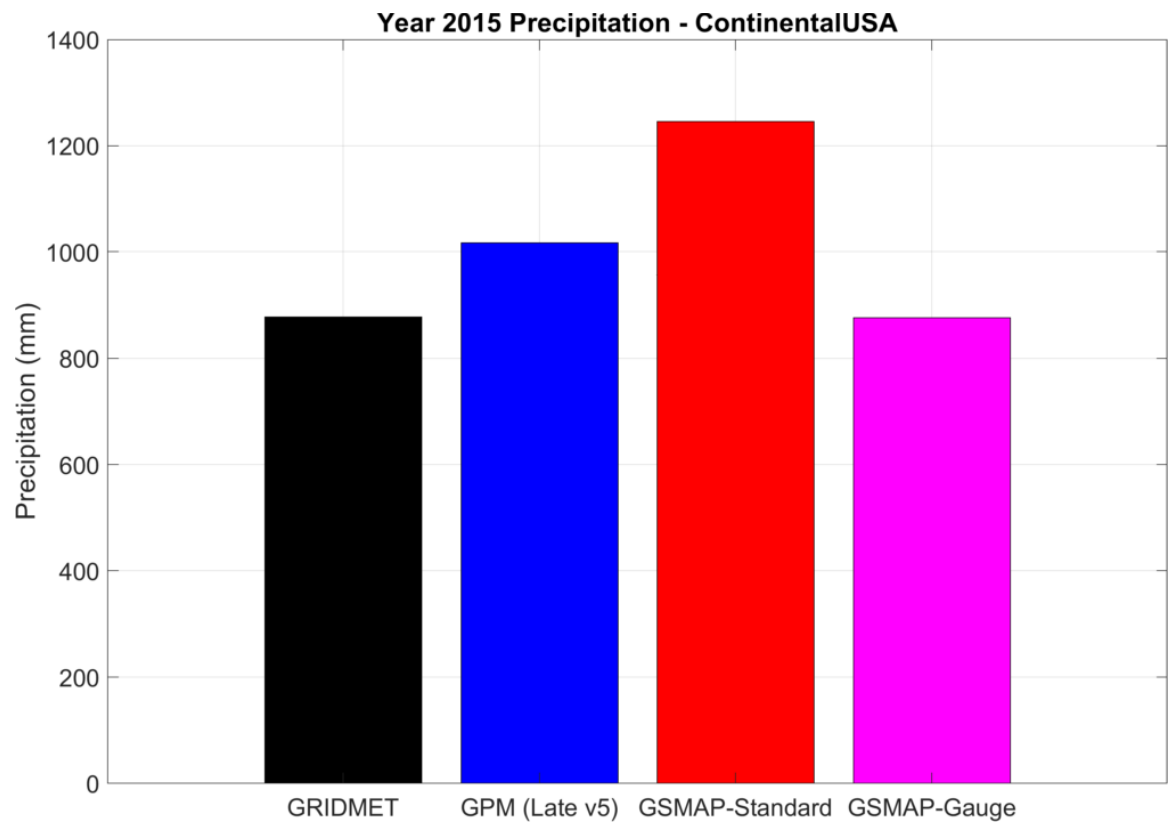


Figure 3-2: Assessment of year 2015 cumulative precipitation from GPM IMERG, GSMap-Standard, and GSMap-Gauge data products.

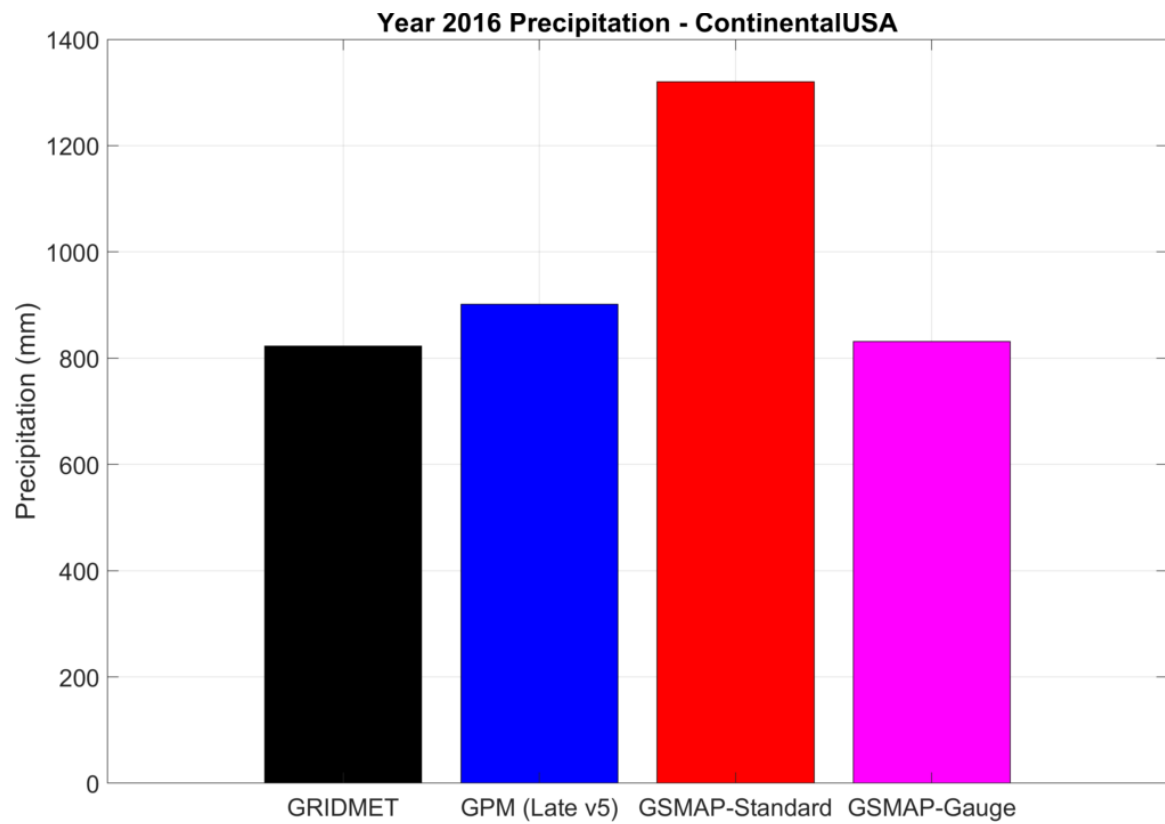


Figure 3-3: Assessment of year 2016 cumulative precipitation from GPM IMERG, GSMap-Standard, and GSMap-Gauge data products.

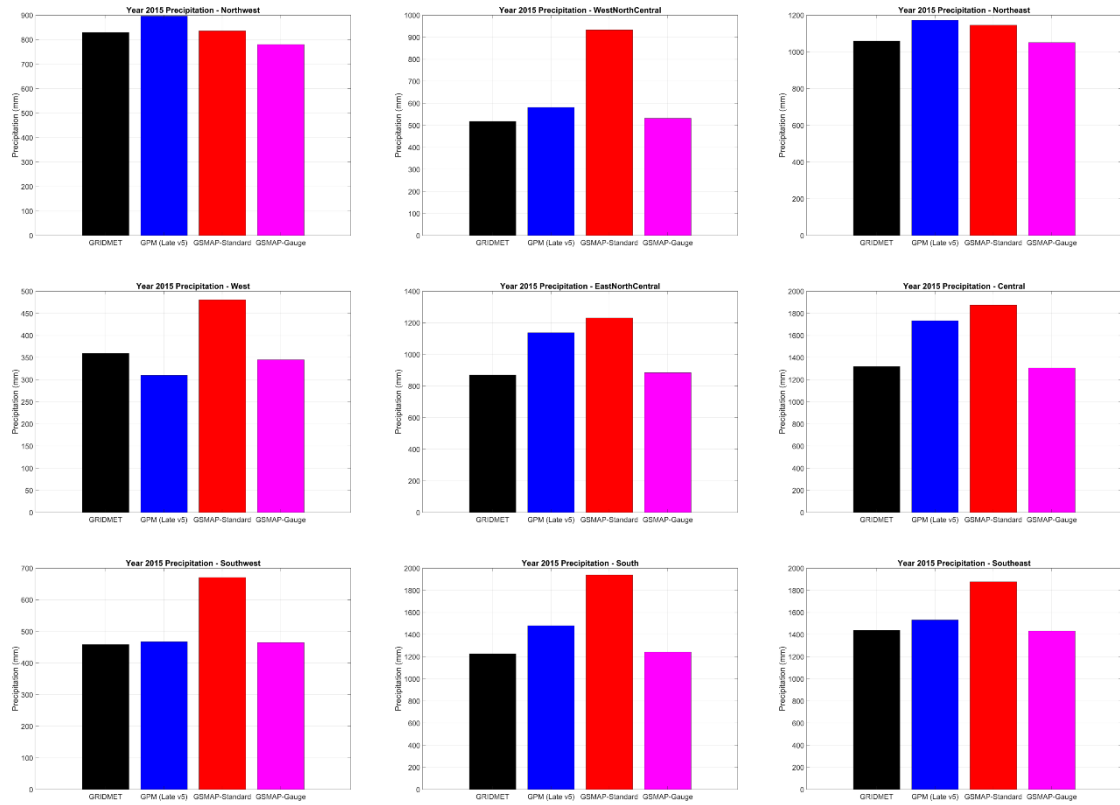


Figure 3-4: Assessment of year 2015 regional cumulative precipitation from GPM IMERG, GSMaP-Standard, and GSMaP-Gauge data products.

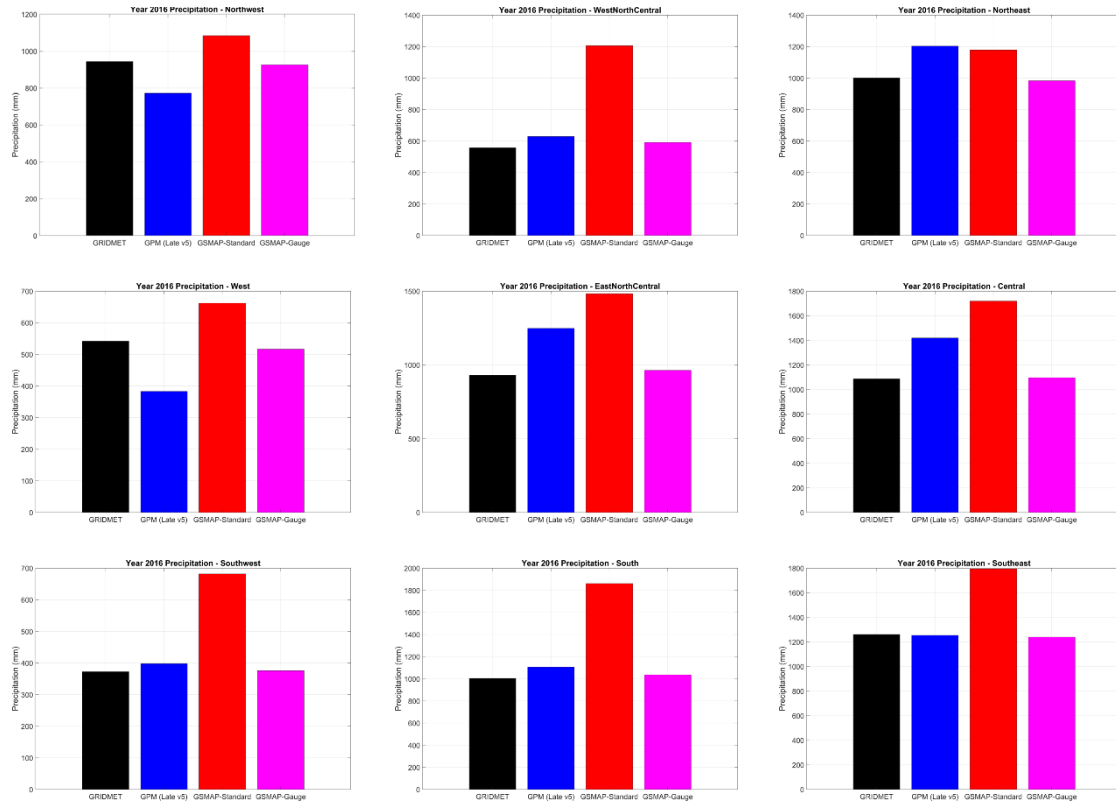


Figure 3-5: Assessment of year 2016 regional cumulative precipitation from GPM IMERG, GSMaP-Standard, and GSMaP-Gauge data products.

3.1.2 Seasonal Assessments

Figure 3-6 and Figure 3-7 present the cumulative precipitation for each season of years 2015 and 2016 for GRIDMET, GPM IMERG, GSMaP-Standard, and GSMaP-Gauge data products. As with the annual assessment, GSMaP-Standard greatly overestimates precipitation in spring, summer, and fall, but the overestimation appears to be remedied in the GSMaP-Gauge product. GPM IMERG also typically overestimates in all seasons.

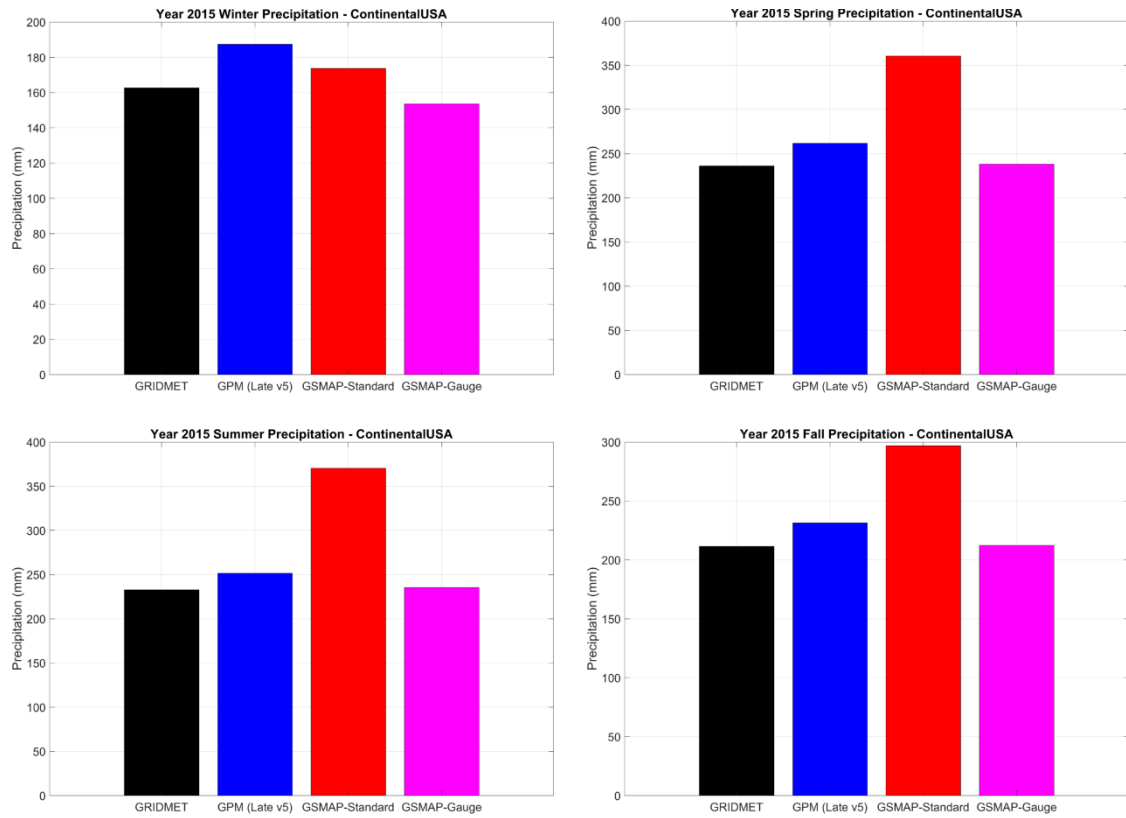


Figure 3-6: Seasonal assessment of year 2015 cumulative precipitation from GPM IMERG, GSMap-Standard, and GSMap-Gauge data products for the Continental US

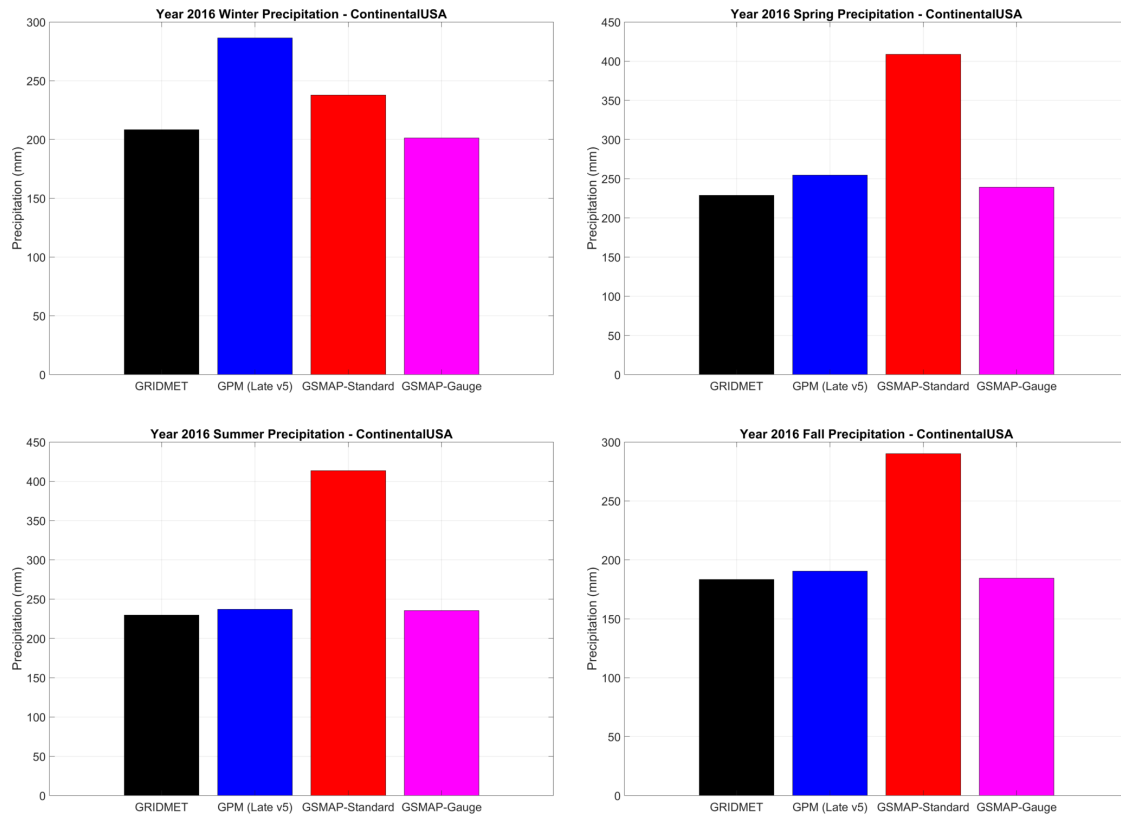


Figure 3-7: Seasonal assessment of year 2016 cumulative precipitation from GPM IMERG, GSMaP-Standard, and GSMaP-Gauge data products for the Continental US

Figure 3-8 and Figure 3-9 present the regional cumulative precipitation for the winter seasons of years 2015 and 2016 for GRIDMET, GPM IMERG, GSMaP-Standard, and GSMaP-Gauge data products. The GPM IMERG product consistently overestimates winter precipitation in the Northwest, Northeast, and Central regions and underestimates in the Southwest. The GSMaP-Standard estimates are generally either lesser or comparable to the GRIDMET reference except for the South and Southeast for which there is substantial overestimation, and the inconsistency with GRIDMET appears to be removed with the incorporation of rain gauge data in the GSMaP-Gauge product.

As shown in Figure 3-10 and Figure 3-11, the GPM IMERG product underestimates spring precipitation in the Northwest, West, and Southwest climate regions, while

overestimating in the Central and East North Central regions. GSMap-Standard overestimates in most regions, and this is rectified by the GSMap-Gauge data set.

Figure 3-12 and Figure 3-13 show that the GPM IMERG summer cumulative precipitation is comparable to the GRIDMET reference except for the the West and Southwest regions for which there is overestimation, in contrast to the underestimation during the winter and spring seasons. GSMap-Standard is conspicuous by its large overestimation for most regions, which similar to the previous assessments, is rectified in the GSMap-Gauge data set.

Figure 3-14 and Figure 3-15 show that the GPM IMERG fall cumulative precipitation is comparable to the GRIDMET reference, but there is a dry bias in the GPM IMERG product in the Northwest and West. GSMap-Standard overestimates in the majority of regions while GSMap-Gauge agrees well with the GRIDMET reference.

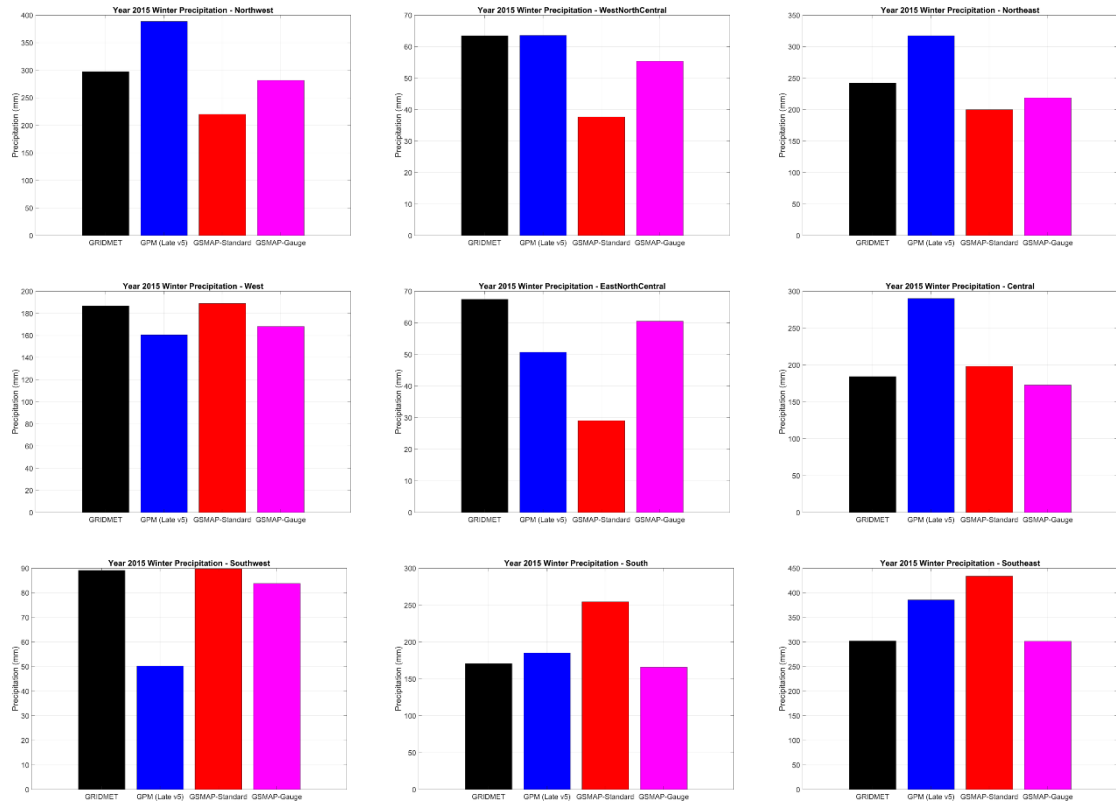


Figure 3-8: Assessment of year 2015 regional winter cumulative precipitation from GPM IMERG, GSMaP-Standard, and GSMaP-Gauge data products.

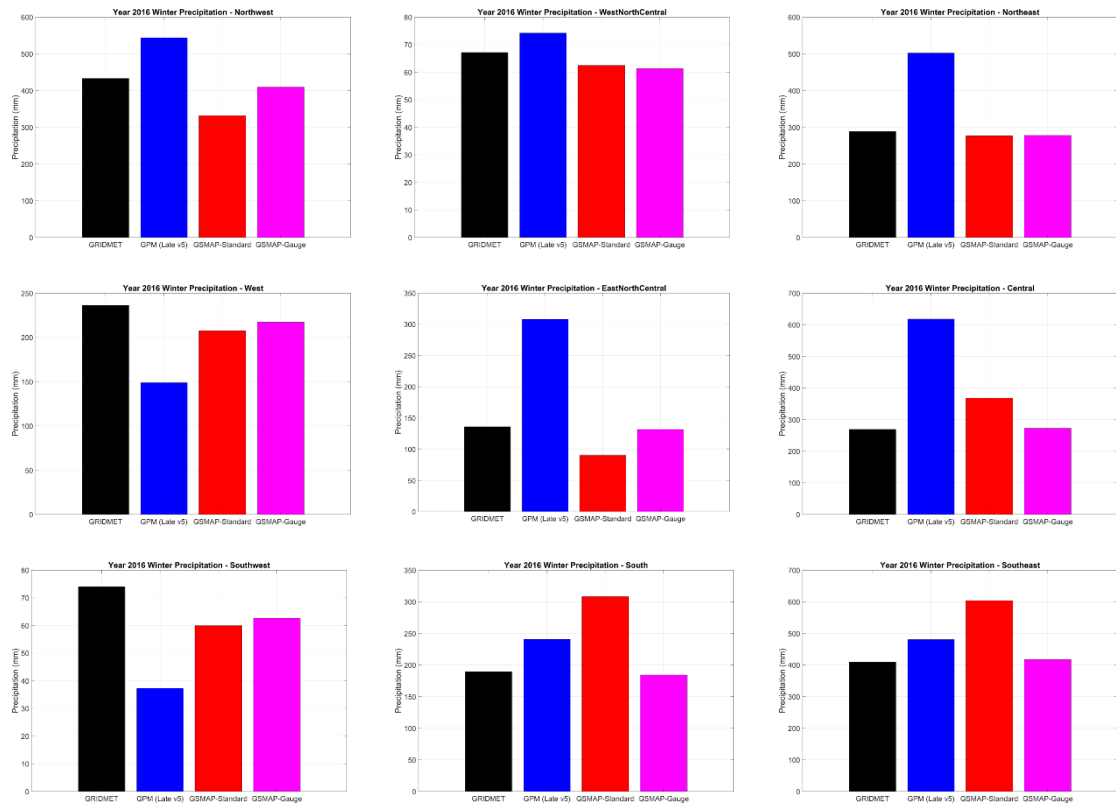


Figure 3-9: Assessment of year 2016 regional winter cumulative precipitation from GPM IMERG, GSMaP-Standard, and GSMaP-Gauge data products.

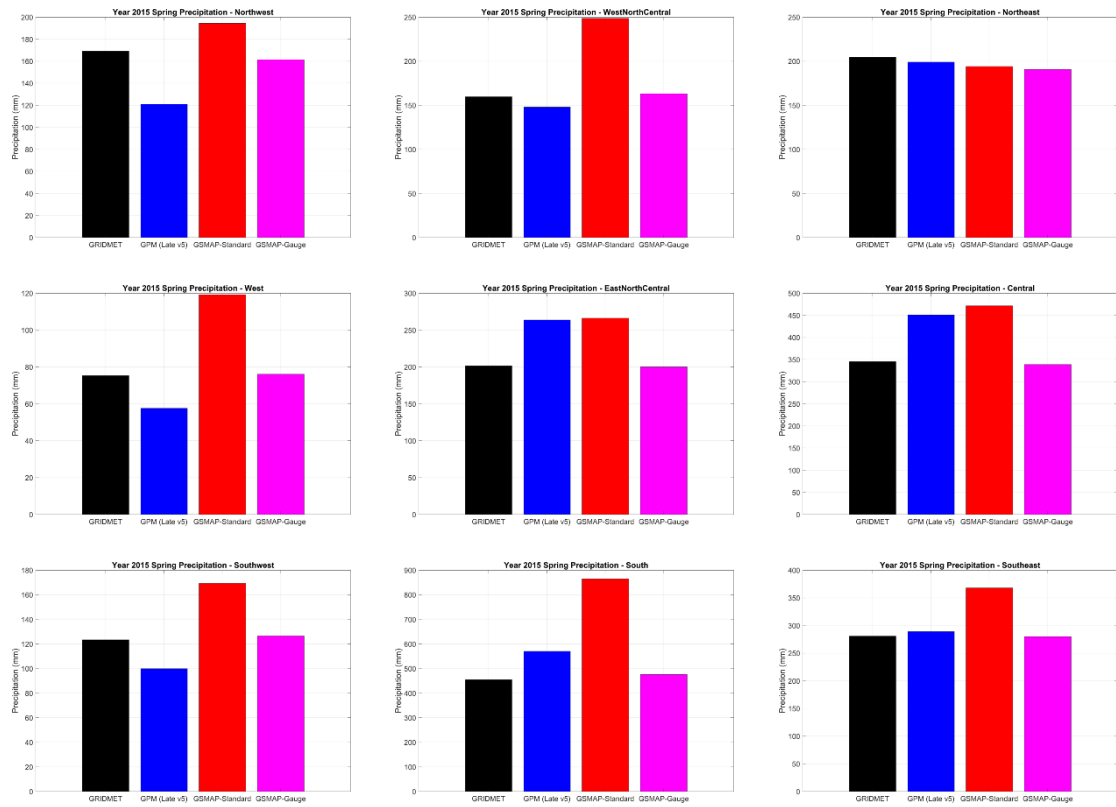


Figure 3-10: Assessment of year 2015 regional spring cumulative precipitation from GPM IMERG, GSMap-Standard, and GSMap-Gauge data products.

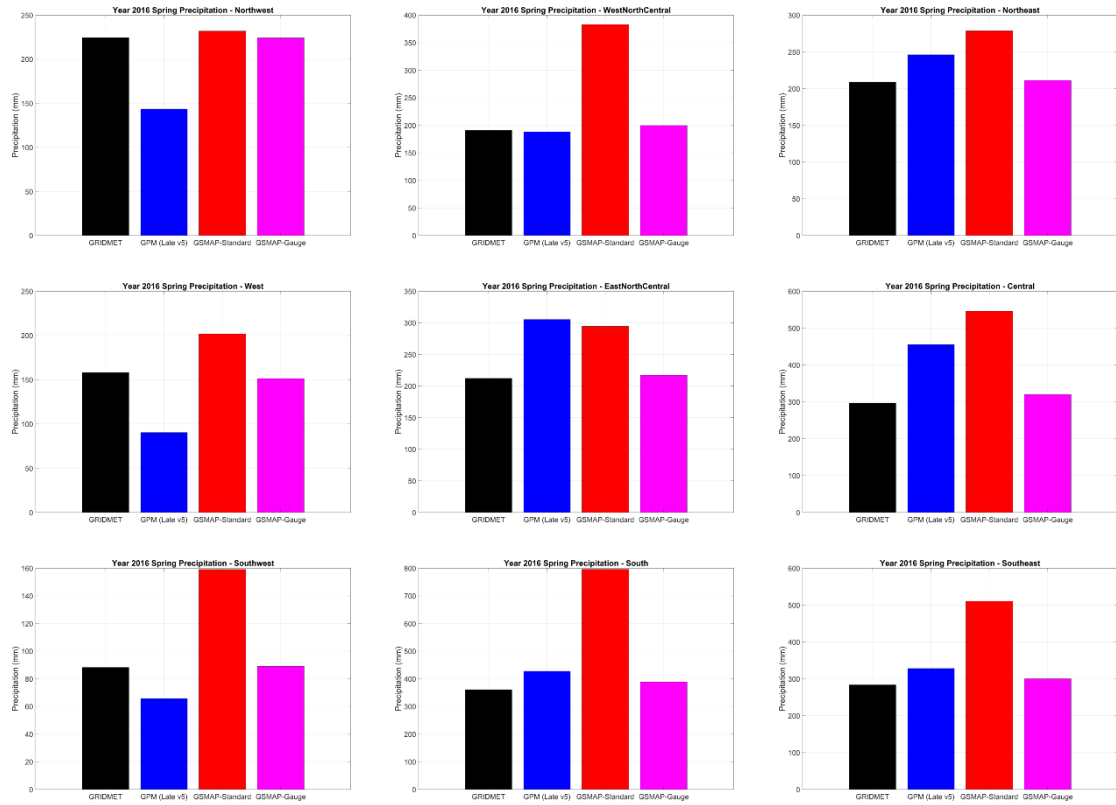


Figure 3-11: Assessment of year 2016 regional spring cumulative precipitation from GPM IMERG, GSMap-Standard, and GSMap-Gauge data products.

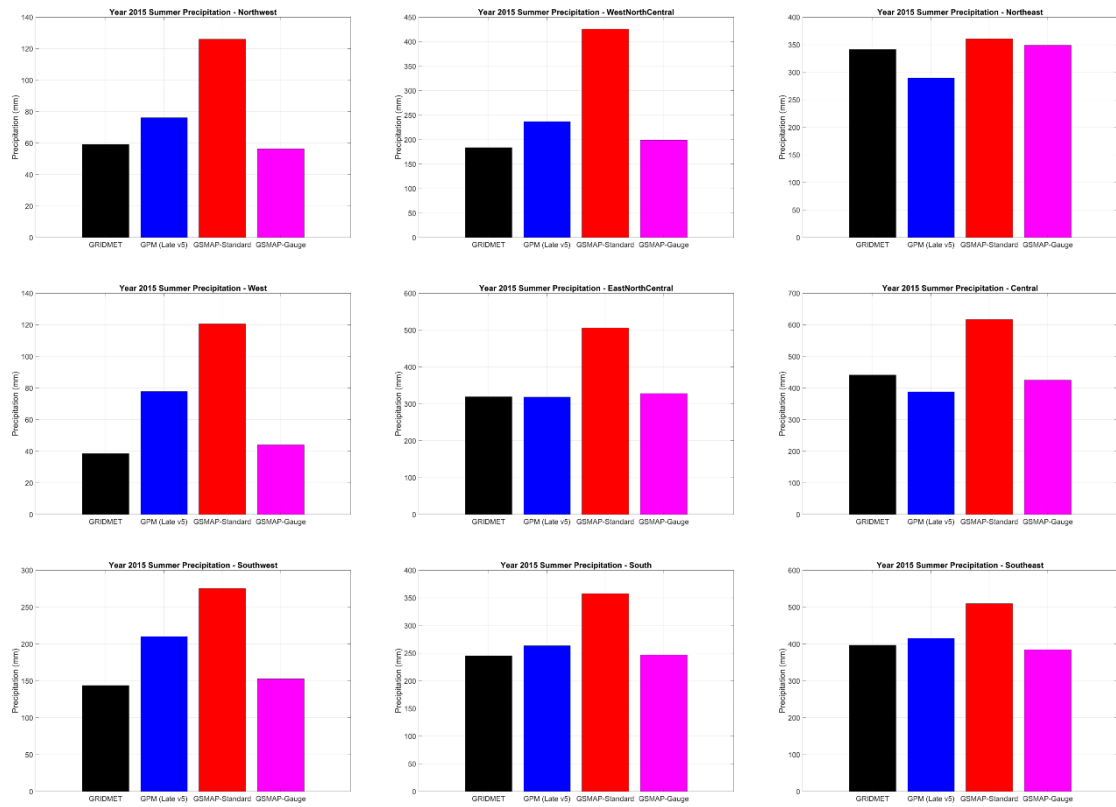


Figure 3-12: Assessment of year 2015 regional summer cumulative precipitation from GPM IMERG, GSMaP-Standard, and GSMaP-Gauge data products.

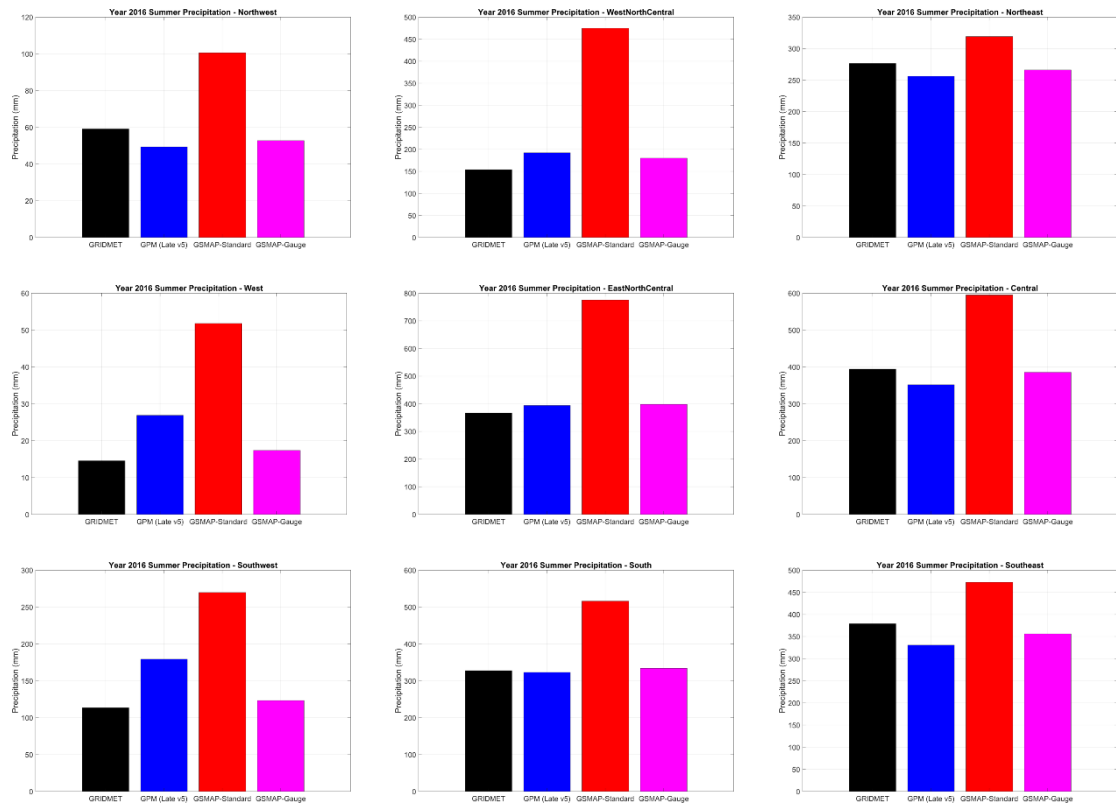


Figure 3-13: Assessment of year 2016 regional summer cumulative precipitation from GPM IMERG, GSMaP-Standard, and GSMaP-Gauge data products.

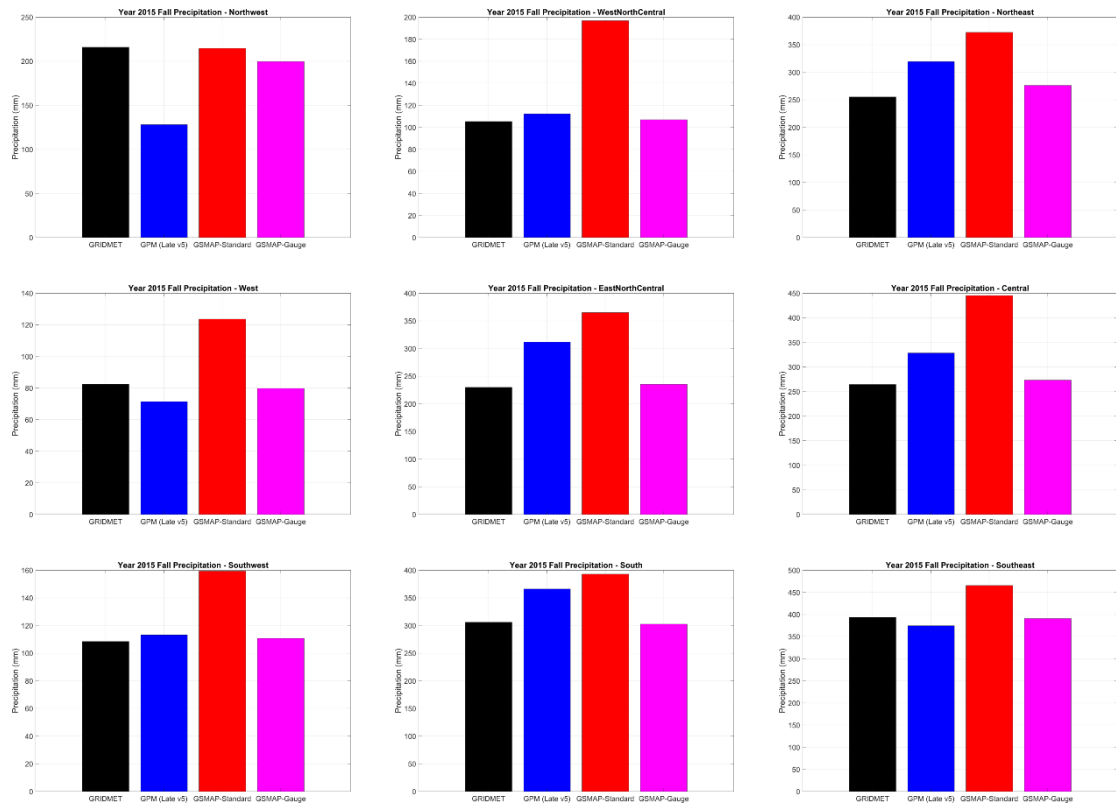


Figure 3-14: Assessment of year 2015 regional fall cumulative precipitation from GPM IMERG, GSMap-Standard, and GSMap-Gauge data products.

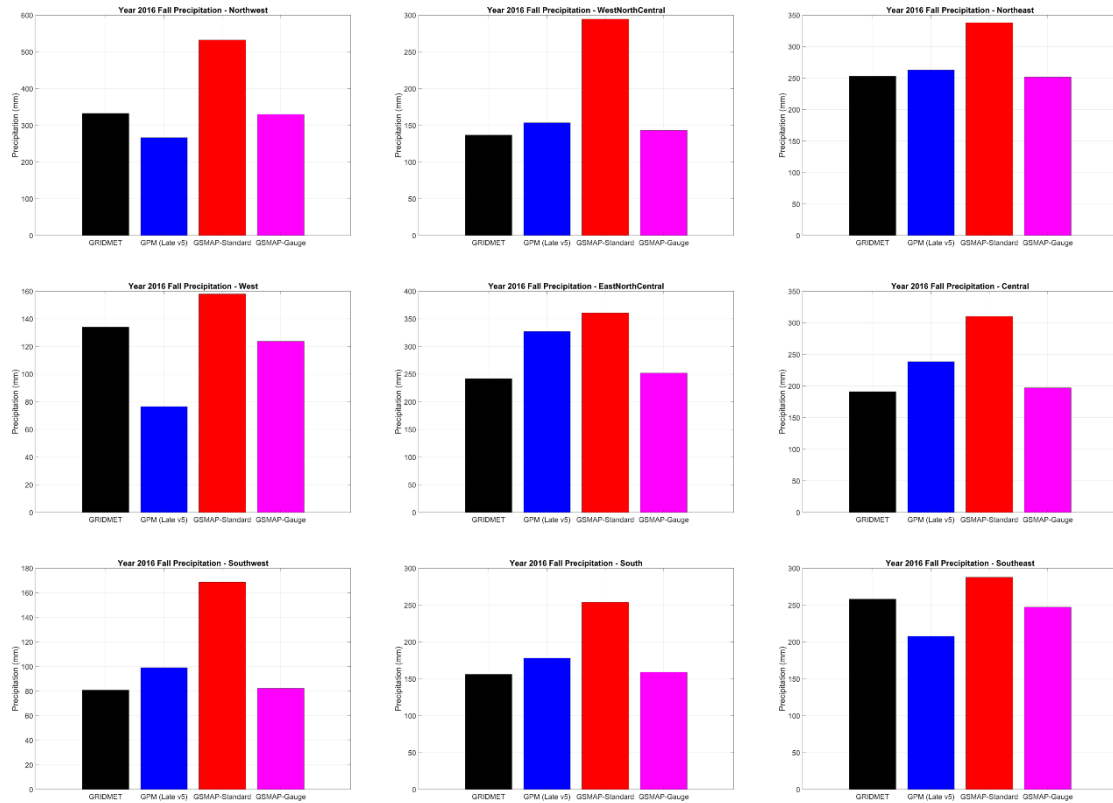


Figure 3-15: Assessment of year 2016 regional fall cumulative precipitation from GPM IMERG, GSMaP-Standard, and GSMaP-Gauge data products.

3.1.3 Assessment of Empirical Probability Density Functions of Daily Precipitation and Summary Statistics

To assess how remote sensing retrievals of precipitation fare with regard to extreme, typical, and dry events, Figure 3-16 presents the empirical probability density function (PDF) and cumulative probabilities (CDF) for daily rainfall from the GRIDMET, GPM IMERG, GSMaP-Standard and GSMaP-Gauge data products for the continental United States. The results indicate that daily precipitation events between 0 and 5 mm occur more frequently in the monitoring-network driven GRIDMET data product, than in all the remote sensing derived products. GSMaP-Gauge follows the GRIDMET closely, while the

GSMaP-Standard has a clear wet bias for non-extreme daily precipitation events. The CDF suggests that the GPM IMERG product may overestimate extreme precipitation events.

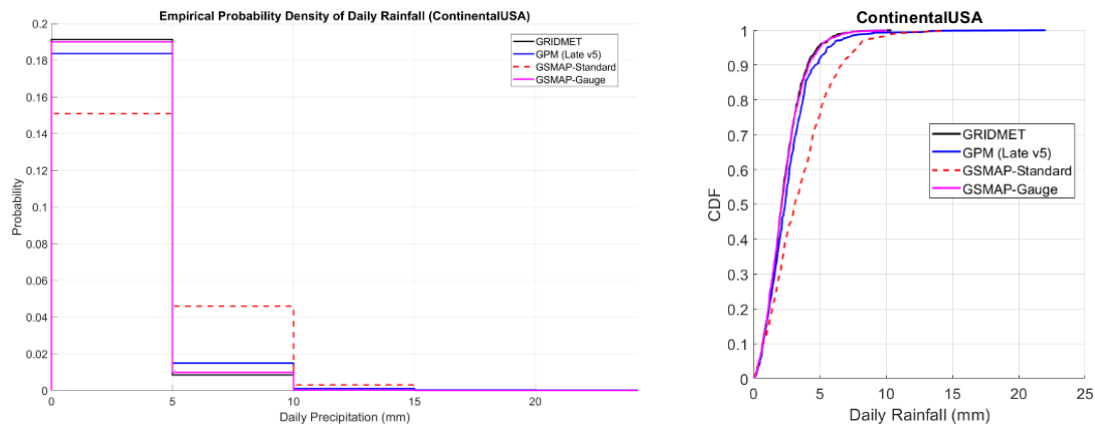


Figure 3-16: Empirical probability (PDF) and cumulative density functions (CDF) for daily precipitation over the 2015-2016 period for the continental United States

Figure 3-17 presents the seasonal empirical probability density functions and cumulative probabilities for daily precipitation. Results confirm the great wet bias in the GSMaP-Standard product. GSMaP standard also overestimates extreme precipitation events relative to the other data products in all seasons except for the winter season in which the GPM IMERG product overestimates precipitation by a greater amount than GSMaP-Standard. The GPM IMERG product appears to agree best with the GRIDMET data product for all types of daily precipitation during the summer and fall, while the GSMaP-Gauge product agrees well with GRIDMET in all seasons.

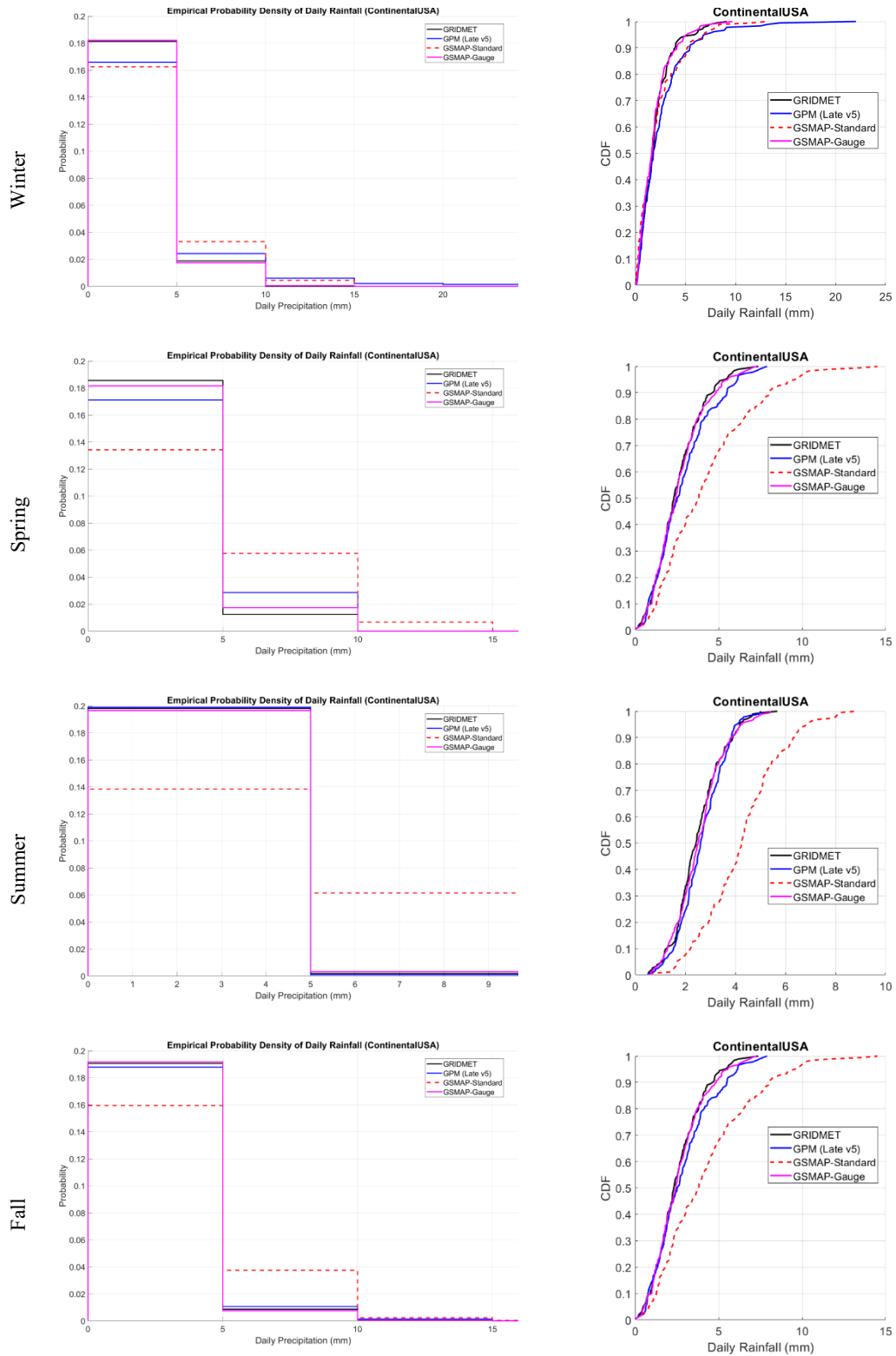


Figure 3-17: Seasonal empirical probability density functions and cumulative probabilities for daily precipitation over the 2015-2016 period for the continental United States.

Figure 3-18 and Figure 3-19 present the empirical probability density functions and cumulative probabilities for daily precipitation over the 2015-2016 period for the nine U.S. climate regions. Features that stand out from the probability densities are the for precipitation events between 0 and 5 mm, GPM IMERG and GSMaP-Standard generally overestimate precipitation with respect to the GRIDMET reference, except for GPM IMERG in the Northwest and West regions. The regional cumulative probabilities also confirm that GSMaP-Standard generally overestimates all types of precipitation (dry, typical, intense) in all climate regions, while the GPM IMERG product appears to greatly overestimate intense precipitation events in the East North Central, Central, South, and Southeast.

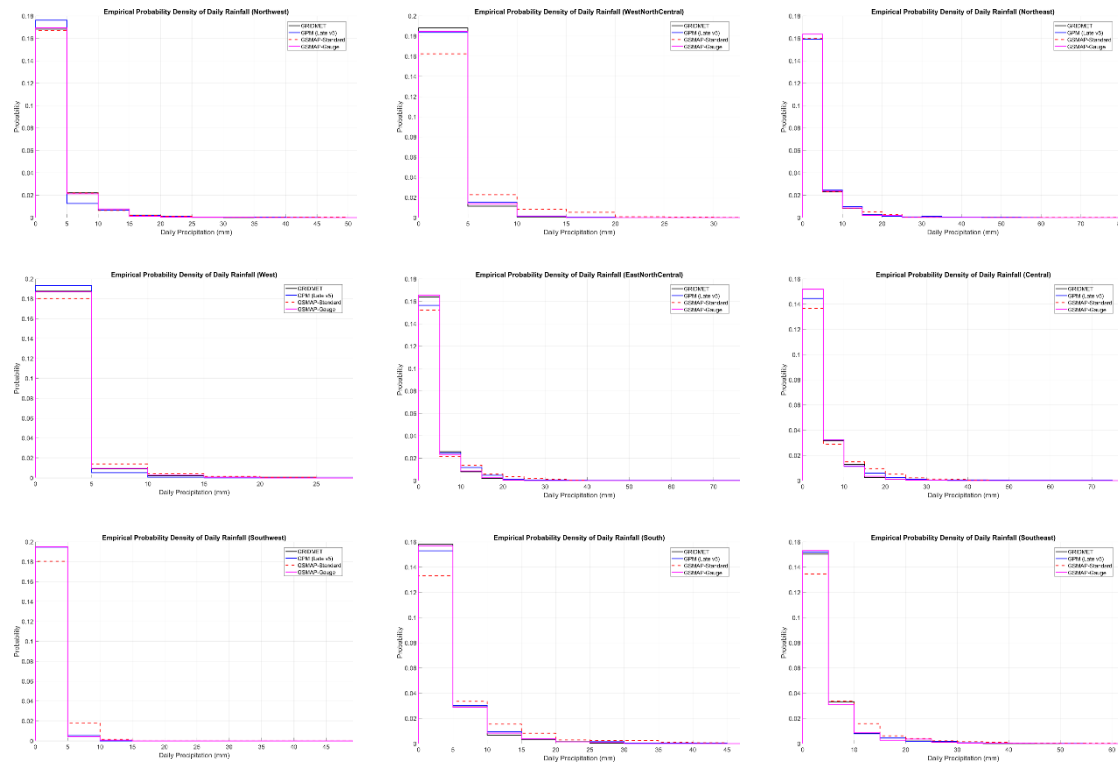


Figure 3-18: Empirical probability density functions for daily precipitation over the 2015-2016 period for nine climate regions of the continental United States.

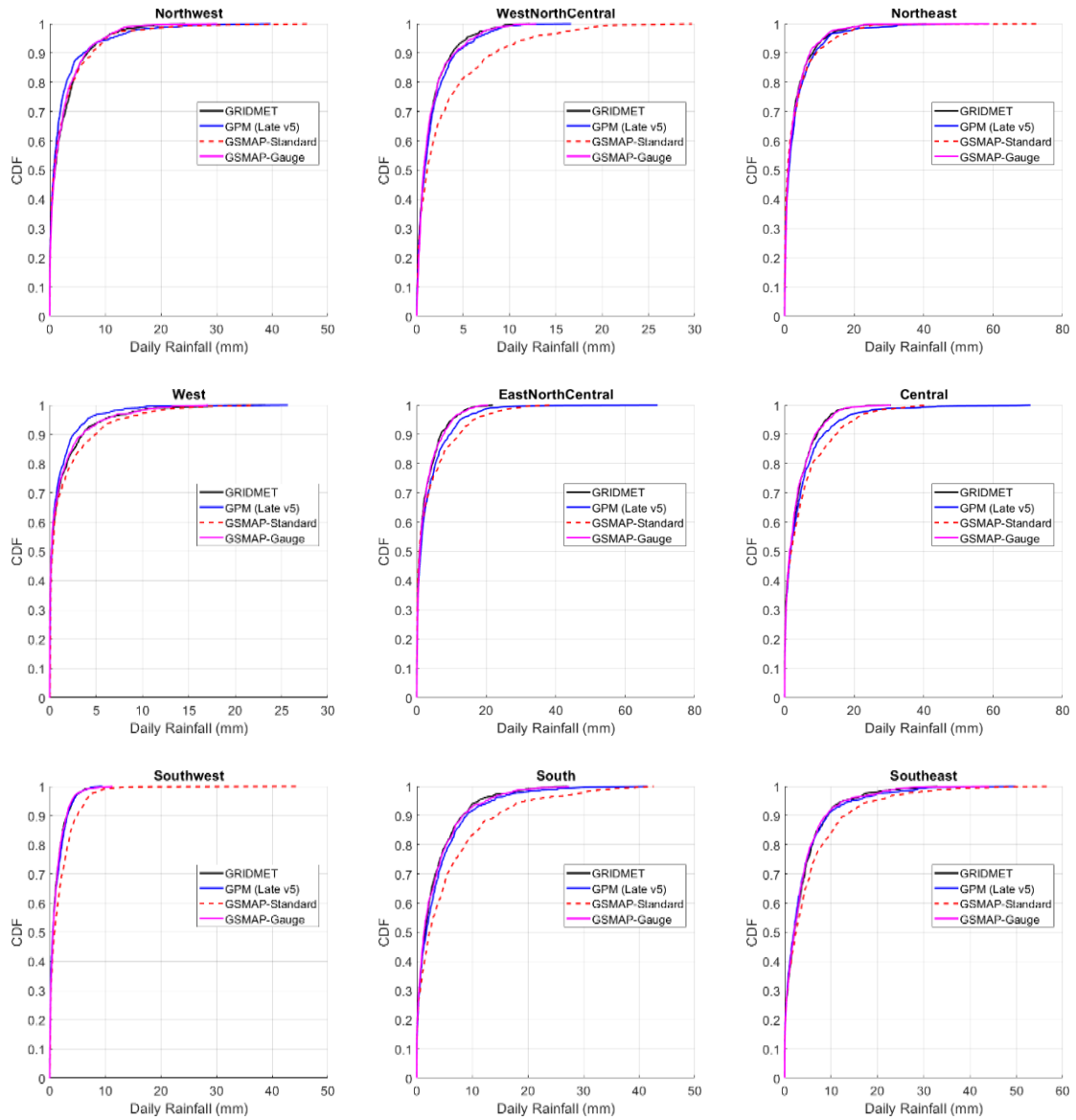



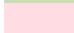


Figure 3-19: Cumulative probabilities for daily precipitation over the 2015-2016 period for nine climate regions of the continental United States.

Table 3-1 summarizes the statistical performance of the remote sensing retrievals of daily precipitation over the 2015-2016 period in comparison to the GRIDMET reference. As expected from the previous assessments in this study, GSMAp-Standard has the lowest correlation, greatest root-mean-squared-error (RMSE), and greatest mean absolute error (MAE) compared to the GPM IMERG and the GSMAp-Gauge product for all climate

regions as well as the entire continental US. The GPM IMERG product is more highly correlated with the GRIDMET reference than the other remote sensing retrievals, with correlations greater than 80 percent for most of the climate regions, suggesting that GPM IMERG captures the occurrence of rain days well (even if there is over/underestimation of the event itself). The RMSE results, which are sensitive to extreme precipitation events, highlight the GPM IMERG biases during extreme events as explored in the previous sections of this assessment.

Table 3-1: Summary performance statistics for remote sensing retrievals of daily precipitation over the 2015-2016 period.

Region Name	Mean Daily Precipitation (mm)				GRIDMET Correlation			GRIDMET RMSE (mm)			GRIDMET MAE (mm)		
	GRIDMET	GPM IMERG	GSMaP-Standard	GSMaP-Gauge	GPM IMERG	GSMaP-Standard	GSMaP-Gauge	GPM IMERG	GSMaP-Standard	GSMaP-Gauge	GPM IMERG	GSMaP-Standard	GSMaP-Gauge
Continental USA	2.33	2.62	3.51	2.34	0.83	0.73	0.80	1.10	2.04	0.90	0.62	1.51	0.61
Northwest	2.43	2.28	2.63	2.33	0.85	0.72	0.84	2.28	3.26	1.96	1.18	1.64	1.05
West North Central	1.47	1.66	2.93	1.54	0.89	0.66	0.74	1.00	3.68	1.39	0.62	1.87	0.84
Northeast	2.82	3.25	3.18	2.78	0.73	0.60	0.66	3.75	4.65	3.60	1.80	2.37	1.88
West	1.23	0.95	1.56	1.18	0.85	0.72	0.82	1.36	2.09	1.45	0.68	1.03	0.64
East North Central	2.46	3.26	3.71	2.53	0.80	0.60	0.67	3.39	5.03	2.88	1.59	2.52	1.67
Central	3.29	4.31	4.92	3.29	0.77	0.68	0.74	4.73	5.39	3.06	2.08	2.95	1.81
Southwest	1.14	1.18	1.85	1.15	0.79	0.66	0.80	0.95	2.21	0.92	0.59	1.06	0.52
South	3.05	3.54	5.20	3.12	0.91	0.73	0.81	2.20	5.52	2.64	1.20	2.99	1.51
Southeast	3.69	3.81	5.02	3.65	0.77	0.68	0.72	3.62	5.45	3.67	1.61	2.82	1.87
Difference in comparison to GRIDMET reference Highlight Legend  > +10% (Wet Bias)  < -10% (Dry Bias)					Metric Performance  Best  Worst								

3.2 Bias assessment of remote sensing precipitation and surface soil moisture with respect to in-situ measurements

As presented in Chapter 2, Chan et al. (2018) listed biases in SMAP L3 Enhanced surface soil moisture products during the April 2015 to October 2016 time period as assessed at SMAP core validation sites. Expanding on this assessment, the following exercise quantifies bias in remote sensing (i.e. GPM IMERG, GSMaP-Standard, and GSMaP-Gauge) and reanalysis (i.e. GRIDMET) retrievals of daily precipitation with respect to a single rain-gauge in the vicinity of select SMAP core validation sites. Table 3-2 lists select SMAP core validation sites along with a neighboring rain gauge from the Global Historical Climatology Network (GHCN) data source made publicly available by the NOAA National Climatic Data Center (NCDC) (Menne et al. 2012). For each GHCN site, the daily precipitation time series from the GRIDMET, NASA GPM IMERG (Version 5 Late Release), JAXA GSMaP-Standard (Version 7), and JAXA GSMaP-Gauge (Version 7) data products spanning April 1, 2015 to October 31, 2016 are retrieved from a 0.1° by 0.1° bounding box centered at the GHCN gauge location.

Table 3-2: Locations of select SMAP core validation sites and neighboring GHCN rain gauges

SMAP Core Validation Sites		GHCN Rain-Gauge Sites		
Site Name	Latitude, Longitude	Site Name	Latitude, Longitude	Distance from SMAP CVS (km)
South Fork, Iowa USA	42.42, -93.41	Iowa Falls, Iowa USA	42.52, -93.25	17
Little River, Georgia USA	31.67, -83.60	Fitzgerald, Georgia USA	31.77, -83.26	34
Fort Cobb, Oklahoma USA	35.38, -98.64	Colony, Oklahoma USA	35.35, -98.67	4
Kenaston, Canada	51.47, -106.48	Loreburn, Canada	51.25, -106.54	25
Monte Buey, Argentina	-32.91, -62.51	Marcos Juarez, Argentina	-32.68, -62.16	41
REMEDIHUS, Spain	41.29, -5.46	Salamanca Aeropuerto, Spain	40.96, -5.50	37
Twente, Netherlands	52.26, 6.77	Hengelo, Netherlands	52.27, 6.77	1
Yanco, Australia	-34.86, 146.16	Coleambally Irrigation, Australia	-34.80, 145.89	26

Table 3-3 presents the biases in the remote sensing and reanalysis precipitation retrievals along with the biases in SMAP L3 Enhanced surface soil moisture retrievals as reported by Chan et al. 2018. As expected, GRIDMET (available only for the U.S.) generally agreed well with the rain gauge data, while the GPM IMERG, GSMaP-Standard, and GSMaP-Gauge products exhibited wet bias at the majority of assessed sites. Wet biases were especially large in the GSMaP-Standard product, and these biases were mitigated substationally in the GSMaP-Gauge product. A major finding from this exercise is that biases in SMAP surface soil moisture retrievals are not necessarily consistent with biases in remote sensing precipitation retrievals. That is, if SMAP surface soil moisture estimates are drier or wetter than the true soil surface soil moisture state, it cannot be assumed that

the corresponding precipitation retrievals will likewise be drier or wetter than the true precipitation.

Table 3-3: Biases in SMAP L3 Enhanced surface soil moisture retrievals paired with percent biases in neighboring daily precipitation retrievals from GRIDMET, GPM, GSMaP-Standard, and GSMaP-Gauge for the April 2015 to October 2016 period.

SMAP Core Validation Sites Analysis (Chan et al 2018)		Precipitation Percent Biases (Neighboring GHCN Rain Gauge)				
SMAP CVS Site Name	SMAP Bias (m³/m³)	GHCN Site Name	GRIDMET (%)	GPM (%)	GSMaP-Standard (%)	GSMaP-Gauge (%)
South Fork	− 0.062	Iowa Falls	− 2.88	28.66	50.13	1.19
Little River	0.087	Fitzgerald	− 1.73	− 1.64	22.17	− 7.35
Fort Cobb	− 0.056	Colony	− 8.63	22.31	129.52	8.18
Kenaston	− 0.040	Loreburn	-	−0.63	30.30	− 8.34
Monte Buey	− 0.020	Marcos Juarez	-	− 32.05	23.28	− 11.89
REMEDIHUS	− 0.007	Salamanca	-	72.18	100.80	21.11
Twente	0.013	Hengelo	-	31.62	13.13	0.98
Yanco	0.020	Coleambally	-	27.27	130.47	6.62

3.3 Correlation of errors in remote sensing retrievals of precipitation and remote sensing retrievals of surface soil moisture

In the previous section, the quality of daily aggregated GPM IMERG (Version 5, Late Release), JAXA GSMaP-Standard (Version 7) and JAXA-GSMaP-Gauge (Version 7) were assessed over the continental U.S. in relation to daily gridded precipitation from the GRIDMET data set. Analysis revealed region-specific errors and biases in remote sensing

retrievals of precipitation. Such errors may adversely impact the accuracy of agricultural models' prediction of crop yield, crop stress, and irrigation demand as well as the accuracy of hydrological streamflow predictions. In this section, a remote-sensing driven remedial strategy for improving the accuracy of daily remote sensing retrievals of precipitation is explored. It is of interest to assess whether errors in remote sensing retrievals of precipitation (in relation to the GRIDMET reference) are correlated with remote sensing retrievals of surface soil moisture from the SMAP mission. The question is asked: can we predict – and therefore remove – errors in remote sensing daily precipitation data, given information of surface soil moisture state? For the nine climate regions of the continental U.S., the correlation between errors in remote sensing daily precipitation data and surface soil moisture from the SMAP Level 3 Enhanced data product is assessed.

Figure 3-20 presents the correlation between errors (in relation to the GRIDMET precipitation reference) in regional daily mean precipitation estimates from the GPM IMERG (Version 5, Late Release) data product and mean regional surface soil moisture estimates from the SMAP Enhanced Level 3 (6AM retrieval) over the continental U.S. during year 2016. For the continental U.S. as a whole, as well as for the nine climate regions, correlations are centered about zero, suggesting that errors in GPM IMERG precipitation data are independent of and cannot be predicted by retrievals of regional mean surface soil moisture state. Similar conclusions can be made regarding the GSMaP-Gauge data product (i.e. surface soil moisture state does not inform what the error in precipitation retrieval would be) as shown by Figure 3-21. The lack of correlation between errors in remote sensing retrievals of daily precipitation and SMAP surface soil moisture estimates persists regardless of season. Figure 3-22 illustrates this lack of correlation for each season

during the 2015-2016 period as evaluated over the continental U.S., and similar results (i.e. no correlation between errors in remote sensing precipitation retrievals and SMAP surface soil moisture estimates) were obtained for each climate region of U.S. These findings suggest that the errors in the remote sensing precipitation data may be random rather than systematic (at least in relation to surface soil moisture state and dynamics) and thusly cannot be remedied by information of surface soil moisture alone. Further research should investigate other avenues for improving the accuracy of the remote sensing precipitation retrievals. At least for the continental U.S., the best data set for incorporating remote sensing precipitation data into agricultural and hydrological models would arguably be the GSMP-Gauge data set. However, due to the relatively large errors in the GSMP-Standard data set as assessed in the previous sections, the preferability of GSMP-Gauge is attributed primarily to the availability of a large network of rain-gauges in the region to locally calibrate the remote sensing retrievals, and not to the gauge-free retrieval algorithm itself. Thusly, it can be assumed that the GSMP-Gauge product may not be suitably accurate for use over gauge-scarce regions (e.g. many parts of the water-sensitive and data-scarce developing world).

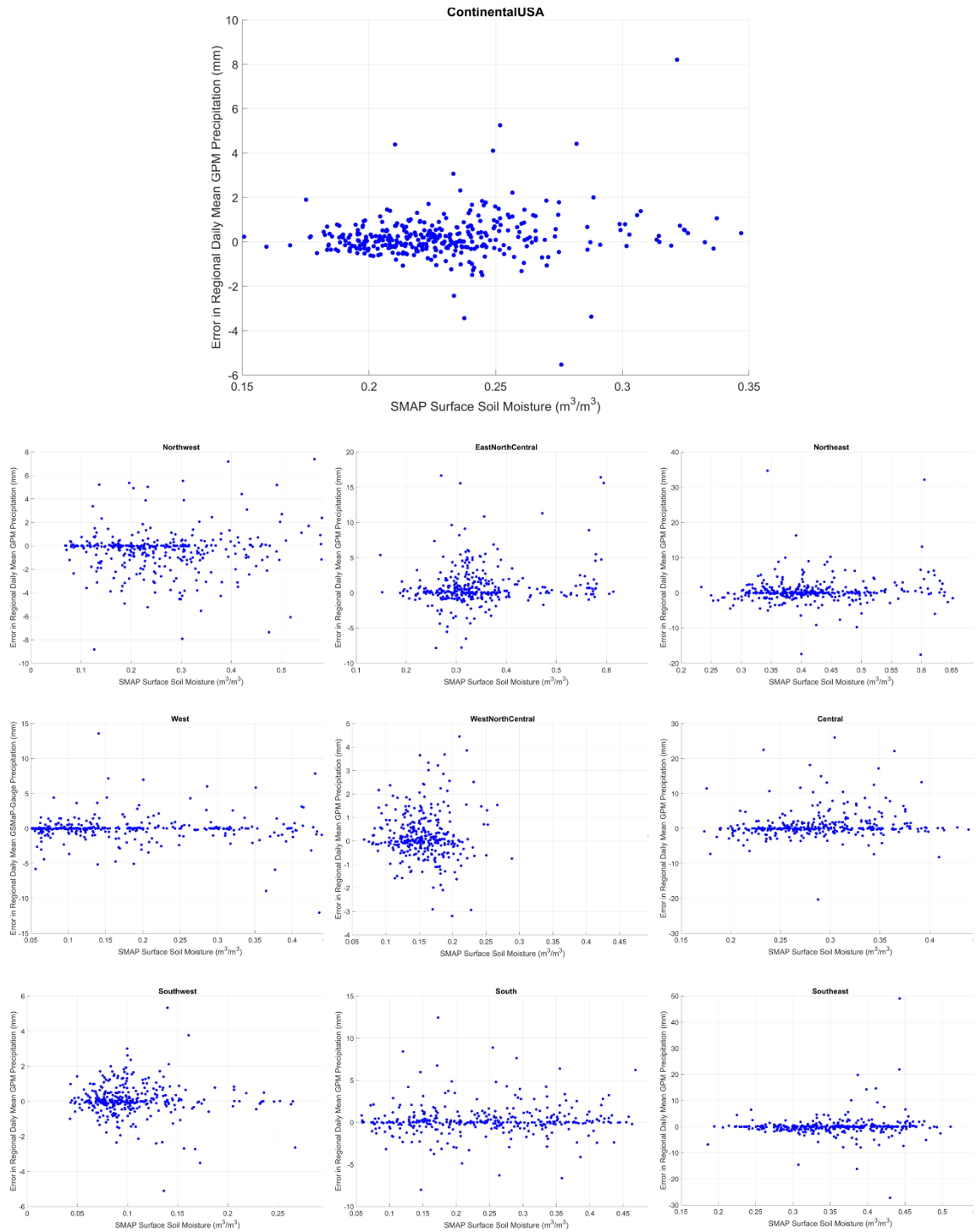


Figure 3-20: Correlation between errors in retrievals of regional mean daily precipitation from GPM IMERG (Version 5, Late Release) and SMAP Enhanced Level 3 regional mean surface soil moisture estimates for year 2016.

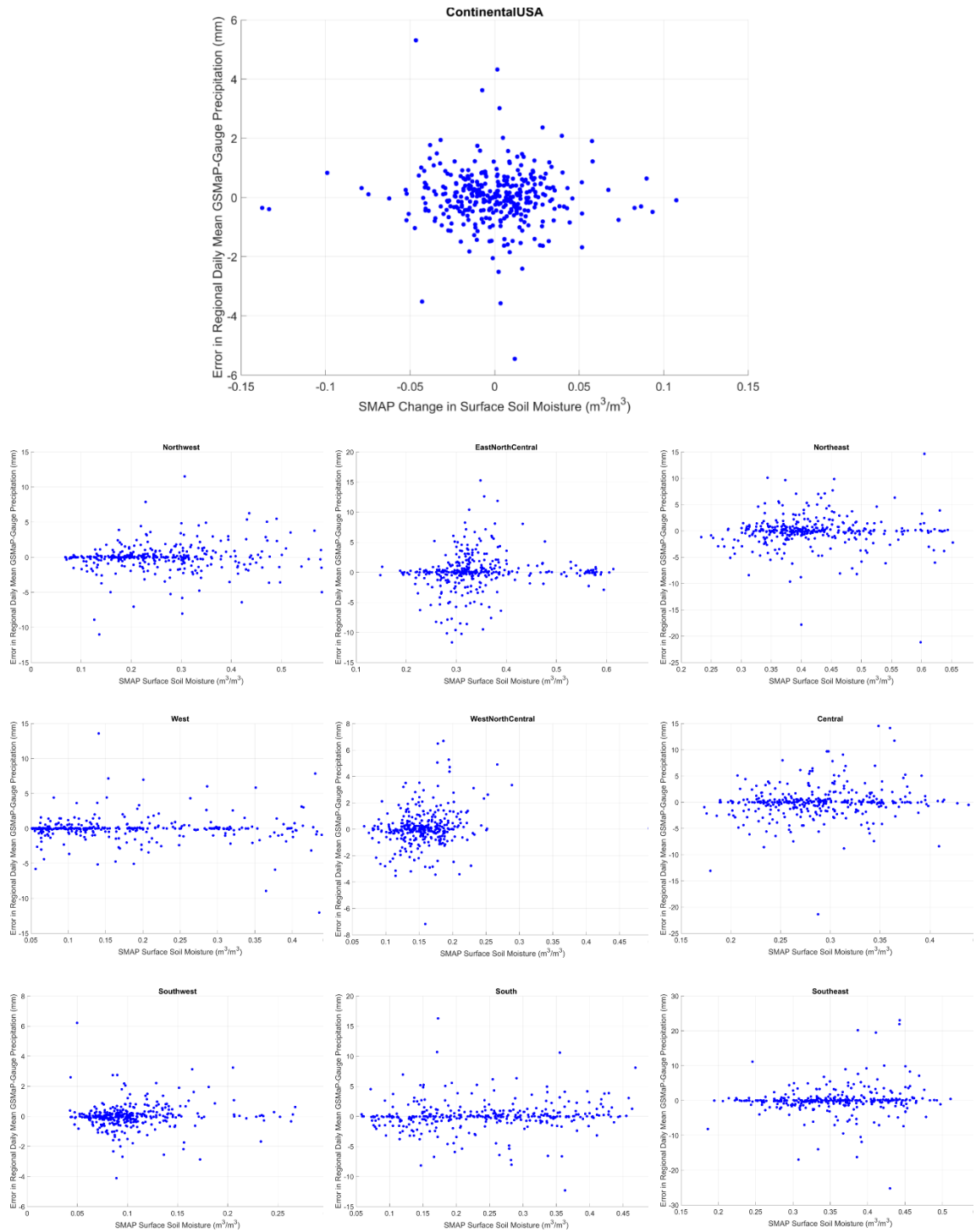


Figure 3-21: Correlation between errors in retrievals of regional mean daily precipitation from GSMap-Gauge (Version 7) and SMAP Enhanced Level 3 regional mean surface soil moisture estimates for year 2016.

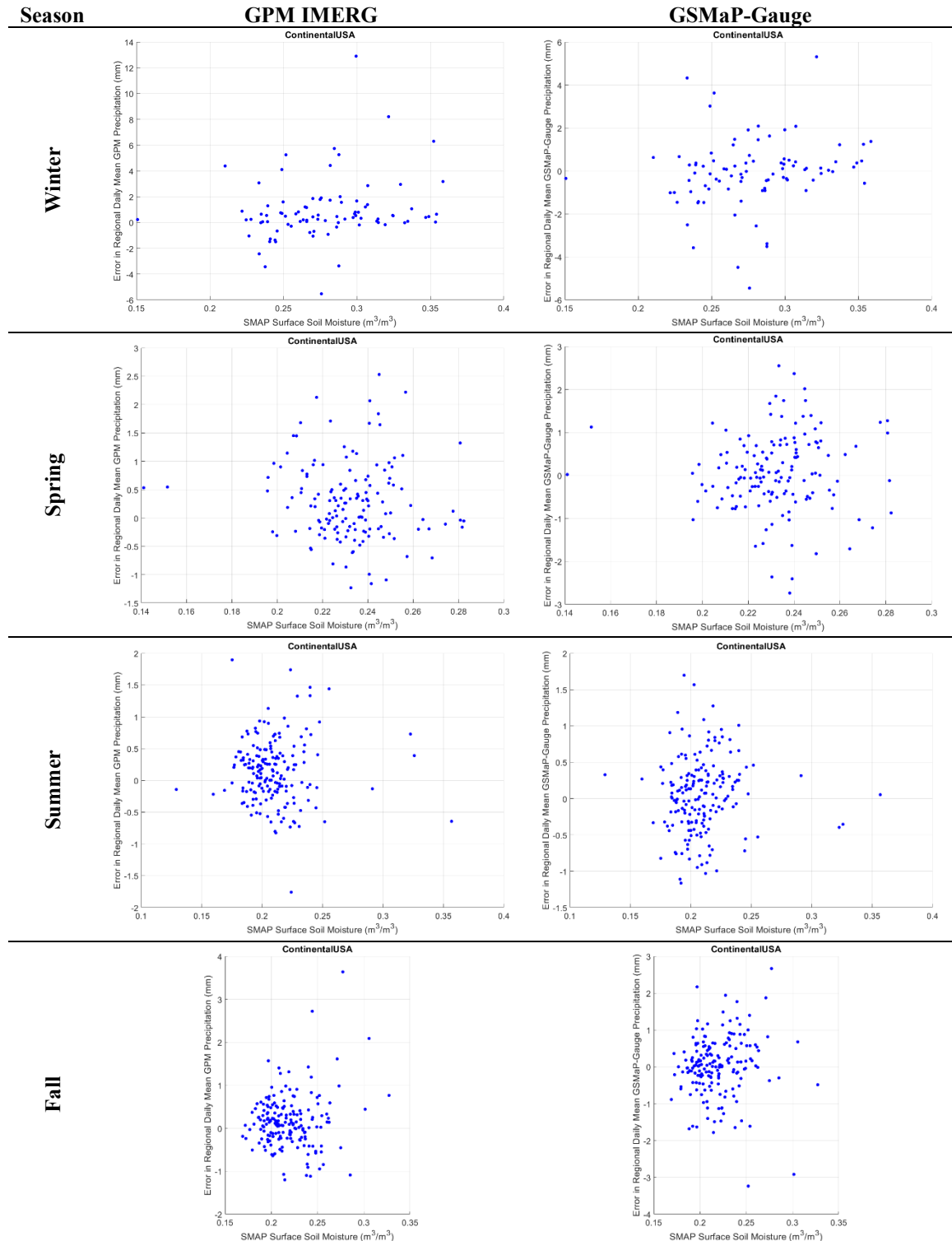


Figure 3-22: Correlation between errors in retrievals of regional mean daily precipitation from GPM IMERG (Version 5 Late Release), GSMaP-Gauge (Version 7), and SMAP Enhanced Level 3 regional mean surface soil moisture estimates for each season during the 2015-2016 period.

Figure 3-23 presents the correlation between retrievals of regional mean daily precipitation from GPM IMERG (Version 5, Late Release) and one-day change (i.e. how much the regional surface soil moisture changes one day after the day of interest) in SMAP Enhanced Level 3 regional mean surface soil moisture estimates during year 2016. Figure 3-24 presents the same figure except that GSMap-Gauge is assessed instead of GPM IMERG. Results suggest that the errors in remote sensing retrievals of regional daily precipitation are not strongly correlated with whether the surface soil moisture is getting wetter or drier.

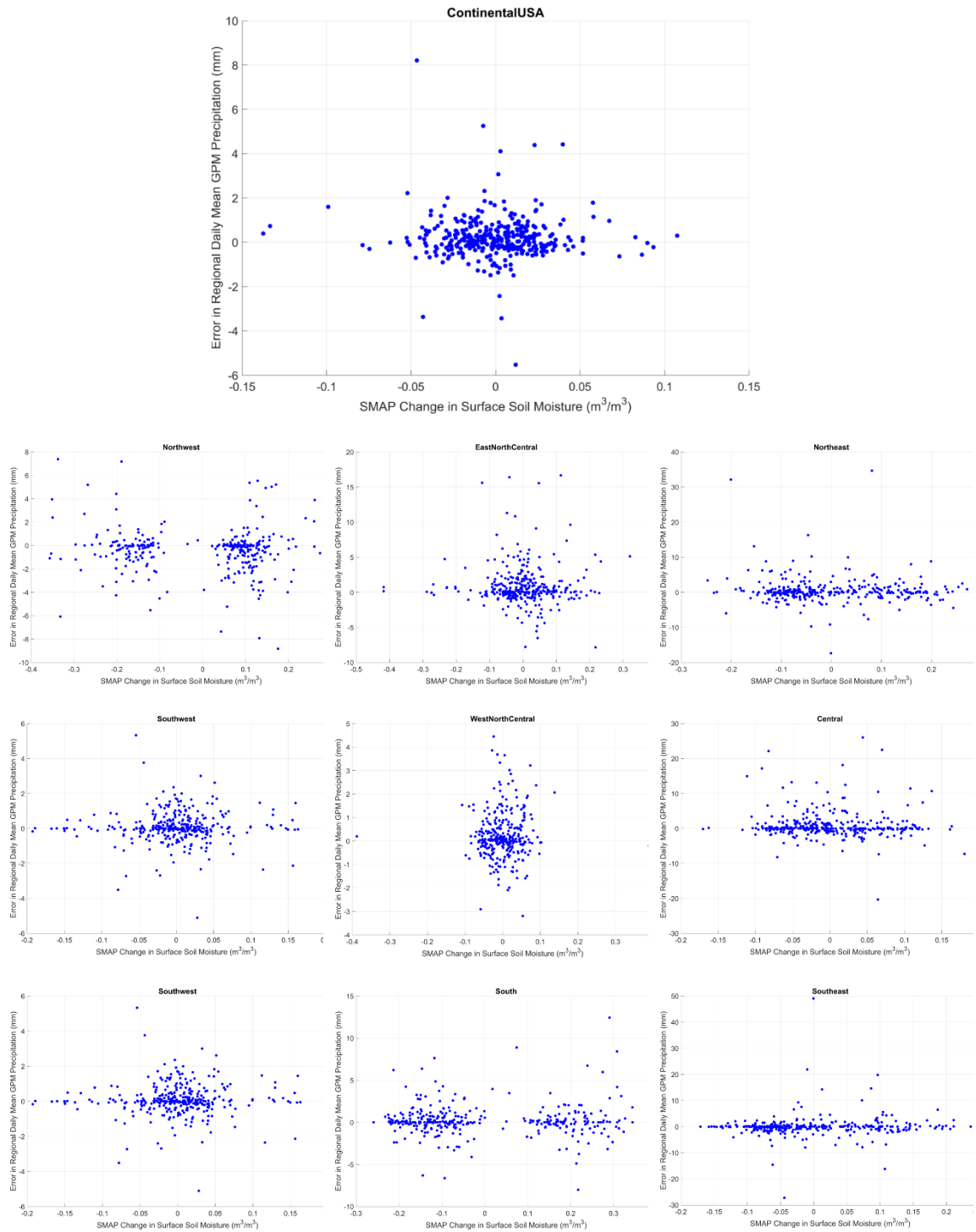


Figure 3-23: Correlation between errors in retrievals of regional mean daily precipitation from GPM IMERG (Version 5, Late Release) and one-day change in SMAP Enhanced Level 3 regional mean surface soil moisture estimates during year 2016.

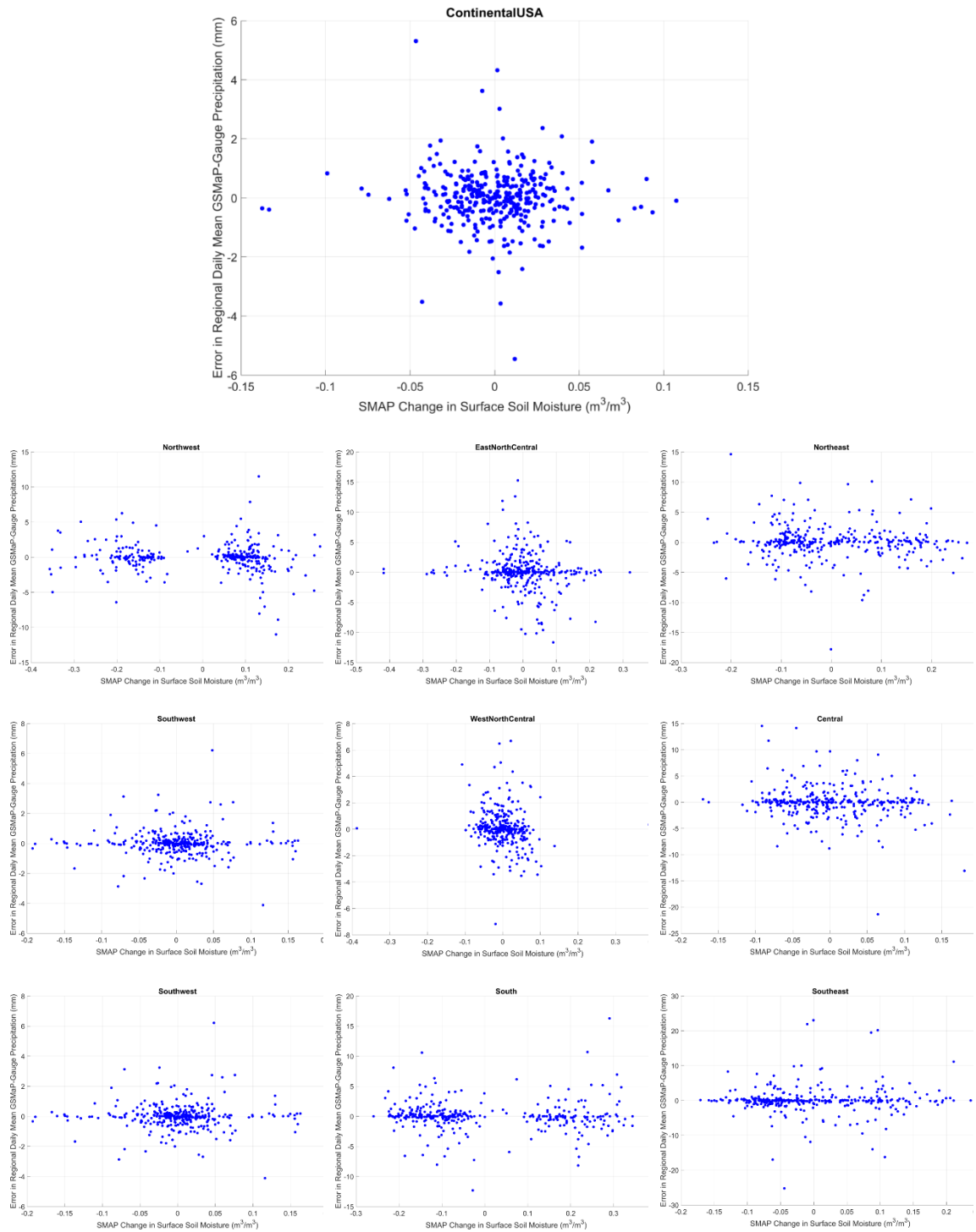


Figure 3-24: Correlation between errors in retrievals of regional mean daily precipitation from GSMap-Gauge (Version 7) and one-day change in SMAP Enhanced Level 3 regional mean surface soil moisture estimates during year 2016.

3.4 Spatial correlation in errors in GPM IMERG and GSMaP-Gauge precipitation products

This exercise takes a preliminary look at the spatial correlations in errors of remote sensing daily precipitation retrievals with respect to the GRIDMET reference. For a sample transect divided into 15 adjacent subregions, the time series of errors in GPM IMERG and GSMaP-Gauge is calculated. Then the correlation between these time series of errors between the 15 subregions is assessed and presented as a function of geographic distance (in degrees of latitude) between subregions. This analysis is carried out for the entire 2015-2016 period, as well as seasonally within years 2015-2016.

Figure 3-25 maps the 15 sub-regions for which spatial correlation of errors in remote sensing retrievals of daily precipitation are assessed. The full transect lies in the southeastern United States and spans 0.2 degrees longitude and 3.0 degrees latitude (approximately 18 km by 334 km). For each of the 15 sub-regions the daily precipitation time series from Jan 1, 2015 to December 31, 2016 is calculated from the GRIDMET, GPM IMERG version 5 Late Release, and GSMaP-Gauge Version 7 data sets. Errors in the remote sensing retrievals are calculated with respect to the GRIDMET precipitation time series. The Pearson correlation coefficient is then calculated between the time series of errors for each of the 15 sub-regions.

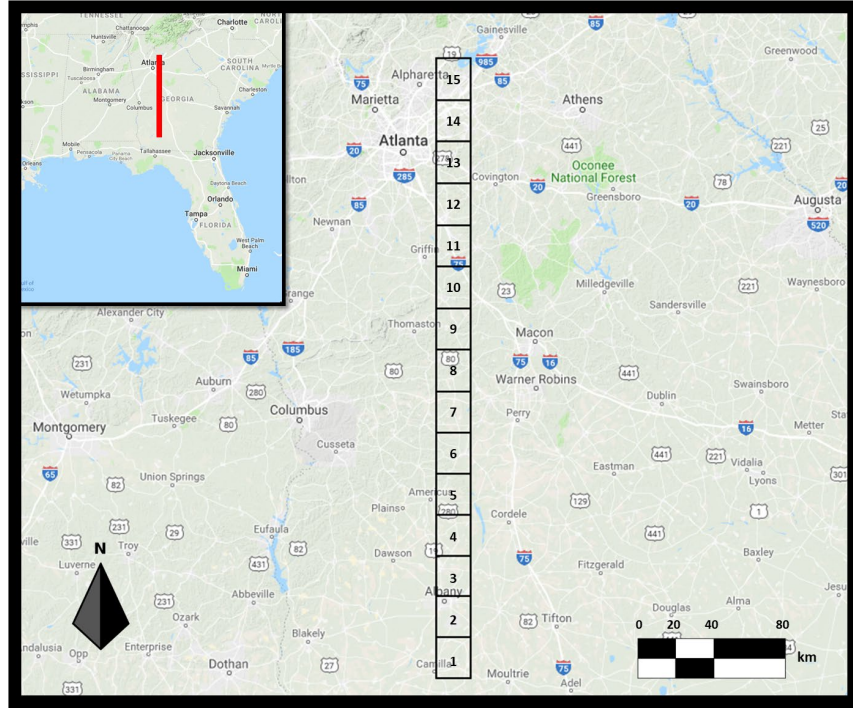


Figure 3-25: 15 sub-regions within a sample transect in the southeastern United States for assessment of spatial correlations in errors of remote sensing retrievals of daily precipitation.

Figure 3-26 plots the spatial correlation of errors in daily precipitation retrievals from GPM IMERG and GSMaP-Gauge data products during the year 2015-2016 period for regions 1 and 8 which are representative of all the 15 regions. Results show the daily precipitation errors in GPM IMERG and GSMaP-Gauge are highly correlated in space up to a distance of 2 degrees latitude (over 200 km), beyond which the correlations are below 30 – 40 percent amongst the 15 sub-regions assessed in this exercise. This finding suggests that it may be possible to implement error mitigation strategies over a large area (e.g. 2 degrees by 2 degrees region); however, it appears unlikely that SMAP surface soil moisture retrievals would be helpful in this effort, as SMAP retrievals were not correlated with precipitation retrievals, and that assessment was conducted for regions much larger than 2 degrees by 2 degrees.

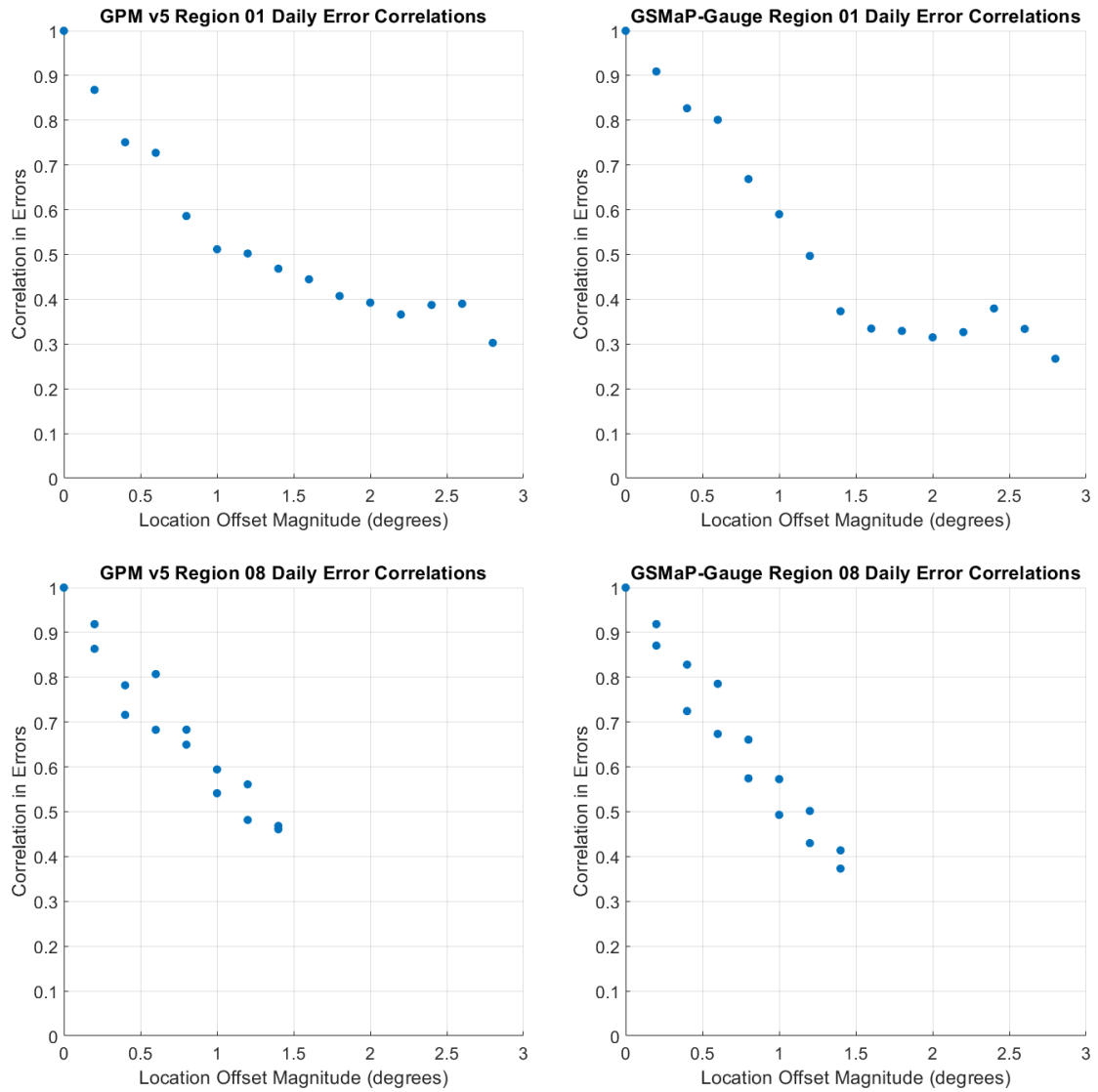


Figure 3-26: Spatial correlations of remote sensing precipitation errors as a function of latitude distance for regions 1 and 8 during the year 2015-2016 period.

Figure 3-27 plots the spatial correlation of errors in region 1 daily precipitation retrievals from GPM IMERG and GSMaP-Gauge data products during each season of the year 2015-2016 period. Results show that the spatial correlation in daily precipitation errors is strongly connected to season. Spatial correlation in errors are strongest during the winter periods, with fall having the next strongest correlations. The strength of correlation drops off most rapidly during the summer and is also relatively weak during springtime beyond the 1.0 degree latitude distance. Precipitation in this region of the U.S. is characterized by frontal systems during the winter and convective systems in the summer; consequently, results suggest that spatial correlations in precipitation retrieval errors are connected to precipitation type, with errors from frontal storms being the most spatially correlated and those from convective storms being the least spatially correlated.

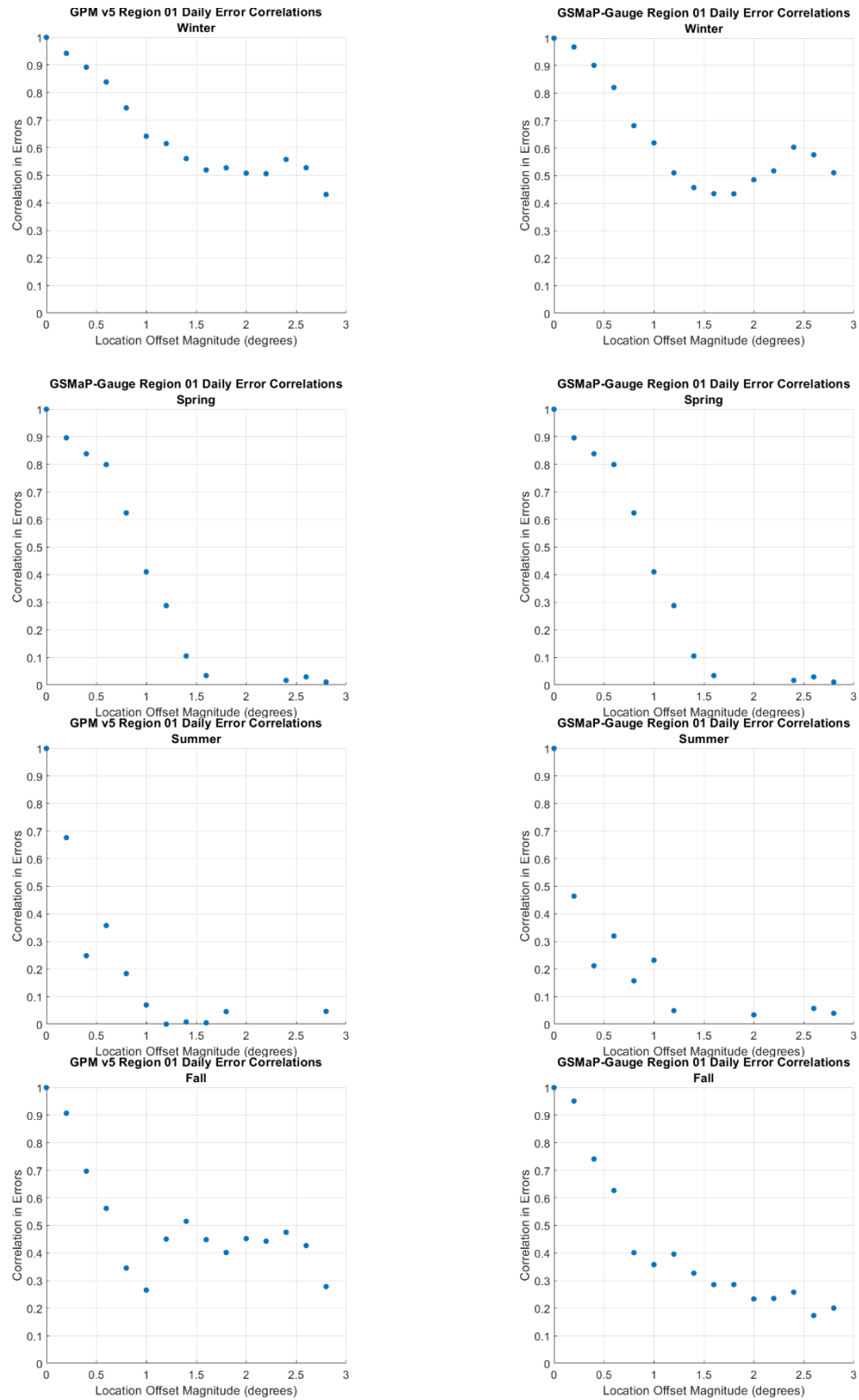


Figure 3-27: Spatial correlations of remote sensing precipitation errors as a function of latitude distance and season for region 1 during the year 2015-2016 period.

3.5 Impact of spatial averaging of high-resolution gridded meteorological and soil data on DSSAT crop model output

Crop systems models, such as DSSAT-CSM, were originally developed to model crop growth and development at the single plot/field scale. For regional scale simulations, crop models often ingest gridded data of meteorological forcings and soil profile characteristics. The spatial resolution of these products may adversely impact the accuracy of such models originally designed for point-scale applications. In this study, the sensitivity of the DSSAT-CSM modeled regional-scale mean crop yield and irrigation demand to coarsening spatial resolution – from 1km to 40km – of soil characteristics and meteorological forcing data is assessed. Year 2005 to 2016 rainfed and irrigated corn is simulated for various U.S. regions with diverse climates. Modeling 12 years worth of regional mean crop yield and irrigation demand also allows for assessing the influence of relatively dry, wet, and normal (with regard to precipitation) growing seasons on this exercise.

First, for each region of interest, a 200km by 200km domain is defined and divided into 25 40km by 40km grid cells as shown in Figure 3-28. Each of the 40km grid cells is comprised of 1,600 1km grid cells, 100 4km grid cells, and 16 10km grid cells.

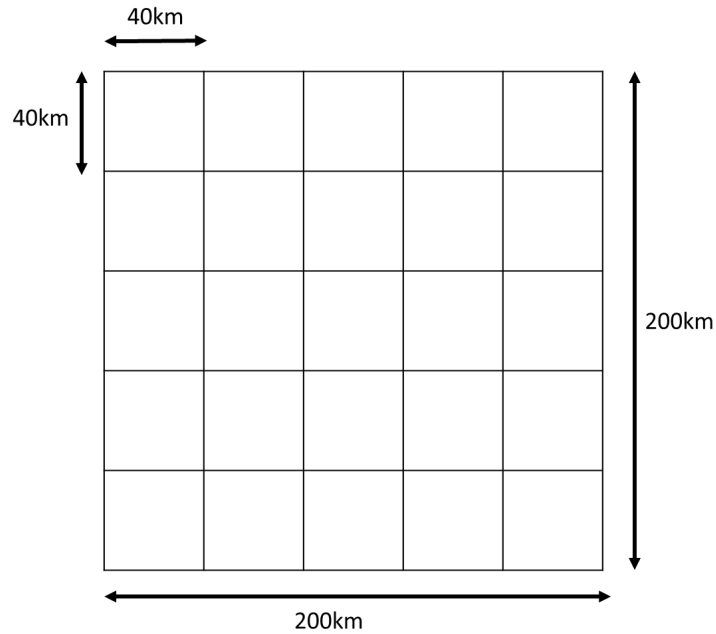


Figure 3-28: Schematic of domain for DSSAT simulations driven by multi-scale weather and soil data products

Next, corn crop yield and irrigation demand are modeled by running DSSAT at a single, randomly selected 1km grid cell within each of the 25 sub-domains. In these simulations, DSSAT is forced by 1km gridded data of daily incoming solar radiation, maximum and minimum air temperature, and precipitation from the DAYMET reanalysis data set, and soil data derived from pedo-transfer functions applied to the 1km Soilsgrid data set (Hengl et al. 2014; Han et al. 2015). The mean of these 25 simulations (one simulation per 40km sub-domain) represent crop yield and irrigation demand within the regional domain using 1km gridded data. This procedure is repeated at the 4km, 10km, and 40km spatial scales after aggregating DAYMET meteorological data and Soilgrids derived soil properties to those scales. As an example, Figure 3-29 illustrates the random selection of 10km grid cells for running DSSAT forced by 10km weather and soil data.

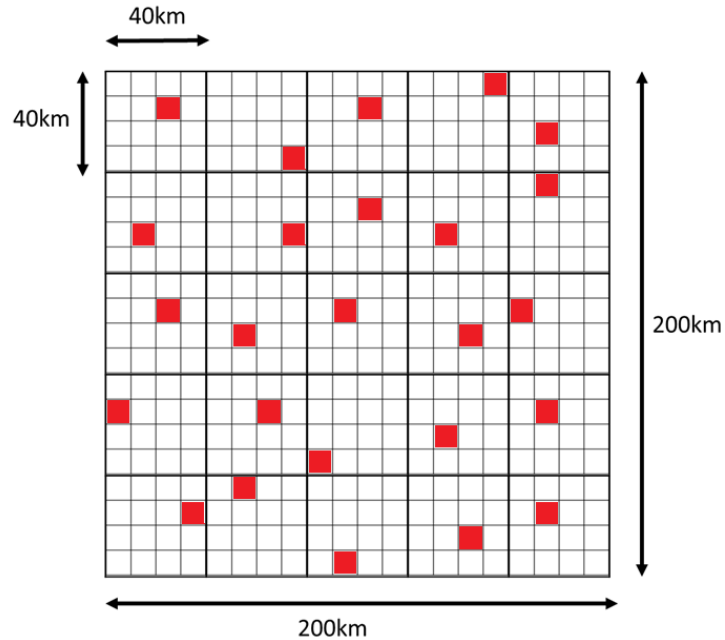


Figure 3-29: Schematic of domain for DSSAT simulations driven by 10km weather and soil data products. One 10km grid cell (red) is randomly selected in each of the 25 40km by 40km subdomains.

For each spatial scale, the sample means (and its standard error) of modeled crop yield and irrigation demand (constructed from 25 values at each spatial scale) are compared across spatial scales to detect at what level(s) of spatial coarsening do modeled regional mean yield and regional mean irrigation demand differ greatly from the simulations drive by the finest resolution 1 km input data. Table 3-4 lists important DSSAT-CSM input parameters for the corn simulations.

Table 3-4: Input parameters for DSSAT-CSM year 2005-2016 maize simulations

Region	Region Centroid (Lat, Lon)	Maize Cultivar	Planting Date (Years 2015 & 2016)	Row Spacing	Plant Population	Irrigation: Soil Management Depth	Irrigation: Available soil water content threshold
Southeast	32.13, -84.03	Jackson Hybrid	March 29 th	30 inches (76 cm)	30,000 plants/acre (7.9 pl/m ²)	12 inches (30 cm)	50%
West	36.43, -120.18	PB 8	April 8 th				70%
South	35.23, -101.62		March 15 th				50%
Midwest	41.86, -95.45		April 26 th			Not Applicable (Rainfed only)	

Figure 3-32 through Figure 3-35 compare the regional-scale means of rainfed and irrigated corn yield and irrigation amount for the case study locations. The figures also indicate the characterization of the growing season based on the 2005-2016 rainfed crop production simulated using 1 km input data. Years with rainfed crop yield below the 25th percentile are “Low Production”, between 25th and 75th percentiles are “Normal Production”, and above the 75th percentile are “High Production”. For the case study region in the west, for which only irrigated corn yield was simulated, years are characterized according to irrigation demand. Years with irrigation demand crop yield above the 75th percentile are “High Irrigation Demand”, between 25th and 75th percentiles are “Normal Irrigation Demand”, and below the 25th percentile are “Low Irrigation Demand”. Due to difficulty of resolving soil characteristics in the west region at the 40km scale, only 1km, 4km, and 10km simulations are performed for this region.

With regard to rainfed and irrigated crop yields, the means are generally consistent across spatial scales regardless if the growing season is dry, wet, or normal. However, mean crop yields simulated using 40km data can be slightly higher than those simulated using 1km data. This bias can be attributed to the impact of the spatial averaging of daily precipitation data over large areas. Averaging over large areas captures isolated precipitation events and redistributes them over the averaging domain. This bias reduces the length of dry spells and artificially boosts simulated crop yields. This same bias is also

responsible for the reduced mean irrigation amount at the 40km spatial scale compared to the simulations forced by finer resolution input data. Figure 3-30 compares year 2005-2016 Daymet daily precipitation at 1km and 40km spatial aggregation scales with the subplots each representing a 40km x 40km domain for different U.S. climate regions. The results at each climate region show that when the 1km precipitation data product reports zero precipitation, the corresponding 40km precipitation data product can report substantial precipitation, sometimes over 10 mm. The effect of this bias is explored in more detail in Figure 3-31 that presents summarized crop production metrics for year 2007 DSSAT simulated rainfed corn in the midwest case study region using 1km and 40km soil and meteorological input data. In this example, the simulation using 40km input data has 50.4 mm less precipitation during the growing season, but crop yield 720 kg/ha greater than the simulation using 1km input data. This seemingly counter-intuitive discrepancy is explained by the lesser water stress and the greater number of rain days in the 40km simulation relative to the 1km simulation.

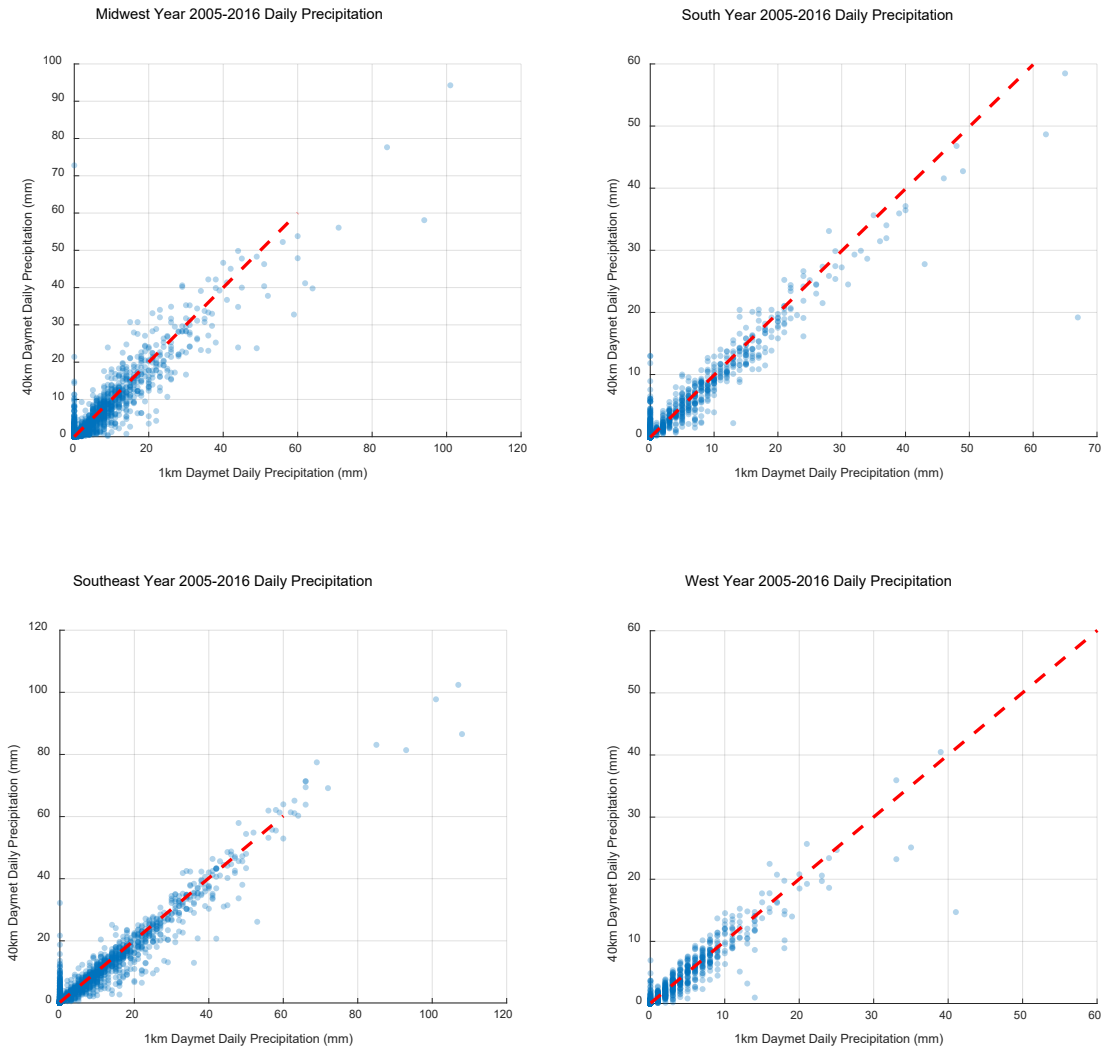


Figure 3-30: Comparison of year 2005-2016 Daymet daily precipitation at 1km and 40km spatial aggregation scales. The subplots each represent a 40km x 40km domain for different U.S. climate regions.

(a) Year 2007 DSSAT Corn Simulation: 1km input data

*ENVIRONMENTAL AND STRESS FACTORS																								
Development Phase					Environment										Stress (0=Min, 1=Max Stress)									
	Time Span days	Temp Max °C	Temp Min °C	Temp Mean °C	Solar Rad MJ/m2	Photop [day] hr	CO2 ppm	Rain mm	Evapo Trans mm	Pot ET mm	TMIN °C	TMIN °C	TMAX °C	TMAX °C	TMAX °C	RAIN mm	Water synth	Nitrogen synth	Phosphorus synth	Photo synth	Growth	Growth	Growth	Growth
Emergence-End Juvenile	26	24.8	11.9	18.3	19.8	14.42	383.3	125.0	77.4	123.5	0	0	2	0	0	8	0.000	0.000	0.000	0.000	0.000	0.000	0.000	0.000
End Juvenil-Floral Init	6	24.1	13.9	19.0	17.4	14.89	383.3	27.0	22.4	23.9	0	0	0	0	0	3	0.000	0.000	0.000	0.000	0.000	0.000	0.000	0.000
Floral Init-End Lf Grow	41	29.4	15.6	22.5	23.1	15.05	383.4	27.0	211.9	216.5	0	0	18	5	1	3	0.003	0.030	0.000	0.000	0.000	0.000	0.000	0.000
End Lf Grth-Beg Grn Fil	10	31.1	18.0	24.6	20.3	14.72	383.6	31.0	38.5	47.6	0	0	7	2	2	1	0.187	0.258	0.000	0.000	0.000	0.000	0.000	0.000
Grain Filling Phase	56	27.7	15.8	21.7	16.7	13.42	383.8	303.0	205.9	208.9	0	1	16	1	0	17	0.008	0.021	0.000	0.000	0.000	0.000	0.000	0.000
Planting to Harvest	150	27.5	14.6	21.1	19.5	14.16	383.5	538.0	587.5	672.2	0	1	45	9	3	34	0.016	0.033	0.000	0.000	0.000	0.000	0.000	0.000
*Resource Productivity																								
Growing season length: 150 days																								
Precipitation during growing season				538.0 mm[rain]																				
Dry Matter Productivity				4.13 kg[DM]/m3[rain]																				
Yield Productivity				1.27 kg[grain yield]/m3[rain]																				
Evapotranspiration during growing season				587.5 mm[ET]																				
Dry Matter Productivity				3.78 kg[DM]/m3[ET]																				
Yield Productivity				1.16 kg[grain yield]/m3[ET]																				
Transpiration during growing season				464.3 mm[EP]																				
Dry Matter Productivity				4.78 kg[DM]/m3[EP]																				
Yield Productivity				1.47 kg[grain yield]/m3[EP]																				
					Maize YIELD :		6840 kg/ha		[Dry weight]															

(b) Year 2007 DSSAT Corn Simulation: 40km input data

*ENVIRONMENTAL AND STRESS FACTORS																								
-----Development Phase-----					-----Environment-----										-----Stress-----									
					-----Average-----					-----Cumulative-----					-----Count of days-----					-----((0=Min, 1=Max Stress))-----				
Time Span days	Temp Max °C	Temp Min °C	Temp Mean °C	Solar Rad MJ/m2	Photop [day] hr	CO2 ppm	Rain mm	Evapo Trans mm	Pot ET mm	TMIN °C	TMIN °C	TMAX °C	TMAX °C	TMAX °C	RAIN mm	Water synth	Growth	Nitrogen synth	Growth	Phosphorus synth	Growth			
Emergence-End Juvenile	26	25.0	11.9	18.4	20.2	14.41	383.3	97.5	74.3	126.0	0	0	2	1	0	9	0.000	0.000	0.000	0.000	0.000			
End Juvenil-Floral Init	6	23.9	13.8	18.9	17.1	14.89	383.3	37.8	22.0	23.3	0	0	0	0	0	5	0.000	0.000	0.000	0.000	0.000			
Floral Init-End Lf Grow	41	29.6	15.7	22.6	23.2	15.05	383.4	34.0	214.9	217.5	0	0	20	8	2	6	0.000	0.011	0.000	0.000	0.000			
End Lf Grth-Beg Grn Fil	10	31.4	18.3	24.9	20.0	14.71	383.6	27.9	44.7	47.2	0	0	8	3	2	1	0.049	0.128	0.000	0.000	0.000			
Grain Filling Phase	55	27.8	15.9	21.9	16.9	13.44	383.8	268.6	205.4	207.2	0	1	24	4	0	25	0.003	0.016	0.000	0.000	0.000			
Planting to Harvest	149	27.7	14.8	21.3	19.6	14.18	383.5	487.6	592.6	672.7	0	1	56	17	4	49	0.004	0.018	0.000	0.000	0.000			
*Resource Productivity																								
Growing season length: 149 days																								
Precipitation during growing season				487.6 mm[rain]																				
Dry Matter Productivity				4.88 kg[DM]/m3[rain]				=				48.8 kg[DM]/ha per mm[rain]												
Yield Productivity				1.55 kg[grain yield]/m3[rain]				=				15.5 kg[yield]/ha per mm[rain]												
Evapotranspiration during growing season				592.6 mm[ET]																				
Dry Matter Productivity				4.02 kg[DM]/m3[ET]				=				40.2 kg[DM]/ha per mm[ET]												
Yield Productivity				1.28 kg[grain yield]/m3[ET]				=				12.8 kg[yield]/ha per mm[ET]												
Transpiration during growing season				474.1 mm[EP]																				
Dry Matter Productivity				5.02 kg[DM]/m3[EP]				=				50.2 kg[DM]/ha per mm[EP]												
Yield Productivity				1.59 kg[grain yield]/m3[EP]				=				15.9 kg[yield]/ha per mm[EP]												
Maize YIELD :				7560 kg/ha [Dry weight]																				

Figure 3-31: DSSAT summarized crop production metrics for year 2007 simulated rainfed corn using (a) 1km and (b) 40km soil and meteorological input data. Midwest case study region.

The behavior of simulated mean corn yields and irrigation demands with coarsening resolution of input data, shown in Figure 3-32 through Figure 3-35 can be explained in most cases by the change of the medians and minimums of growing season precipitation as a result of spatial aggregation of gridded precipitation data (as shown in Figure 3-36).

This finding suggests that the quantities of interest in this analysis (region mean crop yield and irrigation demand) are more sensitive to the spatial averaging of daily precipitation data over the spatial aggregation scale of other meteorological variables and soil input data. To understand the influence of the spatial averaging of soil data, this exercise was repeated except that soil data was always kept at 10km resolution (and meteorological data was allowed to vary from 1km to 40km). The regional scale mean crop yields and irrigation demands were largely indistinguishable compared to what is presented in figures below, suggesting that 10km soil data is sufficient for regional scale crop modeling applications. These are general comments from the simulation results across the tested regions, what follows are summarized observations for each case study region:

Southeast: Any spatial resolution data (from 1km to 40km) can be used for modeling regional mean rainfed production, except for low production (e.g. drought) years, during which the use of 40km input data results in overestimation of crop yield by over 10 percent compared to simulations driven by 1km data. During years with normal or high production (e.g. years with moderate or relatively wet growing seasons), the use of 40km input data results in underestimation of irrigation demand on the order of 10 percent relative to simulations driven by 1km data.

West: For this region, 4km and 10km input data resulted in mean irrigated crop yields that were overestimated and mean irrigation demand that were underestimated relative to using 1km input data; however, these errors were less than 5 percent. Simulations using 40km data were problematic (and thusly not shown) due to the difficulty of resolving soil characteristics at the 40km scale.

South: Comments regarding this region are similar to the other case study regions, except that during high production years there appears to be a drop in the mean of rainfed and irrigated crop yields relative to the 1km simulations when using either 4km and 10km input data. This unexpected finding is attributed to outlier temperature and spatial sampling effects during specific years that were characterized as “high production”. For a few simulations within this region, the random sampling procedure within each 40km subdomain selected pixels containing growing season frost spells that terminated crop production. These frost spells only occurred in simulations driven by the 4km and 10km data, resulting in lower mean values for crop yield, but no such pixels were selected for the 1km and 40km simulations.

Midwest: During low production, normal production, and high production years, any spatial resolution data (from 1km to 40km) can be used for modeling regional mean rainfed crop yield. Input data coarser than 1km do result in higher yields, due to the bias introduced by spatial averaging of precipitation data, but this bias does not exceed 5 percent.

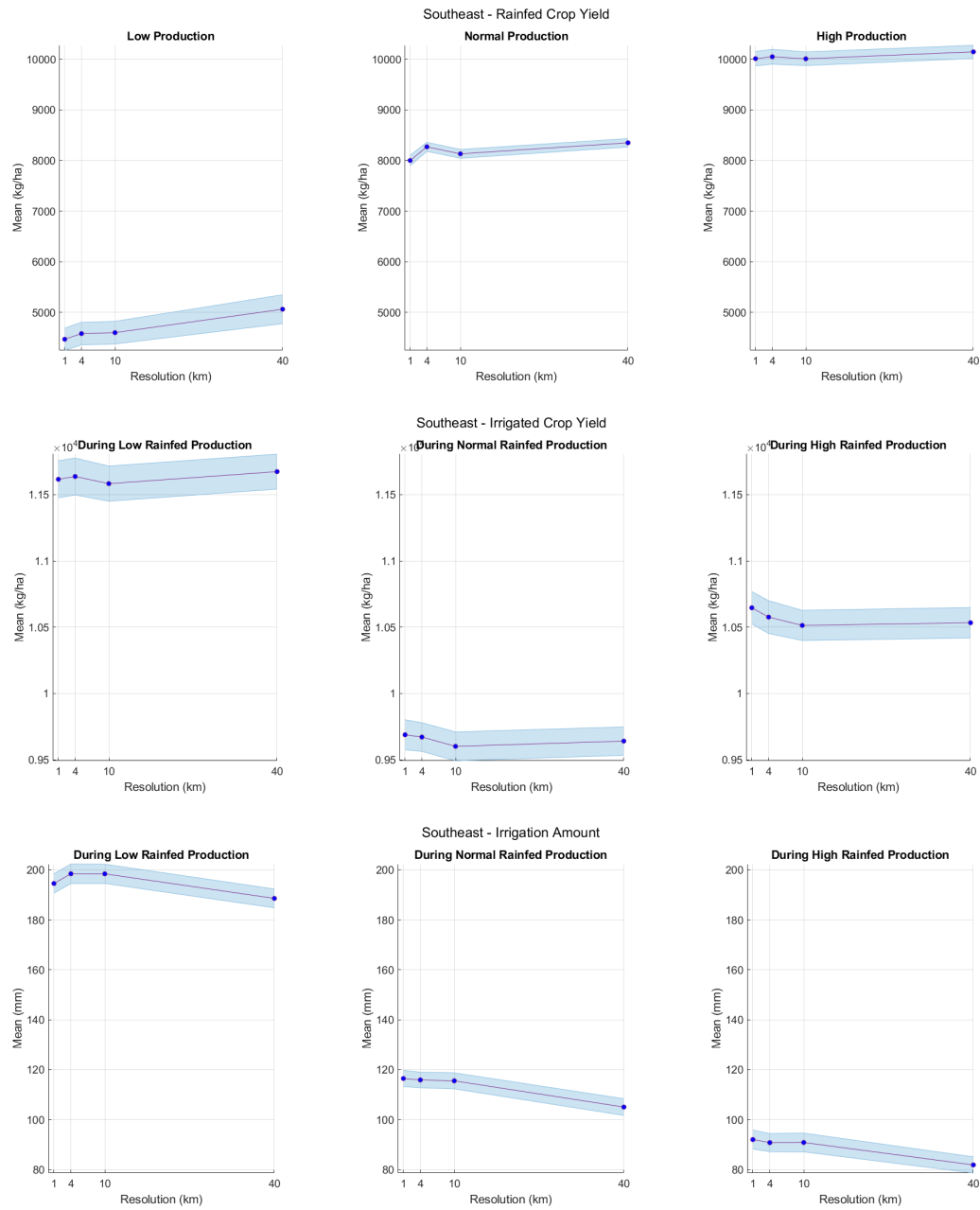


Figure 3-32: Comparison of mean rainfed corn yield, irrigated corn yield, and corn irrigation amount with meteorological forcing and soil input data with spatial resolutions ranging from 1km to 40km. The standard error of the mean is indicated by the shaded region. Southeast case study region.

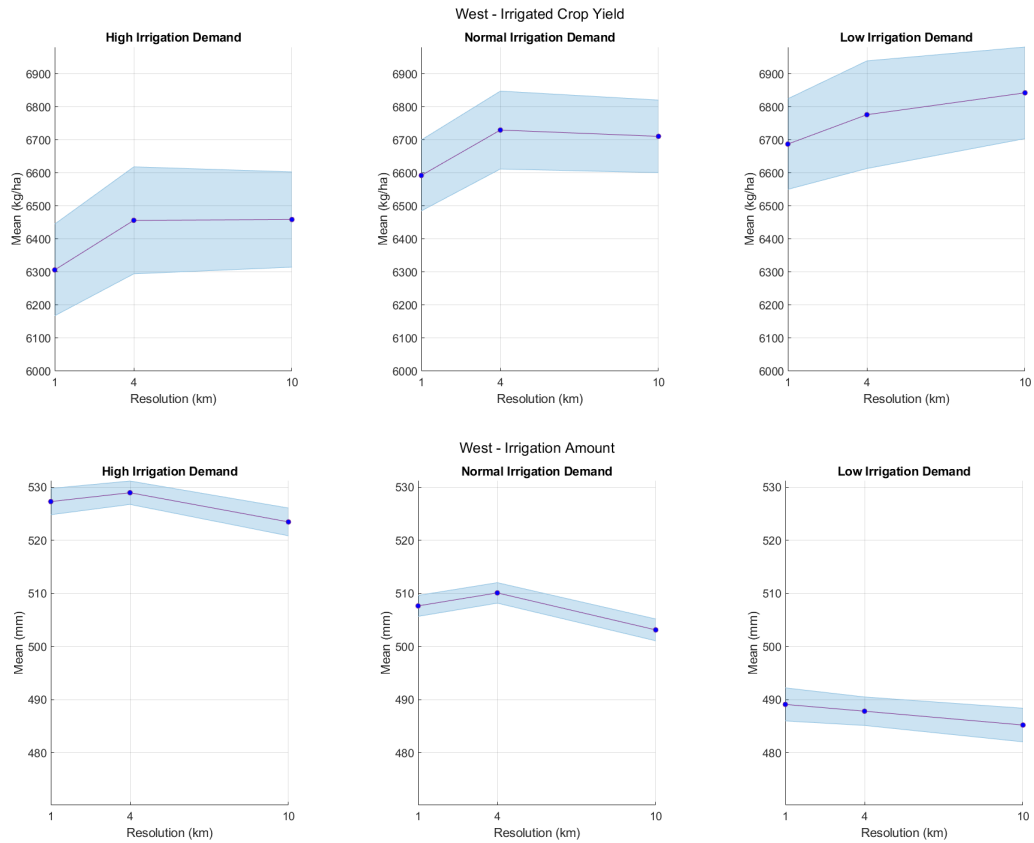


Figure 3-33: Comparison of mean of irrigated corn yield and corn irrigation amount with meteorological forcing and soil input data with spatial resolutions ranging from 1km to 10km. The standard error of the mean is indicated by the shaded region. West case study region.

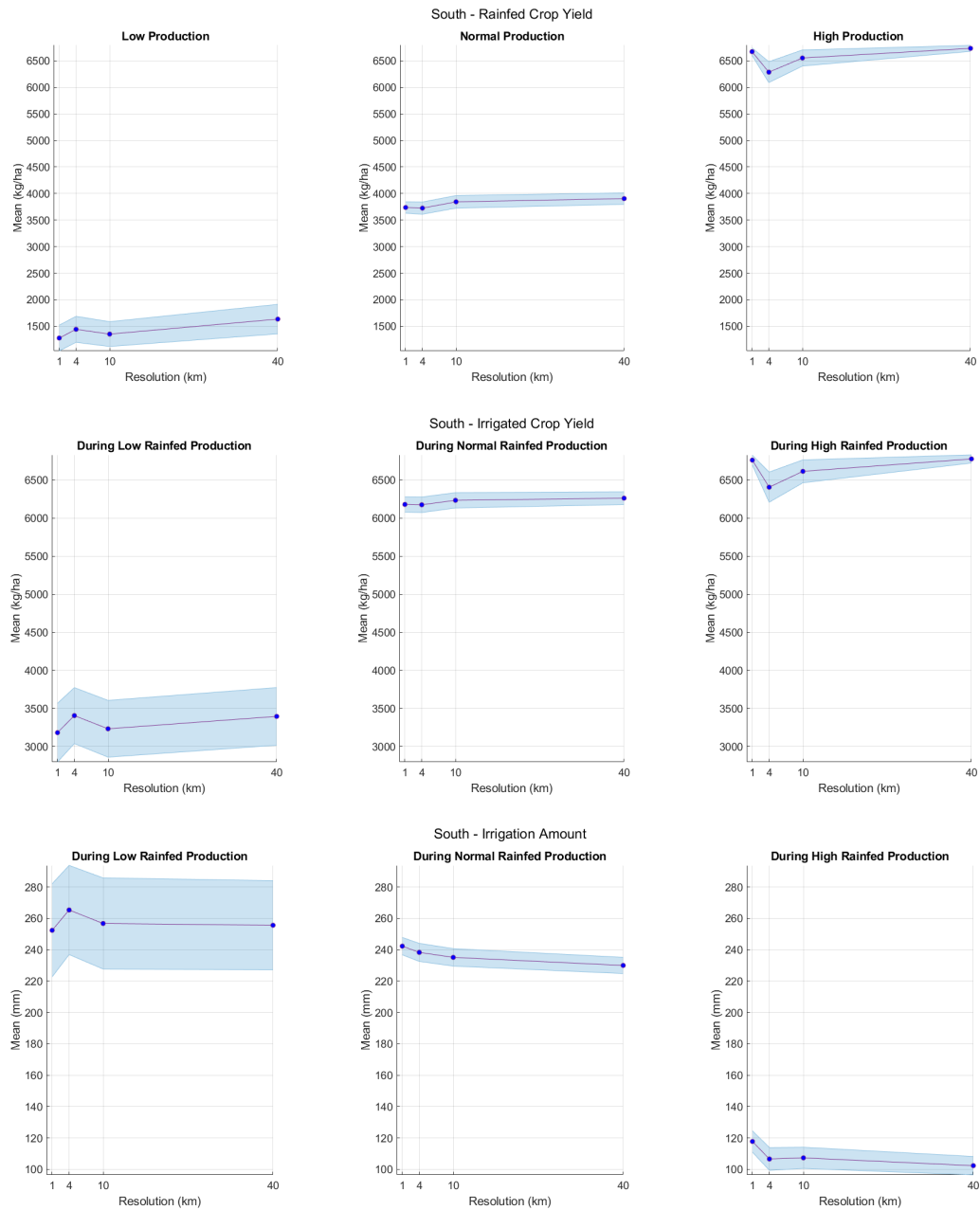


Figure 3-34: Comparison of mean rainfed corn yield, irrigated corn yield, and corn irrigation amount with meteorological forcing and soil input data with spatial resolutions ranging from 1km to 40km. The standard error of the mean is indicated by the shaded region. South case study region.

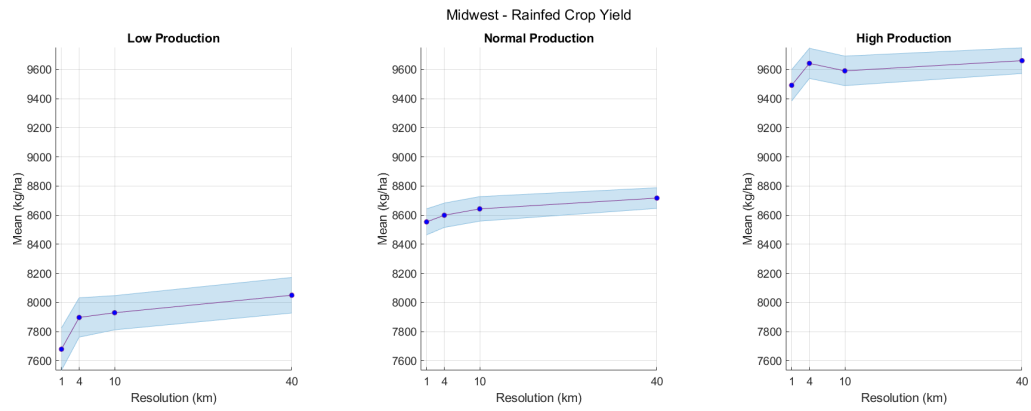


Figure 3-35: Comparison of mean rainfed corn yield with meteorological forcing and soil input data with spatial resolutions ranging from 1km to 40km. The standard error of the mean is indicated by the shaded region. Midwest case study region.

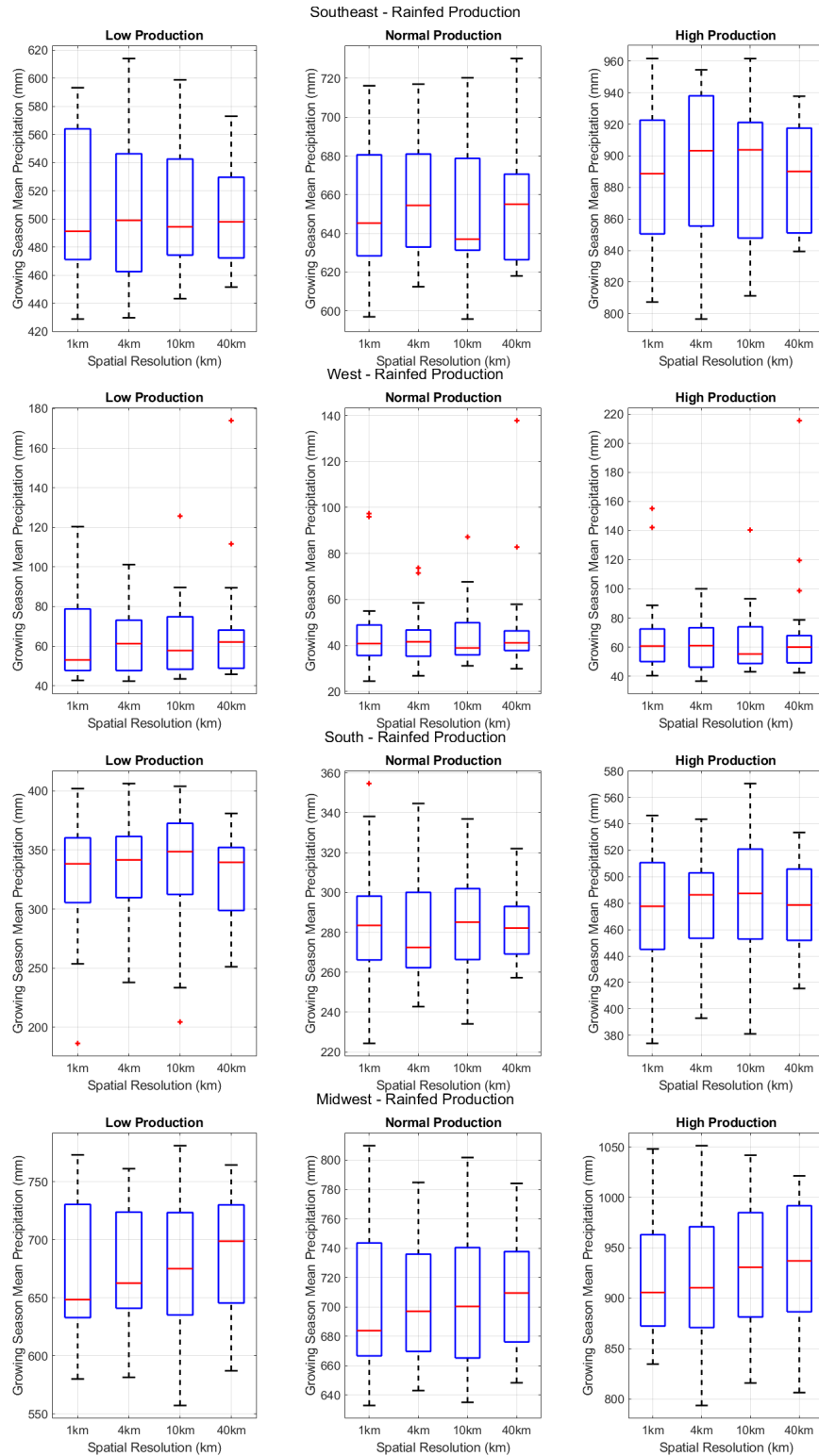


Figure 3-36: Box plots of mean precipitation during the growing season for case studies in the southeast, west, south, and midwest regions as a function of scale of spatial aggregation of GRIDMET precipitation data.

The impact of spatial averaging of high-resolution gridded meteorological and soil property data has implications for regional-scale agricultural modeling and planning, as well as water resources management. For regional-scale assessments using crop model simulations, it is ideal to use the finest spatial resolution and soil data available; however, it may be adequate to use soil data as coarse as 10km and weather data (particularly precipitation data) no coarser than 10km to sufficiently capture the mean crop yield and irrigation demand. The findings of this research also suggest that it may be desirable, but not necessary to spatially downscale remote sensing precipitation products (which are typically no finer than 10km) for applications in regional scale agricultural modeling.

3.6 Summary

In this chapter, the accuracy of modern remote sensing precipitation data and the sensitivity of the DSSAT agricultural model to the spatial resolution of weather and soil input data was assessed.

In relation to the gauge-network based GRIDMET precipitation data set, remote sensing retrievals of precipitation within the continental U.S. generally exhibit a wet bias, but the nature of these biases vary with season and climate region. The most accurate remote sensing precipitation retrievals are those that are heavily calibrated by rain gauge data, which raises questions on whether such retrievals can be trusted over scarcely gauged regions. Despite issues in accurately estimating the magnitude of precipitation events, the remote sensing precipitation retrievals were highly correlated with the GRIDMET reference data set, suggesting the occurrence of rain events is captured in the remote sensing retrievals.

GPM IMERG Version 5 Late Release tends to underestimate precipitation in the western (West and Northwest) climate regions, while overestimating everywhere else. The most severe overestimation is in the winter season, particularly in the Northwest, Northeast, and Central climate regions. While winter time underestimation of precipitation is apparent in the arid West and Southwest climate regions. The JAXA GSMap-Gauge product agrees well with the GRIDMET reference; however, this agreement is due entirely to the assimilation of rain gauge data with the satellite retrievals.

With regard to removing errors from remote sensing precipitation retrievals by way of using surface soil moisture data from the recent SMAP mission, at least two challenges were found. Firstly, SMAP retrievals of surface soil moisture were uncorrelated with errors in daily precipitation retrievals. Secondly, the errors in the remote sensing precipitation retrievals are highly correlated in space.

It can be expected that if remote sensing retrievals of daily precipitation are incorporated into calibrated agricultural decision support models (e.g. DSSAT), then rainfed and irrigated crop yields would be substantially overestimated, except in regions with dry bias. Likewise, irrigation demand would likely be underestimated. If incorporated with streamflow models (such as SAC-SMA), it is expected that while the timing of peak flows may be accurately captured, the magnitude of such flows would be severely overestimated, especially during extreme events. Only remote sensing precipitation products that are calibrated by gauges in the region may prove useful for incorporation into agricultural and hydrologic models.

With regard to the sensitivity of the DSSAT model to the spatial averaging of daily weather and soil inputs, this assessment shows that while finest spatial information of daily

weather data is ideal, atmospheric variables and soil data with spatial resolution no coarser than ~10km are acceptable for crop yield and irrigation assessments. Thus, it may not be necessary to downscale modern remote sensing precipitation data products for the study purpose; however, near-real-time correction of remote sensing precipitation data using rain gauge data is essential to accurately capture the timing and magnitude of precipitation events for applications in agricultural and streamflow modeling.

CHAPTER 4

HINDCASTING AND NEAR-REAL-TIME PREDICTION OF CROP YIELD, IRRIGATION DEMAND, DROUGHT, AND HYDROLOGICAL FLOWS

4.1 Preliminary Study: Modeling regional crop yield and irrigation demand using SMAP type of soil moisture data (El Sharif, et al. 2015)

In this section, a preliminary study completed by El Sharif et al. (2015) is presented which explores a novel method for incorporating SMAP soil moisture data into the DSSAT-CSM crop model for estimating regional crop yield and irrigation demand. This study was performed before the advent of the SMAP satellite launch and before the availability of SMAP data products. What follows is excerpted from what was published in the *Journal of Hydrometeorology*.

4.1.1 Abstract

Agricultural models, such as the Decision Support System for Agrotechnology Transfer – Cropping Systems Model (DSSAT-CSM), have been developed for predicting crop yield at field and regional scales and to provide useful information for water resources management. A potentially valuable input to agricultural models is soil moisture. Presently, no observations of soil moisture exist covering the entire U.S. at adequate time (daily) and space (~10 km or less) resolutions desired for crop yield assessments. Data products from NASA's upcoming Soil Moisture Active Passive (SMAP) mission will fill the gap. The

objective of this study is to demonstrate the usefulness of the SMAP soil moisture data in modeling and forecasting crop yields and irrigation amount. A simple, efficient data assimilation algorithm is presented in which the agricultural crop model DSSAT-CSM is constrained to produce modeled crop yield and irrigation amounts that are consistent with SMAP-type data. Numerical experiments demonstrate that incorporating the SMAP data into the agricultural model provides an added benefit of reducing the uncertainty of modeled crop yields when the weather input data to the crop model are subject to large uncertainty.

4.1.2 Capsule

SMAP-type soil moisture data is used to increase the precision of modeled crop yield and irrigation application forecasts at the ~10km spatial scale using DSSAT-CSM.

4.1.3 Section 1: Introduction

4.1.3.1 Background

Agricultural production systems have evolved significantly in recent years to address a growing national and global demand for food supply. The advent of modern measurement technologies such as geographic information systems (GIS), global positioning systems (GPS), and other remote sensing tools at finer spatio-temporal resolutions, and crop system models have provided the opportunity to guide agricultural related water resources management at both field and regional scales with reduced dependency on costly and uncertain in-situ field experiments. Precision agriculture has been largely focused on maximizing field and regional crop yields and associated economic benefits. The tools involved in precision agriculture may also guide regional water resources management as more accurate modeling and forecasting of water demand for crop production would lead

to a more efficient allocation of limited water supplies. Careful monitoring and provision of water resources for agricultural use is critical as agriculture demands a large fraction of total water use in the United States and the world. In 2005, irrigation in the United States consumed 128 billion gallons per day, accounting for 37 percent of all freshwater withdrawals and 62 percent of all freshwater withdrawals excluding thermoelectric withdrawals (Kenny et al. 2009). The 2013 National Climate Assessment (NCA) (NCADAC 2013) indicates that under the A2 emissions scenario, U.S. freshwater withdrawals will increase by 25 to 35% in the coming 50 years, with $\frac{3}{4}$ of this increase due to irrigation and $\frac{1}{4}$ to landscape watering and power generation (Brown et al. 2013; Georgakakos et al. 2014). Because of these and other stresses, a key message of the 2014 NCA is that “in most U.S. regions, water resources managers and planners will encounter new risks, vulnerabilities, and opportunities that may not be properly managed with existing practices.” The information of space-time distribution of soil moisture is critical for irrigation decisions and for more efficient use of water resources across multiple sectors.

Agricultural models, such as Decision Support System for Agrotechnology Transfer – Cropping Systems Model (DSSAT-CSM) (Tsuji et al. 1994), have been developed to predict the yield of various crops at field and regional scales. Crop yield modeling and prediction provide essential information for water resources management. One key output of the agricultural models is soil moisture. Presently, no soil moisture observations covering the entire U.S. exist with adequate time (daily) and space (~10 km or less) resolutions preferred for crop yield assessments. Instead, estimates of soil moisture at fine spatial scales are commonly derived from downscaling remotely-sensed soil moisture data

(Cheng et al. 2008; El-Sharkawy 2011; NCDC 2006; NRCS 2013; WRF 2013). The NASA Soil Moisture Active Passive (SMAP) mission satellite is scheduled for launch on 8 January 2015 and aims to measure soil moisture from space at fine (down to 9 km for the combined active radar and passive radiometer product) spatial and temporal (2-3 days global coverage) resolution for the first time. The depth of soil moisture retrieval will be the topmost 5cm of the soil profile. Incorporating SMAP soil moisture data products into crop system models such as DSSAT-CSM has the potential to improve the accuracy of crop yield prediction especially with regard to regional irrigation forecasting and water resources management. Although agricultural water use dominates consumption of water in many parts of the world, reliable estimates of historical and future agricultural water demand are lacking for some times and regions. In the southeastern U.S., for example, individual farmers do not routinely monitor or record their water usage, and they are not obligated to report their water use to any governing body. This situation presents significant challenges for retrospective analysis of inter-annual and seasonal water demand. Irrigation practice is strongly dependent on soil moisture conditions, and accurate fine resolution soil moisture data are vital to regional water resources managers and related stakeholders who strive to efficiently and equitably allocate limited water resources especially in the face of a changing climate.

4.1.3.2 Problem Statement

Crop yield and water demand estimates depend on accurate, high resolution spatio-temporal data of weather and/or soil moisture that are not available at sufficient resolutions for all regions. NASA's SMAP mission will provide much needed soil moisture data at relatively high spatio-temporal resolution with global coverage. This data can potentially

support more accurate crop yield and irrigation demand forecasts, which would be particularly useful in regions where observed weather or soil moisture data are sparse or unavailable. In the developing world, for example, where food-security is a major concern, the current and historical weather data critical to forecasting crop yield and irrigation demand are subject to substantial uncertainty (WFP and IFAD 2011), leading to large uncertainty in the modeled crop yield and irrigation demand. A potential benefit of SMAP-type data is to reduce the uncertainty in modeled crop yield and irrigation demand by constraining model simulations to be consistent with the remotely-sensed top soil moisture data.

4.1.3.3 Objectives

The objectives of this study are to:

- 1) Develop an algorithm by which daily SMAP-type top soil moisture data can be assimilated into the DSSAT-CSM for modeling of crop yield and irrigation amount at the ~10km spatial scale.
- 2) Reduce the uncertainty in the forecast of crop yield and irrigation demand by combining SMAP-type remotely-sensed soil moisture data with other weather measurement data products.

4.1.3.4 Outline

The article is organized as follows:

Section 1 introduces the value of precision agriculture models – models designed to explore site-specific, high-efficiency, sustainable agriculture with the help of detailed, modern data sets (McLoud and Gronwald 2007; Shibusawa 1998; Zhang et al. 2002) – and the potential benefit the upcoming SMAP remotely-sensed soil moisture data products can

provide in forecasting crop yield and irrigation demand. The objectives of this study are also stated. An overview of previous studies on crop system models, in particularly DSSAT-CSM, the role of soil moisture data in such models, and the description of the upcoming SMAP mission and its data products is also provided. Section 2 presents the methodology for developing a synthetic “ground truth” soil moisture sequence using observed weather data and DSSAT-CSM top soil moisture output and describes how the SMAP data product is expected to be within a specified error tolerance of the synthetic soil moisture data set. SMAP-derived information on soil moisture is then combined with supplementary data and incorporated into the DSSAT-CSM agricultural model to simulate crop yield and irrigation demand. Section 3 describes the study region for which the methodology is applied and identifies relevant data sources. Results and conclusions are presented in Sections 4 and 5 respectively.

4.1.3.5 Literature Review

DSSAT-CSM:

The Decision Support System for Agrotechnology Transfer – Cropping Systems Model (DSSAT-CSM) is a widely used bio-physical model for simulating the phenology, growth, development, and yield of various crops and cultivars given inputs of soil, weather, and management conditions (Jones et al. 2003). DSSAT-CSM version 4.5 (Hoogenboom et al. 2012) includes 29 crops and fallow fields (Daroub et al. 2003; Hoogenboom et al. 1999; Jones et al. 2001; Jones et al. 2003; Liu et al. 2011; Tsuji et al. 1994). DSSAT-CSM is composed of a main driver program, a land unit module, and modules of weather, soil, plant, soil-plant-atmosphere interaction, and management. The main driver program controls each of the primary modules and allows each module to read inputs, initialize

variables, compute rates, integrate variables, and write outputs independent of other modules (Jones et al. 2003). A brief description of the modules included in DSSAT-CSM is presented in Table 1 (Jones et al. 2003).

History of incorporating soil moisture data into agricultural models:

Improving agricultural models by incorporating soil moisture measurements and/or remote-sensing data has become a growing field of study. Baier and Robertson (1968) found that wheat yields from 39 plantings in Canada over five seasons were more closely related to soil moisture conditions than rainfall and maximum and minimum temperatures, a significant finding as the DSSAT-CSM soil water balance algorithm still uses precipitation and maximum and minimum temperatures as model input (Jones et al. 2003). Batts and Kaleita (2008) investigated the impact of synthetic top 5cm soil moisture data on the DSSAT-CSM model simulations in a series of modeling experiments for a maize field in Ames, Iowa. Differences in modeled yield using their assimilation method in some cases were greater than 10 percent depending on year, soil type, and nitrogen fertilizer application rate of the synthetic experiments. Groenendyk (2011) investigated assimilation of in-situ soil moisture data into the DSSAT-CSM through a Kalman Filter to simulate the winter-wheat crop growing seasons of 2003-05 in Maricopa, Arizona. Model improvement (defined by closer agreement with field measurements of crop yield and canopy biomass) occurred when soil moisture data was assimilated into the top 3cm and top 5cm of the soil layer. Ines et al. (2013) utilized an Ensemble Kalman Filter to assimilate remotely-sensed AMSR-E soil moisture and MODIS Leaf Area Index (LAI) data products into DSSAT-CSM to model year 2003 – 2009 maize yields in Story County, Iowa. Data assimilation improves the correlation between modeled and observed crop yield from 0.47 (no data

assimilation) to 0.65 (with combined assimilation of soil moisture and LAI data). Maas (1988) explored four techniques for incorporating remotely-sensed data into a simulation of a white-maize monoculture at a USDA Research Farm in Texas with direct input of remotely-sensed data being the simplest of data assimilation methods under test. However, the direct input method required frequent observations that were not available. Moulin et al. (1998) addressed challenges in incorporating coarse resolution remote-sensing data to estimate regional crop yields using a similar approach. Delécolle et al. (1992) also used remote-sensing data assimilation techniques for several categories of crop models and recommended that regional analysis may be performed by aggregating simulated crop yields from individual fields. Mo et al. (2005) used remotely-sensed data of crop canopy leaf area index (LAI) with a process-based soil-vegetation-atmosphere transfer (SVAT) model to predict crop yield, water consumption, and water use efficiency for a sub-region of the North China Plain. Mishra et al. (2012) have tested the Atmospheric Land Exchange Inverse (ALEXI) satellite-derived soil moisture estimates as a surrogate for precipitation data in the DSSAT-CSM for crop yield simulation for two climatically contrasting locations in Alabama and Indiana. The soil moisture data with the required resolutions are often obtained through downscaling. Blöschl et al. (2009) provide a statistical technique for downscaling 25 km remotely-sensed soil moisture data to 1 km resolution over Europe. Lin, et al. (2011, 2013) used a coupled the WRF-tRIBS-VEGGIE hydrologic model to downscale Early Adopter SMAP data products. Use of high spatio-temporal resolution soil moisture data for modeling crop yields is an active field of research.

SMAP and other soil moisture measurement missions:

Remote-sensing soil moisture data sets have been derived from signals of active and passive microwave sensors on satellites (Bartalis et al. 2007; Njoku et al. 2003; Owe et al. 2008) since the early 1980s. Without such observations, soil moisture estimates often depend on reanalysis data subject to large uncertainties (Dorigo et al. 2012; Ferguson and Wood 2011). Satellite missions include, SkyLab (Entekhabi et al. 2010), ERS-1, ERS-2, AMSR-E, SMMR, SSM/I, TMI, ASCAT, and SMOS (Dorigo et al. 2010). These soil moisture data products have spatial resolutions ranging from 12km to 50km and daily, weekly, and monthly temporal resolutions covering various regions of the earth.

According to the National Research Council's (NRC) Decadal Survey (NRC 2007), the data product of SMAP mission, whose satellite is scheduled to be launched on 8 January 2015, was characterized with high scientific and practical applications value in multi-scale hydrologic and environmental studies (Entekhabi et al. 2010). The SMAP mission will measure the top 5 cm layer soil moisture and soil freeze/thaw state from space at fine (down to 9 km) spatial and temporal (2-3 days global coverage) resolution using (the first space-borne) L-band (active) radar and an L-band (passive) radiometer instrumentation (Entekhabi et al. 2010). One standard deviation about true soil moisture in the Level 2 9km SMAP data product is specified not to exceed 0.04 cm³cm⁻³. Incorporating SMAP soil moisture data into crop system models such as DSSAT-CSM has the potential to improve the accuracy of crop yield simulations related to regional irrigation forecasting and water resources management.

4.1.4 Section 2: Methodology and Data

The purpose of this study is to quantify the impact of SMAP-like remote-sensing soil moisture data on DSSAT-CSM agricultural model forecasts of agricultural yield and

irrigation demand using synthetically generated data sets with statistical characteristics (uncertainty) similar to those of the upcoming SMAP products. This soil moisture data product is then used to “filter” an ensemble of DSSAT-CSM model runs using synthetic weather input data. In this study, stochastic forcing is introduced by adding measurement noise to daily weather inputs. The “control” scenario refers to DSSAT-CSM modeled results using the entire ensemble of synthetic input data in DSSAT-CSM model runs. The “SMAP” scenario refers to DSSAT-CSM model runs in which modeled top soil moisture is consistent with the SMAP-like data. Agreement is assessed via the absolute difference between modeled and the “ground truth” top layer soil moisture content for each day of the simulated growing season. Model runs in which the SMAP-derived error tolerance criteria for soil moisture content is violated less than five percent of the growing season are selected as “feasible” or “SMAP-consistent” model runs. The SMAP-derived absolute difference threshold is assumed to be a function of the “true” soil moisture for the current day of simulation. “SMAP-consistent” model runs are used to generate samples of simulated rain-fed and irrigated crop yield and irrigation demand. Under the irrigation scenarios, the DSSAT-CSM is programmed to automatically irrigate the top soil layer to saturation when the modeled top layer soil moisture drops below a user-specified threshold. An overview of the filtering procedure is illustrated in Figure 1. Details regarding the acceptance criteria for a model run to be considered either feasible (SMAP-consistent) or infeasible is shown in the Figure 2 flowchart. Metrics used to assess the usefulness of soil moisture data include the reduction in the standard deviation of modeled crop yield and year-end irrigation application depth after the soil moisture data filter is applied. It is also of interest to record

whether incorporation of SMAP-like data impacts the mean modeled crop yield and irrigation amount.

The experiments involved in this study are listed in Table 2. Experiment #1 explores how daily soil moisture data can reduce uncertainty in modeled crop yield under the scenario in which daily precipitation is subject to random measurement errors. Experiment #2 builds on this premise and subjects all required daily weather variables – precipitation, maximum and minimum air temperature, and solar radiation – to measurement errors. These two experiments represent scenarios in which field data on weather are available, but are subject to modest uncertainties due to measurement error or spatial interpolation/extrapolation of weather data, as may be the case in data-scarce regions. The method of generating the surrogate “ground truth” soil moisture data set and weather measurement sequences for a case study region and incorporating them into DSSAT-CSM experiments mentioned in Table 2 is described below.

4.1.4.1 SMAP-like soil moisture data

In this study, DSSAT-CSM modeled soil moisture driven by observed weather input is referred to as “ground truth”. The SMAP-like 9km spatial and daily temporal resolution data product is assumed to be within a specified error tolerance of the synthetic “ground-truth” data set. Operating over a SMAP 9km pixel, the DSSAT-CSM point-scale model simulates crop yield and irrigation amount assuming homogeneous field, soil, crop, and weather conditions. DSSAT-CSM is then constrained to keep modeled top layer soil moisture within SMAP-derived error tolerances for each day of the growing season while measurement errors are introduced into daily weather inputs. When these constraints are

fulfilled for at least 95 percent of the growing season, it is concluded that DSSAT-CSM has “assimilated” SMAP-like data.

While the upper bound of the error (one-sigma) in SMAP Level 2 (combined radar and radiometer) data product is $0.04 \text{ cm}^3\text{cm}^{-3}$, pre-launch tests of the SMAP retrieval algorithm suggest that the actual error is expected to be smaller (e.g. approximately $0.03 \text{ cm}^3\text{cm}^{-3}$) (Das et al. 2011). The error may be further reduced through constraining the SMAP-like data by the information of case study site. Under this condition, we suggest that the actual, or “effective” effective error for the SMAP product varies with true soil moisture: peaking halfway between wilting point and saturation and diminishing near wilting point and saturation. Figure 3 illustrates a characterization of the effective error σ in the SMAP data product with a wilting point near zero and saturation water content of $0.361 \text{ cm}^3\text{cm}^{-3}$. The maximum effective error is set at a $0.025 \text{ cm}^3\text{cm}^{-3}$ according to our analysis of SMAP calibration mission results from Das et al. (2011). For each day of the DSSAT-CSM simulated growing season, modeled soil moisture content for a feasible model run must remain within 1.96 times the effective error (representing two standard deviations) of the synthetic “ground truth” soil moisture data set for at least 95 percent of the modeled growing season. If this acceptance criteria is achieved, then the model run is considered to be “feasible” and consistent with SMAP-like data.

4.1.4.2 Experiment #1: Soil moisture data corrects errors in daily rainfall input

When precipitation observations are available with significant uncertainty, the DSSAT-CSM may be used to “correct” rainfall input through DSSAT-CSM modeling the dynamics of top layer soil moisture with soil moisture data used as a rainfall correction “filter”. Using

information on the percent error in daily rainfall measurements, an ensemble of stochastic rainfall sequences is simulated. Each of these weather realizations are used as input into a model run of DSSAT-CSM. Whenever a weather realization results in a modeled daily time series of top soil moisture within the effective error threshold for at least 95 percent of the growing season, the model run is selected as a “SMAP-consistent”. Modeled rain-fed and irrigated crop yields are sampled from these feasible model runs. In this experiment, daily precipitation data is stochastically generated based on daily observations. For each day of simulation, 2,000 samples of precipitation are generated from a truncated normal distribution with a mean equal to the observed precipitation and a standard deviation equal to 20 percent of the observation. The distribution is bounded by zero and 1.1 times the observation (to allow for both under- and over-estimation errors). Introducing this type of noise into rainfall data mimics measurement and/or spatial interpolation/extrapolation errors. In this experiment, other daily weather variables (incoming solar radiation, maximum and minimum air temperatures) are assumed to be known and equivalent to observations as mentioned in Table 2. In this study, the absolute error threshold for DSSAT-CSM modeled daily top soil moisture is set at 1.96 times the daily effective SMAP error shown in Figure 3.

4.1.4.3 Experiment #2: Soil moisture data corrects errors in daily weather input

When observed meteorological variables such as incoming solar radiation, precipitation, and maximum and minimum air temperatures are available with significant errors, incorporating SMAP-like top soil moisture data into DSSAT-CSM can mitigate model errors due to incorrect weather input. Error-contaminated measurement data sets are

developed using different methods appropriate for each weather variable. The rainfall data is obtained using the method described in Experiment #1. The daily solar radiation data is simulated using a truncated Gaussian distribution with a mean equal to the day's observation of solar radiation. The truncated distribution is bounded by zero and 1.2 times the historical data of radiation to cover the cases of both over- and under-estimation. The standard deviation is set as 10 percent of each day's historically recorded solar radiation. Daily maximum and minimum temperatures were simulated from the observation data superimposed with a white noise following a truncated Gaussian distribution between -1 and +1 °C with a mean of zero and standard deviation of 0.5 °C. Experiment #2 represents a practical scenario in which observations are available for multiple weather variables, all subject to measurement and/or interpolation/extrapolation error.

Each of these weather realizations are used as input to DSSAT-CSM model runs. The synthetic soil moisture data, with the SMAP-derived effective error threshold, is used to select SMAP-consistent model runs just as in Experiment #1. Similarly, modeled rain-fed and irrigated yields are sampled from these feasible model runs.

4.1.5 Section 3: Data

4.1.5.1 Ames, Iowa

The case study site was Ames, Iowa USA located at 42°1' N, 93°44'W (Central Iowa, USA) at an elevation of 327 meters (NRCS 2013). As published by the National Climatic Data Center (NCDC) Climate Services Branch (NCDC 2006), the Iowa terrain is mostly comprised of rolling hills with a climate dominated by moist southerly wind from the Gulf of Mexico in the summer, northwesterly wind of cold, dry Canadian air in the winter, and occasionally air masses from the Pacific Ocean and the Desert Southwest. Summer daily

high temperatures (July) reach 28°C and winter daily low temperatures (January) drop to -15.6°C. Statewide annual precipitation is 864mm with the majority of precipitation occurring during the late April to early October growing season. Iowa's climate and rich soils are ideal for rain-fed corn and soybean crops.

4.1.5.2 Weather Data

This study uses 2003 weather data from Station 2031 (Ames, Iowa) from the Soil Climate Analysis Network (SCAN) managed by the Natural Resources Conservation Service (NRCS) (USDA-NRCS-NWCC 2014). Minimum weather inputs for DSSAT-CSM include daily data of incoming solar radiation, maximum and minimum temperatures, and precipitation. The SCAN station includes temperature probes and a rain gauge to provide the rainfall and temperature data. For daily measurement entries from the SCAN site containing erroneous or missing data, data entries were replaced with available data from the previous day. Only three days during 2003 had missing data at the SCAN site. Daily solar radiation data were taken from the NASA-POWER Agro-climatology (NASA 2014) data set.

4.1.5.3 DSSAT-CSM Initialization

DSSAT-CSM model simulations for 2003 in this study were based upon crop, soil-type, and management parameters from a 1999 Ames, Iowa rain-fed maize cropping scenario. The 1999 scenario data files were provided as one of the default maize experiments in DSSAT-CSM version 4.5.0.0. and were developed by Drs. J. Lizaso and B. Batchelor of the Department of Agricultural and Biosystems Engineering, Iowa State University. Model results from the 1999 experiment agreed well with in-situ measurements of crop yields. DSSAT-CSM simulation of Ames, Iowa crop yields using weather observations from years

1996 – 1999 are compared with averaged county-level crop yields reported by the United States Department of Agriculture National Agricultural Statistics Service (USDA: NASS) as shown in Figure 4. Modeled crop yields in these years were generally within 20 percent of the county average, suggesting that the DSSAT-CSM model reasonably simulates the region’s hydrology, soil-type, expected crop growth, and crop stresses, at least for the non-drought years of 1996 – 1999. One of the required inputs for DSSAT-CSM initialization is the initial soil moisture profile. Initial conditions for 2003 soil moisture profile were obtained from a 2002 DSSAT-CSM model run using a fallow crop. The soil moisture profile from December 31, 2002 was assigned to the soil water profile for January 1, 2003. Year 2003 model runs were initialized from January 1, 2003 with the simulated growing season from May 27, 2003 to October 31, 2003. Table 3 lists some management parameters used to initialize DSSAT-CSM simulations, and Table 4 lists soil layer and soil-type parameters used in the study.

4.1.5.4 Crop Yield Statistics

Results from the numerical experiments are compared to the reported annual (growing season) maize yields for year 2003 from the United States Department of Agriculture National Agricultural Statistics Service (USDA:NASS). To facilitate comparison with USDA reported yields, DSSAT-CSM calculated dry yields were reduced by five percent to account for mechanical losses during the harvest process. USDA reported yields were converted to dry weight assuming a grain moisture content of 15.5 percent. Relevant county level statistics are presented in Table 5 (USDA 2013). It is important to note that this study models crop yield at the scale of a single SMAP pixel (~10km) and not county-level yield; comparison of model results to county level data is done only for reference.

4.1.6 Section 4: Results

As shown in Figure 5, the soil moisture filtering procedure was able to reduce the uncertainty in modeled rain-fed crop yield for Experiments #1 and #2 in which measurement uncertainties were introduced into daily weather variables. Simulated rain-fed crop yields in those experiments were brought closer to the modeled rain-fed crop yield from true weather input. The USDA county-level yield for year 2003 (an average of Boone and Story counties in Iowa) converted to dry weight is indicated in Figure 5 for reference.

For Experiment #1, in which only daily rainfall was subject to measurement error, the soil moisture filter selected 727 SMAP-consistent model runs from a pool of 2,000. The mean modeled rain-fed crop yield did not change significantly after the soil moisture filter was applied (increasing by only 2 percent); however, the uncertainty (standard deviation) in the modeled crop yield was reduced by approximately 30 percent as shown in Table 6. Similarly, when measurement error was introduced into all daily weather inputs (Experiment #2), the soil moisture filter selected 872 SMAP-consistent model runs from a pool of 2,000, and the standard deviation in modeled rain-fed crop yield was reduced by approximately 18 percent.

As evidenced by the uncertainty in the control modeled crop yields, measurement errors in weather input to DSSAT-CSM can introduce significant uncertainty in model results. Errors such as those introduced in Experiment #1, directly influence the evolution of soil moisture in each layer of the soil profile. Water flux downwards through the soil profile (via drainage) and upwards (via diffusion and root water uptake) is also affected. Lack of predictive skill, due to erroneous water input, would introduce errors with regard to modeling nutrient transport and would cause inaccurate yield estimates. Likewise, errors

in solar radiation and temperature data, such as those included in Experiment #2, cause errors in crop photosynthesis, soil evaporation, and crop transpiration, which, in turn, affect the transport of water and nutrients through the soil profile and lead to errors in crop growth and yield. Due to the highly non-linear relationship between weather variables, soil water and nutrient transport dynamics, and crop growth, it is not entirely clear what type of error (over- or under-estimation) would be introduced to crop yield due to combined (and/or competing) errors in precipitation, solar radiation, and air temperature. Overestimation of low precipitation events and underestimation of extreme (and rare) precipitation events could lead to water surpluses offsetting drought effects. However, when coupled with reduced photosynthesis and reduced evaporation due to underestimation of solar radiation, any benefit from the plentiful supply of water would be lost. Water surplus coupled with overestimation of solar radiation would obviously accelerate photosynthesis leading to overestimation of crop yield. It is of interest to note that the errors introduced to rainfall input for Experiment #1 and to weather inputs for Experiment #2 resulted in modeled top soil moisture content that was outside of SMAP specifications for 65 percent and 56 percent of the crop yield simulations respectively. Guiding the DSSAT-CSM to produce results consistent with the SMAP-type top soil moisture data, as accomplished by the novel soil moisture filtering procedure developed in this study, can correct some potentially dramatic model biases introduced by such input/measurement errors.

Under the automated irrigation scenario, drought stresses on photosynthesis and crop growth were virtually eliminated, and crop yield approached the modeled irrigated levels using true weather input as shown in Figure 6. This occurs regardless of whether external soil moisture data was available or not. Because of the achievement of potential production

in the absence of water stresses, modeled crop yield variation was negligible in the irrigated crop simulations. Mean irrigated crop yield and mean irrigation amount for Experiments #1 and #2 did not significantly change with application of the soil moisture filter as shown in Figure 6 and Figure 7; however, the standard deviation in irrigation amount was reduced (marginally) by 14 and 9 percent respectively for Experiments #1 and #2 as shown in Table 7.

4.1.7 Section 5: Conclusions and on-going research

This study introduces an efficient algorithm for assimilating SMAP top layer daily soil moisture data into the DSSAT-CSM model. The soil moisture filtering procedure constrains the agricultural model to produce results consistent with SMAP-like remotely-sensed soil moisture data, thereby reducing the uncertainty in forecasted crop yield and irrigation amount. Incorporating SMAP-like top layer soil moisture data into DSSAT-CSM resulted in increased precision of modeled rain-fed crop yield, bringing model estimates of mean crop yield into closer agreement with DSSAT-CSM rain-fed yield using observed weather input. Furthermore, the data assimilation algorithm developed for this study mitigated the impact of measurement errors in critical weather inputs on modeled crop yield and irrigation amount, highlighting the potential utility of both this algorithm and of the SMAP top soil moisture data product.

This study is limited to a single site (an experimental “field” in Ames, Iowa) for a single growing season (2003). Further research will expand the case-study spatially and temporally to the regional scale, multiple years, and for various rain-fed and irrigated crops. This study is also limited by the assumption that “ground-truth” 9km soil moisture can be

accurately determined from weather observations, detailed site specific soil properties, and the other required minimum input to the point-scale DSSAT-CSM.

As the SMAP satellite data products will not be available until early 2015, and reliable soil moisture observations at the Ames, Iowa case study site were not available, DSSAT-CSM modeled top layer soil moisture driven by observed daily weather input served as a surrogate for “ground-truth” soil moisture and is assumed to mimic the SMAP soil moisture data product. Likewise, the potential to merge information on local physical constraints with SMAP data products to further reduce the error in SMAP remotely-sensed beyond the 0.04cm³cm⁻³ mission specification needs further investigation. It is of interest to validate the conclusions of this study as soon as soil moisture data from the SMAP mission are available.

Merging remotely-sensed SMAP soil moisture data with DSSAT-CSM is a topic of ongoing research, and we look forward to conducting on-going research on the following topics:

- The impact of lower effective error in top layer soil moisture data, (e.g., 0.01 cm³cm⁻³) on precision in crop model output.
- How SMAP-like data can guide DSSAT-CSM model runs in which other inputs such as crop cultivars, soil type, and soil hydraulic characteristics are uncertain.
- Performing DSSAT-CSM simulation of drought years to further investigate the benefit of SMAP-type data to reduce uncertainty in irrigation forecasts.
- Incorporating the SMAP Level 4 Root-Zone soil moisture product to further reduce uncertainties in DSSAT-CSM forecasts.

4.1.8 Acknowledgments

This work was supported by USGS GWRI grant G11AP20073, NSF grant EAR-1331846 and ARO grants W911NF-10-1-0236/W911NF-12-1-0095. We are also greatly appreciative of the efforts of the NASA: SMAP Early Adopters team whose members provided beneficial feedback during preliminary stages of this research. The authors also thank the anonymous reviewers for their valuable comments that helped improve the quality of this paper.

4.1.9 References

- Baier, W., and G. W. Robertson, 1968: The performance of soil moisture estimates as compared with the direct use of climatological data for estimating crop yields. *Agricultural Meteorology*, **5**, 17-31.
- Bartalis, Z., and Coauthors, 2007: Initial soil moisture retrievals from the METOP-A Advanced Scatterometer (ASCAT). *Geophysical Research Letters*, **34**, L20401.
- Batts, C., and A. L. Kaleita, 2008: Data Assimilation of Near-Surface In-Situ Soil Moisture Using the DSSAT Crop Model. *2008 ASABE Annual International Meeting* Providence, RI, American Society of Agricultural and Biological Engineers (ASABE).
- Blöschl, G., J. Komma, and S. Hasenauer, 2009: Hydrological downscaling of soil moisture: Final Report to the H-SAF (Hydrology Satellite Application Facility) via the Austrian Central Institute for Meteorology and Geodynamics (ZAMG).
- Brown, T. C., R. Foti, and J. A. Ramirez, 2013: Projected freshwater withdrawals in the United States under a changing climate. *Water Resources Research*, **49**, 1259-1276.
- Cheng, K., Y. Lin, and J. Liou, 2008: Rain-gauge network evaluation and augmentation using geostatistics. *Hydrological Processes*, **22**, 2554-2564.
- Daroub, S. H., A. Gerakis, J. T. Ritchie, D. K. Friesen, and J. Ryan, 2003: Development of a soil-plant phosphorus simulation model for calcareous and weathered tropical soils. *Agricultural Systems*, **76**, 1157-1181.
- Das, N. N., D. Entekhabi, and E. G. Njoku, 2011: An Algorithm for Merging SMAP Radiometer and Radar Data for High-Resolution Soil-Moisture Retrieval. *IEEE Transactions on Geoscience and Remote Sensing*, **49**, 1504-1512.
- Delécolle, R., S. J. Maas, M. Guérif, and F. Baret, 1992: Remote sensing and crop production models: present trends. *ISPRS Journal of Photogrammetry and Remote Sensing*, **47**, 145-161.

Dorigo, W., R. de Jeu, D. Chung, R. Parinussa, Y. Liu, W. Wagner, and D. Fernández-Prieto, 2012: Evaluating global trends (1988–2010) in harmonized multi-satellite surface soil moisture. *Geophysical Research Letters*, **39**, L18405.

Dorigo, W. A., K. Scipal, R. M. Parinussa, Y. Y. Liu, W. Wagner, R. A. M. de Jeu, and V. Naeimi, 2010: Error characterisation of global active and passive microwave soil moisture datasets. *Hydrol. Earth Syst. Sci.*, **14**, 2605-2616.

El-Sharkawy, M. A., 2011: Overview: Early history of crop growth and photosynthesis modeling. *Biosystems*, **103**, 205-211.

Entekhabi, D., and Coauthors, 2010: The Soil Moisture Active Passive (SMAP) Mission. *Proceedings of the IEEE*, **98**, 704-716.

Ferguson, C. R., and E. F. Wood, 2011: Observed Land–Atmosphere Coupling from Satellite Remote Sensing and Reanalysis. *Journal of Hydrometeorology*, **12**, 1221-1254.

Georgakakos, A. P., and Coauthors: Water Resources Chapter, 2014 U.S. National Climate Assessment. [Available online at <http://ncadac.globalchange.gov/>.]

Groenendyk, D. G., 2011: Assimilating in situ soil moisture measurements into the DSSAT-CSM using a Kalman filter. *Agricultural and Biosystems Engineering Conference Papers, Posters and Presentations*, ASABE.

Hoogenboom, G., P. Wilkens, and G. Tsuji, 1999: *Decision support system for agrotechnology transfer (DSSAT) v.3*. Vol. 4, University of Hawaii.

Hoogenboom, G., and Coauthors, 2012: Decision Support System for Agrotechnology Transfer (DSSAT) Version 4.5.1.023 [CD-ROM]. University of Hawaii.

Ines, A. V. M., N. N. Das, J. W. Hansen, and E. G. Njoku, 2013: Assimilation of remotely sensed soil moisture and vegetation with a crop simulation model for maize yield prediction. *Remote Sensing of Environment*, **138**, 149-164.

Jones, J. W., B. A. Keating, and C. H. Porter, 2001: Approaches to modular model development. *Agricultural Systems*, **70**, 421-443.

Jones, J. W., and Coauthors, 2003: The DSSAT cropping system model. *European Journal of Agronomy*, **18**, 235-265.

Kenny, J. F., N. L. Barber, S. S. Hutson, K. S. Linsey, J. K. Lovelace, and M. A. Maupin, 2009: Estimated use of water in the United States in 2005 U.S. Geological Survey Circular 1344, 52 p pp.

Lin, L.-F., R. L. Bras, A. N. Flores, and J. Wang, 2013: Dynamic downscaling GPM like precipitation data --- a case study of 4DVAR Data Assimilation of Rain Rates. *PMM Science Team Meeting*, Washington, DC.

Lin, L.-F., A. N. Flores, G. Bisht, U. Narayan, J. Wang, and R. L. Bras, 2011: Dynamic downscaling of GPM precipitation and SMAP soil moisture using WRF-ptRIBS-VEGGIE model – a preliminary test. *PMM Science Team Meeting*, Denver, CO.

Liu, H. L., and Coauthors, 2011: Using the DSSAT-CERES-Maize model to simulate crop yield and nitrogen cycling in fields under long-term continuous maize production. *Nutr Cycl Agroecosyst*, **89**, 313-328.

Maas, S. J., 1988: Use of remotely-sensed information in agricultural crop growth models. *Ecological Modelling*, **41**, 247-268.

McLoud, P. R., and R. Gronwald, 2007: Agronomy Technical Note No. 1: Precision Agriculture: NRCS Support for Emerging Technologies.

Mishra, V., J. Cruise, and J. Mecikalski, 2012: Agricultural Decision Support Through Robust Assimilation of Satellite Derived Soil Moisture Estimates. *AGU 2012 Fall Meeting, Poster Session, H31F-1177*, American Geophysical Union.

Mo, X., S. Liu, Z. Lin, Y. Xu, Y. Xiang, and T. R. McVicar, 2005: Prediction of crop yield, water consumption and water use efficiency with a SVAT-crop growth model using remotely sensed data on the North China Plain. *Ecological Modelling*, **183**, 301-322.

Moulin, S., A. Bondeau, and R. Delecolle, 1998: Combining agricultural crop models and satellite observations: From field to regional scales. *International Journal of Remote Sensing*, **19**, 1021-1036.

NASA, cited 2014: Prediction Of Worldwide Energy Resource (POWER): Agroclimatology. [Available online at http://power.larc.nasa.gov/common/php/POWER_AboutAgroclimatology.php.]

NCADAC, cited 2013: Federal Advisory Committee Draft Climate Assessment. [Available online at <http://ncadac.globalchange.gov/>.]

NCDC: Climate of Iowa. [Available online at http://www.crh.noaa.gov/images/dvn/downloads/Clim_IA_01.pdf.]

Njoku, E. G., T. J. Jackson, V. Lakshmi, T. K. Chan, and S. V. Nghiem, 2003: Soil moisture retrieval from AMSR-E. *Geoscience and Remote Sensing, IEEE Transactions on*, **41**, 215-229.

NRC, 2007: *Earth Science and Applications from Space: National Imperatives for the Next Decade and Beyond*. The National Academies Press.

NRCS, cited 2013: Ames (2031) - Site Information and Reports. [Available online at <http://www.wcc.nrcs.usda.gov/nwcc/site?sitenum=2031&state=ia>.]

Owe, M., R. de Jeu, and T. Holmes, 2008: Multisensor historical climatology of satellite-derived global land surface moisture. *Journal of Geophysical Research: Earth Surface*, **113**, F01002.

Shibusawa, S., 1998: Precision Farming and Terra-mechanics. *Fifth ISTVS Asia-Pacific Regional Conference in Korea*, Seoul, South Korea.

Tsuji, G., G. Uehara, and S. Balas, 1994: *DSSAT V3*. University of Hawaii.

USDA-NRCS-NWCC, cited 2014: Ames (SCAN Site 2031) Site Information and Reports. [Available online at <http://www.wcc.nrcs.usda.gov/nwcc/site?sitenum=2031&state=ia>.]

USDA: USDA NASS: Quick Stats: Data and Statistics. [Available online at http://www.nass.usda.gov/Quick_Stats/.]

WFP, and IFAD, 2011: *Weather Index-based Insurance in Agricultural Development: A Technical Guide*. International Fund for Agricultural Development (IFAD), World Food Programme (WFP), 61 pp.

WRF: The Weather Research & Forecasting Model. [Available online at <http://www.wrf-model.org/index.php>.]

Zhang, N., M. Wang, and N. Wang, 2002: Precision agriculture—a worldwide overview. *Computers and Electronics in Agriculture*, **36**, 113-132.

Table 1: Description of DSSAT-CSM modules and sub-modules

Modules	Sub modules	Behavior
Main program (DSSAT-CSM)		Controls time loops, determines which modules to call based on user input switches, controls print timing for all modules
Land unit		Provides a single interface between cropping system behavior and applications that control the use of the cropping system. It serves as a collection point for all components that interact on a homogenous area of land
Weather		Reads or generates daily weather parameters used by the model. Adjusts daily values if required, and computes hourly values
Soil	Soil dynamics	Computes soil structure characteristics by layer. This module currently reads values from a file, but future versions can modify soil properties in response to tillage, etc.
	Soil temperature module	Computes soil temperature by layer
	Soil water module	Computes soil water processes including snow accumulation and melt, runoff, infiltration, saturated flow and water table depth. Volumetric soil water content is updated daily for all soil layers. Tipping bucket approach is used
	Soil nitrogen and carbon module	Computes soil nitrogen and carbon processes, including organic and inorganic fertilizer and residue placement, decomposition rates, nutrient fluxes between various pools and soil layers. Soil nitrate and ammonium concentrations are updated on a daily basis for each layer
SPAM		Resolves competition for resources in soil-plant-atmosphere system. Current version computes partitioning of energy and resolves energy balance processes for soil evaporation, transpiration, and root water extraction
CROPGRO Crop Template module		Computes crop growth processes including phenology, photosynthesis, plant nitrogen and carbon demand, growth partitioning, and pest

		and disease damage for crops modeled using the CROPGRO model Crop Template (soybean, peanut, dry bean, chickpea, cowpea, faba bean, tomato, Macuna, Brachiaria, Bahiagrass)
Individual plant growth modules	CERES-Maize; CERES-Wheat; CERES-Rice; SubStor-Potato; Other plant models	Modules that simulate growth and yield for individual species. Each is a separate module that simulates phenology, daily growth and partitioning, plant nitrogen and carbon demands, senescence of plant material, etc.
Management operations module	Planting	Determines planting date based on read-in value or simulated using an input planting window and soil, weather conditions
	Harvesting	Determines harvest date, based on maturity, read-in value or on a harvesting window along with soil, weather conditions
	Irrigation	Determines daily irrigation, based on read-in values or automatic applications based on soil water depletion
	Fertilizer	Determines fertilizer additions, based on read-in values or automatic conditions
	Residue	Application of residues and other organic material (plant, animal) as read-in values or simulated in crop rotations

Table 2: Experiment description

Exp. No.	Description	Incoming Solar Radiation (MJ/m ²)	Max. and Min. Air Temp. (°C)	Precipitation (mm)
1	Soil moisture data corrects errors in daily rainfall input.	Known	Known	Subject to 20% daily measurement error.
2	Soil moisture data corrects errors in daily weather input.	Subject to $\pm 10\%$ daily measurement error.	Subject to $\pm 0.5^\circ\text{C}$ daily measurement error.	Subject to 20% daily measurement error.

Table 3: DSSAT-CSM Initialization

Experiment Parameter	Description
Maize Cultivar	DK 611
Plant Population	4.7 plants/m ²
Nitrogen Fertilizer Application	Not applicable*,
Soil Type	Clarion Loam
Planting Date	May 27, 2003
Harvest Date	October 31, 2003

* Crop nitrogen demand is assumed to be fully met throughout growing season; nitrogen transport and nitrogen-deficit plant stress is not simulated.

Table 4: Site specific soil profile characteristics for Ames, Iowa USA

Depth (cm)	Soil Water Lower Limit	Drained Upper Limit	Sat. Water Content	Sat. Hyd. Cond. (cm/h)	Org. Carbon Content (%)	Sand (%)	Clay (%)	Silt (%)
10	0.110	0.300	0.361	3.3	2.03	79	21	0
30	0.110	0.300	0.361	3.3	2.03	79	21	0
60	0.129	0.310	0.371	3.3	0.44	73	27	0
90	0.129	0.310	0.371	3.3	0.44	73	27	0
120	0.107	0.229	0.369	3.3	0.15	83	17	0

Table 5: USDA: NASS Year 2003 Iowa Maize yield

Region	Dry Yield (kg/ha)
Story County	8,725
Boone County	9,038
Average (Boone & Story Counties)	8,882

Table 6: Change in uncertainty of modeled rain-fed crop yield after applying daily soil moisture (SM) filter

Exp. No.	Description	Standard Deviation in modeled rain-fed crop yield (kg/ha)		Percent Change
		Before SM Filter	After SM Filter	
1	Soil moisture data corrects errors in daily rainfall input.	223	157	- 30%
2	Soil moisture data corrects errors in daily weather input.	302	249	- 18%

Table 7: Change in uncertainty of modeled cumulative irrigation amount after applying daily soil moisture (SM) filter

Exp. No.	Description	Standard Deviation in modeled irrigation amount (mm)		Percent Change
		Before SM Filter	After SM Filter	
1	Soil moisture data corrects errors in daily rainfall input.	5.9	5.1	- 14%
2	Soil moisture data corrects errors in daily weather input.	6.1	5.6	- 9%

4.1.11 Figures

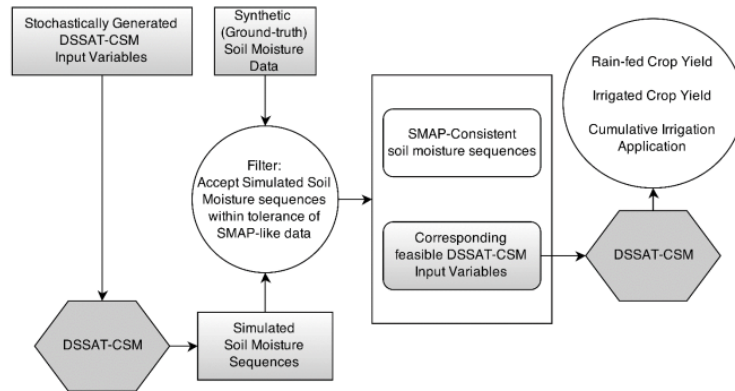


Figure 1: Flow chart describing process of using “ground truth” soil moisture data and SMAP-derived error tolerances in modeled top layer soil moisture to “filter” through DSSAT-CSM model runs.

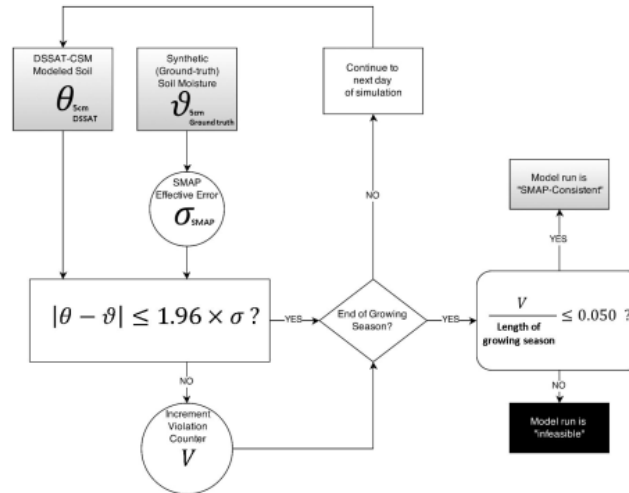


Figure 2: Flow chart detailing process of determining the SMAP-Consistency (feasibility) of a DSSAT-CSM model run. For each day of the growing season, the absolute difference between the DSSAT-CSM modeled soil moisture θ and the "ground truth" synthetic soil moisture θ is compared to the effective error in SMAP-like measurement σ . A violation counter V is incremented each day the acceptance criteria is not fulfilled. If acceptance criteria is violated more than five percent of the days of the growing season, then the model run is deemed as "infeasible", and if otherwise, then "SMAP-Consistent".

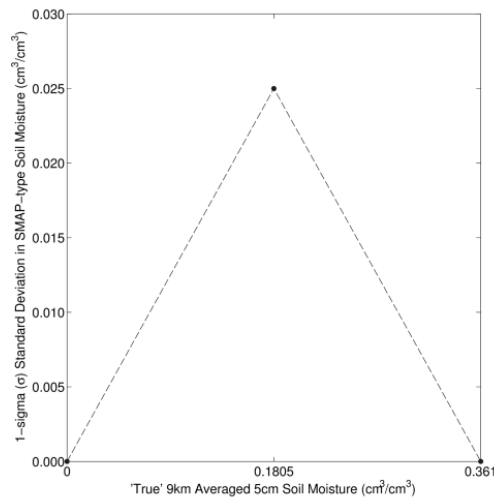


Figure 3: Simple characterization of effective error in the Level 2 9km SMAP data product for a soil type with a wilting point near zero and saturation water content of 0.361 cm³/cm³. Maximum error is assigned where the soil moisture has more freedom to vary; minimum error is assigned at the extremes of wilting point and saturation.

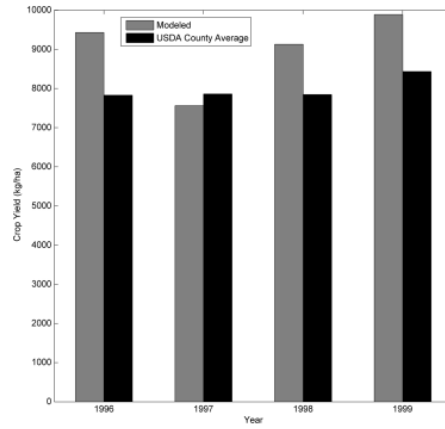


Figure 4: Comparison of DSSAT-CSM modeled crop yield to USDA-NASS averaged county yield. Yield average reported for Boone and Story counties near Ames, Iowa USA.

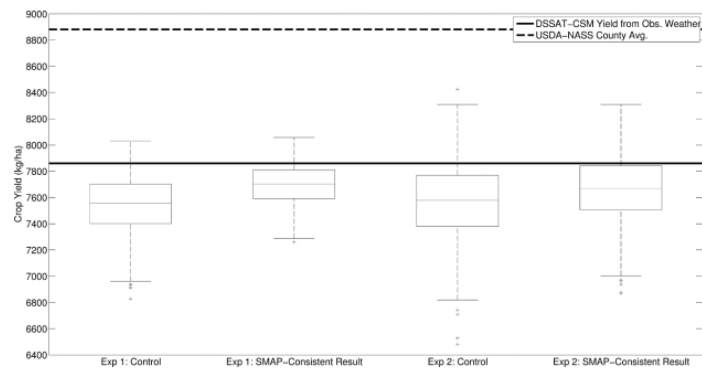


Figure 5: Modeled rain-fed crop yields for Experiments #1 and #2.

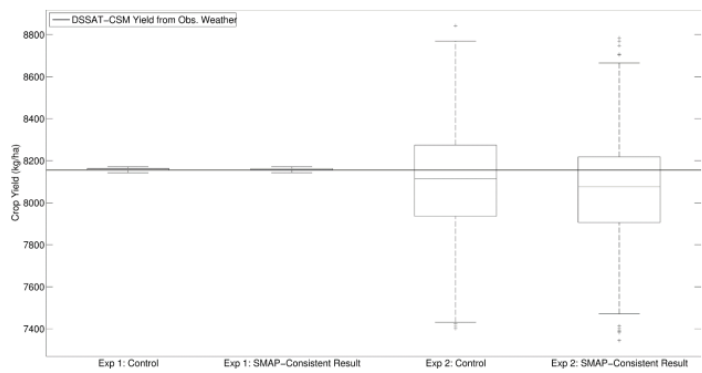


Figure 6: Modeled irrigated crop yields for Experiments #1 and #2.

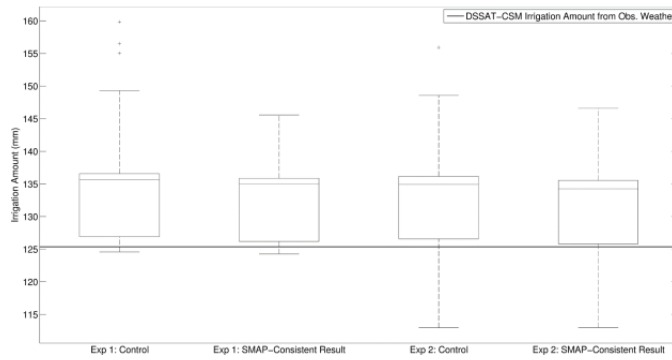


Figure 7: Modeled cumulative irrigation amounts for Experiments #1 and #2.

4.2 Incorporation of remote sensing SMAP L3 Enhanced surface soil moisture data in DSSAT-CSM rainfed crop simulations

In the following case studies, surface soil moisture estimates from the SMAP L3 Enhanced data product are incorporated into year 2015 and 2016 county-level rain-fed maize DSSAT-CSM simulations. Simulations are also driven by daily meteorological forcing from the GRIDMET data set and gridded soil profile data from the Harvest Choice Global High Resolution Soil Profile Data set. In these hindcasting exercises, when data availability allows, remote sensing surface soil moisture estimates replace the DSSAT-CSM modeled daily 5 cm soil moisture estimates. In this way, it is hoped that incorporation of SMAP estimates would “correct” the soil moisture dynamics in the DSSAT model simulations as the growing season progresses, thereby bringing calibrated DSSAT estimates of county-level rain-fed crop yield in closer agreement with USDA NASS reported crop yields. DSSAT crop yield estimates resultant from incorporation of SMAP data are also compared with simulated crop yields without SMAP data incorporation (referred to as DSSAT Control) to assess improved agreement with USDA NASS reported crop yields.

Table 4-1 lists some of the important input data and parameters for modeling of rain-fed maize for year 2015 and 2016. The DSSAT-CSM model is run at multiple point locations within the county boundaries. The same locations are used for the control run simulations and simulations that incorporate SMAP estimates of surface soil moisture. With regard to gridded data, DSSAT simulations are driven by data from the pixel nearest to each point location. To facilitate comparison of simulated crop yields with USDA NASS reported yields, USDA yields are converted from bushels per acre to kilograms per acre with an assumed moisture content of 15.5 percent.

Table 4-1: Calibrated input parameters for rainfed county-level DSSAT-CSM maize simulations.

Location	DSSAT-CSM Input Parameter				
	Number of point locations	Maize cultivar	Planting date	Plant Population [plants/m ² (plants/acre)]	Row Spacing [cm (in)]
Story County, Iowa	88	PB 8	April 26 th	7.9 (30,000)	76 (30)
Livingston County, New York	110	AS 740	May 11 th		
Lancaster County, Pennsylvania	159	Cargill 111S	May 17 th		

Figure 4-1 illustrates the box plots of simulated county-level rain-fed maize both with and without incorporation of SMAP surface soil moisture data, while Figure 4-2 compares DSSAT simulated 5 cm soil moisture (without incorporation of remote sensing soil moisture data) and the corresponding SMAP surface soil moisture retrieval. For year 2015 in Story County, IA, the rain-fed maize crop received sufficient rainfall such that the crop yields with or without SMAP data incorporation were identical, even though the SMAP surface soil moisture estimates were clearly drier than the 5 cm soil moisture modeled in the DSSAT control experiment. In year 2016 however, the dry bias (relative to the DSSAT

control) caused a substantial reduction in modeled crop yield and a broadening of variability in the county-level estimate. In both years, modeled crop yields were not brought in closer agreement with the USDA reported mean county-level crop yield. For Livingston County, NY, SMAP surface soil moisture estimates were typically wetter than the DSSAT Control, and this translated to higher crop yields, but did not greatly reduce variability in the crop yields. For Lancaster County, PA, SMAP bias in surface soil moisture (relative to the DSSAT control) was not as clear as the other case study locations, as a result, DSSAT Control and DSSAT+SMAP crop yields were nearly identical. In evaluating the case studies collectively, the variability in modeled crop yield due to meteorological forcing data and model error (as assessed by deviation from the USDA reported county-level crop yield) appears to be much greater than can be mitigated by incorporation of SMAP surface soil moisture retrievals, especially when SMAP surface soil moisture retrievals may themselves be subject to substantial biases.

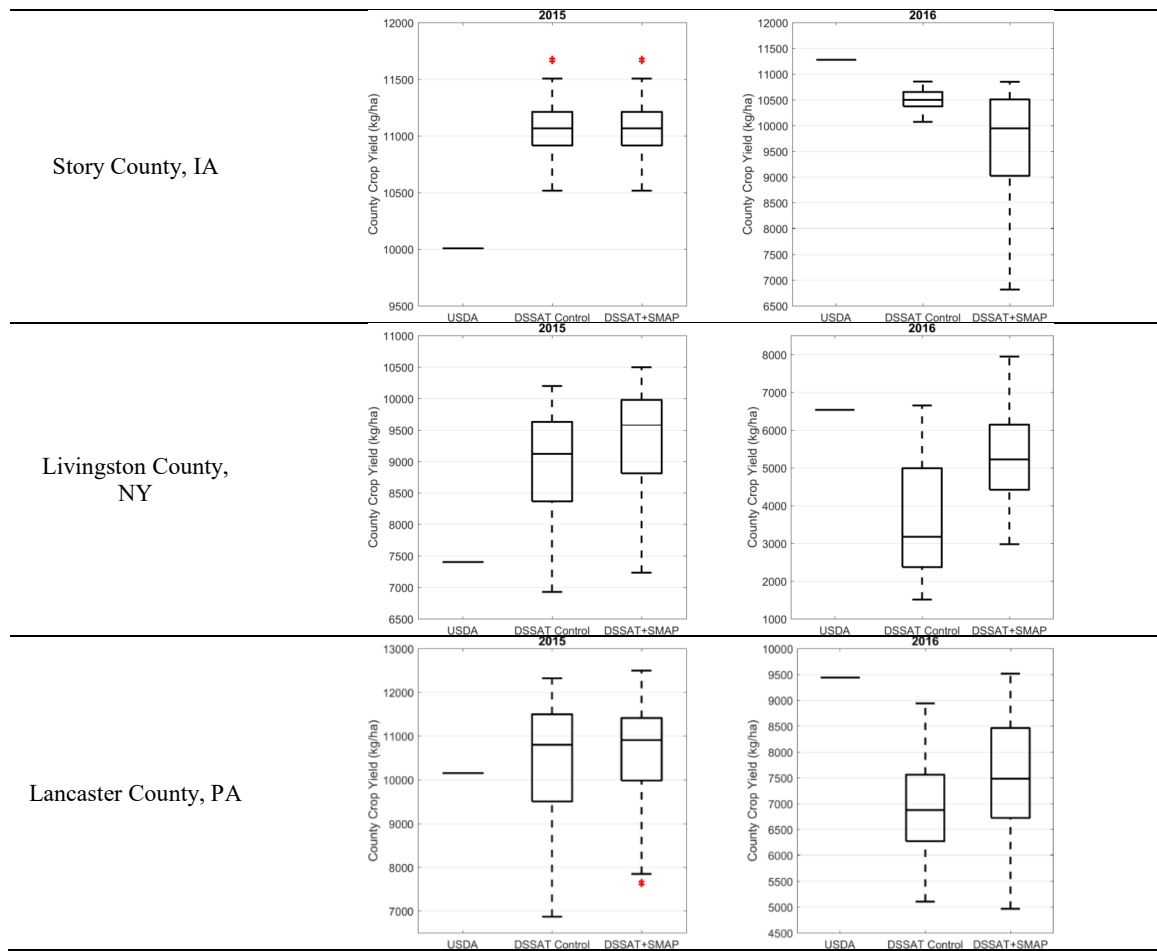


Figure 4-1: Box plots of simulated year 2015 and 2016 county-level rain-fed maize yield without SMAP data incorporation (DSSAT control) and with SMAP data incorporation (DSSAT+SMAP)

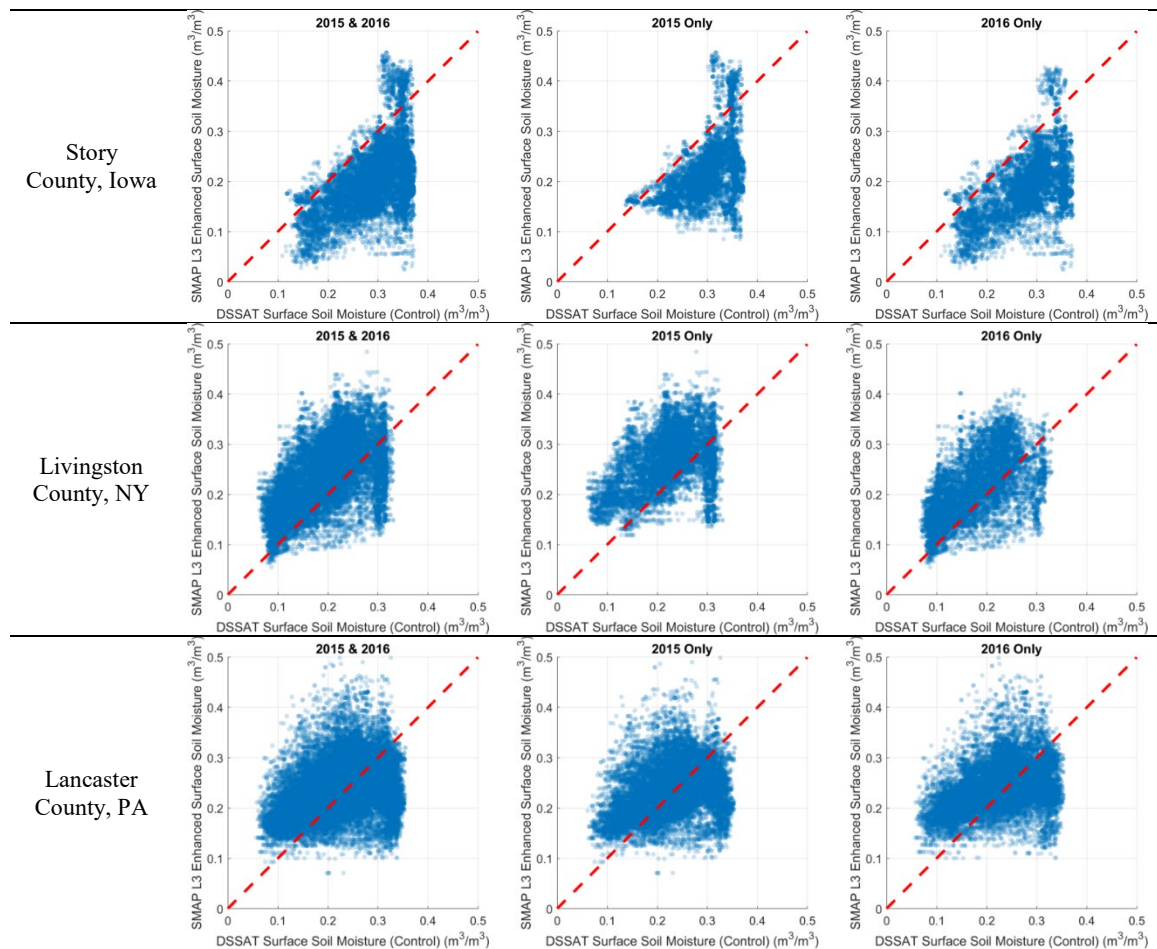


Figure 4-2: Comparison of DSSAT simulated and SMAP estimated surface soil moisture for the rain-fed maize case study locations

4.3 Incorporation of remote sensing GPM IMERG daily precipitation in DSSAT-CSM crop simulations

In the following case studies, daily cumulative precipitation estimates from the GPM IMERG Version 5 Late Release data product are incorporated into year 2015 and 2016 county-level rain-fed and irrigated maize DSSAT-CSM simulations. Simulations are also driven by daily meteorological forcing (excluding rainfall, as GPM IMERG is being used for precipitation forcing) from the GRIDMET data set and gridded soil profile data from the Harvest Choice Global High resolution Soil Profile Data set. DSSAT crop yield

estimates resultant from incorporation of GPM IMERG data are also compared with simulated crop yields without GPM IMERG data incorporation (referred to as DSSAT Control) to assess improved agreement with USDA NASS reported crop yields.

Table 4-2 lists some of the important input data and parameters for modeling of rainfed and irrigated maize for year 2015 and 2016. The case study counties in Iowa, New York, and Pennsylvania are entirely rainfed while the counties in Georgia, California, and Texas have crop acreages that are split between rainfed and irrigated acreages as listed in Table 4-3. For simulation of irrigated crops, the DSSAT-CSM “Automatic-Irrigation” option is used in which the simulated available soil moisture within a user specified depth is monitored daily. When the available soil moisture drops below a threshold percentage value, the DSSAT-CSM model applies irrigation on that day until the soil profile saturated. The DSSAT-CSM model is run at multiple point locations within the county boundaries. The same locations are used for the control run simulations and simulations that incorporate GPM IMERG estimates of daily precipitation. With regard to gridded data, DSSAT simulations are driven by data from the pixel nearest to each point location. To facilitate comparison of simulated crop yields with USDA NASS reported yields, USDA yields are converted from bushels per acre to kilograms per acre with an assumed moisture content of 15.5 percent.

Table 4-2: Calibrated input parameters for rainfed and irrigated county-level DSSAT-CSM maize simulations.

Location	DSSAT-CSM Input Parameter				
	Number of point locations	Maize cultivar	Planting date	Plant Population [plants/m ² (plants/acre)]	Row Spacing [cm (in)]
Story County, Iowa	88	PB 8	April 26 th	7.9 (30,000)	76 (30)
Livingston County, New York	110	AS 740	May 11 th		
Lancaster County, Pennsylvania	159	Cargill 111S	May 17 th		
Miller County, Georgia	36	PIO 3382	March 29 th		
San Joaquin County, California	218	PB 8	April 8 th		
Wayne County, Nebraska	70	DK 611	May 4 th		
Dallam County, Texas	231	WASH-GRAIN-1	March 15 th		

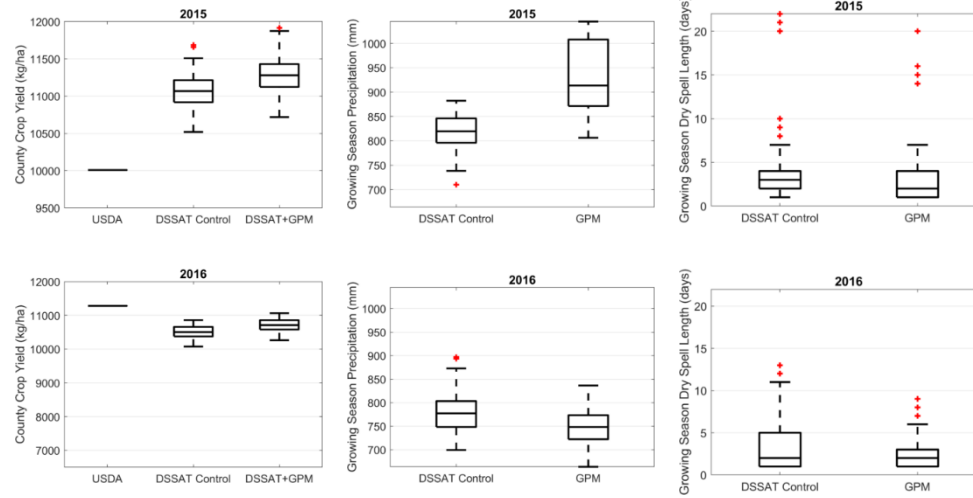
Table 4-3: Calibrated DSSAT-CSM input parameters for automatic-irrigation of maize

Location	DSSAT-CSM Automatic-Irrigation Input Parameter		
	Percentage of acreage with irrigation (%)	Soil moisture monitoring depth [cm (in)]	Available soil moisture threshold (%)
Miller County, Georgia	77	30 (12)	50
San Joaquin County, California	100		70
Wayne County, Nebraska	20		50
Dallam County, Texas	47		

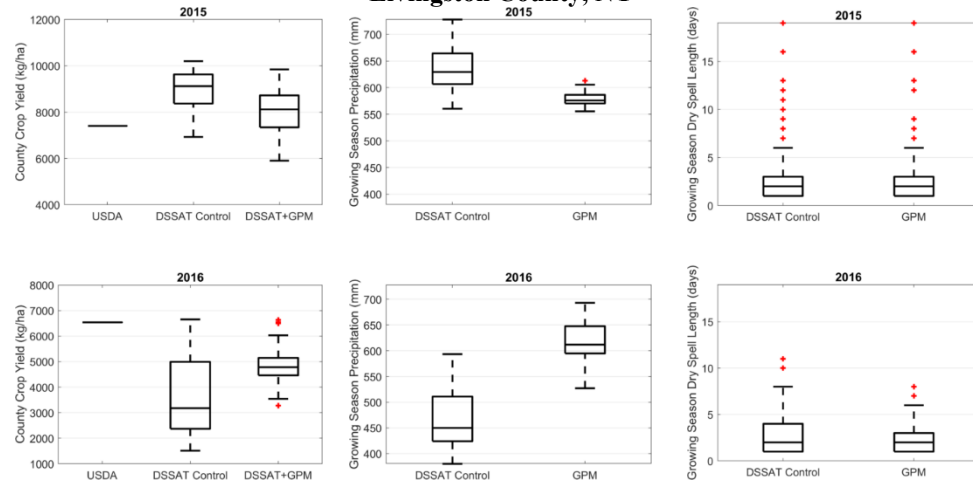
As shown in the box plots of maize yield and irrigation amount in Figure 4-3, incorporation of remote sensing precipitation data makes a substantial difference in model results; however, it is not clear that incorporation of GPM IMERG data improves the accuracy DSSAT-CSM simulated yields relative to USDA reported yields. For Story County (year 2015), Livingston County (year 2016), Miller County (year 2015), San Joaquin County (years 2015 and 2016), Wayne County (years 2015 and 2016), and Dallas

County (years 2015 and 2016), overestimation of growing season precipitation (relative to the GRIDMET reference) led to increased crop yields and reduced irrigation demand. Cases in which the amount of overestimation in GPM growing season precipitation exceeds the amount of underestimation in irrigation application suggest that extreme events are being overestimated by GPM IMERG. When this data is incorporated into DSSAT, large amounts of runoff and drainage from the bottom of the soil profile (both types of water are useless to crops) are estimated by the DSSAT-CSM model. The difference in dry spell lengths (consecutive days of zero precipitation during the growing season), between the GRIDMET reference and GPM IMERG also impact modeled crop yield results. At the Story County, Iowa 2016 and Miller County, Georgia 2016 locations, cumulative growing season precipitation was less in the GPM IMERG product than in the GRIDMET reference; however, crop yields driven by GPM IMERG data were still higher than the control scenario. This is attributed to the shorter dry spell lengths in the remote sensing precipitation product.

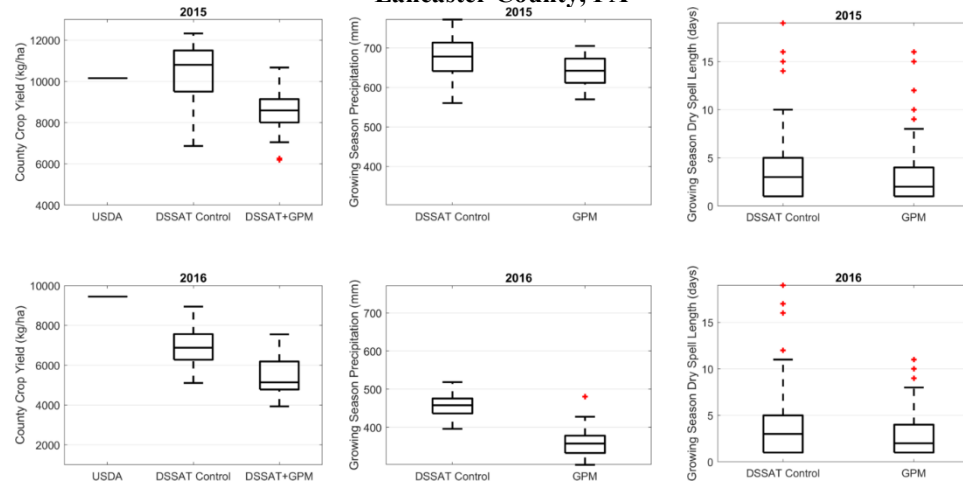
Story County, IA



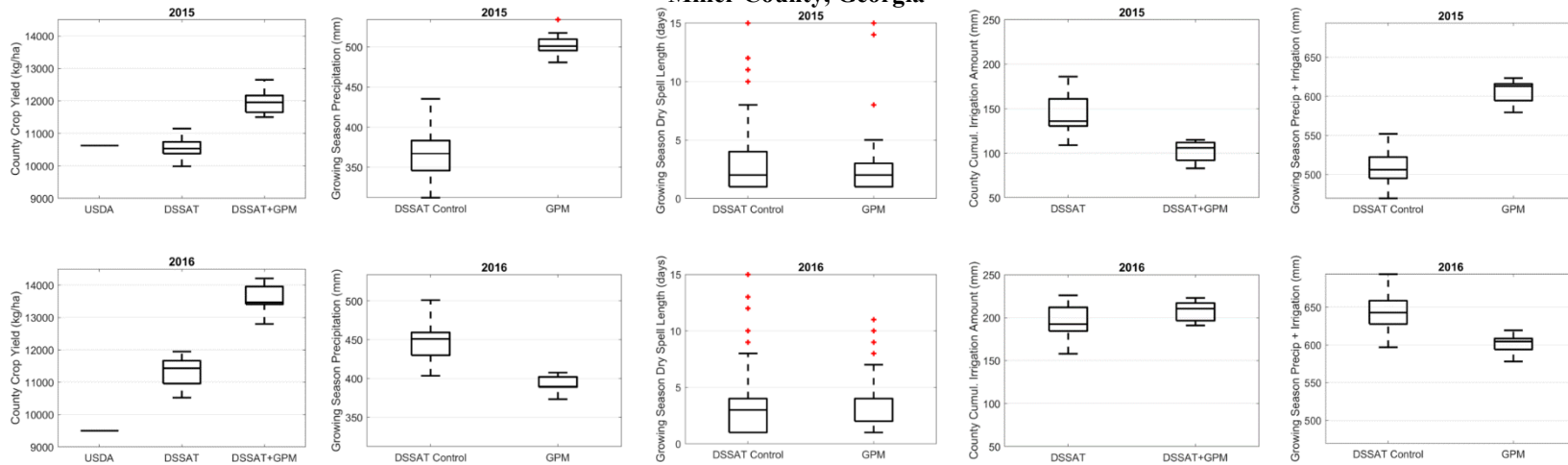
Livingston County, NY



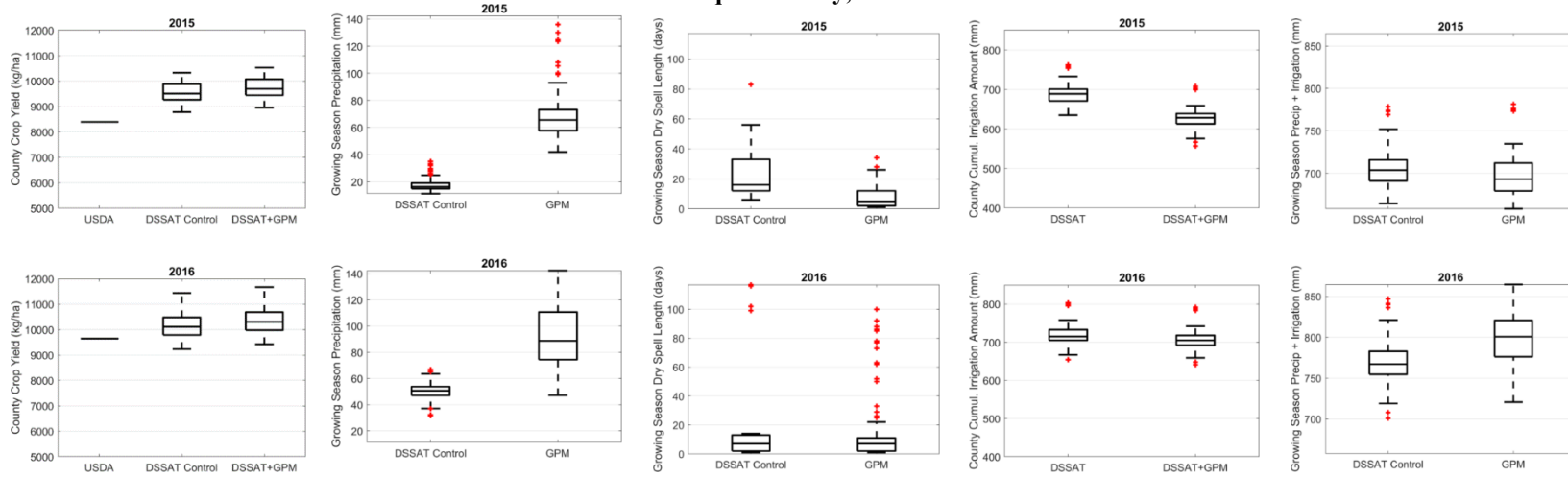
Lancaster County, PA



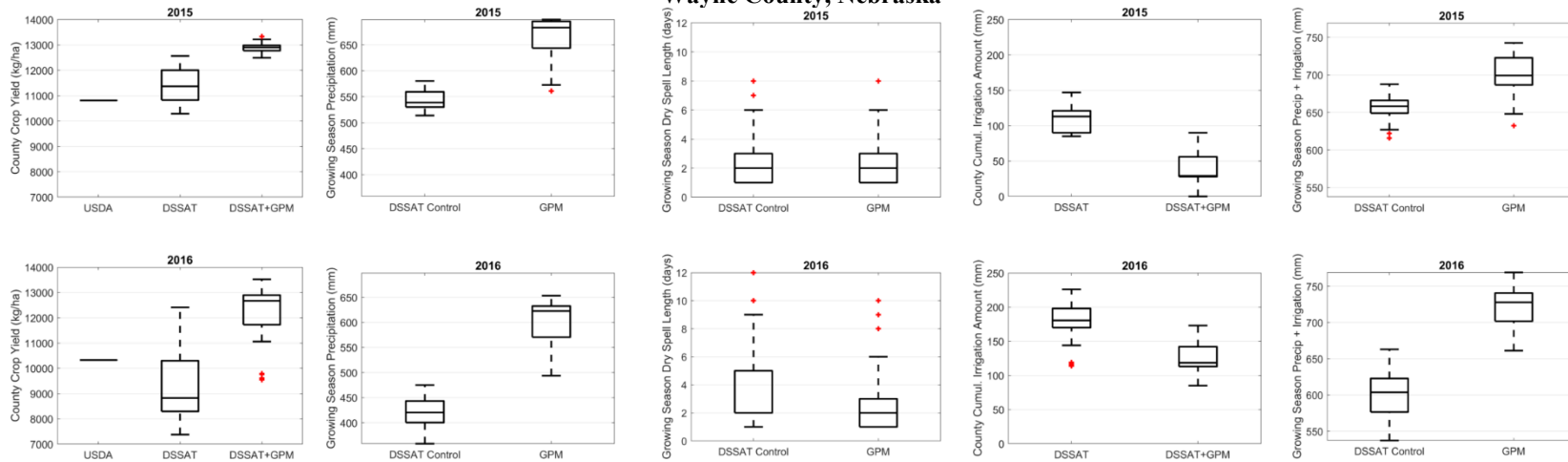
Miller County, Georgia



San Joaquin County, California



Wayne County, Nebraska



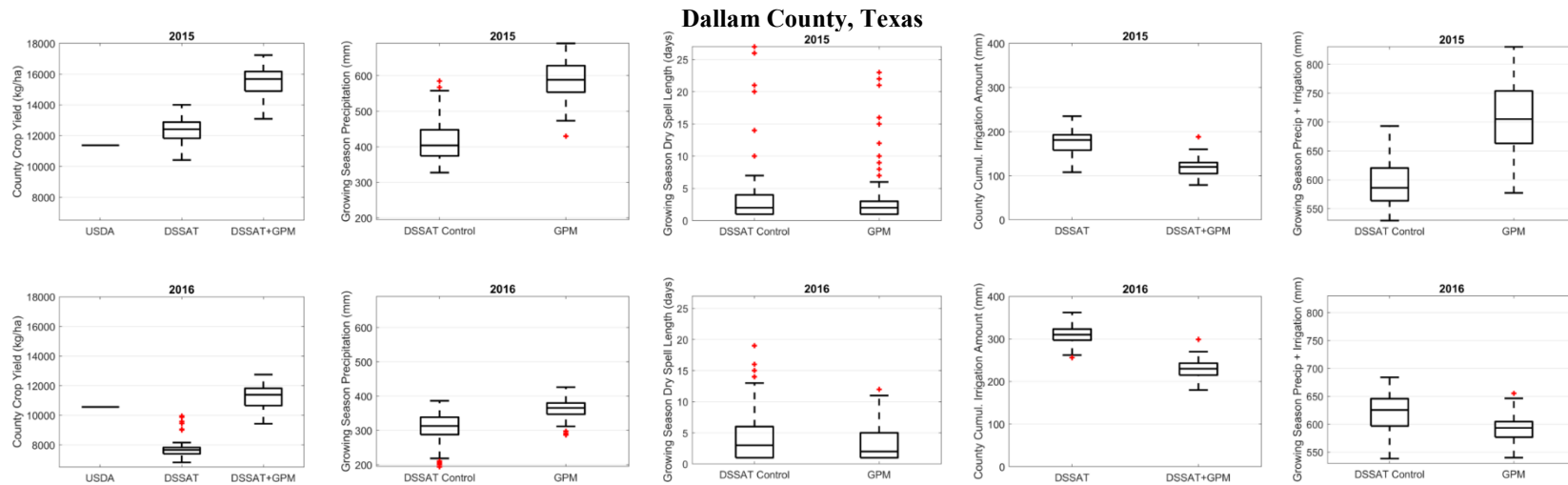


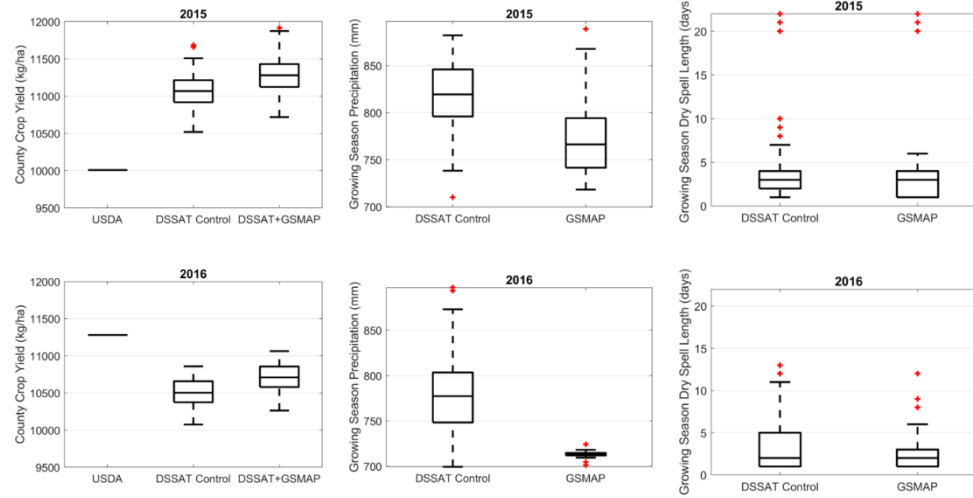
Figure 4-3: Box plots of simulated year 2015 and 2016 county-level maize yield and irrigation amount without GPM IMERG data incorporation (DSSAT Control) and with GPM IMERG data incorporation. Box plots of growing season cumulative precipitation and consecutive dry days derived from GRIDMET (DSSAT Control) and GPM IMERG are also provided for reference.

4.4 Incorporation of remote sensing JAXA GSMP daily precipitation products in DSSAT-CSM crop simulations

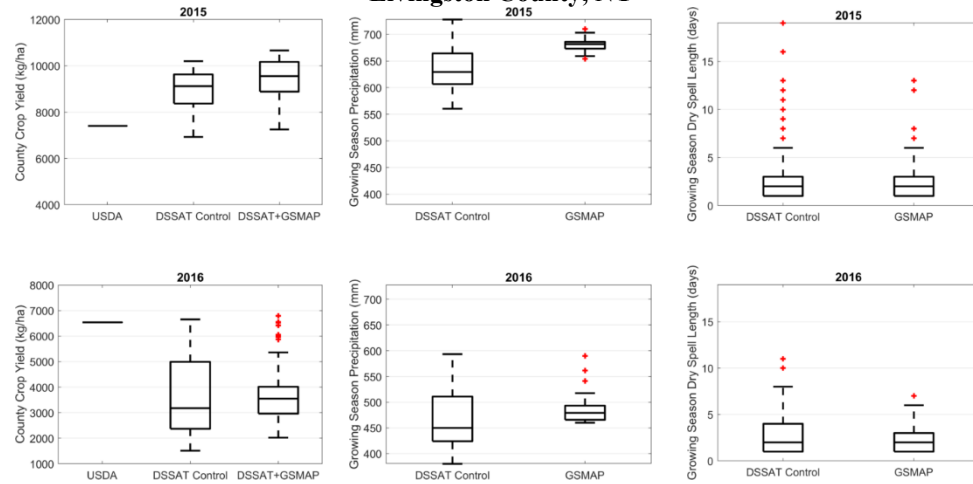
In this section, DSSAT-CSM crop simulations incorporating remote sensing retrievals of daily cumulative precipitation are carried out with the same method as the previous section, except that instead of GPM IMERG data, JAXA GSMP-Gauge data is incorporated into the DSSAT-CSM model.

As shown in the box plots of maize yield and irrigation amount in Figure 4-4, incorporation of remote sensing precipitation data makes a substantial difference in model results; however, it is not clear that incorporation of GSMP-Gauge data improves the accuracy DSSAT-CSM simulated yields relative to USDA reported yields. In general, growing season rainfall in the GSMP-Gauge data product is in closer agreement with the GRIDMET reference than the GPM IMERG Late Release Version 5 data product. The GSMP-Gauge data also appears to be more spatially homogenous than GPM IMERG as evidenced by the relatively smaller spread in growing season precipitation and simulated irrigation amount for some of the case study sites. However, similar to the conclusion from incorporating SMAP surface soil moisture estimates in the DSSAT model, errors in remote sensing retrieval or precipitation, combined with errors in the DSSAT model, are still too large to be mitigated by remote sensing retrievals of daily precipitation. At the Story County, Iowa 2015 and 2016; Miller County, Georgia 2015 and 2016; and Dallam County, Texas 2015 locations, cumulative growing season precipitation was less in the GSMP-Gauge product than in the GRIDMET reference; however, crop yields driven by GSMP-Gauge data were still higher than the control scenario. This is attributed to the shorter dry spell lengths in the remote sensing precipitation product.

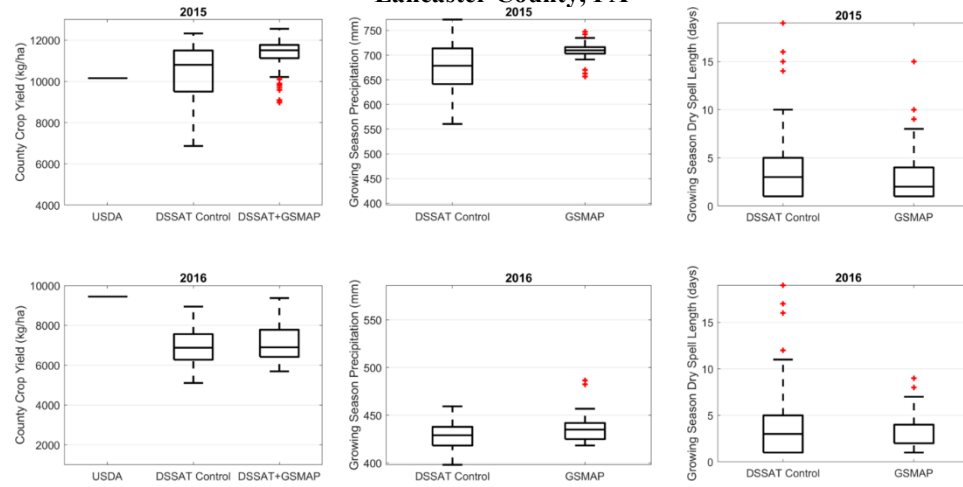
Story County, IA



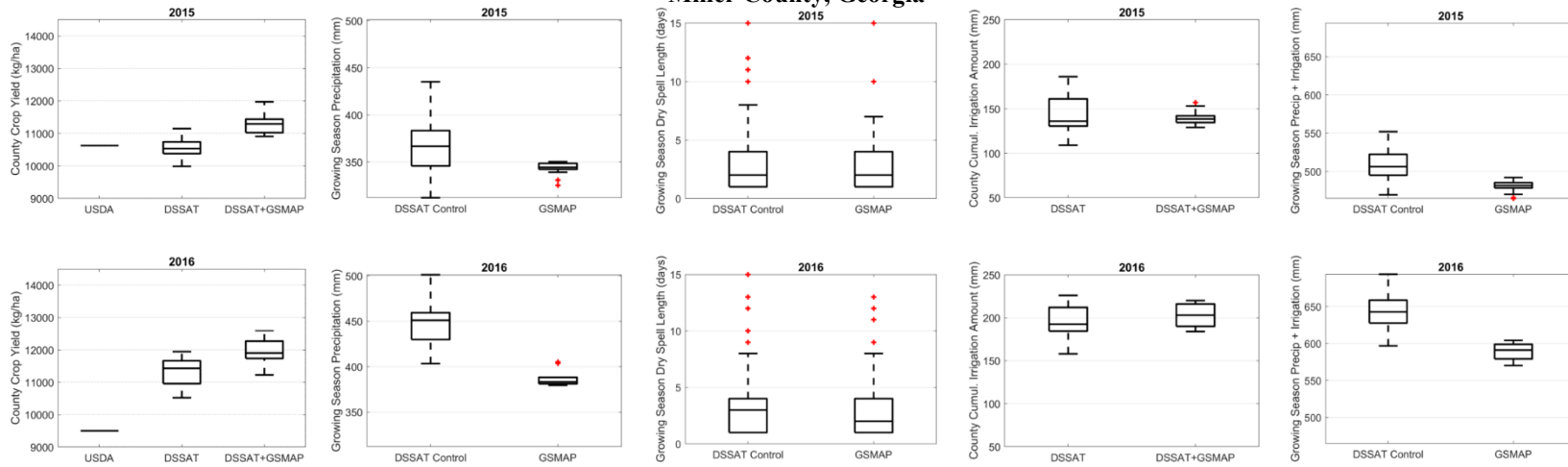
Livingston County, NY



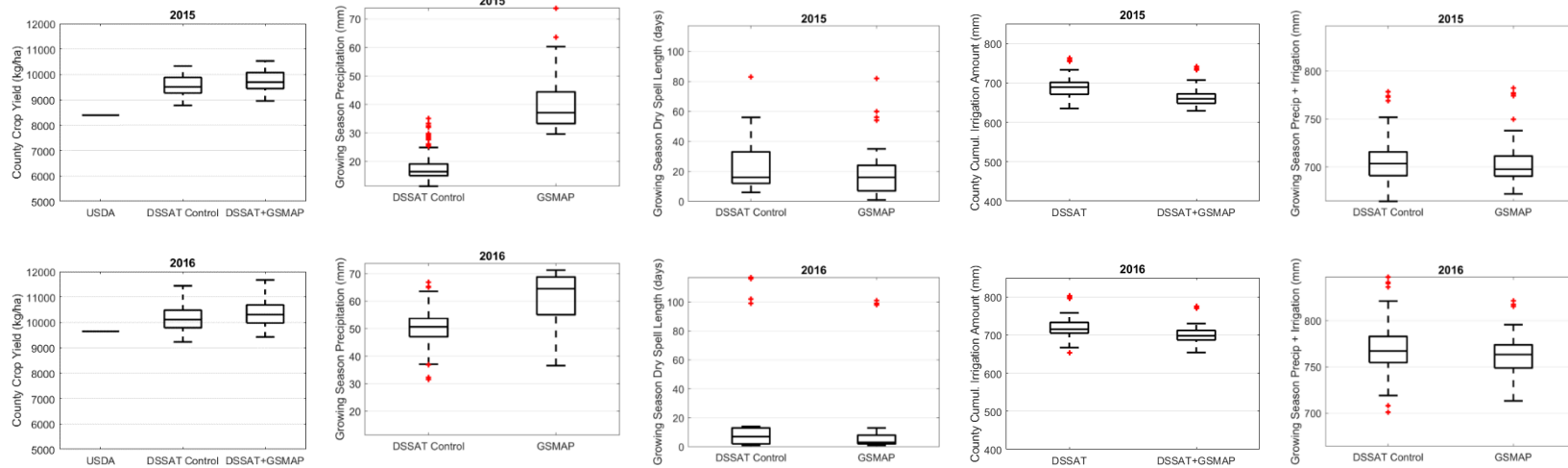
Lancaster County, PA



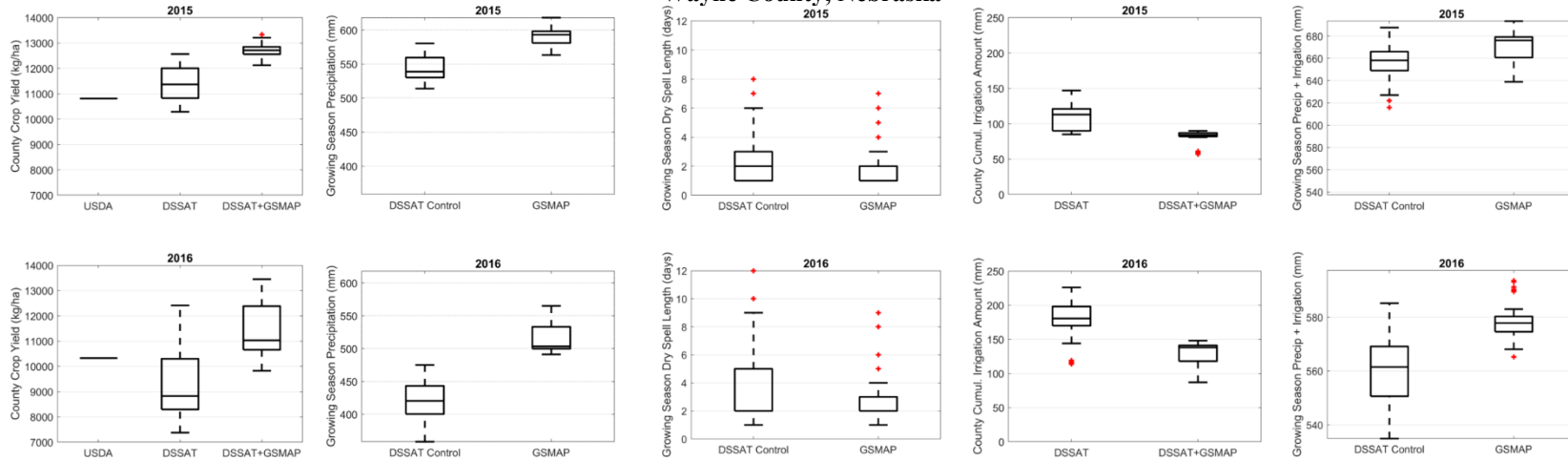
Miller County, Georgia



San Joaquin County, California



Wayne County, Nebraska



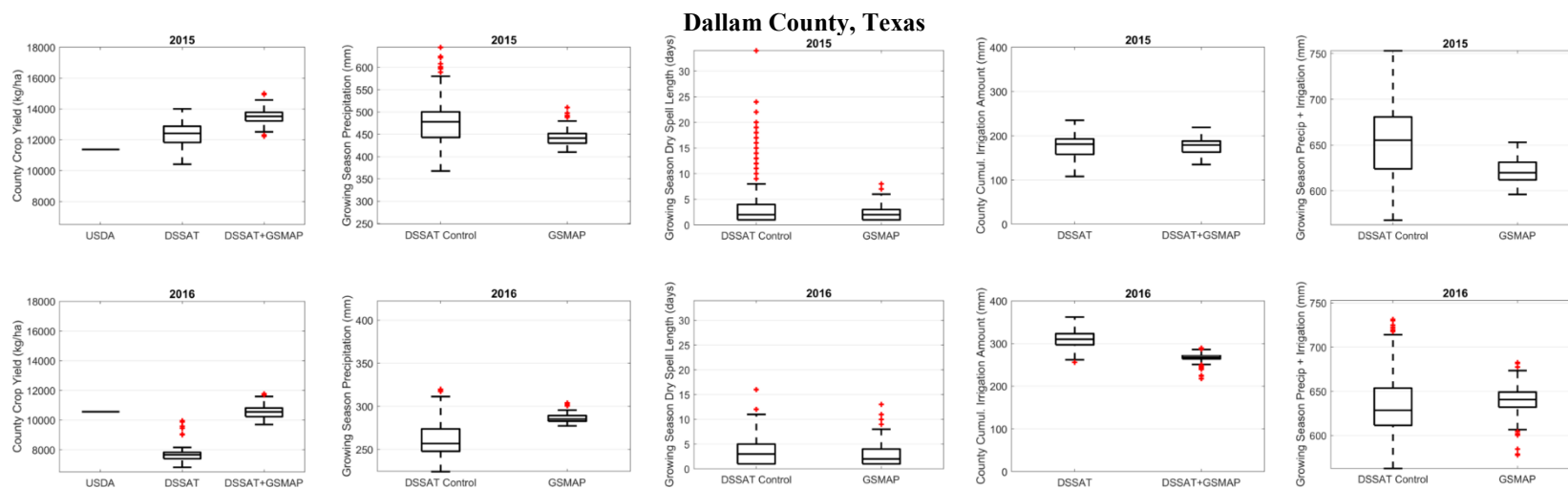


Figure 4-4: Box plots of simulated year 2015 and 2016 county-level maize yield and irrigation amount without JAXA GSmaP-Gauge data incorporation (DSSAT Control) and with GSmaP-Gauge data incorporation. Box plots of growing season cumulative precipitation and consecutive dry days derived from GRIDMET (DSSAT Control) and GSmaP-Gauge are also provided for reference.

4.5 Historical Climate Variability and Crop Yield / Irrigation Assessment: Case Study in the Apalachicola-Chattahoochee-Flint (ACF) River Basin

In this case study, multi-sensor gridded data products including University of Idaho GRIDMET daily meteorological data (GRIDMET), HarvestChoice Global high-resolution soil profile database for crop modeling applications (HC-GHRSPD), and USDA-NASS CropScape Cropland Data Layer, are innovatively integrated with the DSSAT cropping system model (DSSAT-CSM) to assess crop yield and irrigation demand for various staple crops harvested in the Apalachicola-Chattahoochee-Flint (ACF) river basin. The top crops grown in the region include peanuts, corn, soybeans, and cotton.

The ACF basin and its 14 sub-basins (located in the states of Georgia, Alabama, and Florida, USA) are shown in the figure below. In this study, the impact of historical climate variability on current (year 2016) cropping and irrigation practices in each of the 14 ACF sub-basins is assessed.

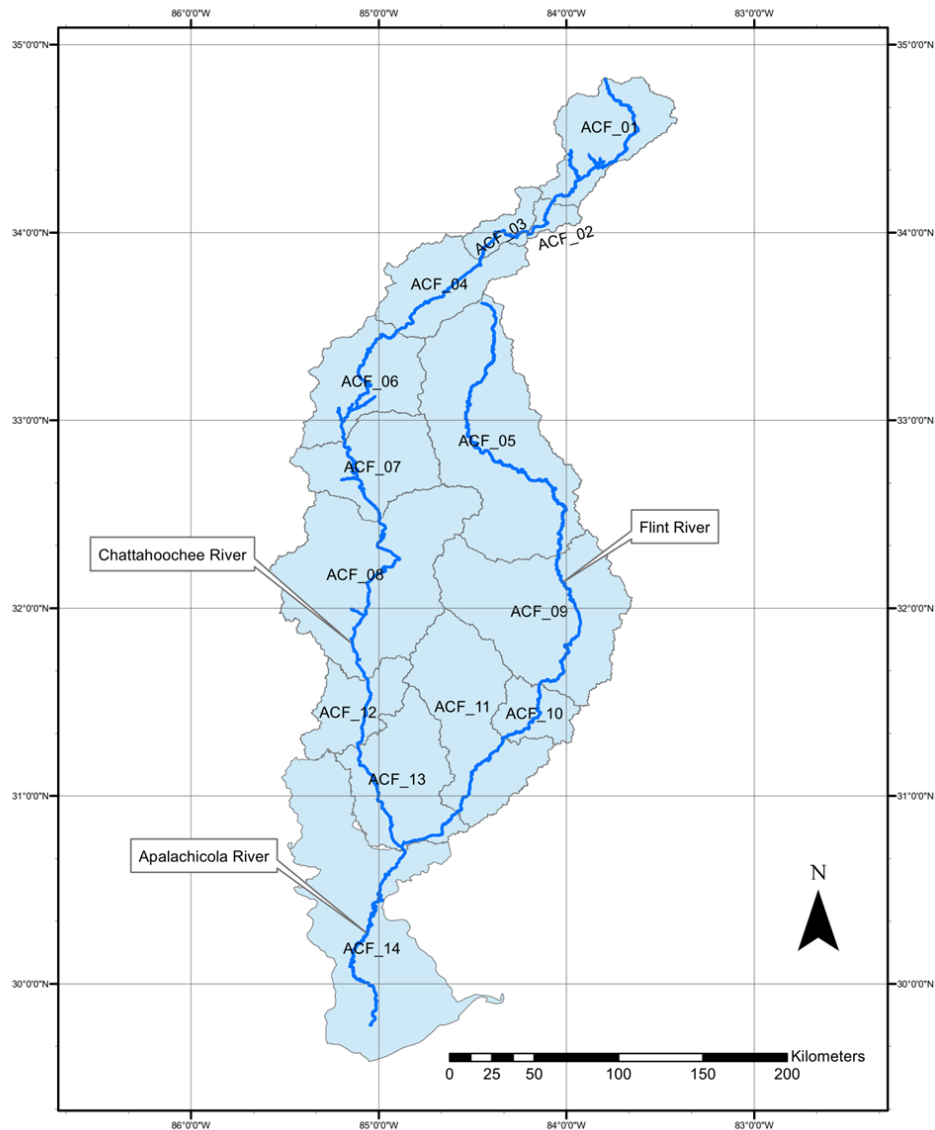


Figure 4-5: A map of the ACF basin and its 14 sub-basins.

To simulate crops at multiple point locations, the location coordinates (latitude-longitude pairs) for each crop field of interest within each of the ACF sub-basins are extracted from the pixels of the USDA-NASS CropScape data set from year 2016. The number of CDL single-planting field pixels (in year 2016) were identified for each major crop in the ACF sub-basins as listed in the following table.

Table 4-4: Quantity of 30 x 30 m² single-planting corn, peanut, cotton, and soybean field pixels identified in the 2016 USDA-NASS Cropland Data Layer for each ACF sub-basin.

ACF	Quantity of USDA-NASS CDL Pixels				
Sub-basin	Corn	Peanut	Cotton	Soybean	All Crops
1	11,193	1	9	1,486	12,689
2	13	0	0	48	61
3	86	0	0	40	126
4	179	0	38	257	474
5	20,999	11,487	44,690	46,998	124,174
6	2,214	1	510	1,077	3,802
7	2,016	13	380	2,910	5,319
8	18,561	40,692	65,383	3,351	127,987
9	239,078	262,004	732,300	62,665	1,296,047
10	51,905	55,931	76,923	2,792	187,551
11	297,168	460,481	552,651	37,226	1,347,526
12	32,567	109,355	120,469	9,698	272,089
13	190,871	450,847	459,888	21,702	1,123,308
14	27,201	196,768	182,688	16,462	423,119

This assessment uses the University of Idaho GRIDMET gridded meteorological data set. For computational efficiency, the individual crop fields (identified earlier) are each mapped to the nearest 4 x 4 km² pixel of the GRIDMET. Then, DSSAT-CSM is run to simulate the annual crop yield from 1980–2016 (37 years) with GRIDMET meteorological forcing and soil characterization data from the HarvestChoice Global High-Resolution Soil Profile Database (HC-GHRSPD). Model results (rainfed and irrigated crop yields as well as irrigation amounts) are subsequently weighted and aggregated based on the number of crop fields mapped to a unique pixel of GRIDMET meteorological forcing. This procedure allows us to capture the impact of spatial variability in sub-basin weather on crop yield and irrigation demand without the computational expense of running DSSAT-CSM for each 30 x 30 m² crop field in the ACF sub-basins.

4.5.1 DSSAT-CSM Calibration

DSSAT-CSM calibration for rainfed crop simulation requires selection of the crop cultivar, planting date, row spacing, and plant population. Simulation of irrigated crops additionally requires specification of a soil moisture management depth and corresponding available soil-water content threshold to trigger an irrigation application using DSSAT-CSM's "Auto-Irrigation" Water Management Option. The option to simulate nitrogen stress is also available and has been incorporated into the cotton simulations which are particularly sensitive to nitrogen stresses. The remaining crops, (corn, peanut, and soybean) are assumed to have all their nitrogen demands met during the growing season, thus, nitrogen stress is not modeled for those crops. Using historical data from USDA on reported corn crop yields and assumptions regarding typical irrigation practices in the ACF region, the calibration inputs for rainfed and irrigated corn, peanut, cotton, and soybean simulations were specified as shown in the table below.

Table 4-5: DSSAT-CSM input parameters for the rainfed and irrigated corn, peanut, cotton, and soybean simulations in the ACF basin.

Model Parameter	Corn	Peanut	Cotton	Soybean
Planting Date (1980-2016)	March 29 th	May 16 th	May 5 th	May 25 th
Cultivar	B73 X MO17	Georgia Green	DP 555 BG/RR	DP 5634 (Maturity Group V)
Row Spacing	30 inches (76 cm)	36 inches (90 cm)	36 inches (90 cm)	30 inches (76 cm)
Plant Population	30,000 plants/acre (7.9 plants/m ²)	85,000 plants/acre (21 plants/m ²)	50,000 plants/acre (12.4 plants/m ²)	90,000 plants/acre (22.2 plants/m ²)
Irrigation: Soil Management Depth	12 inches (30 cm)	20 inches (50 cm)	12 inches (30 cm)	12 inches (30 cm)
Irrigation: Available soil water content threshold	50%	60%	50%	50%
Nitrogen Fertilizer	Nitrogen stress not simulated	Nitrogen stress not simulated	45 lbs/acre (50 kg/ha) of N fertilizer applied at 4 inch (10 cm) depth at planting and again at 46 days after planting	Nitrogen stress not simulated

4.5.2 ACF Assessment Methodology

For each crop in each ACF sub-basin, the simulated rainfed and irrigated yields for present-day (2016) crop fields forced by historical (1980-2016) meteorological conditions are illustrated in time-series plots. Crop yields are reported in dry mass units normalized by area (kilogram/hectare). Similarly, the modeled irrigation demand is also reported. Variability bars are included for each year of meteorological forcing to show the variability of modeled crop yield and irrigation demand (due to variation in meteorological forcing and soil property data) in each sub-basin. This exercise assesses how present-day rainfed and irrigated fields would have produced had they been subjected to the historical meteorology. These results could reasonably be extrapolated to estimate the actual historical production and total amount of water used by these major crops of the agricultural sector if the total area of rainfed and the total area of irrigated crop fields are known for each historical year and for each sub-basin.

Included with each figure are corresponding linear regression equations with the probability that the estimated slope of the linear trend (in units of kg/ha per year for crop yield and depth units of mm per year for irrigation demand) is greater than zero. The regression equations are estimated using Bayesian Linear Regression. Under the conservative assumption of non-informative priors for the regression parameters, Bayesian Linear Regression provides a data-dominated and analytical derivation of the posterior probability distribution of the trend – a non-central Student t-distribution (Elster et al. 2015) – and thereby facilitates a more comprehensive assessment of the trend's direction (e.g., positive or negative) than provided by traditional, frequentist simple linear regressions (Kéry 2010; Baldwin and Larson 2017). As indicated in Figure 4-6, once the

posterior probability distribution of the linear regression slope parameter is derived, the certainty regarding slope's direction can be characterized in terms of intuitively meaningful probability statements (e.g “the slope is very likely positive”, “the slope is virtually certain to be negative”, etc.) based on what proportion of the slope probability distribution lies to the right of zero, indicated as “+prob” in subsequent figures. For convenience, the probability statements and associated probability ranges used in this study are modified from those adopted by the Intergovernmental Panel on Climate Change (IPCC) in their most recent assessment report (IPCC 2014).

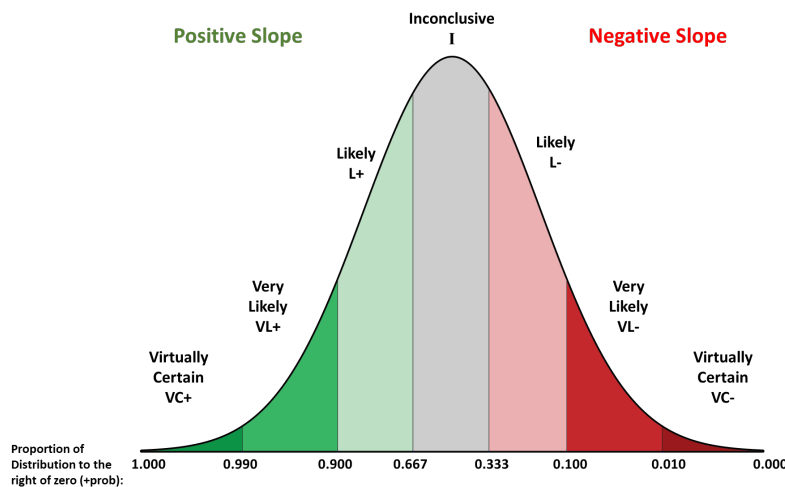


Figure 4-6: an example posterior Student t-distribution for the regression slope determined using Bayesian Linear Regression. Probability statements (with concise abbreviations) describe the certainty regarding the slope's sign (i.e. positive or negative).

The assessments presented here do not incorporate the influence of technology innovation on crop yield. Crop yield gains due to technology innovations are significant and need to be considered when comparing simulated versus observed crop yield data; this investigation however, focuses on the impact of historical climate variability on yield and irrigation demand given current crop management and irrigation practices and technology.

4.5.3 ACF Assessment Results: Corn

Figure 4-7 illustrates the simulated rainfed corn yields for present-day (2016) corn fields forced by historical (1980–2016) meteorological conditions for each of the ACF sub-basins. The figure also indicates the mean crop yield (in units of kilograms of dry weight per hectare, kg/ha) for the 37 year period (1980 – 2016) , and two 18 year periods (1980 – 1997, and 1998 – 2015) along with corresponding annual trends (calculated using the previously mentioned Bayesian linear regression methodology) and the probability of these trends being positive. During the 1980 – 2016 historical period, the ACF sub-basins in the Lower portions of the Chattahoochee and Flint basins and the Apalachicola basin (sub-basins 10 to 14) show rainfed corn crop yields that are “likely” or “very likely” decreasing annually. Furthermore, the results show that after 2005, agricultural droughts are increasing in intensity and duration, compared to the pre-2005 period, especially in the southern sub-basins. Analysis of the two 18-year periods (1980 – 1997 and 1998 – 2015) in sub-basins 10 to 14 shows that the decline in rainfed crop yield is a phenomenon of the latter period, as the mean rainfed crop yield during the 1998 – 2015 period is 13 to 21 percent less than that of the 1980 – 1997 period.

Corn (Rainfed - Mean Crop Yields)

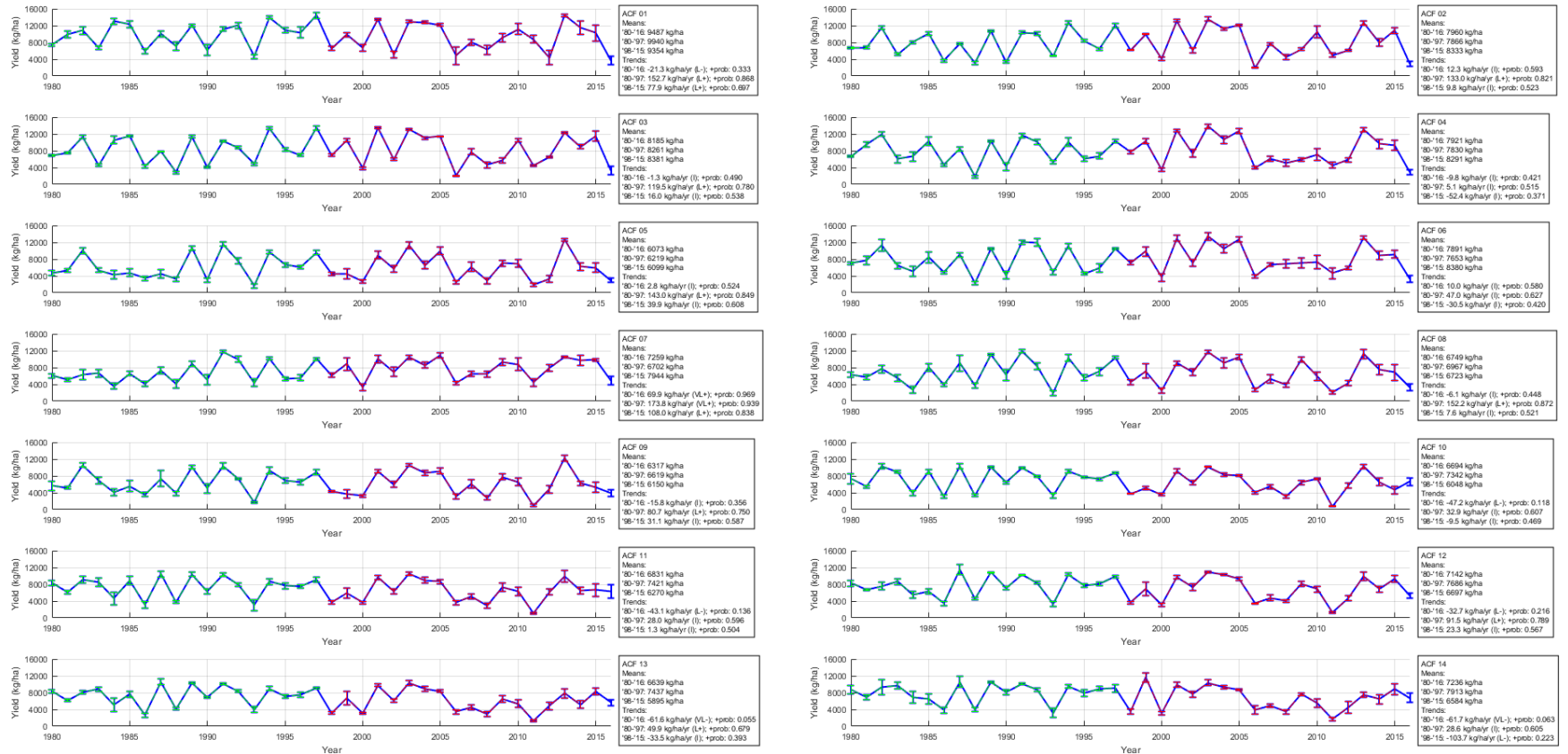


Figure 4-7: Simulated ACF mean *rainfed* corn yield for 1980–2016 and present-day corn fields.

Figure 4-8 and Figure 4-9 illustrate the simulated irrigated yields and corresponding irrigation amounts for present-day (2016) corn fields forced by historical (1980–2016) meteorology for each ACF sub-basin. Similar to the rainfed analysis, mean and trend information is also presented for the 1980 – 1997 and 1998 – 2015 periods. Simulation results show that irrigated corn yields are increasing annually in the northern sub-basins (which are not heavily cropped), but decreasing in the more heavily cropped southern sub-basins. The post-2005 period clearly shows that the demand for water has markedly increased in response to the increased severity and duration of agricultural droughts. In the southern half of the ACF, the impact of the year 2011 drought stands out with over 300 mm of irrigation demand, the greatest simulated demand for the entire 1980 – 2016 period. A review of local and national news during summer 2011 confirms the severe effects of this historic drought. The New York Times (Severson and Johnson 2011) reported:

COLQUITT, Ga. — The heat and the drought are so bad in this southwest corner of Georgia ... Corn, a lucrative crop with a notorious thirst, is burning up in fields. Cotton plants are too weak to punch through soil so dry it might as well be pavement.

Farmers with the money and equipment to irrigate are running wells dry in the unseasonably early and particularly brutal national drought that some say could rival the Dust Bowl days.

Another finding from this analysis is that despite the “very likely” positive trend in applied irrigation in the southern half of the ACF, these sub-basins surprisingly still report decreasing irrigated corn yield. This indicates that some climatic variable, other than water availability (through precipitation and irrigation), impacts corn yield negatively. After

examination of the ACF meteorological data, the declining yield trend is attributed to the change of the mean daily and minimum daily temperatures. Assessment of GRIDMET air temperature data shows that both of these temperatures are steadily increasing in recent years. Furthermore, a temperature-plant stress relationship is known to exist limiting carbohydrate production when daily temperature exceeds the ideal temperature for photosynthesis (DSSAT-CSM captures this relationship through a quadratic penalty function). For corn in particular, the ideal daily temperature is 26 degrees Celsius (Ritchie et al. 1998).

Lastly, Figure 4-9 shows that the irrigation amount to achieve optimal crop yield varies markedly from year to year depending on drought conditions. This is true for all ACF sub-basins but especially for sub-basins 6 to 14, after 2005. The assessment results show that minimum, average, and maximum irrigation amounts have increased considerably in recent years, with the maximum irrigation often exceeding mean irrigation by 100%. Similar results were also found for the irrigation depths of the other crops investigated in this study.

The agricultural assessments presented here are consistent with the climatological trends in the ACF, which indicate that seasonal air temperature is increasing and seasonal precipitation is decreasing in the majority of ACF sub-basins. These findings suggest a decline in crop water productivity (amount of crop yield per unit of irrigation application/precipitation) and raise concerns about the long term sustainability of the current water and agricultural management practices.

Corn (Irrigated) - Mean Crop Yields

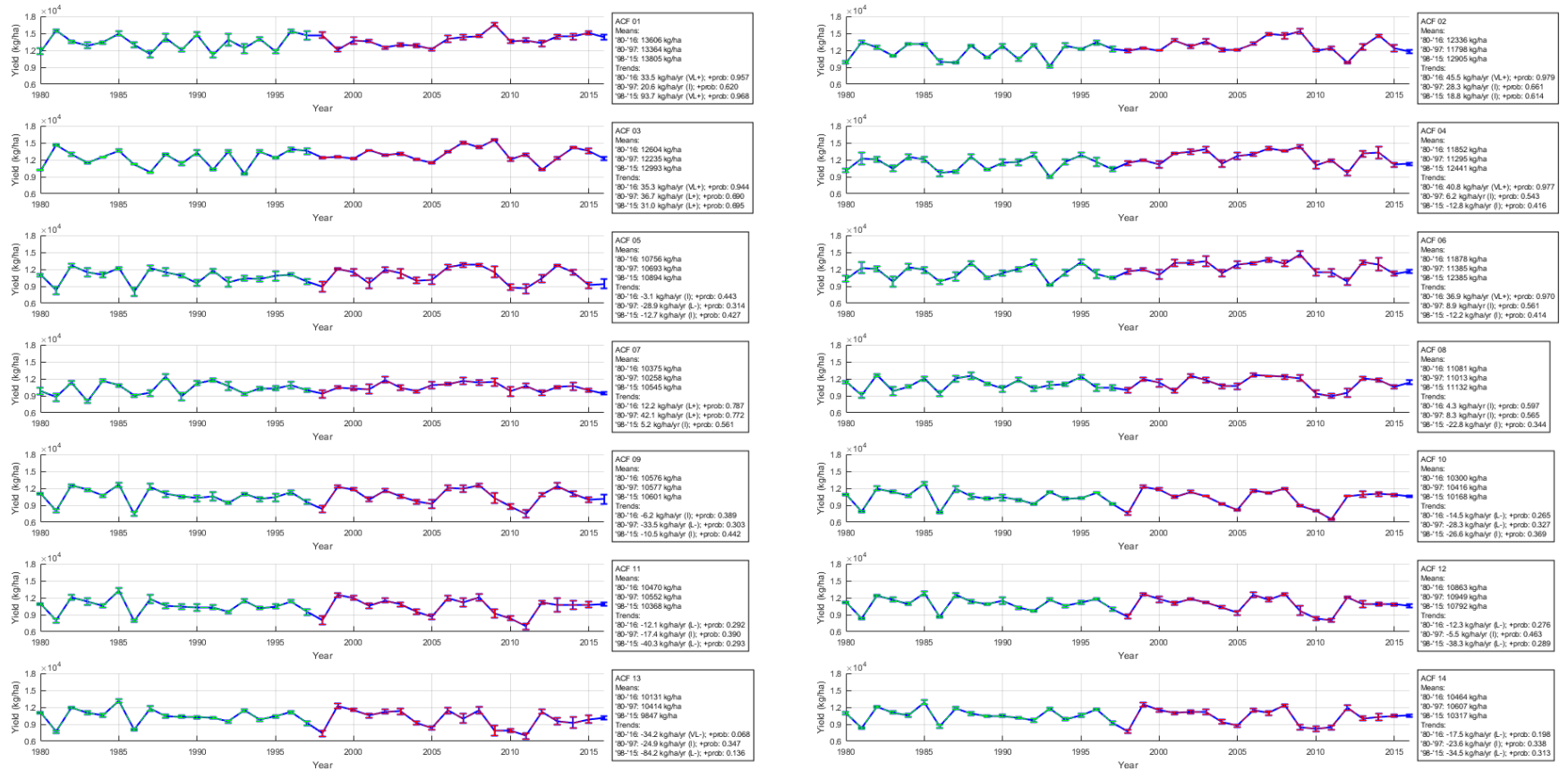


Figure 4-8: Simulated ACF mean irrigated corn yield for historical meteorology and present-day corn fields.

Corn (Irrigated - Mean Irrigation Amount)

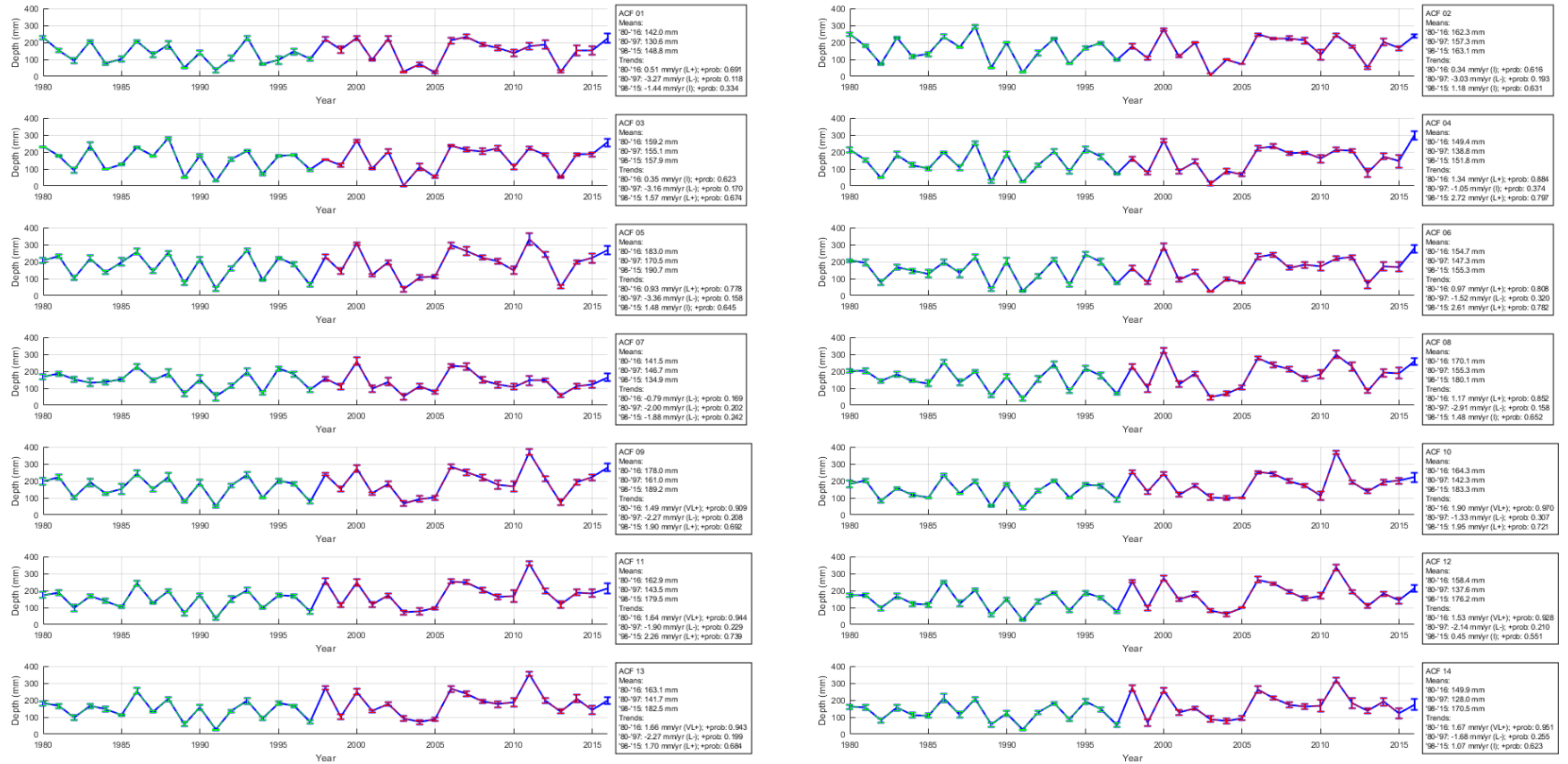


Figure 4-9: Simulated ACF mean irrigation amount for historical meteorology and present-day corn fields.

4.5.4 ACF Assessment Results: Peanut

Figure 4-10 illustrates the DSSAT-CSM simulated rainfed peanut yields for present-day (2016) peanut fields forced by historical (1980–2016) meteorological conditions for each of the ACF sub-basins. In contrast with corn (discussed earlier) ACF sub-basins with significant peanut acreage do not generally report a strong trend when considering the full 1980 – 2016 period. However, when focusing on the 1998 – 2015 period, sub-basins 9 – 14 show relatively strong trends that are either “likely” or “very likely” negative. During the 1980 – 1997 period, these sub-basins report rainfed peanut yields increasing by 20 to 32 kg/ha (dry weight) per year; however, during the 1998 – 2015 period, nearly all sub-basins report rainfed peanut yields as *decreasing* by 30 to 60 kg/ha per year. It is noted that in spite of the trend reversal, mean rainfed peanut yield during the 1998 – 2015 period generally exceeds that of the 1980 – 1997 period. However, this finding is attributed to a short-lived benefit that peanut crops may receive, in the absence of water stress, from rising temperatures (until an optimal temperature threshold is surpassed) and increased atmospheric CO₂ concentrations. The analysis of irrigated peanut yields which follows highlights the ephemeral nature of these positive influences on peanut yield as increases in irrigated peanut yield are slowed during the 1998 – 2015 period despite raised temperatures, increased CO₂ concentrations, and the absence of water stress.

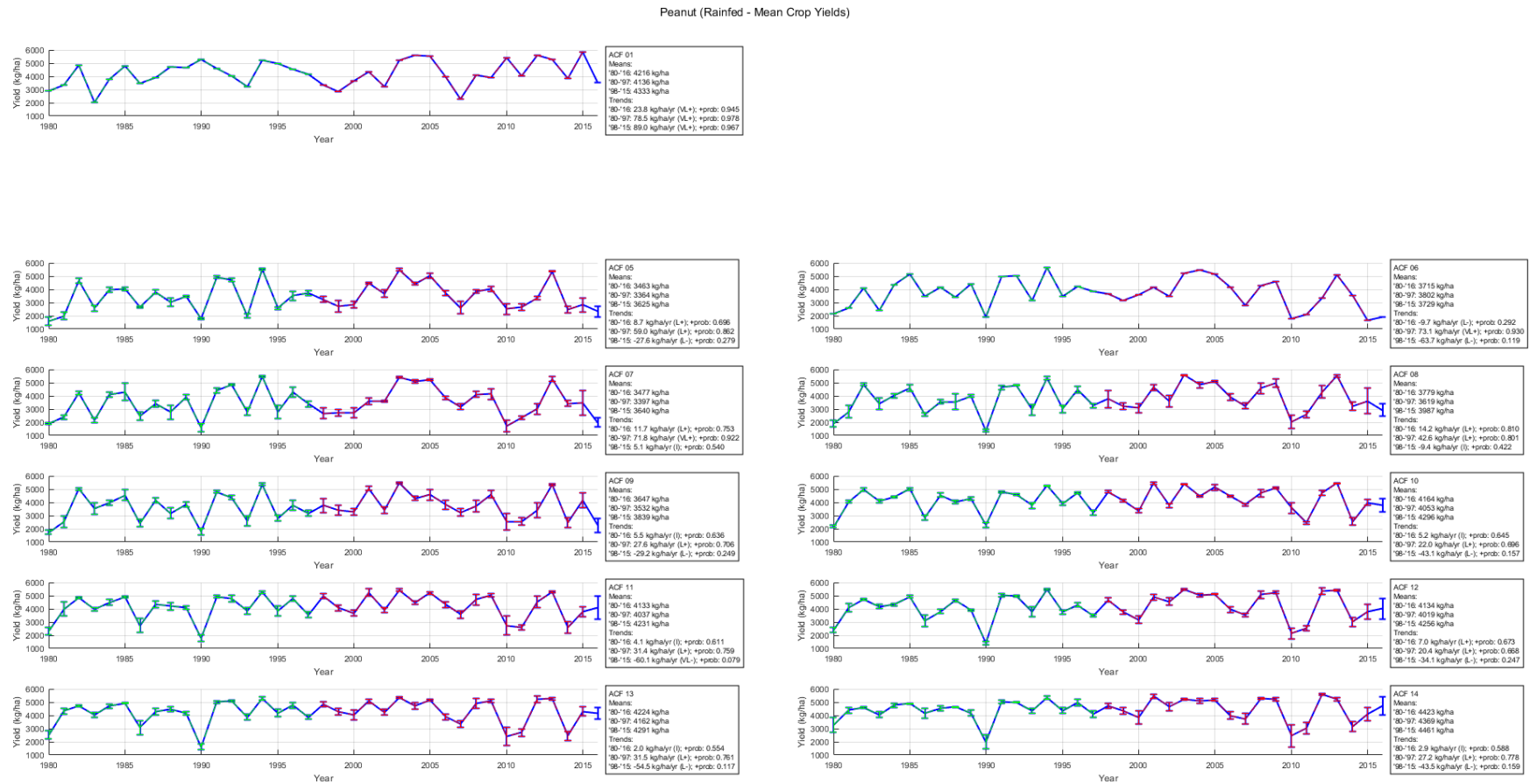


Figure 4-10: Simulated ACF mean *rainfed* peanut yield for 1980–2016 and present-day peanut fields.

Figure 4-11 and Figure 4-12 illustrate the simulated irrigated yields and corresponding irrigation amounts for present-day (2016) peanut fields forced by historical (1980–2016) meteorology for each ACF sub-basin. Irrigated peanut yields are increasing in all sub-basins in tandem with irrigation demand. However, the post-2005 period clearly shows that the demand for water has increased markedly in response to the increased severity and duration of agricultural droughts. It is of interest to note that the positive trend in irrigated peanut yield during the 1998 – 2015 period is only a fraction of the positive trend during the 1980 – 1997 period. In the southernmost basins, for example, the trend in irrigated yield during the 1998 – 2015 period is only 14 to 30 percent of that from the 1980 – 1997 period.

The result of increasing peanut yields (both rainfed and irrigated) seems to highlight the resilience of the peanut plant in the face of rising temperatures in the ACF. In contrast to corn, the optimal air temperature for peanut vegetative growth is relatively higher, ranging from 25° to 28° C (Wood 1968; Cox 1979; Vara Prasad et al. 2000). Furthermore, previous studies have shown that peanut may benefit from increased atmospheric CO₂ concentrations, more so than corn (Jones et al. 2012). However, as suggested by the apparent negative trend in rainfed peanut yields in nearly all sub-basins with substantial peanut acreage after year 2005 and the considerably slowed increase in irrigated peanut yield during the 1998 – 2015 period, ambient mean temperatures may have already surpassed the optimal. As a result, further increases in atmospheric CO₂ concentrations may not offset the negative impacts of continued increases in temperature beyond the optimal, even in the absence of water stress (e.g. when the crop is fully irrigated). This finding portends that, similar to corn, peanut crop will be subject to reduced crop water productivity, even if projected increases in irrigation demand are sufficiently met.

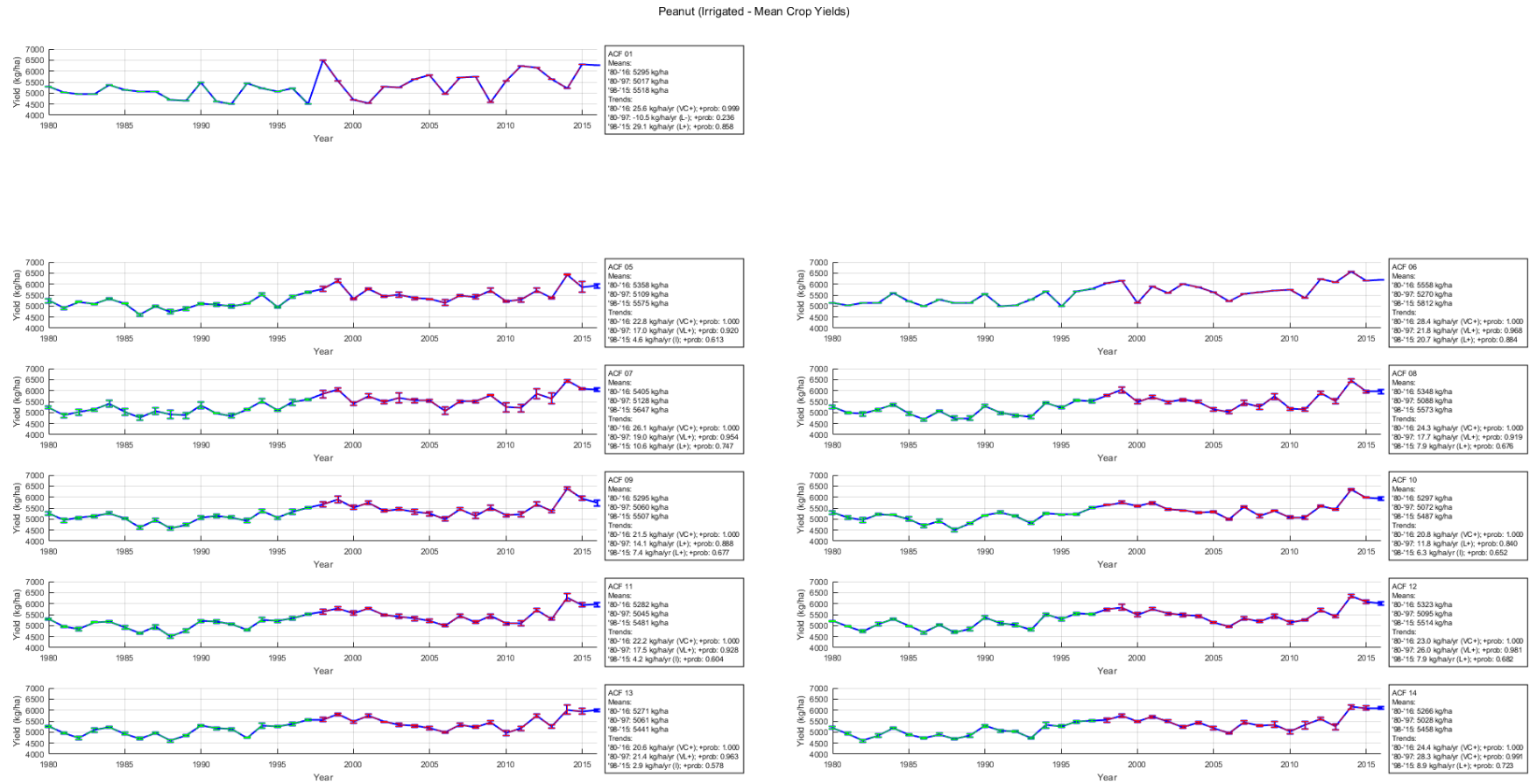


Figure 4-11: Simulated ACF mean irrigated peanut yield for historical meteorology and present-day peanut fields.

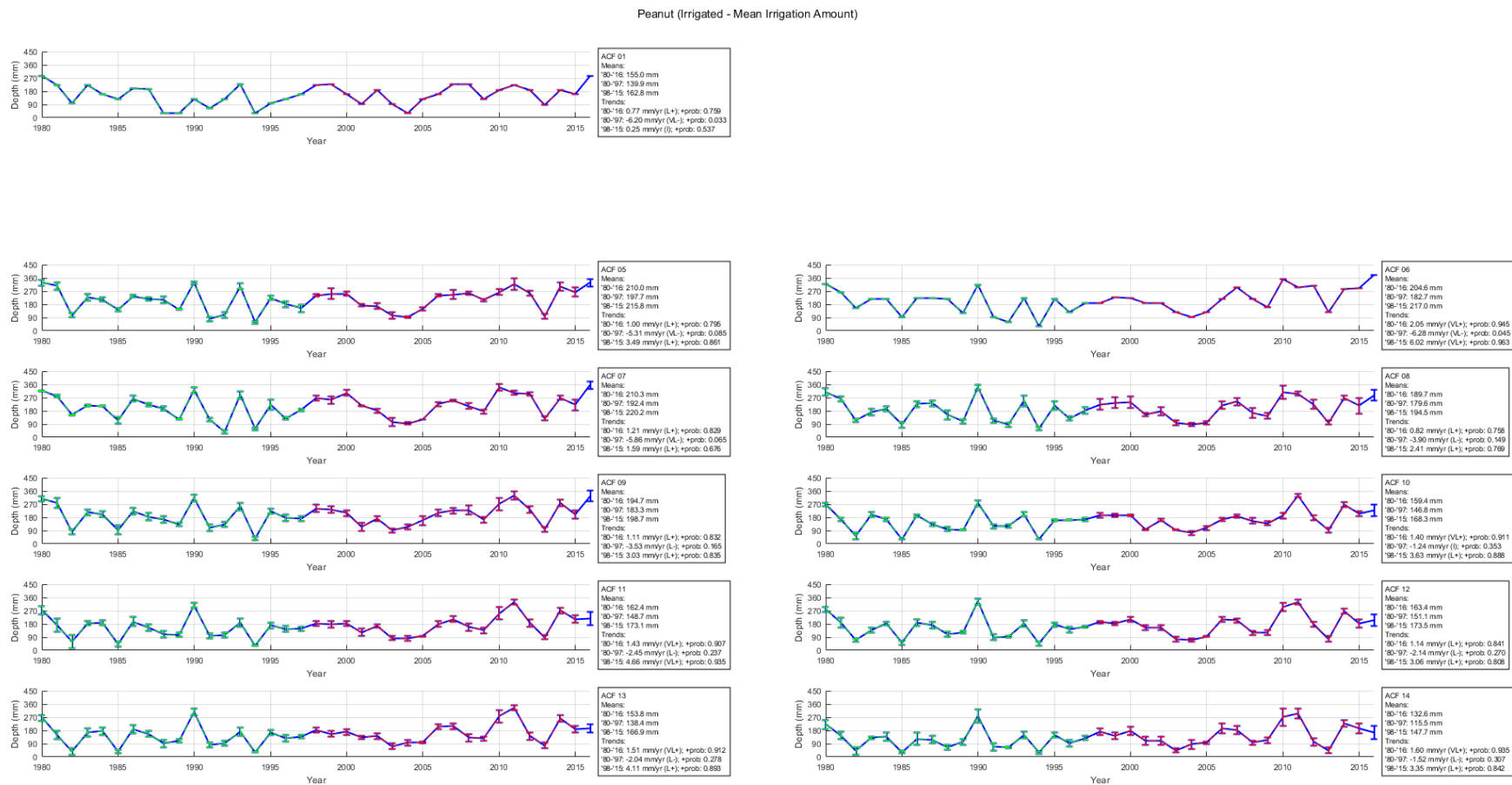


Figure 4-12: Simulated ACF mean irrigation amount for historical meteorology and present-day peanut fields.

4.5.5 ACF Assessment Results: Cotton

Figure 4-13 illustrates the DSSAT-CSM simulated rainfed cotton yields for present-day (2016) cotton fields forced by historical (1980–2016) meteorological conditions for each of the ACF sub-basins. The ACF sub-basins with significant cotton acreage report stable rainfed cotton yield, as shown by the small magnitude of the regression slopes and the near 50% probability of positive trends. However, similar to peanut, the “inconclusive” trend in rainfed cotton crop yield over the 1980-2016 period masks the reality that the temperature stresses of recent years (which are expected to continue into the future) and decreases in precipitation are severely impacting yield. In the more recent 1998-2015 period, crop yields are decreasing rapidly as shown by the regression slopes characterized as “likely” or “very likely” to be negative.

Cotton (Rainfed - Mean Crop Yields)

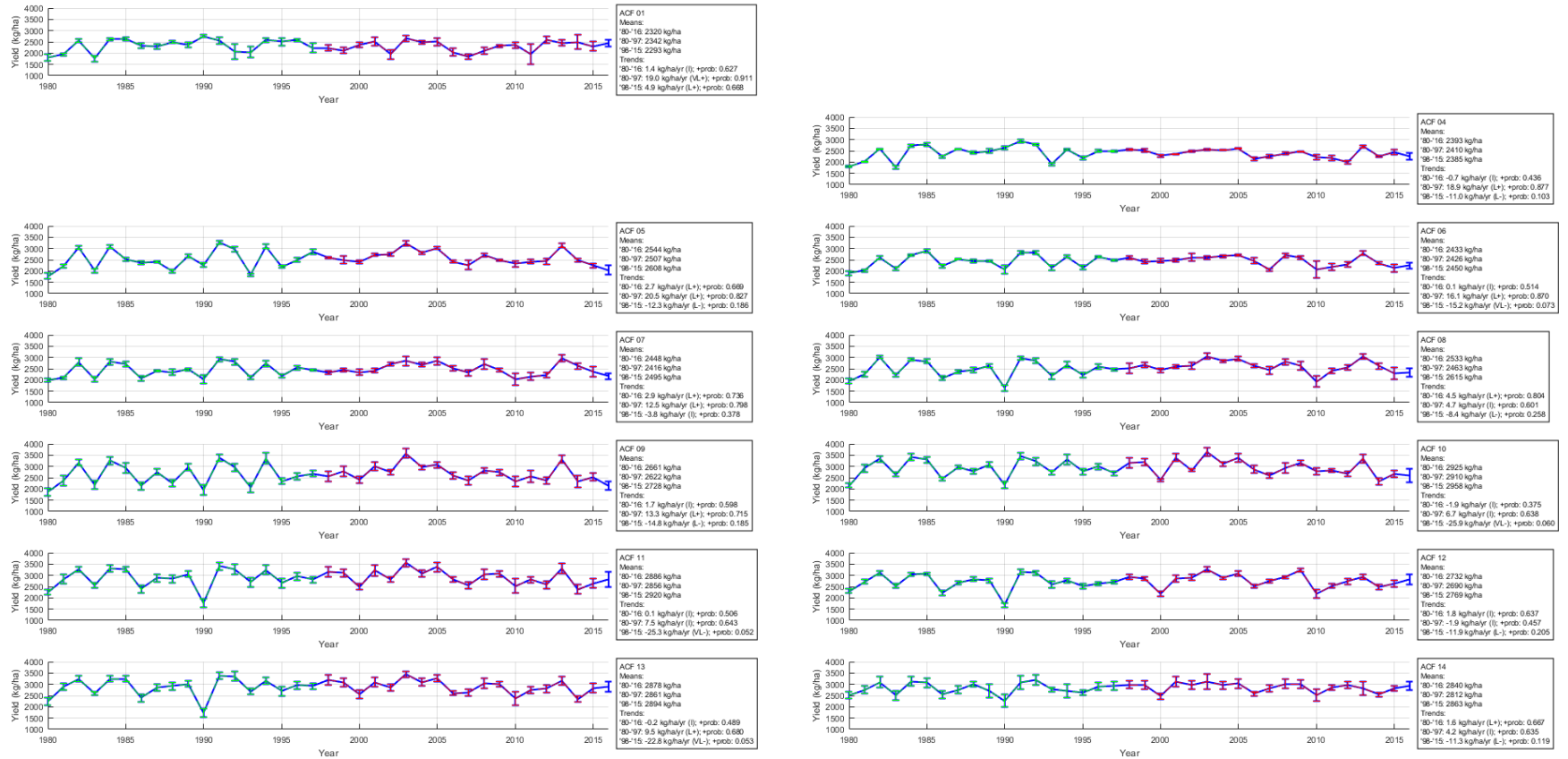


Figure 4-13: Simulated ACF mean rainfed cotton yield for 1980–2016 and present-day cotton fields.

Figure 4-14 and Figure 4-15 illustrate the simulated irrigated yields and corresponding irrigation amounts for present-day (2016) cotton fields forced by historical (1980–2016) meteorology for each ACF sub-basin. Irrigated cotton yields are increasing in all sub-basins as well as irrigation demand. However, the positive annual trend over the 1980-2016 period in irrigated yields is reduced in the warmer, southernmost basins in comparison to the rest of the ACF. This finding suggests, that similar to the other major crops assessed, mean air temperatures have exceeded the optimal for crop yield. In reviewing the literature, a series of well-watered, temperature- and CO₂-controlled studies in Mississippi showed that optimal mean temperatures for cotton yield were between 25° and 28° C, with fruit retention steeply declining until zero with temperature increases from 28° C to beyond 33°C (Reddy et al. 1992; Hodges et al. 1993).

Comparison of the trends in irrigated cotton yield from the 1980 – 1997 period with those of the 1998 – 2015 emphasize in negative impact of increased temperatures despite the absence of water stress. During the 1980-1997 period, irrigation demand for cotton was stable or decreasing, even for the southernmost sub-basins, while irrigated crop yields were increasing in the majority of sub-basins with extensive cotton acreage. The 1998-2015 period stands in sharp contrast to this, with irrigation demand generally increasing in the sub-basins as indicated by the “likely positive” regression slopes during this period. For example, in the southern sub-basins, mean irrigation depth during the 1998-2015 period has increased by 25 up to 40 percent compared to the 1980 – 1997 period. It is also concerning that despite the increase in irrigation application during the 1998-2015 period, irrigated cotton yields continued to decline annually (indicated by slopes that are “virtually certain” or “very likely” to be negative) in the southern half the ACF basins where the most

cotton acreage lies. This finding indicates a sharp reduction in cotton's crop water productivity (e.g. increased water application coupled with persistently decreasing yields) in the face of rising temperatures and reduced precipitation in the ACF.

Cotton (Irrigated - Mean Crop Yields)

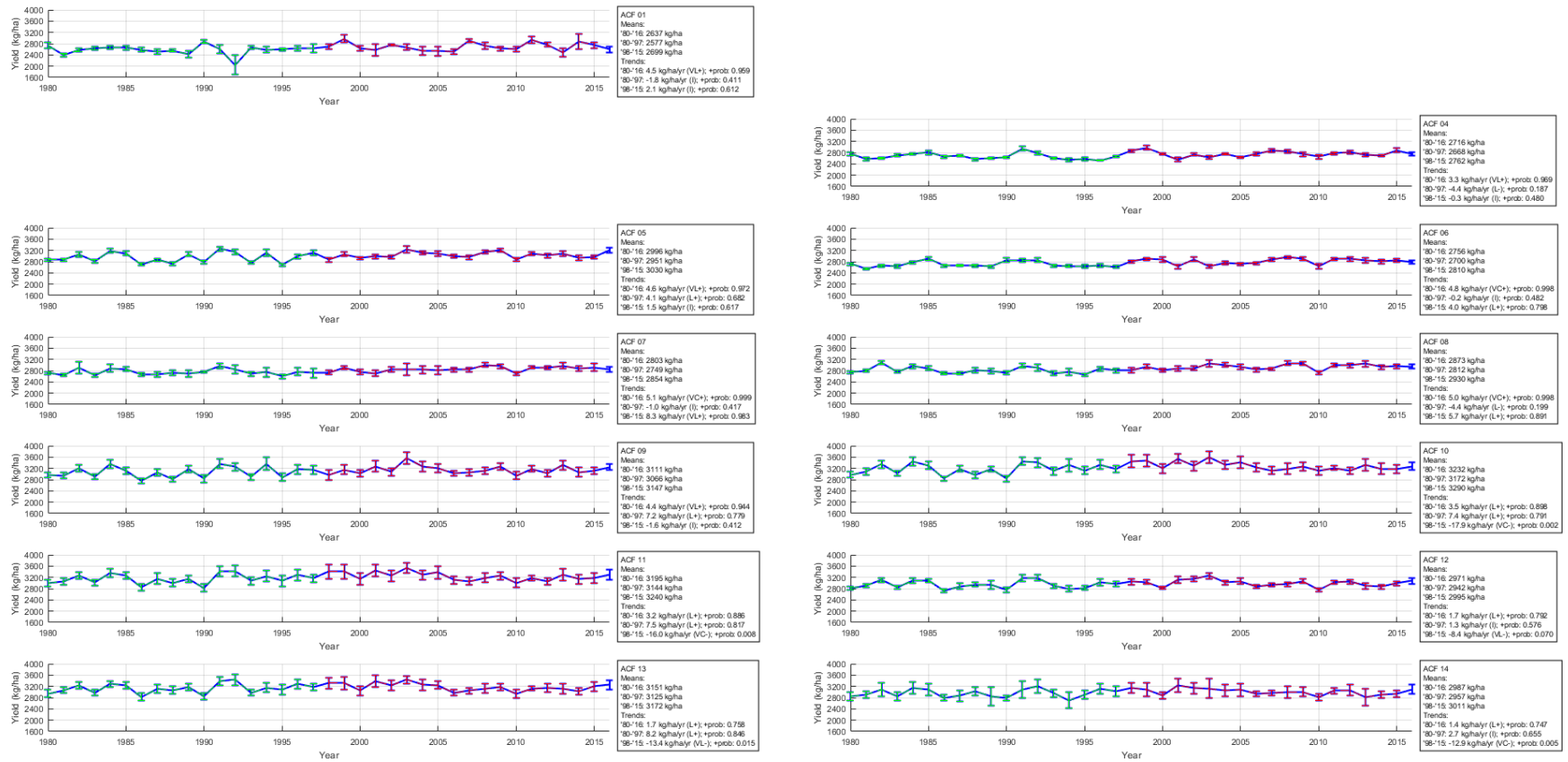


Figure 4-14: Simulated ACF mean irrigated cotton yield for historical meteorology and present-day cotton fields.

Cotton (Irrigated - Mean Irrigation Amount)

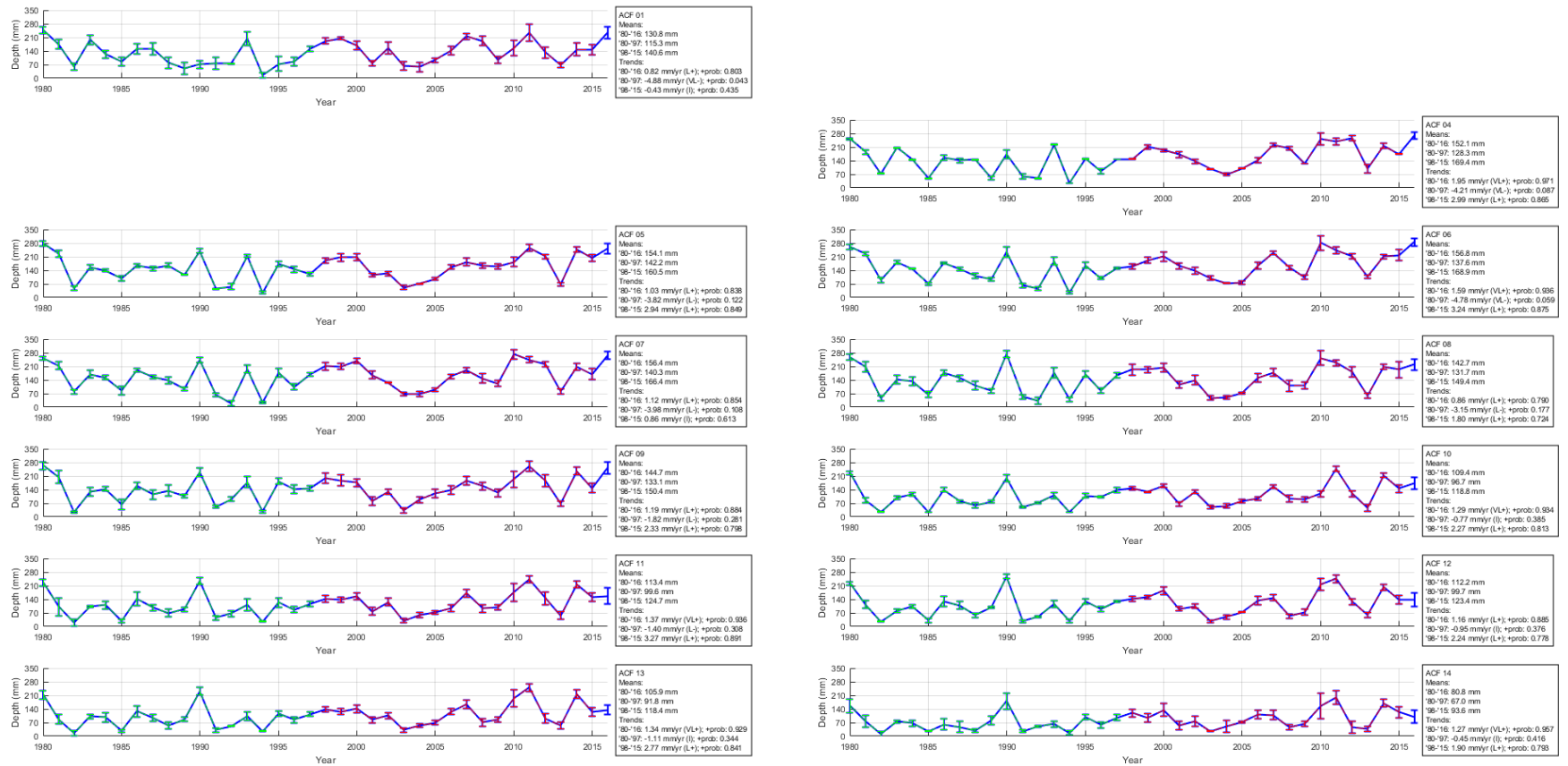


Figure 4-15: Simulated ACF mean irrigation amount for historical meteorology and present-day cotton fields.

4.5.6 ACF Assessment Results: Soybean

Figure 4-16 illustrates the simulated rainfed soybean yields for present-day (2016) soybean fields forced by historical (1980–2016) meteorological conditions for each of the ACF sub-basins. The linear trend in soybean yields over this period is positive in the sub-basins with the most soybean acreage (sub-basins 5, 9, and 11 along the Flint River). However, similar to other major crops tested in this report, the overall positive trend in rainfed soybean crop yield over the 1980-2016 period masks the reality that the temperature stresses of recent years (which are expected to continue into the future) and decreases in precipitation are adversely impacting yield. Rainfed soybean yields were generally increasing annually in ACF during the 1980-1997 sub-period, but are now “likely” decreasing in the southern basins as shown by the negative regression slopes during the 1998-2015 period.

Soybean (Rainfed - Mean Crop Yields)

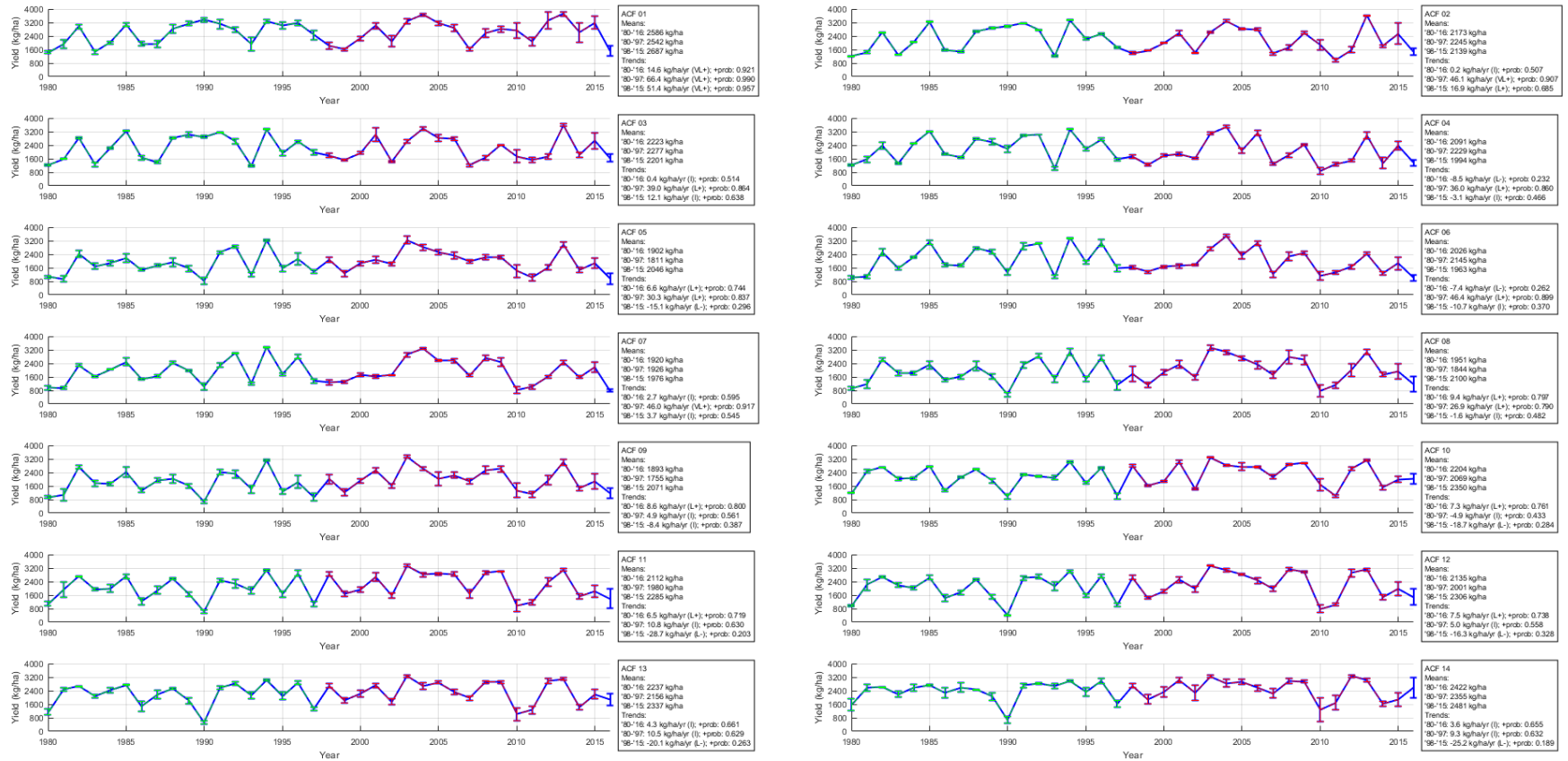


Figure 4-16: Simulated ACF mean rainfed soybean yield for 1980–2016 and present-day soybean fields.

Figure 4-17 and Figure 4-18 illustrate the simulated irrigated yields and corresponding irrigation amounts for present-day (2016) soybean fields forced by historical (1980–2016) meteorology for each ACF sub-basin. Irrigated soybean yields are increasing steadily with “virtual certainty” throughout the period in all sub-basins. Irrigation demand is increasing as well. In contrast to other crops, irrigated soybean yields are increasing in both the 1980-1997 and 1998-2015 periods. In fact, in many of the sub-basins the 1998-2015 positive trend, exceeds that of the 1980-1997 period. In the Upper Chattahoochee for example, the 1998-2015 trend in irrigated soybean yield is nearly three times that of the 1980-1997 period. These findings suggest that the increasing temperatures in the ACF have not yet exceeded the optimal maximum temperature for the crop, provided that the markedly increased water demands are satisfied.

It remains to be seen however for how long can the annual increases in irrigated soybean yield can be sustained in the face of the ACF’s changing climate. Previous studies have shown that soybean yield in the absence of water stress increases until daytime/nighttime temperatures exceed 26°C/20°C, after which yield declines due to temperature stresses (Huxley et al. 1976; Sionit et al. 1987). CO₂ enrichment has been reported to reduce seed weight, but this deleterious effect is balanced by an increase in seed number, such that soybean yields generally benefit from elevated CO₂ concentrations; however, increase in yield components due to increases in CO₂ is highly dependent on temperature (Baker et al. 1989; Baker and Allen 1993).

Soybean (Irrigated) - Mean Crop Yields

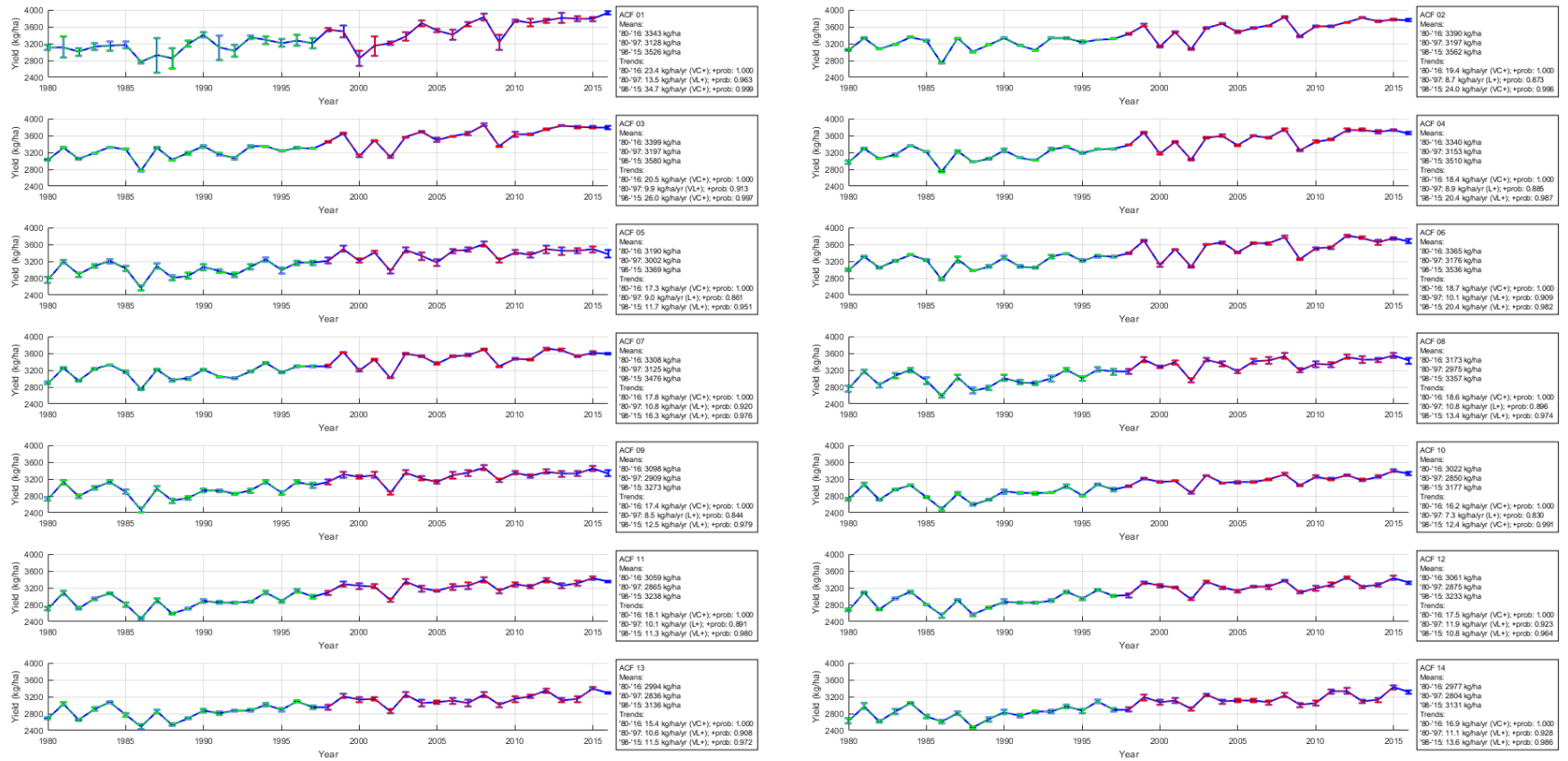


Figure 4-17: Simulated ACF mean irrigated soybean yield for historical meteorology and present-day soybean fields.

Soybean (Irrigated - Mean Irrigation Amount)

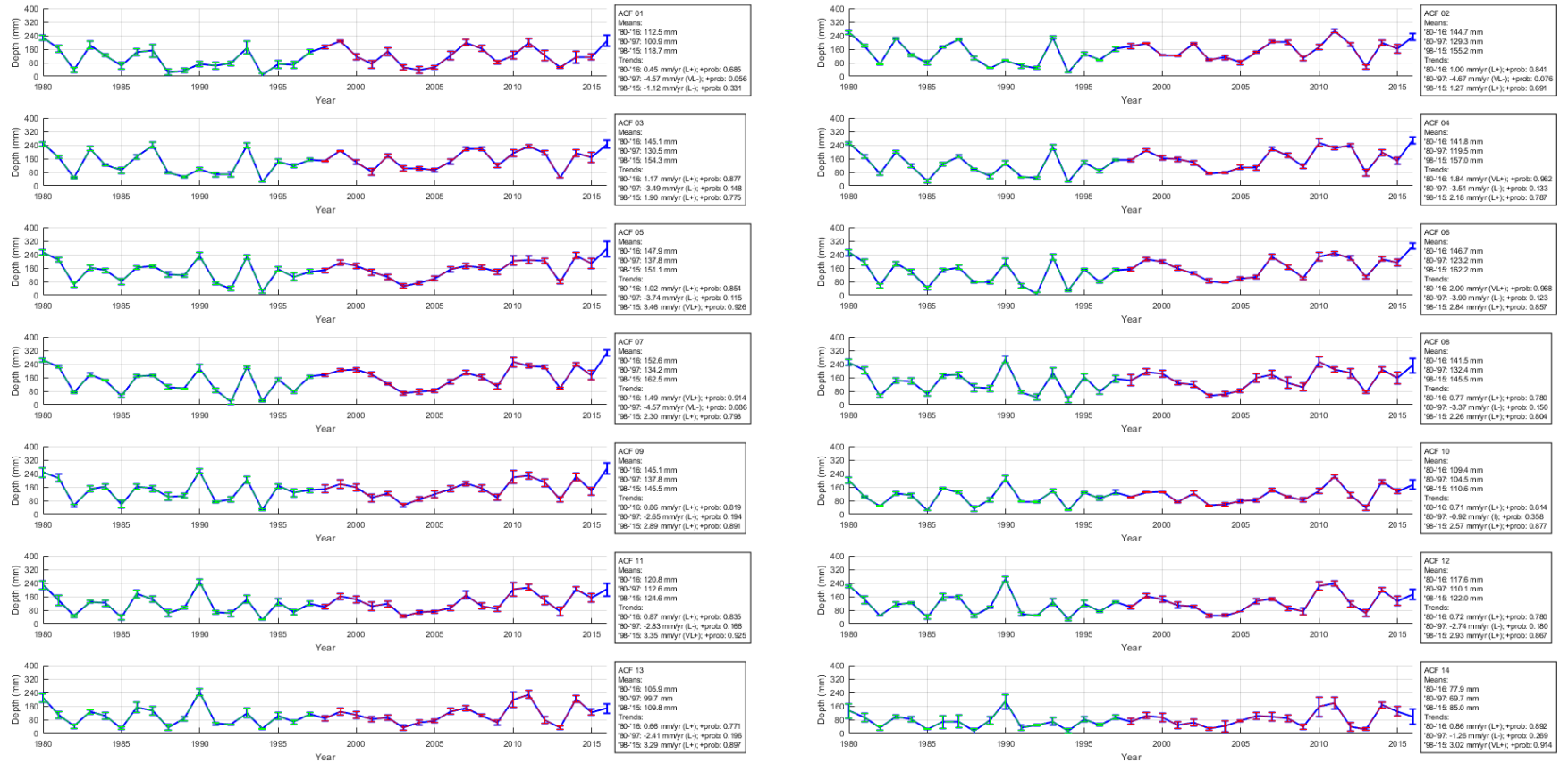


Figure 4-18: Simulated ACF mean irrigation amount for historical meteorology and present-day soybean fields.

4.5.7 ACF Assessment Results: Summary Statistics

Table 4-6 through Table 4-9 list summary statistics related to crop yield and irrigation demand for the major crops in the ACF during the 1980 – 1997 period and the 1998 – 2015 period. Bootstrap sampling (Efron and Tibshirani 1993) of data from these two periods is used to estimate the probability distribution of the change in summary statistics between these two periods. Depending on how much of the “change distribution” lies to the right of zero, the change in the statistic of interest can be characterized as shown in Figure 4-19. The summary statistics of interest include the mean of rainfed and irrigated crop yields, the 25th percentile of rainfed and irrigated crop yields (indicative of agricultural drought), the mean of irrigation amount, and the 75th percentile of irrigation amount (indicative of agricultural drought).

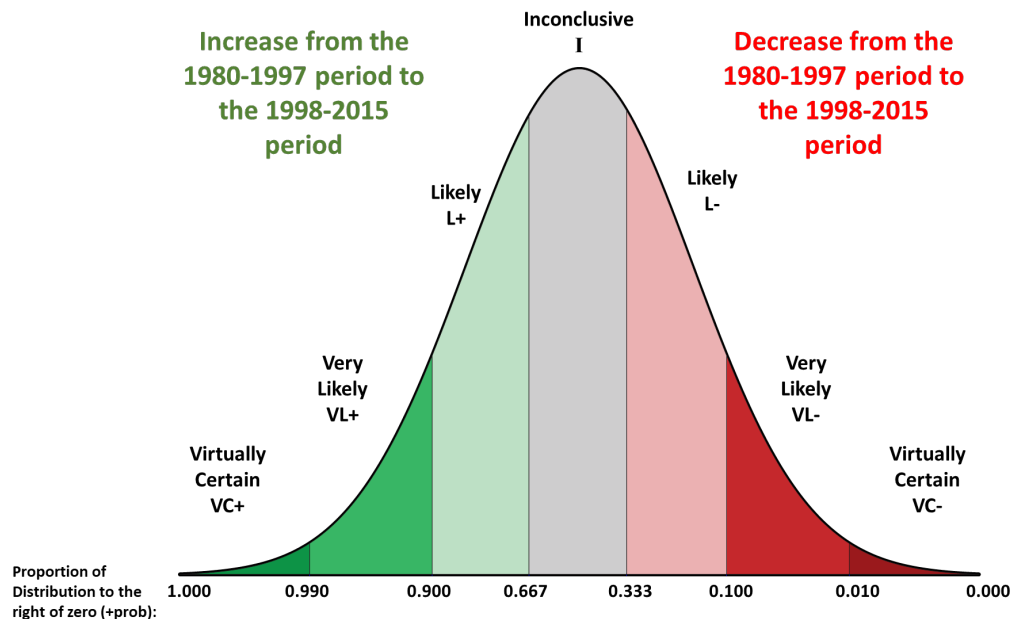


Figure 4-19: Probability statements describing the change in a summary statistic going from the 1980-1997 period to the 1998-2015 period.

Results confirm that for both rainfed and irrigated corn, the mean and 25th percentile of corn yields have decreased going from the 1980 – 1997 period to the 1998 – 2015 period (as indicated by “VL-“ [very likely decrease] and “L-“ [likely decrease] in Table 4-6) in the southern half of the ACF, while the corn yields have increased or stabilized in the northern sub-basins (as indicated by “L+” [likely increase] and “I” [change inconclusive]). Mean and 75th percentile corn irrigation amounts have generally increased throughout the ACF, especially in the southern basins. For peanut, there is not a clear distinction between the north and south. Rainfed peanut yields have “likely” increased or stabilized going from the 1980 – 1997 period to the 1998 – 2015 period. Irrigated peanut yields have increased throughout the ACF, but so has the irrigation demand to support these higher yields. Cotton and soybean also show similar behavior of increasing or stabilized crop yields with an increase in irrigation demand. These findings are consistent with the trend analyses discussed in the preceeding sections.

Table 4-6: Summary statistics for corn crop yield and irrigation demand for the 1980-1997 and 1998-2015 periods and characterization of the change going from the former period to the latter.

ACF Sub-basin	Rainfed Corn Yield (kg/ha)						Irrigated Corn Yield (kg/ha)						Irrigation Amount Corn (mm)					
	Mean			25th Percentile			Mean			25th Percentile			Mean			75th Percentile		
	1980- 1997	1998- 2015	Change	1980- 1997	1998- 2015	Change	1980- 1997	1998- 2015	Change	1980- 1997	1998- 2015	Change	1980- 1997	1998- 2015	Change	1980- 1997	1998- 2015	Change
1	9940	9354	L-	7109	6548	L-	13364	13805	L+	12035	12952	L+	131	149	L+	185	210	L+
2	7866	8333	L+	5150	6117	I	11798	12905	VC+	10394	12079	VL+	157	163	I	221	223	I
3	8261	8381	I	4829	5694	I	12235	12993	VL+	11212	12236	VL+	155	158	I	205	214	I
4	7830	8291	L+	6025	5817	I	11295	12441	VC+	10312	11315	VL+	139	152	L+	200	207	L+
5	6219	6099	I	4259	3373	I	10693	10894	L+	9812	9557	L-	171	191	L+	220	243	L+
6	7653	8380	L+	4862	6695	L+	11385	12385	VC+	10488	11430	VL+	147	155	I	201	219	I
7	6702	7944	VL+	5109	6454	L+	10258	10545	L+	9324	9983	L+	147	135	L-	187	149	L-
8	6967	6723	I	5490	4275	L-	11013	11132	I	10285	9988	I	155	180	L+	201	228	L+
9	6619	6150	L-	5065	3714	L-	10577	10601	I	10089	9608	L-	161	189	L+	201	239	L+
10	7342	6048	VL-	5489	4021	L-	10416	10168	L-	9927	8887	L-	142	183	VL+	183	242	L+
11	7421	6270	VL-	6099	3777	L-	10552	10368	I	10167	9241	L-	144	179	VL+	174	248	VL+
12	7686	6697	L-	6354	4045	L-	10949	10792	I	10206	9748	I	138	176	VL+	173	241	VL+
13	7437	5895	VL-	6198	3404	VL-	10414	9847	L-	9786	8371	L-	142	183	VL+	182	237	VL+
14	7913	6584	VL-	6925	3919	VL-	10607	10317	L-	9866	8734	L-	128	171	VL+	161	212	VL+

Table 4-7: Summary statistics for peanut crop yield and irrigation demand for the 1980-1997 and 1998-2015 periods and characterization of the change going from the former period to the latter.

ACF Sub-basin	Rainfed Peanut Yield (kg/ha)						Irrigated Peanut Yield (kg/ha)						Irrigation Amount Peanut (mm)					
	Mean			25th Percentile			Mean			25th Percentile			Mean			75th Percentile		
	1980-1997	1998-2015	Change	1980-1997	1998-2015	Change	1980-1997	1998-2015	Change	1980-1997	1998-2015	Change	1980-1997	1998-2015	Change	1980-1997	1998-2015	Change
1	4136	4333	L+	3462	3677	I	5017	5518	VC+	4692	5206	L+	140	163	L+	198	223	I
5	3364	3625	L+	2569	2714	L+	5109	5575	VC+	4960	5331	VC+	198	216	L+	236	256	I
6	3802	3729	I	3127	3148	I	5270	5812	VC+	5039	5594	VC+	183	217	VL+	221	288	L+
7	3397	3640	L+	2440	2722	L+	5128	5647	VC+	4921	5487	VC+	192	220	L+	264	268	L+
8	3619	3987	L+	2965	3237	L+	5088	5573	VC+	4876	5266	VC+	180	195	L+	233	241	I
9	3532	3839	L+	2579	3293	L+	5060	5507	VC+	4941	5238	VC+	183	199	L+	222	235	I
10	4053	4296	L+	3756	3766	I	5072	5487	VC+	4906	5304	VL+	147	168	L+	193	194	I
11	4037	4231	L+	3829	3683	I	5045	5481	VC+	4838	5220	VC+	149	173	L+	188	211	L+
12	4019	4256	L+	3771	3511	I	5095	5514	VC+	4843	5253	VC+	151	174	L+	182	212	VL+
13	4162	4291	I	3874	3893	I	5061	5441	VC+	4838	5227	VC+	138	167	L+	171	205	L+
14	4369	4461	I	4181	3845	L-	5028	5458	VC+	4838	5239	VC+	116	148	VL+	146	193	VL+

Table 4-8: Summary statistics for cotton crop yield and irrigation demand for the 1980-1997 and 1998-2015 periods and characterization of the change going from the former period to the latter.

ACF Sub-basin	Rainfed Cotton Yield (kg/ha)						Irrigated Cotton Yield (kg/ha)						Irrigation Amount Cotton (mm)					
	Mean			25th Percentile			Mean			25th Percentile			Mean			75th Percentile		
	1980-1997	1998-2015	Change	1980-1997	1998-2015	Change	1980-1997	1998-2015	Change	1980-1997	1998-2015	Change	1980-1997	1998-2015	Change	1980-1997	1998-2015	Change
1	2342	2293	L-	2062	2117	I	2577	2699	VC+	2555	2572	I	115	141	VL+	152	192	L+
4	2410	2385	I	2169	2249	L+	2668	2762	VC+	2580	2695	VL+	128	169	VL+	173	216	VL+
5	2507	2608	L+	2194	2415	VL+	2951	3030	VL+	2785	2959	VL+	142	160	L+	172	206	I
6	2426	2450	I	2152	2281	L+	2700	2810	VC+	2634	2742	VL+	138	169	VL+	182	214	L+
7	2416	2495	L+	2095	2333	VL+	2749	2854	VC+	2669	2812	VC+	140	166	L+	190	210	L+
8	2463	2615	VL+	2210	2439	VL+	2812	2930	VC+	2733	2866	VC+	132	149	L+	175	194	L+
9	2622	2728	L+	2193	2413	VL+	3066	3147	VL+	2898	3033	VL+	133	150	L+	178	188	L+
10	2910	2958	I	2696	2664	I	3172	3290	VL+	3034	3188	VL+	97	119	L+	117	148	L+
11	2856	2920	L+	2656	2589	I	3144	3240	VL+	3013	3136	VL+	100	125	VL+	118	154	VL+
12	2690	2769	L+	2537	2532	I	2942	2995	L+	2826	2902	L+	100	123	L+	129	151	VL+
13	2861	2894	I	2677	2631	I	3125	3172	L+	2975	3043	L+	92	118	VL+	112	141	VL+
14	2812	2863	L+	2648	2812	L+	2957	3011	L+	2848	2932	VL+	67	94	VL+	80	123	VL+

Table 4-9: Summary statistics for soybean crop yield and irrigation demand for the 1980-1997 and 1998-2015 periods and characterization of the change going from the former period to the latter.

ACF Sub-basin	Rainfed Soybean Yield (kg/ha)						Irrigated Soybean Yield (kg/ha)						Irrigation Amount Soybean (mm)					
	Mean			25th Percentile			Mean			25th Percentile			Mean			75th Percentile		
	1980-1997	1998-2015	Change	1980-1997	1998-2015	Change	1980-1997	1998-2015	Change	1980-1997	1998-2015	Change	1980-1997	1998-2015	Change	1980-1997	1998-2015	Change
1	2542	2687	L+	1923	2089	L+	3128	3526	VC+	3030	3374	VC+	101	119	L+	150	163	I
2	2245	2139	L-	1494	1547	I	3197	3562	VC+	3078	3477	VL+	129	155	L+	180	194	I
3	2277	2201	I	1590	1654	I	3197	3580	VC+	3062	3487	VL+	130	154	L+	170	195	I
4	2229	1994	L-	1557	1337	L-	3153	3510	VC+	3051	3370	VC+	120	157	VL+	173	210	L+
5	1811	2046	L+	1363	1632	L+	3002	3369	VC+	2879	3222	VC+	138	151	L+	170	193	I
6	2145	1963	L-	1568	1353	I	3176	3536	VC+	3054	3406	VC+	123	162	VL+	185	214	VL+
7	1926	1976	I	1353	1593	I	3125	3476	VC+	3005	3355	VC+	134	163	VL+	176	205	L+
8	1844	2100	L+	1410	1710	L+	2975	3357	VC+	2844	3279	VC+	132	146	L+	176	185	I
9	1755	2071	VL+	1256	1602	L+	2909	3273	VC+	2795	3215	VC+	138	145	I	166	181	I
10	2069	2350	VL+	1794	1694	I	2850	3177	VC+	2724	3123	VC+	105	111	I	130	135	I
11	1980	2285	VL+	1652	1669	I	2865	3238	VC+	2715	3183	VC+	113	125	L+	144	162	L+
12	2001	2306	L+	1495	1829	L+	2875	3233	VC+	2727	3196	VC+	110	122	L+	140	146	L+
13	2156	2337	L+	1804	1813	I	2836	3136	VC+	2690	3050	VC+	100	110	L+	127	129	I
14	2355	2481	L+	2189	1883	I	2804	3131	VC+	2661	3063	VC+	70	85	L+	91	104	VL+

4.5.8 ACF Assessment Results: Monthly Irrigation Volumes

After estimating the irrigation timings and depths for the major crops of the ACF basin for the 1980 – 2016 historical period, these depths are converted to monthly irrigation volumes by way of the following equation:

$$V_{i,m} = \sum_{c=1}^n \frac{1}{E} \cdot F_{i,c} \cdot A_{i,c} \cdot D_{i,c,m}$$

Where V is the irrigation volume, in cubic meters, for ACF sub-basin i , in the of the month (and year) of interest m ; c , the index representing a major crop (i.e. 1=Corn, 2=Peanut, 3=Cotton, and 4=Soybean); n , the number of crops (4 in this study); E , the efficiency of applied irrigation, i.e. the percentage of simulated irrigation that is actually utilized by crop. In this report E is conservatively set as 0.85; $F_{i,c}$, the fraction of acreage which is irrigated in sub-basin i for crop c ; and $A_{i,c}$ and $D_{i,c,m}$ refer to the total acreage (square meters) and irrigation depth (meters) in the month (and year) m of interest within sub-basin i for crop c respectively.

The term $A_{i,c}$ is estimated based on the quantity of year 2016 USDA-NASS Cropland Data Layer pixels presented earlier in Table 4-4 in which each pixel represents 900 square meters. $D_{i,c,m}$ is determined from the irrigated crop simulations completed in the previous sections of this report, except that the irrigation applications are aggregated monthly instead of annually.

$F_{i,c}$, the fraction of crop acreage that is irrigated within a sub-basin, is estimated following a review of year 2014-2016 county-level crop acreage data publicly available from the USDA Farm Service Agency (USDA FSA 2015, 2016, 2017). For each county

included within each ACF sub-basin, the USDA FSA data set is queried (from years 2014 to 2016 to ensure coverage of relatively dry, normal, and wet growing seasons) for the quantity of irrigated and non-irrigated acreages for corn, cotton, peanut, and soybean. Review of the data showed that $F_{i,c}$ is not overly sensitive to the dryness/wetness of the growing season, so a time-constant value for $F_{i,c}$ has been estimated based on a weighted average of county-level data for each ACF sub-basin for each major crop as listed in Table 4-10. The estimates show that the major crops grown in the Upper Chattahoochee to Middle Chattahoochee (sub-basins 1-4, and 6) are rainfed ($F_{i,c} = 0$), while in the remaining basins representing the Flint, Apalachicola, and Middle to Lower Chattahoochee, 10 to 90 percent of the fields are irrigated depending on crop type.

Table 4-10: Fraction of acreage that is irrigated ($F_{i,c}$) for corn, peanut, cotton, and soybean fields in each ACF sub-basin, estimated from year 2014-2016 county-level crop acreage data provided by the USDA Farm Service Agency.

ACF Sub-basin	Irrigation Acreage Fraction ($F_{i,c}$)			
	Corn	Peanut	Cotton	Soybean
1	0	0	0	0
2	0	0	0	0
3	0	0	0	0
4	0	0	0	0
5	0.9	0.6	0.5	0.2
6	0	0	0	0
7	0.3	0.2	0.2	0.1
8	0.7	0.4	0.4	0.3
9	0.8	0.6	0.5	0.4
10	0.9	0.6	0.6	0.6
11	0.9	0.7	0.6	0.5
12	0.7	0.3	0.3	0.4
13	0.9	0.5	0.6	0.5
14	0.7	0.4	0.4	0.3

4.5.9 ACF Monthly Irrigation Volumes: Upper Chattahoochee

For the Upper Chattahoochee (ACF sub-basins 1 – 4, and 6), the major crops corn, cotton, soybean, and peanut are rainfed as shown previously in Table 4-10.

4.5.10 ACF Monthly Irrigation Volumes: Middle Chattahoochee and Upper Flint

For the Middle Chattahoochee and Upper Flint (ACF sub-basins 5, 7, and 8), the irrigation season spans from April through October. As shown in Figure 4-20 through Figure 4-22, monthly irrigation volumes have large inter-annual variations, with irrigation volumes easily reaching double or more of the long term (1980-2016) mean during droughts, especially in the summer months. The 1980-2016 trends in irrigation volumes are generally positive (indicating increasing irrigation volumes annually) except for September and October in sub-basin 5; April, June, and July in sub-basin 7; and April and October in sub-basin 8. These findings are for the most part consistent with the trends in monthly precipitation and potential evapotranspiration. As a result, the mean irrigation volumes of the 1998-2015 period are greater than their counterparts from the 1980-1997 period for the majority of the growing season. When comparing 1980-1997 trends to those of 1998-2015, there are trend reversals in which irrigation volumes go from decreasing annually during the 1980-1997 period, to increasing during the 1998-2015 period. This occurs in June and July for sub-basin 5; October for sub-basin 7; and July for sub-basin 8.

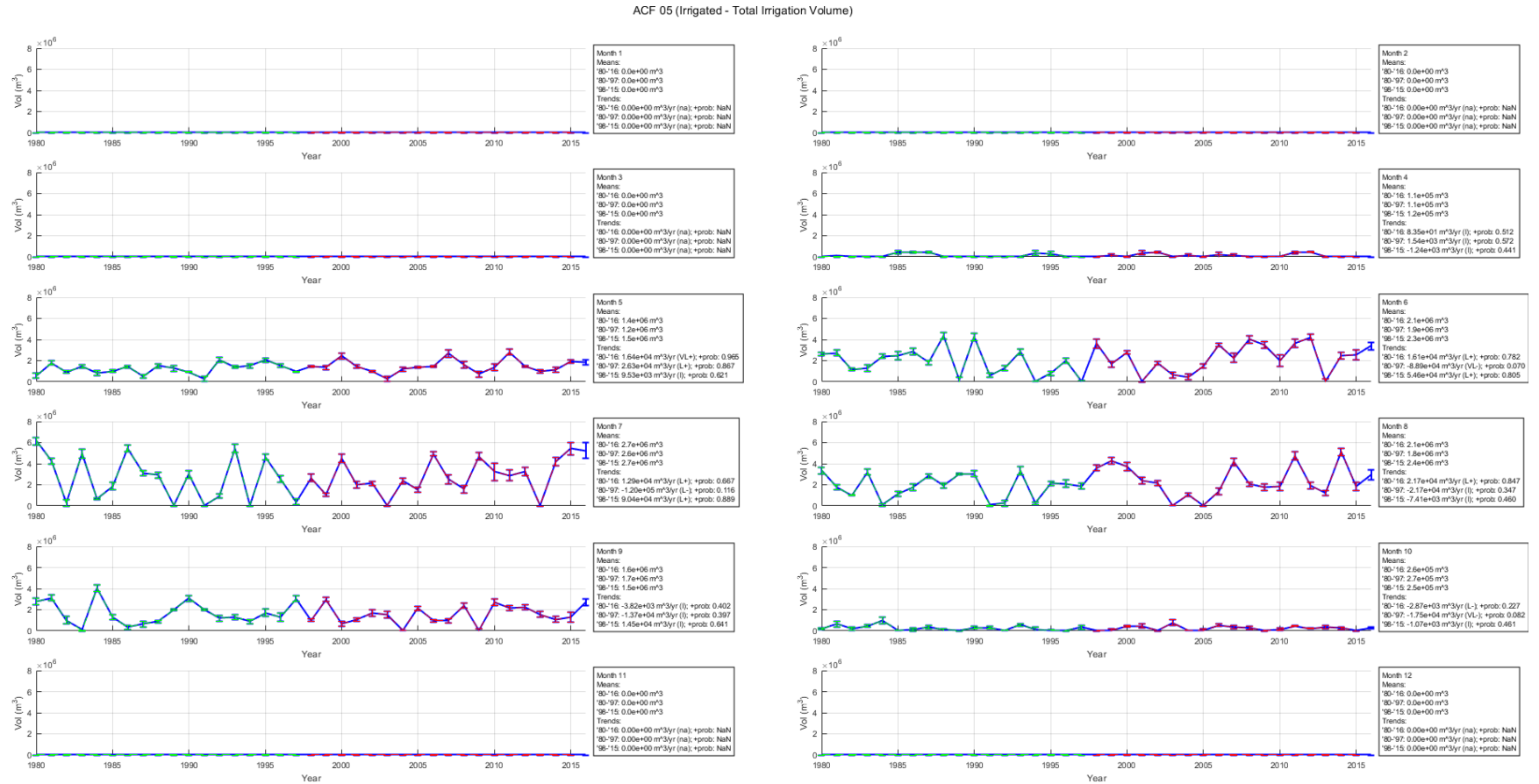


Figure 4-20: Monthly irrigation volumes for ACF Sub-basin 5

Figure 10 displays 8 line plots showing monthly mean lake volume (Vol in m^3) from 1980 to 2015 for Lake Tanganyika. The y-axis is scaled by 10^4 . Each plot includes a legend for the month, mean values for three periods (1980-1989, 1990-1999, 2000-2009), and trends for three periods (1980-1989, 1990-1999, 2000-2009).

Month 1:
 Means:
 1980-1989: $0.0e+00 \text{ m}^3$
 1990-1999: $0.0e+00 \text{ m}^3$
 2000-2009: $0.0e+00 \text{ m}^3$
 Trends:
 1980-1989: $0.00e+00 \text{ m}^3/\text{yr}$ (na); +prob: NaN
 1990-1999: $0.00e+00 \text{ m}^3/\text{yr}$ (na); +prob: NaN
 1990-1999: $0.00e+00 \text{ m}^3/\text{yr}$ (na); +prob: NaN

Month 2:
 Means:
 1980-1989: $0.0e+00 \text{ m}^3$
 1990-1999: $0.0e+00 \text{ m}^3$
 2000-2009: $0.0e+00 \text{ m}^3$
 Trends:
 1980-1989: $0.00e+00 \text{ m}^3/\text{yr}$ (na); +prob: NaN
 1990-1999: $0.00e+00 \text{ m}^3/\text{yr}$ (na); +prob: NaN
 1990-1999: $0.00e+00 \text{ m}^3/\text{yr}$ (na); +prob: NaN

Month 3:
 Means:
 1980-1989: $0.0e+00 \text{ m}^3$
 1990-1999: $0.0e+00 \text{ m}^3$
 2000-2009: $0.0e+00 \text{ m}^3$
 Trends:
 1980-1989: $0.00e+00 \text{ m}^3/\text{yr}$ (na); +prob: NaN
 1990-1999: $0.00e+00 \text{ m}^3/\text{yr}$ (na); +prob: NaN
 1990-1999: $0.00e+00 \text{ m}^3/\text{yr}$ (na); +prob: NaN

Month 4:
 Means:
 1980-1989: $9.8e+02 \text{ m}^3$
 1990-1999: $1.0e+03 \text{ m}^3$
 2000-2009: $9.8e+02 \text{ m}^3$
 Trends:
 1980-1989: $-3.76e+01 \text{ m}^3/\text{yr}$ (L-); +prob: 0.219
 1990-1999: $-8.85e+01 \text{ m}^3/\text{yr}$ (L-); +prob: 0.288
 1990-1999: $-1.88e+02 \text{ m}^3/\text{yr}$ (VL-); +prob: 0.073

Month 5:
 Means:
 1980-1989: $3.3e+04 \text{ m}^3$
 1990-1999: $3.2e+04 \text{ m}^3$
 2000-2009: $3.4e+04 \text{ m}^3$
 Trends:
 1980-1989: $-1.82e+02 \text{ m}^3/\text{yr}$ (L-); +prob: 0.812
 1990-1999: $-5.05e+02 \text{ m}^3/\text{yr}$ (L-); +prob: 0.828
 1990-1999: $-1.68e+01 \text{ m}^3/\text{yr}$ (L-); +prob: 0.489

Month 6:
 Means:
 1980-1989: $3.6e+04 \text{ m}^3$
 1990-1999: $3.7e+04 \text{ m}^3$
 2000-2009: $3.3e+04 \text{ m}^3$
 Trends:
 1980-1989: $-3.19e+02 \text{ m}^3/\text{yr}$ (L-); +prob: 0.161
 1990-1999: $-2.02e+03 \text{ m}^3/\text{yr}$ (VL-); +prob: 0.022
 1990-1999: $-5.53e+01 \text{ m}^3/\text{yr}$ (L-); +prob: 0.476

Month 7:
 Means:
 1980-1989: $3.8e+04 \text{ m}^3$
 1990-1999: $3.9e+04 \text{ m}^3$
 2000-2009: $3.6e+04 \text{ m}^3$
 Trends:
 1980-1989: $-5.93e+01 \text{ m}^3/\text{yr}$ (L-); +prob: 0.445
 1990-1999: $-6.69e+02 \text{ m}^3/\text{yr}$ (L-); +prob: 0.374
 1990-1999: $-4.31e+01 \text{ m}^3/\text{yr}$ (L-); +prob: 0.514

Month 8:
 Means:
 1980-1989: $2.0e+04 \text{ m}^3$
 1990-1999: $1.7e+04 \text{ m}^3$
 2000-2009: $2.3e+04 \text{ m}^3$
 Trends:
 1980-1989: $-1.72e+02 \text{ m}^3/\text{yr}$ (L-); +prob: 0.781
 1990-1999: $-2.07e+02 \text{ m}^3/\text{yr}$ (L-); +prob: 0.370
 1990-1999: $-1.32e+02 \text{ m}^3/\text{yr}$ (L-); +prob: 0.429

Month 9:
 Means:
 1980-1989: $1.7e+04 \text{ m}^3$
 1990-1999: $1.6e+04 \text{ m}^3$
 2000-2009: $1.7e+04 \text{ m}^3$
 Trends:
 1980-1989: $-7.86e+01 \text{ m}^3/\text{yr}$ (L-); +prob: 0.678
 1990-1999: $-5.73e+02 \text{ m}^3/\text{yr}$ (L-); +prob: 0.138
 1990-1999: $-2.02e+02 \text{ m}^3/\text{yr}$ (L-); +prob: 0.325

Month 10:
 Means:
 1980-1989: $5.4e+03 \text{ m}^3$
 1990-1999: $5.1e+03 \text{ m}^3$
 2000-2009: $5.3e+03 \text{ m}^3$
 Trends:
 1980-1989: $-2.81e+01 \text{ m}^3/\text{yr}$ (L-); +prob: 0.663
 1990-1999: $-2.74e+02 \text{ m}^3/\text{yr}$ (VL-); +prob: 0.089
 1990-1999: $-1.30e+02 \text{ m}^3/\text{yr}$ (L-); +prob: 0.765

Month 11:
 Means:
 1980-1989: $0.0e+00 \text{ m}^3$
 1990-1999: $0.0e+00 \text{ m}^3$
 2000-2009: $0.0e+00 \text{ m}^3$
 Trends:
 1980-1989: $0.00e+00 \text{ m}^3/\text{yr}$ (na); +prob: NaN
 1990-1999: $0.00e+00 \text{ m}^3/\text{yr}$ (na); +prob: NaN
 1990-1999: $0.00e+00 \text{ m}^3/\text{yr}$ (na); +prob: NaN

Month 12:
 Means:
 1980-1989: $0.0e+00 \text{ m}^3$
 1990-1999: $0.0e+00 \text{ m}^3$
 2000-2009: $0.0e+00 \text{ m}^3$
 Trends:
 1980-1989: $0.00e+00 \text{ m}^3/\text{yr}$ (na); +prob: NaN
 1990-1999: $0.00e+00 \text{ m}^3/\text{yr}$ (na); +prob: NaN
 1990-1999: $0.00e+00 \text{ m}^3/\text{yr}$ (na); +prob: NaN

164

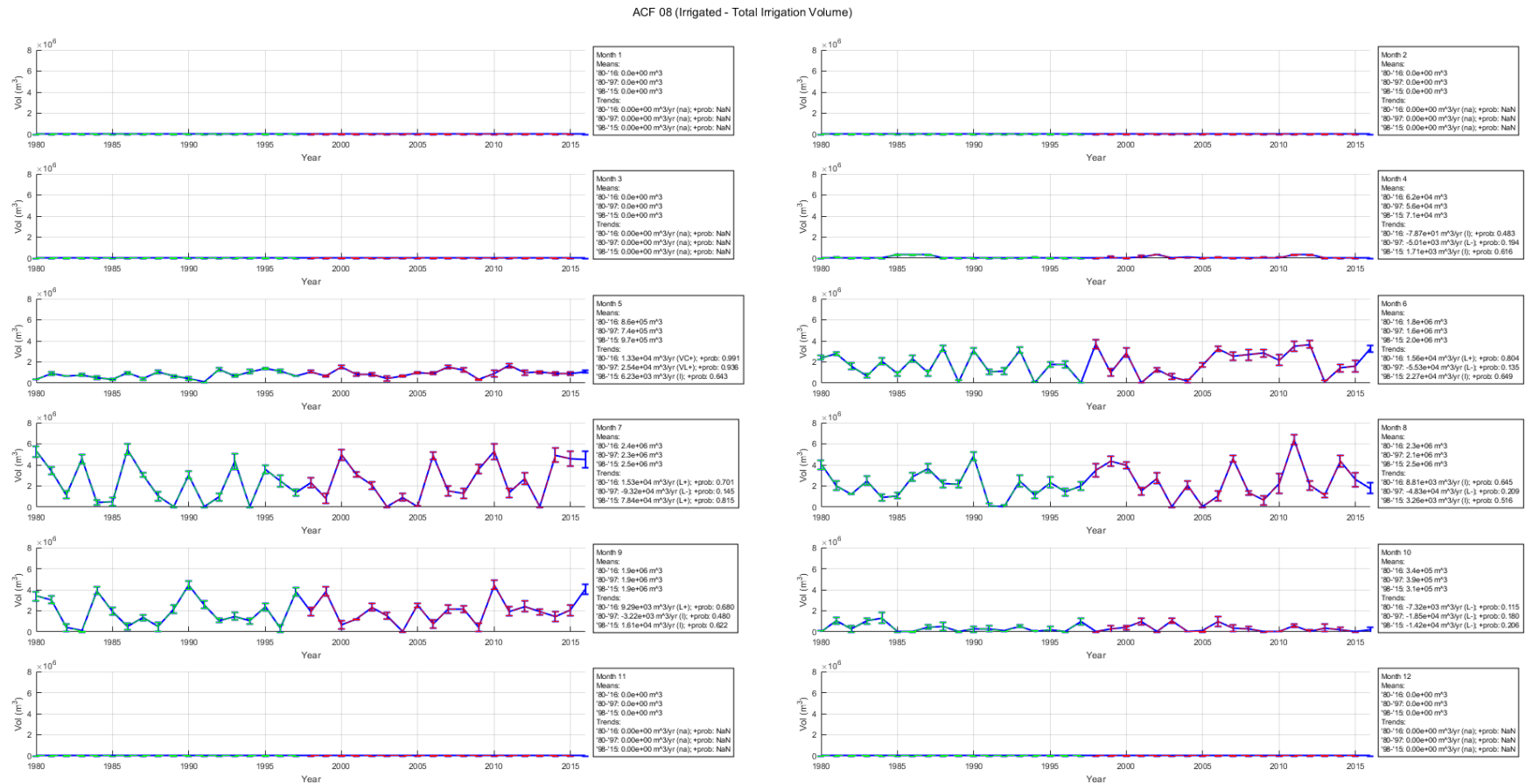


Figure 4-22: Monthly irrigation volumes for ACF Sub-basin 8

4.5.11 ACF Monthly Irrigation Volumes: Middle and Lower Flint and Lower Chattahoochee

For the Middle and Lower regions of the Flint sub-basins and the Lower Chattahoochee (sub-basins 9-13), the irrigation season spans from April through October. As shown in Figure 4-23 through Figure 4-27, monthly irrigation volumes have large inter-annual variations, with irrigation volumes reaching up to three times or more of the long term (1980-2016) mean during droughts, especially in the summer months of the 1998-2015 period. Also in these months, peak irrigation volumes are generally greater in magnitude and occur more frequently during the 1998-2015 period than the 1980-1997 period. Mean irrigation volumes of the 1998-2015 period are generally greater than their counterparts from the 1980-1997 period throughout the growing season except for the months of September and October. It is also of interest to note the mean irrigation volume in April during the 1998-2015 period is nearly double or even more than the corresponding April volume from the 1980-1997 period for the sub-basins in this region. The 1980-2016 trends in irrigation volumes are generally positive (indicating increasing irrigation volumes annually) except for October in all sub-basins, and except for September in sub-basins 9, 10, 12, and 13 in which the slope's direction is "inconclusive". When comparing 1980-1997 trends to those of 1998-2015, in the summer months there are trend reversals in which irrigation volumes go from "likely decreasing" annually during the 1980-1997 period, to "likely increasing" during the 1998-2015 period.

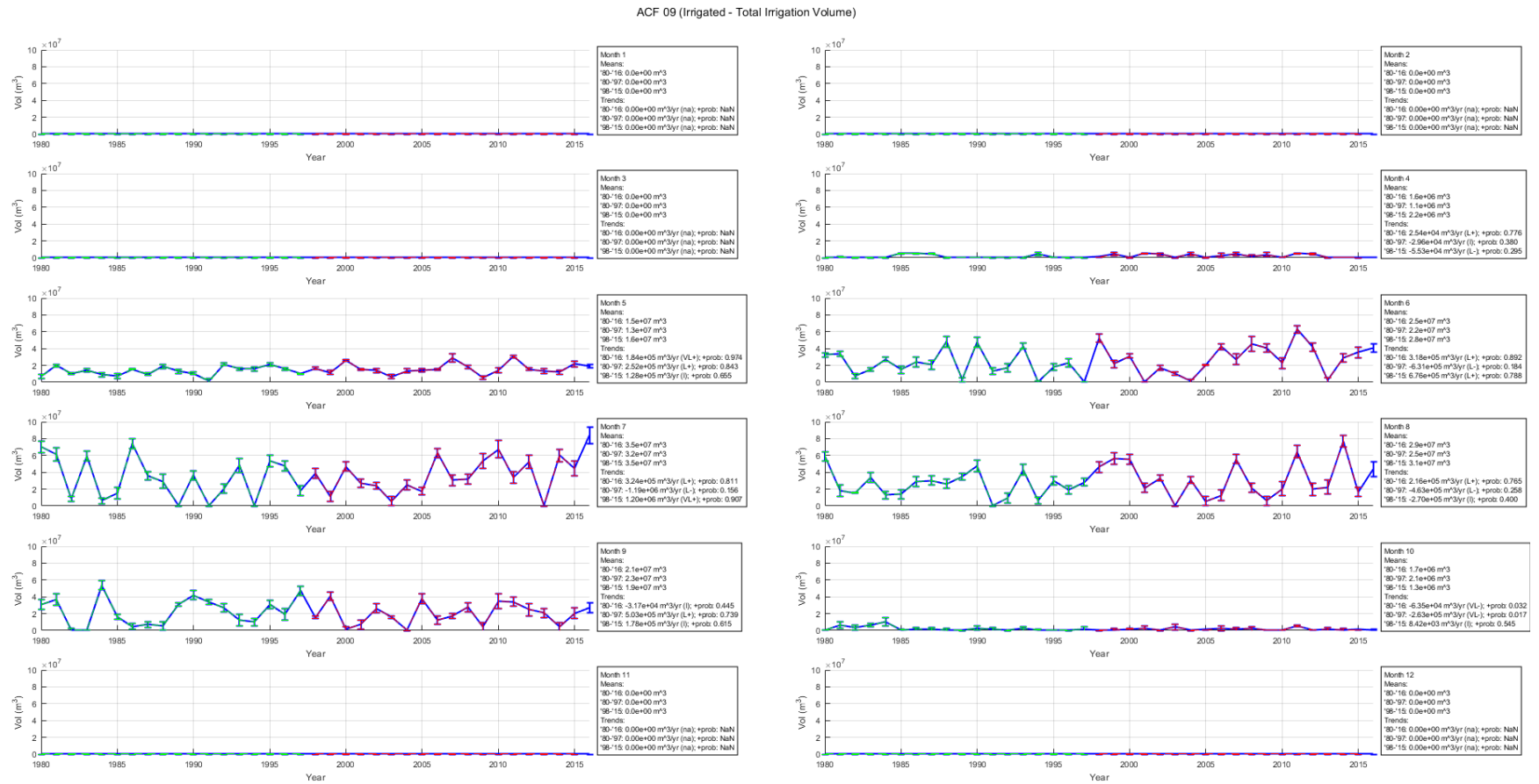


Figure 4-23: Monthly irrigation volumes for ACF Sub-basin 9

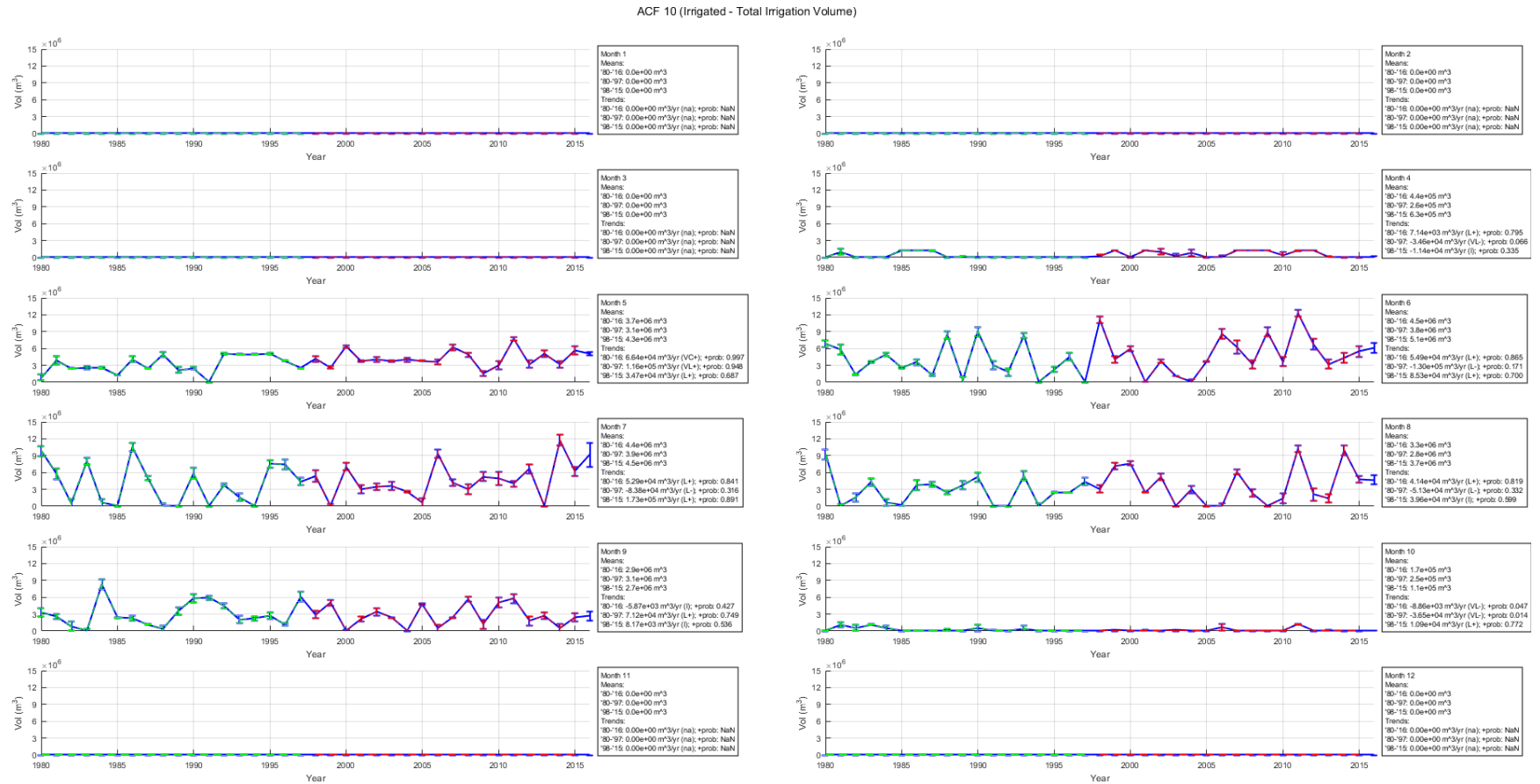


Figure 4-24: Monthly irrigation volumes for ACF Sub-basin 10

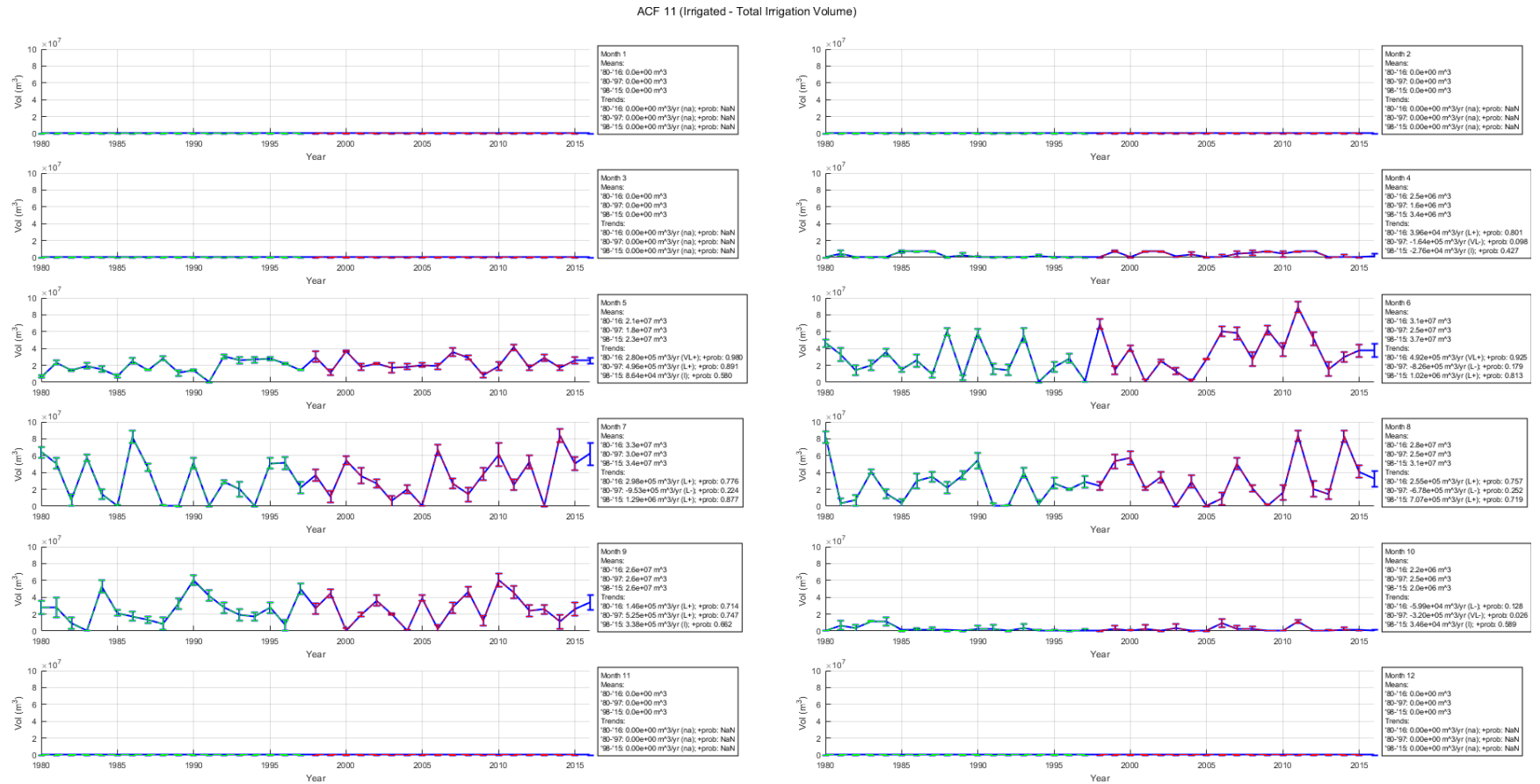


Figure 4-25: Monthly irrigation volumes for ACF Sub-basin 11

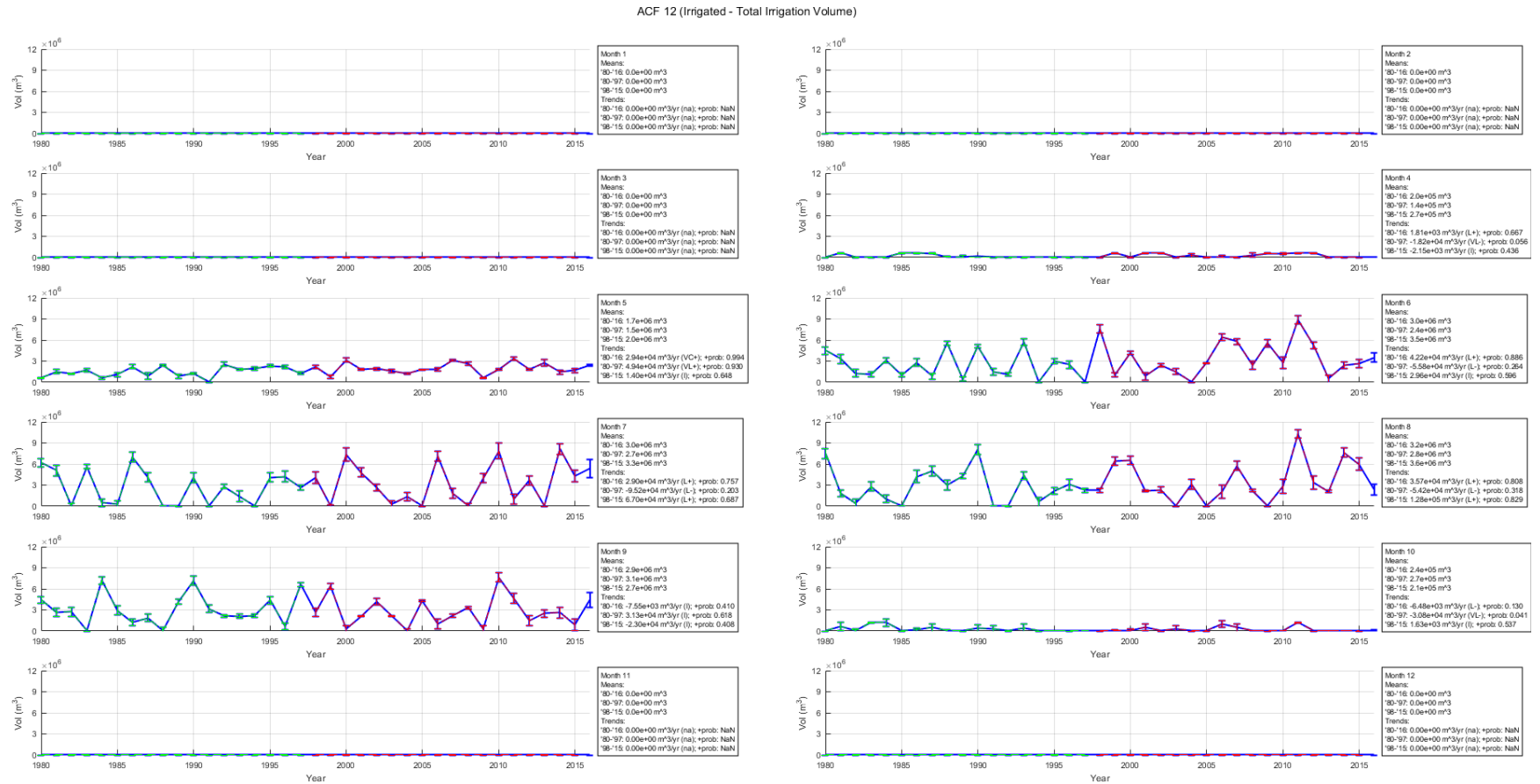


Figure 4-26: Monthly irrigation volumes for ACF Sub-basin 12

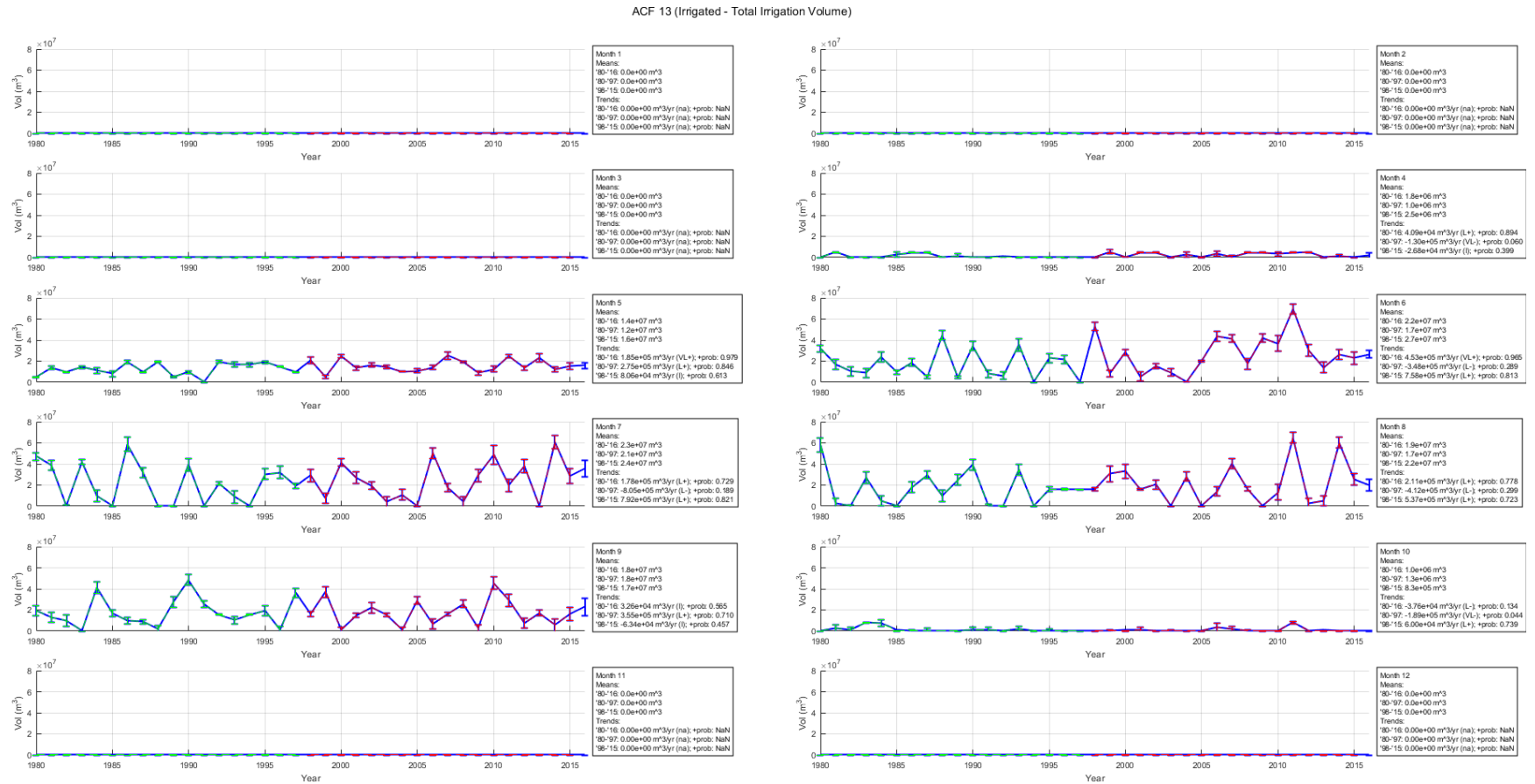


Figure 4-27: Monthly irrigation volumes for ACF Sub-basin 13

4.5.12 ACF Monthly Irrigation Volumes: Apalachicola

For the Apalachicola sub-basin (sub-basin 14), the irrigation season spans from April through October. As shown in Figure 4-28, monthly irrigation volumes have large inter-annual variations, with irrigation volumes reaching up to four times or more of the long term (1980-2016) mean during droughts, especially in the summer months of the 1998-2015 period. Also in these months, peak irrigation volumes are generally greater in magnitude and occur more frequently during the 1998-2015 period than the 1980-1997 period, indicating that droughts are becoming more common and more severe. Mean irrigation volumes of the 1998-2015 period are greater than their counterparts from the 1980-1997 period throughout the growing season except for the month of October. The mean irrigation volume in April during the 1998-2015 period is more than double the corresponding April volume from the 1980-1997 period. The 1980-2016 trends in irrigation volumes are “very likely” positive (indicating increasing irrigation volumes annually) for most of the summer.

ACF 14 (Irrigated - Total Irrigation Volume)

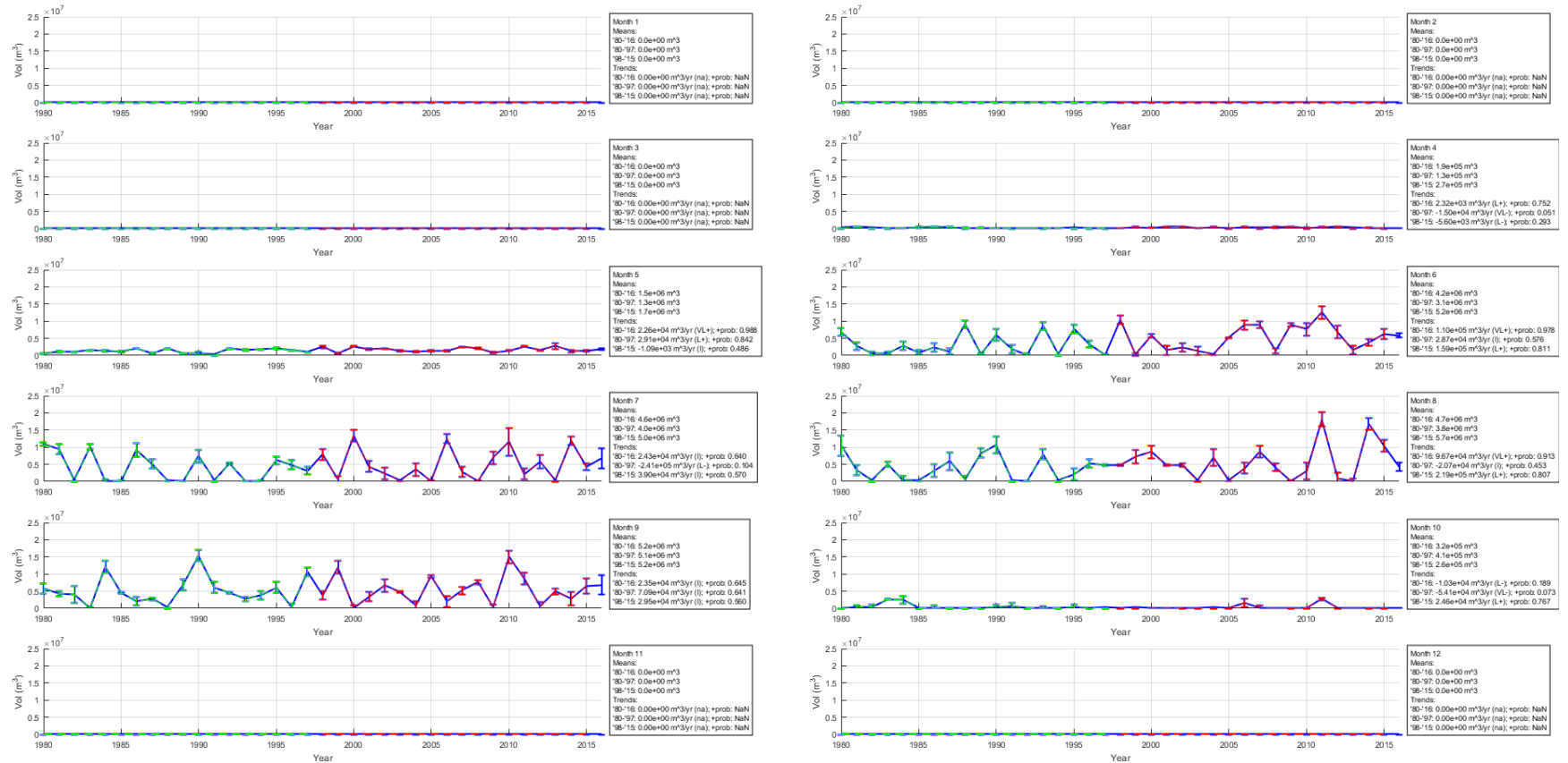


Figure 4-28: Monthly irrigation volumes for ACF Sub-basin 14

4.5.13 ACF Agricultural and Irrigation Demand Assessments: Summary

Crop yields and irrigation volumes simulated by way of integrating multi-sensor gridded climate, soil, and crop data with the DSSAT-CSM illustrate how crop yield and irrigation demand represent highly non-linear integrators of temperature, precipitation, potential evaporation, crop genetics, and agricultural and irrigation management practices. These simulations provide valuable insights that cannot readily be discerned from analysis of climate variables or individual gridded data products alone. Major crops in the Upper Chattahoochee are largely rainfed, but considering the slowed increase and/or decrease in rainfed crop yields in the region, the Upper Chattahoochee may have to consider expanding irrigated acreage. For the remainder of the ACF, summertime rising temperatures and precipitation shortfalls would place considerable stress on surface and groundwater reservoirs during droughts as monthly irrigation demands could peak to multiple times the long term historical means that are conventionally used to assess irrigation allowances. This analysis also confirms that droughts are occurring with increasing frequency and severity throughout the ACF and that the crops themselves may be reaching biophysical limits with regard to resilience towards the changing climate. These findings highlight the need to develop an adaptive management strategy to safeguard agricultural production and water resources especially during drought periods.

4.6 Hindcasting of natural streamflows using GPM IMERG daily precipitation retrievals

In the following hindcasting case studies, remote sensing retrievals of daily cumulative precipitation from the GPM IMERG Version 5 Late Release are incorporated into the Sacramento Soil Moisture Accounting (SAC-SMA) model for estimation of natural streamflows. As mentioned in Chapter 2, SAC-SMA accepts input of daily precipitation and potential evapotranspiration and provides daily estimates of streamflow. In this study, snow precipitation is converted to daily snowmelt discharge (a surrogate for SAC-SMA precipitation input during the winter season) using the simple SNOW-17 model which only requires input of daily precipitation and air temperature. Daily potential evapotranspiration is estimated using the similarly parsimonious Hamon model (Hamon 1961) which ingests latitude and daily mean temperature as input. As SAC-SMA is a lumped model, daily input variables (i.e. temperature and precipitation data from GRIDMET and remote sensing precipitation data) are spatially averaged over the watershed of each case study site. The case study locations tested in this study are listed in Table 4-11.

Table 4-11: Case study locations for assessing SAC-SMA performance with incorporation of remote sensing precipitation retrievals

Watershed Name	HUC-8 Number	USGS Station Number	Station Latitude	Station Longitude	Area (km ²)
East Fork White River at Columbus, Indiana	05120205	03364000	39.200	-85.926	4,421
Grand River at Lansing, Michigan	04050004	04113000	42.751	-84.555	3,186
North Fork John Day River at Monument, Oregon	17070202	14046000	44.814	-119.431	6,527
Greens Bayou near Houston, Texas	12040104	08076000	29.918	-95.307	178
French Broad River at Asheville, North Carolina	06010105	03451500	35.609	-82.579	2,448
Sacramento R.A. Delta, California	18020005	11342000	40.940	-122.416	1,101
North Fork of Clearwater River near Canyon Ranger Station, Montana	17060307	13340600	46.841	-115.621	3,357

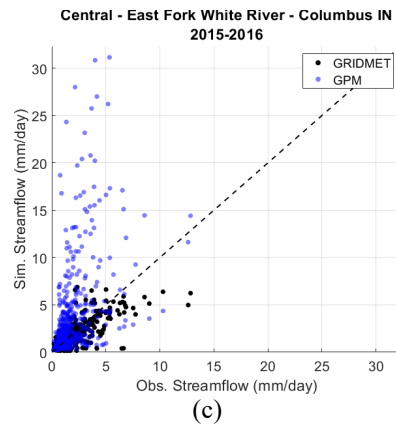
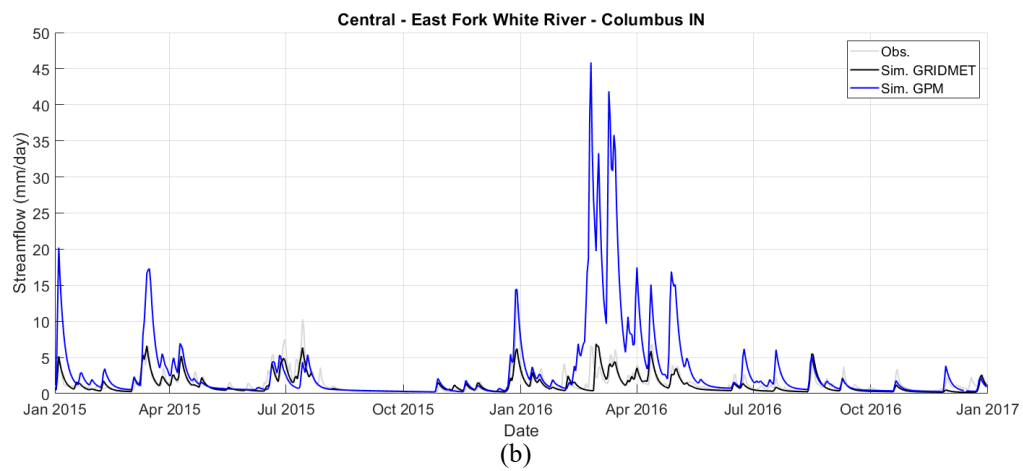
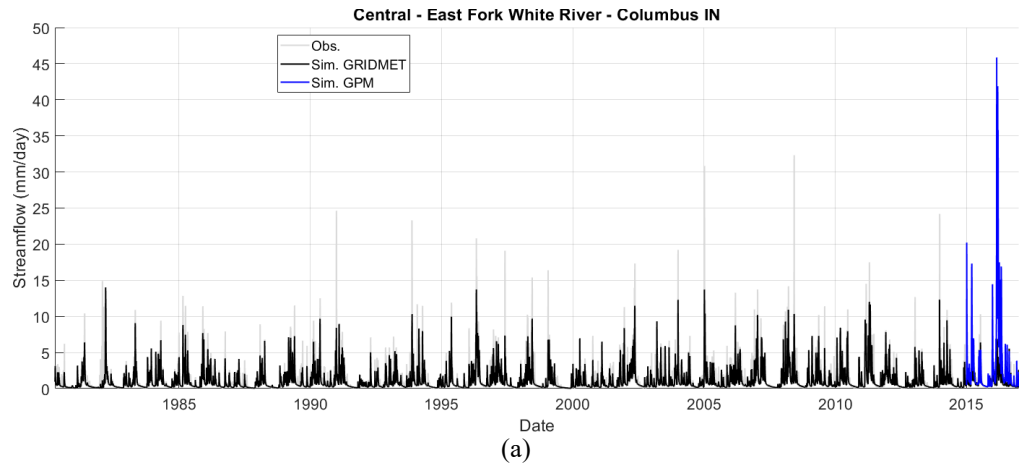
The SAC-SMA model is first calibrated for each case study site with historical streamflow data provided by the U.S. Geological Survey (USGS). Year 1980 to 2000 USGS Daily streamflow data, GRIDMET precipitation and temperature data, and potential evapotranspiration estimates from the Hamon model are used to calibrate the 13 parameters of SAC-SMA using the Hydromad software package. The Hydromad package includes data-optimization tools for calibrating SAC-SMA model parameters. For these case studies, SAC-SMA parameters are optimized in terms of the Nash-Sutcliffe model efficiency coefficient.

After calibration, SAC-SMA is run from years 2014 to 2016 both without (Control) and with incorporation of remote sensing precipitation input during years 2015 to 2016. Year 2014 is included in the simulation period (but without incorporation of remote sensing precipitation data) to serve as the model's "spin up" period. Simulated streamflows are subsequently compared to measured streamflows from USGS stream gauge data. Model performance during the 2015-2016 period is assessed by way of three metrics, NRMSE (root-mean-squared-error normalized by the standard deviation of observations), Nash-Sutcliffe model efficiency coefficient (NSE), and PBIAS (percent bias). According to Moriasi et al. (2007), a watershed streamflow model can be judged as satisfactory if the NRMSE is less than 70 percent, NSE is greater than 0.5, and PBIAS is within ± 25 percent.

4.6.1 East Fork White River at Columbus, Indiana

Figure 4-29 summarizes the performance of the calibrated SAC-SMA model at the East Fork White River at Columbus, Indiana site. The watershed is located in the Central climate region. Even though the model was satisfactorily calibrated for the 1980-2000 period, extreme peak streamflows (e.g. streamflows exceeding 10 mm/day) were underestimated

during the calibration period. During the 2015-2016 period, SAC-SMA had satisfactory performance under the Control scenario; however, when daily precipitation data was replaced with GPM IMERG Version 5 Late Release retrievals, model performance suffered greatly, with all three performance metrics (NSE, NRMSE, and PBIAS) far exceeding acceptable values. With incorporation of GPM IMERG data at this site, streamflows are overestimated, especially during the spring and early summer of year 2016. This finding is consistent with the GPM IMERG wet bias (relative to the GRIDMET reference) in the Central climate region as assessed in Chapter 3.



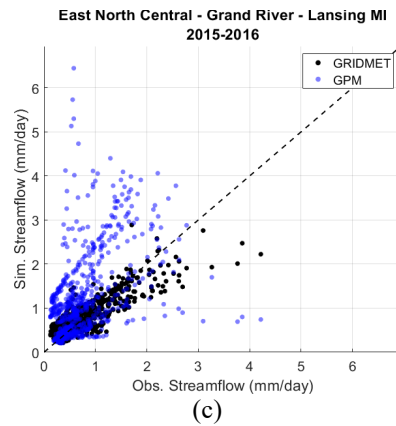
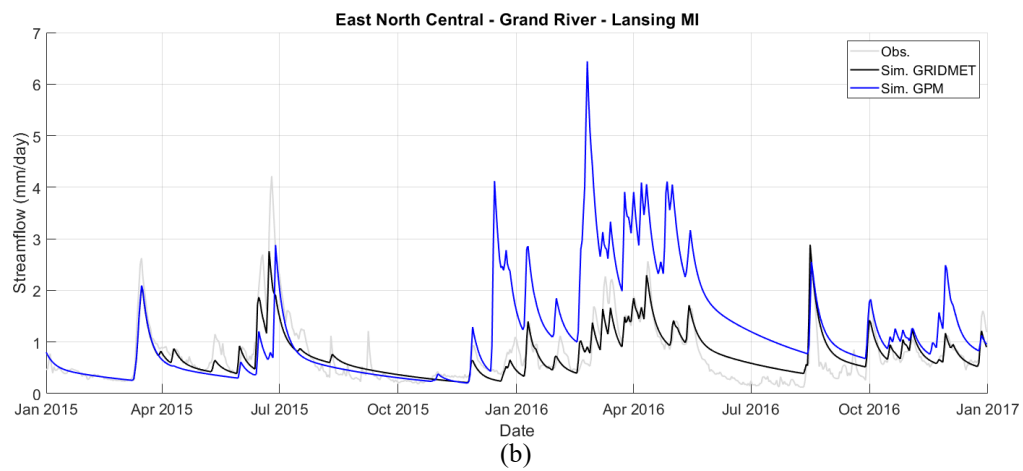
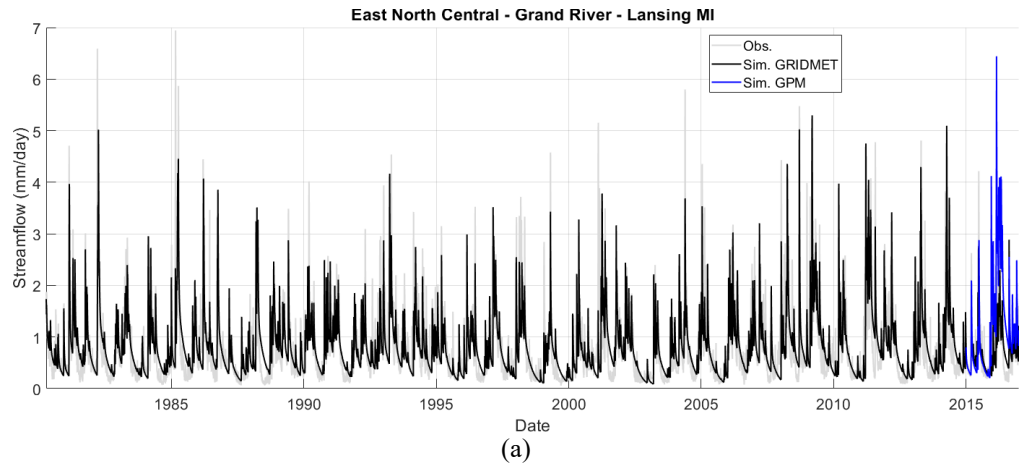
Performance Metric	Control	GPM IMERG
NSE	0.633	-10.97
NRMSE	60.5	345.8
PBIAS	-17.0	120.1

Note: Red values in table above indicate unsatisfactory performance

Figure 4-29: Year 2015-2016 SAC-SMA performance at East Fork White River at Columbus, Indiana site with incorporation of GPM IMERG daily precipitation retrievals. (a) Streamflow time series during the calibration (1980-2000) and validation (2015-2016) period. (b) Time series during 2015-2016 period (c) Year 2015-2016 scatter plot (d) Summary performance metrics during the 2015-2016 period

4.6.2 Grand River at Lansing, Michigan

Figure 4-30 summarizes the performance of the calibrated SAC-SMA model at the Grand River at Lansing, Michigan site. The watershed is located in the East North Central climate region. During the 2015-2016 period, SAC-SMA had satisfactory performance under the Control scenario; however, when daily precipitation data was replaced with GPM IMERG Version 5 Late Release retrievals, model performance suffered greatly, with all three performance metrics (NSE, NRMSE, and PBIAS) far exceeding acceptable values. Similar to the East Fork White River site, with incorporation of GPM IMERG data at this site, streamflows are overestimated, especially during the winter through summer of year 2016. This finding is consistent with the GPM IMERG wet bias (relative to the GRIDMET reference) in the East North Central climate.



Performance Metric	Control	GPM IMERG
NSE	0.729	-2.01
NRMSE	52.1	173.5
PBIAS	-0.3	60.5

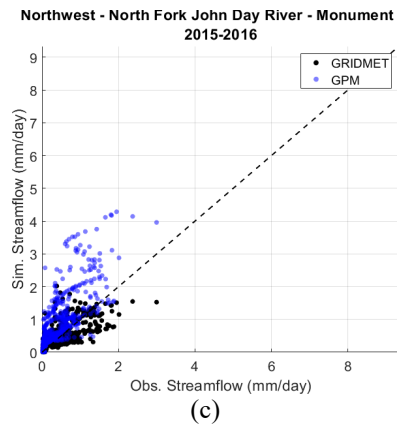
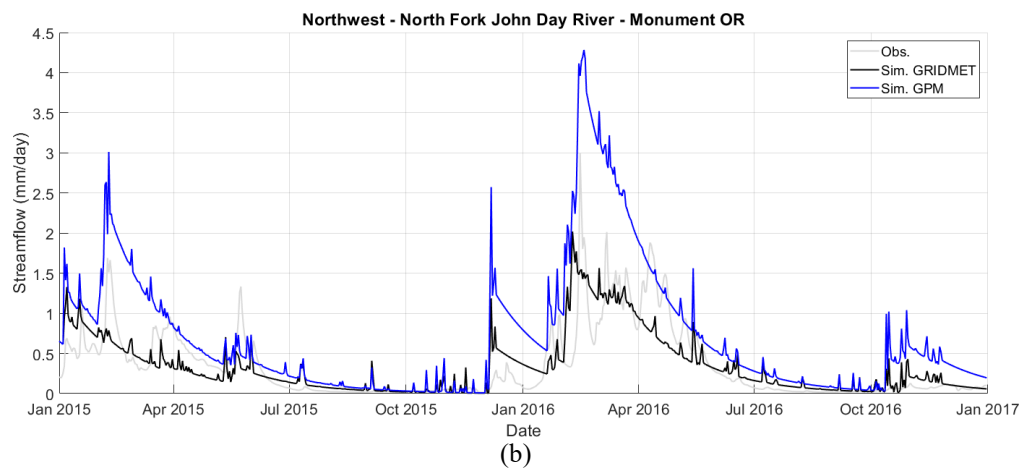
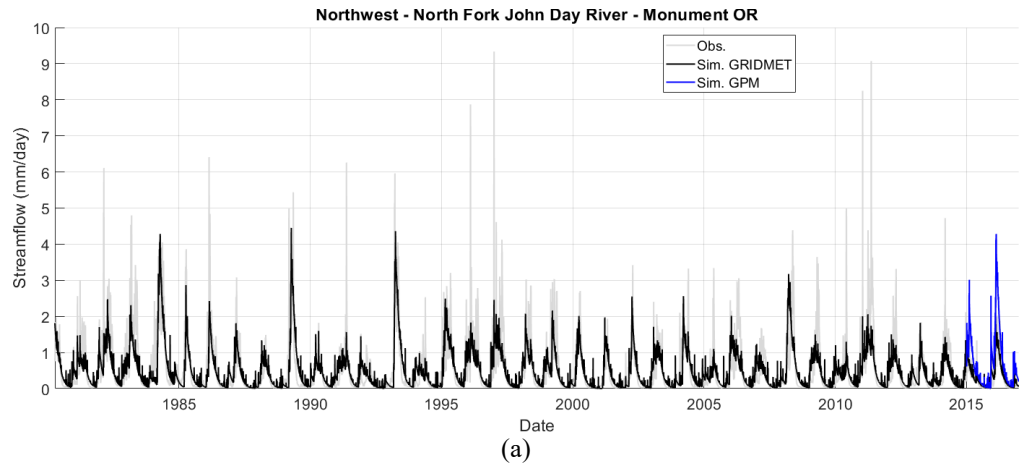
Note: Red values in table above indicate unsatisfactory performance

(d)

Figure 4-30: Year 2015-2016 SAC-SMA performance at Grand River at Lansing, Michigan site with incorporation of GPM IMERG daily precipitation retrievals

4.6.3 North Fork John Day River at Monument, Oregon

Figure 4-31 summarizes the performance of the calibrated SAC-SMA model at the North Fork John Day River at Monument, Oregon site. The watershed is located in the Northwest climate region. During the 2015-2016 period, SAC-SMA had satisfactory performance under the Control scenario; however, when daily precipitation data was replaced with GPM IMERG Version 5 Late Release retrievals, model performance suffered greatly, with all three performance metrics (NSE, NRMSE, and PBIAS) far exceeding acceptable values. With incorporation of GPM IMERG data at this site, streamflows are overestimated, especially during the winter, spring, and early summer seasons.



Performance Metric	Control	GPM IMERG
NSE	0.572	-1.22
NRMSE	65.4	149.0
PBIAS	-0.2	107.0

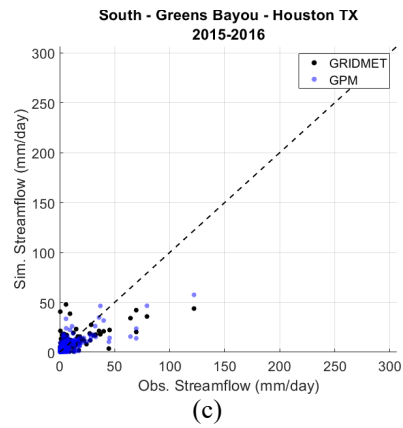
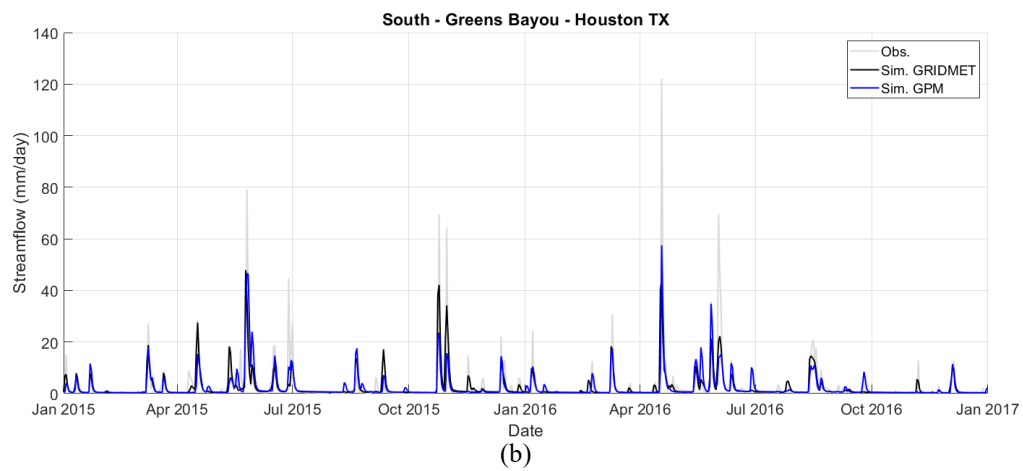
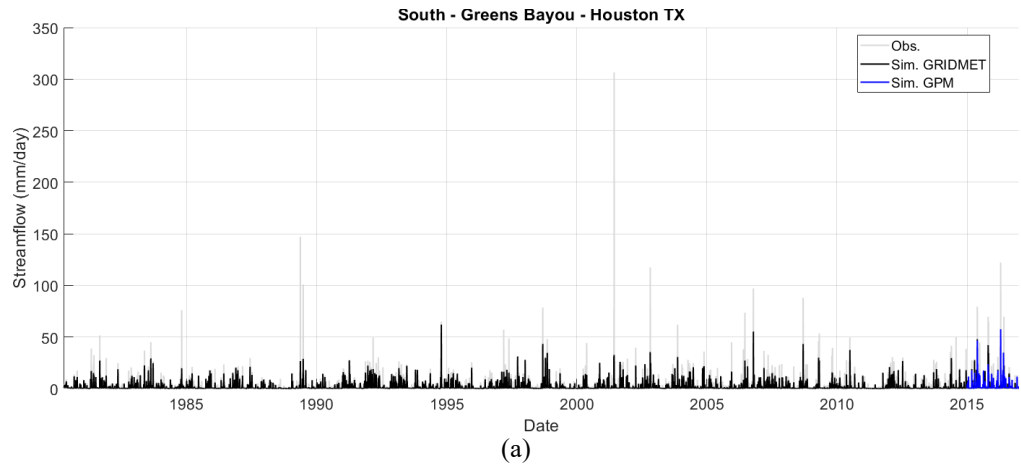
Note: Red values in table above indicate unsatisfactory performance

(d)

Figure 4-31: Year 2015-2016 SAC-SMA performance at North Fork John Day River at Monument, Oregon site with incorporation of GPM IMERG daily precipitation retrievals

4.6.4 Greens Bayou near Houston, Texas

Figure 4-32 summarizes the performance of the calibrated SAC-SMA model at the Greens Bayou near Houston, Texas site. The watershed is located in the South climate region. During the 2015-2016 period, SAC-SMA had satisfactory performance both under the Control scenario and when daily precipitation data was replaced with GPM IMERG Version 5 Late Release retrievals, with all three performance metrics (NSE, NRMSE, and PBIAS) within acceptable bounds, despite underestimation of extreme peak flows.



Performance Metric	Control	GPM IMERG
NSE	0.529	0.585
NRMSE	68.6	64.4
PBIAS	-14.3	-16.3

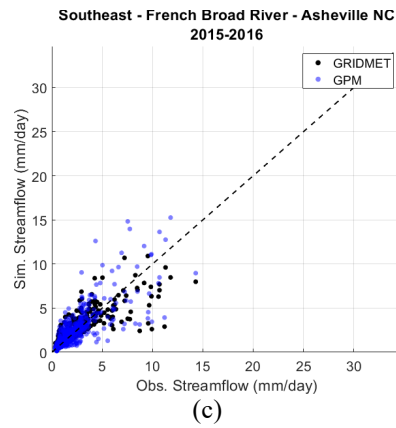
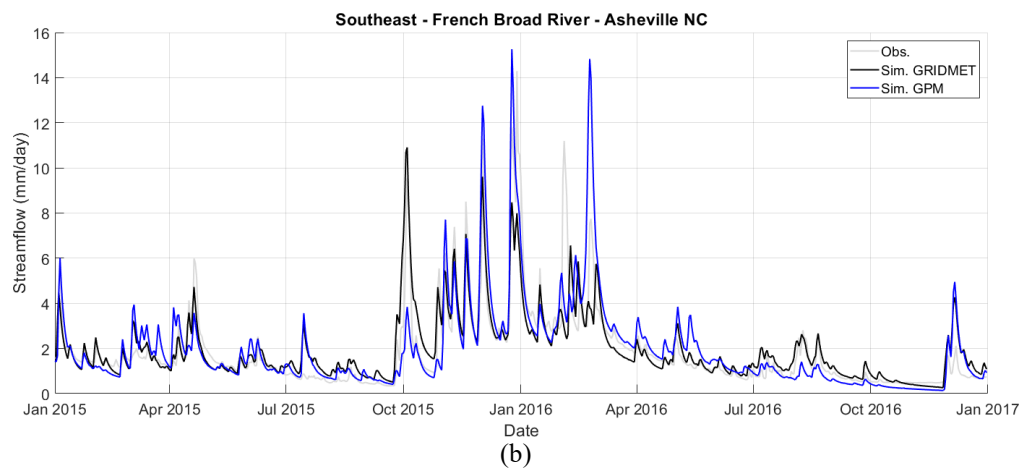
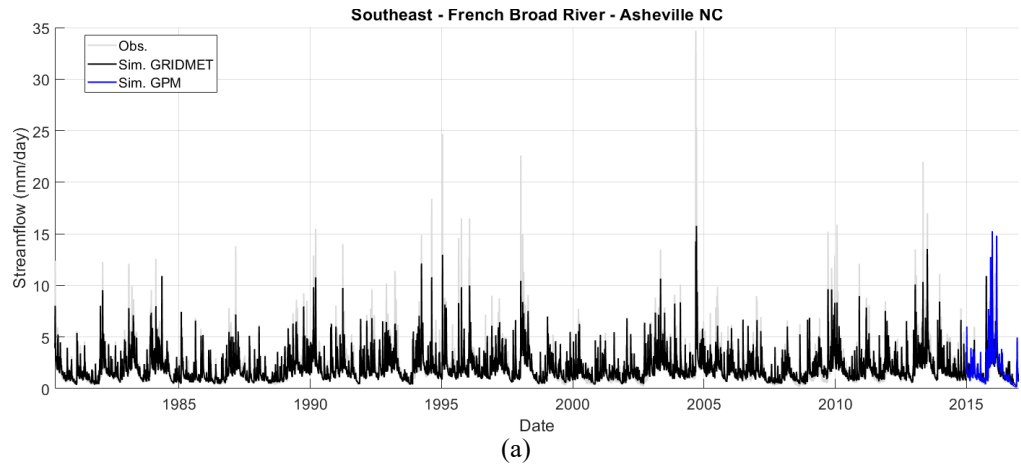
Note: Red values in table above indicate unsatisfactory performance

(d)

Figure 4-32: Year 2015-2016 SAC-SMA performance at Greens Bayou near Houston, Texas site with incorporation of GPM IMERG daily precipitation retrievals

4.6.5 French Broad River at Asheville, North Carolina

Figure 4-33 summarizes the performance of the calibrated SAC-SMA model at the French Broad River at Asheville, North Carolina site. The watershed is located in the Southeast climate region. During the 2015-2016 period, SAC-SMA had satisfactory performance under the Control and GPM IMERG scenarios.



Performance Metric	Control	GPM IMERG
NSE	0.701	0.582
NRMSE	54.6	64.6
PBIAS	4.8	6.2

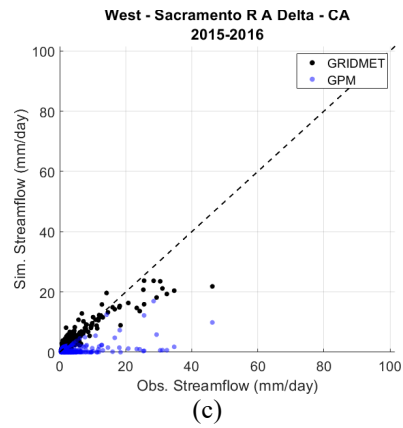
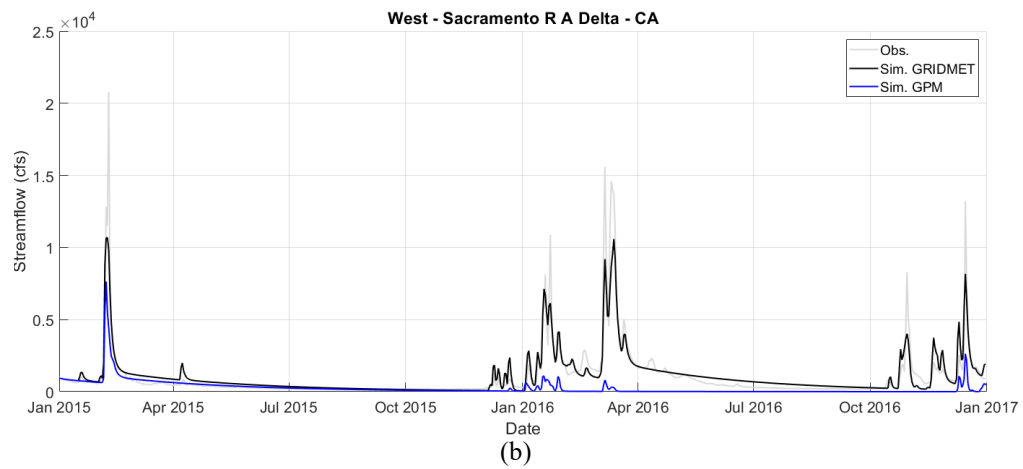
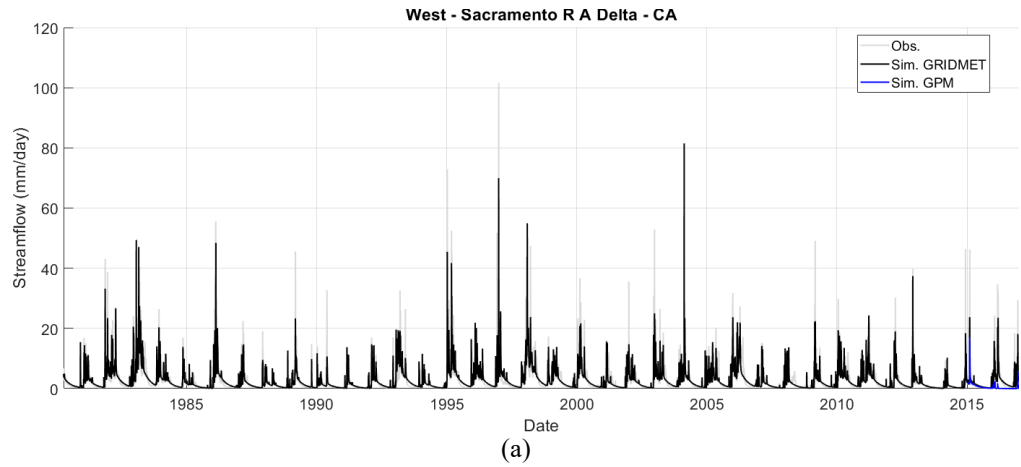
Note: Red values in table above indicate unsatisfactory performance

(d)

Figure 4-33: Year 2015-2016 SAC-SMA performance at French Broad River at Asheville, North Carolina site with incorporation of GPM IMERG daily precipitation retrievals

4.6.6 Sacramento R.A. Delta, California

Figure 4-34 summarizes the performance of the calibrated SAC-SMA model at the Sacramento R.A. Delta, California site. The watershed is located in the West climate region. During the 2015-2016 period, SAC-SMA had satisfactory performance under the Control scenario; however, when daily precipitation data was replaced with GPM IMERG Version 5 Late Release retrievals, model performance suffered greatly, with all three performance metrics (NSE, NRMSE, and PBIAS) exceeding acceptable values. Incorporation of GPM IMERG data resulted in severe underestimation of flows, especially the peak flows of winter and early spring. Results suggest that some large precipitation events were entirely missed by the GPM IMERG retrieval (e.g. Fall 2016). These finds are consistent with the dry bias (relative to the GRIDMET reference) in the GPM IMERG product for the West climate region as assessed in Chapter 3.



Performance Metric	Control	GPM IMERG
NSE	0.835	0.034
NRMSE	40.5	98.2
PBIAS	5.6	-74.5

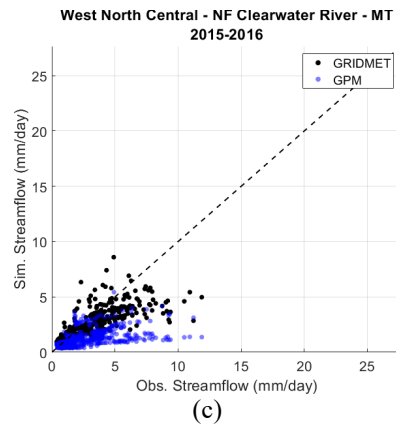
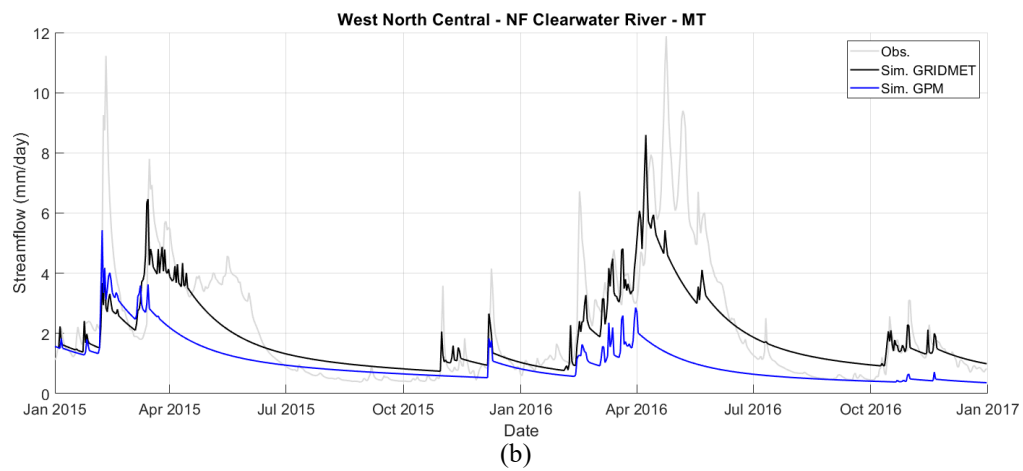
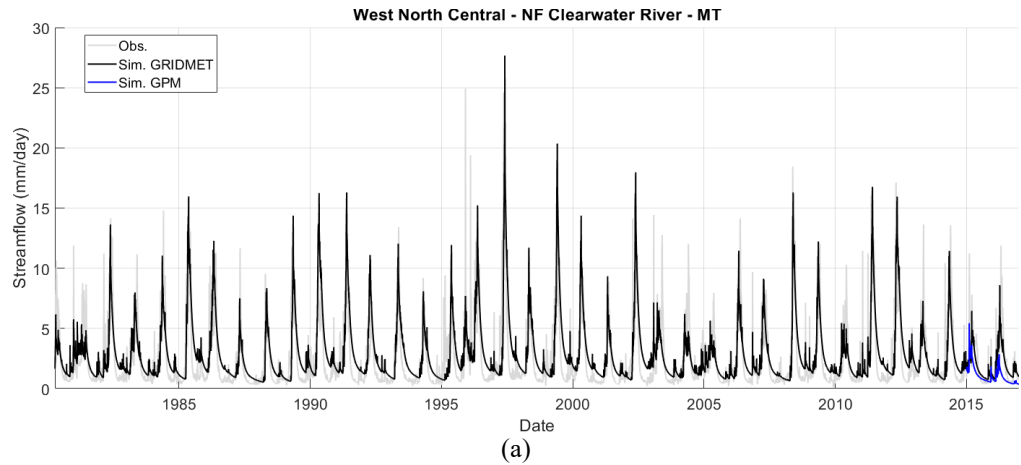
Note: Red values in table above indicate unsatisfactory performance

(d)

Figure 4-34: Year 2015-2016 SAC-SMA performance at Sacramento R.A. Delta, California site with incorporation of GPM IMERG daily precipitation retrievals

4.6.7 North Fork of Clearwater River near Canyon Ranger Station, Montana

Figure 4-35 summarizes the performance of the calibrated SAC-SMA model at the North Fork of Clearwater River near Canyon Ranger Station, Montana site. The watershed is located in the West North Central climate region. During the 2015-2016 period, SAC-SMA had satisfactory performance under the Control scenario; however, when daily precipitation data was replaced with GPM IMERG Version 5 Late Release retrievals, model performance suffered greatly, with all three performance metrics (NSE, NRMSE, and PBIAS) far exceeding acceptable values. Incorporation of GPM IMERG data resulted in severe underestimation of flows, especially during the spring and summer periods.



Performance Metric	Control	GPM IMERG
NSE	0.620	-0.019
NRMSE	61.6	100.9
PBIAS	-10.5	-51.1

Note: Red values in table above indicate unsatisfactory performance

(d)

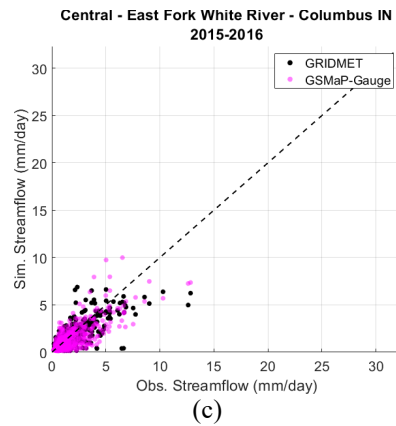
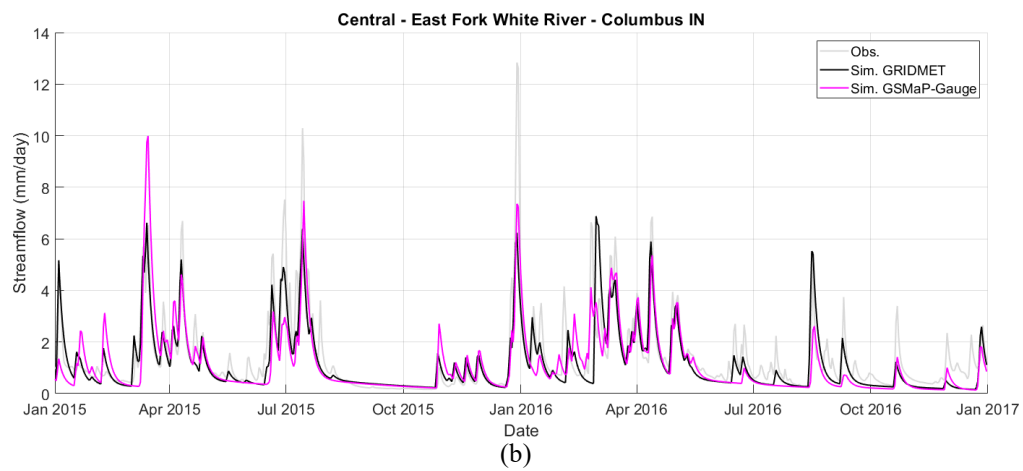
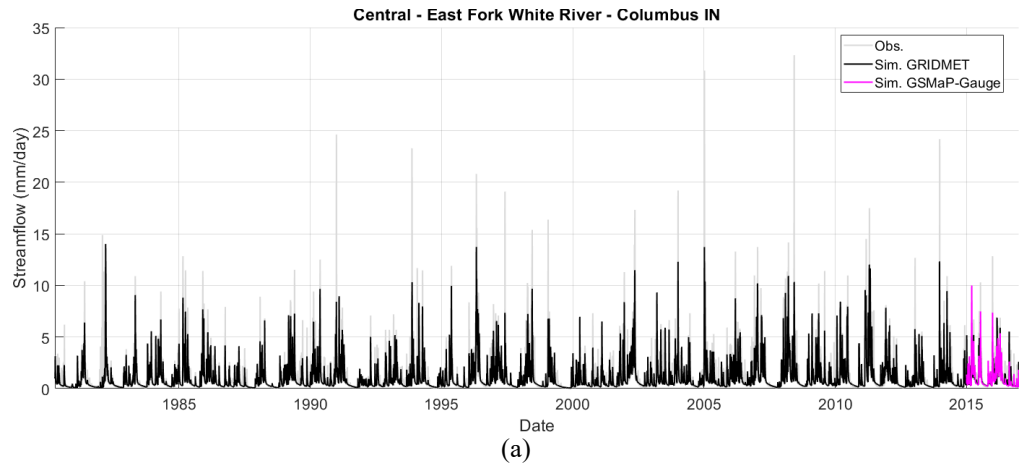
Figure 4-35: Year 2015-2016 SAC-SMA performance at North Fork of Clearwater River near Canyon Ranger Station, Montana site with incorporation of GPM IMERG daily precipitation retrievals

4.7 Hindcasting of natural streamflows using JAXA GSMP daily precipitation retrievals

The following hindcasting case studies are conducted just as those mentioned in the previous section, except that remote sensing retrievals of daily cumulative precipitation from the JAXA GSMP-Gauge Version 7 are incorporated into the Sacramento Soil Moisture Accounting (SAC-SMA) model for estimation of natural streamflows.

4.7.1 East Fork White River at Columbus, Indiana

Figure 4-36 summarizes the performance of the calibrated SAC-SMA model at the East Fork White River at Columbus, Indiana site. During the 2015-2016 period, SAC-SMA had satisfactory performance under the Control scenario, but unlike the GPM IMERG data incorporation experiment, SAC-SMA model performance was also satisfactory with incorporation of GSMP-Gauge daily cumulative precipitation retrievals.



Performance Metric	Control	GSMaP-Gauge
NSE	0.633	0.595
NRMSE	60.5	63.6
PBIAS	-17.0	-20.3

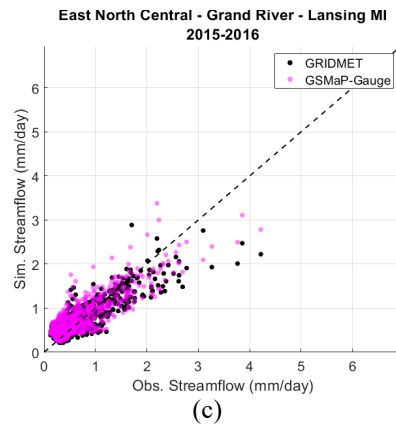
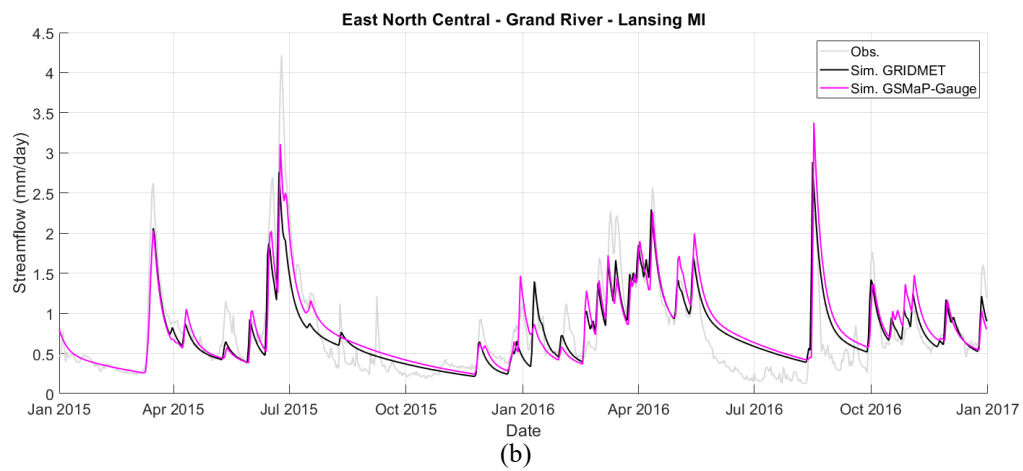
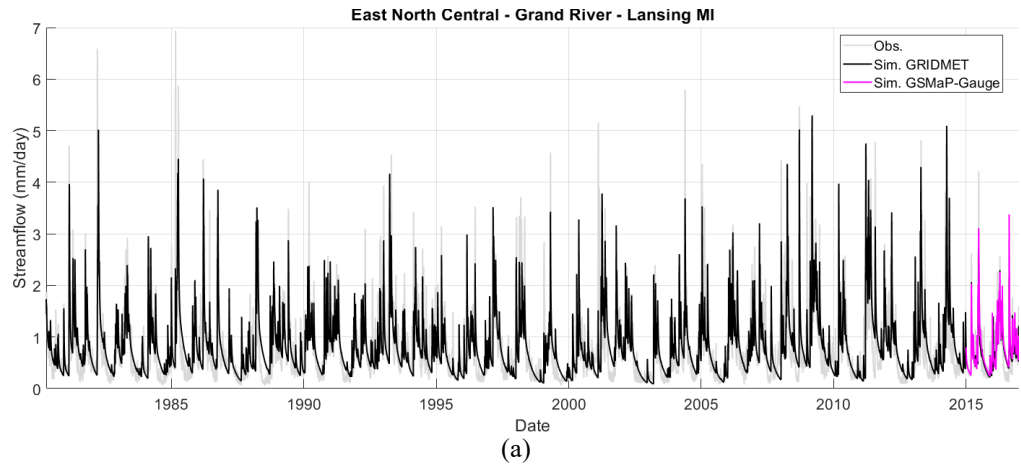
Note: Red values in table above indicate unsatisfactory performance

(d)

Figure 4-36: Year 2015-2016 SAC-SMA performance at East Fork White River at Columbus, Indiana site with incorporation of JAXA GSMaP-Gauge daily precipitation retrievals. (a) Streamflow time series during the calibration (1980-2000) and validation (2015-2016) period. (b) Time series during 2015-2016 period (c) Year 2015-2016 scatter plot (d) Summary performance metrics during the 2015-2016 period

4.7.2 Grand River at Lansing, Michigan

Figure 4-37 summarizes the performance of the calibrated SAC-SMA model at the Grand River at Lansing, Michigan site. The watershed is located in the East North Central climate region. During the 2015-2016 period, SAC-SMA had satisfactory performance under the Control and GSMaP-Gauge scenarios.



Performance Metric	Control	GSMaP-Gauge
NSE	0.729	0.704
NRMSE	52.1	54.3
PBIAS	-0.3	6.7

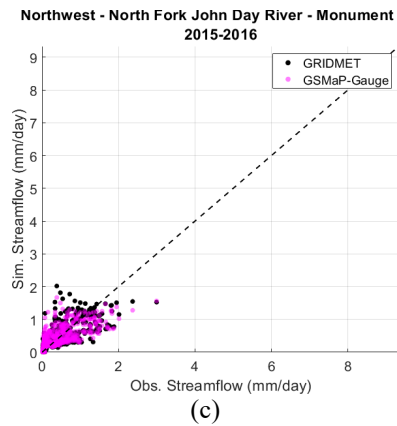
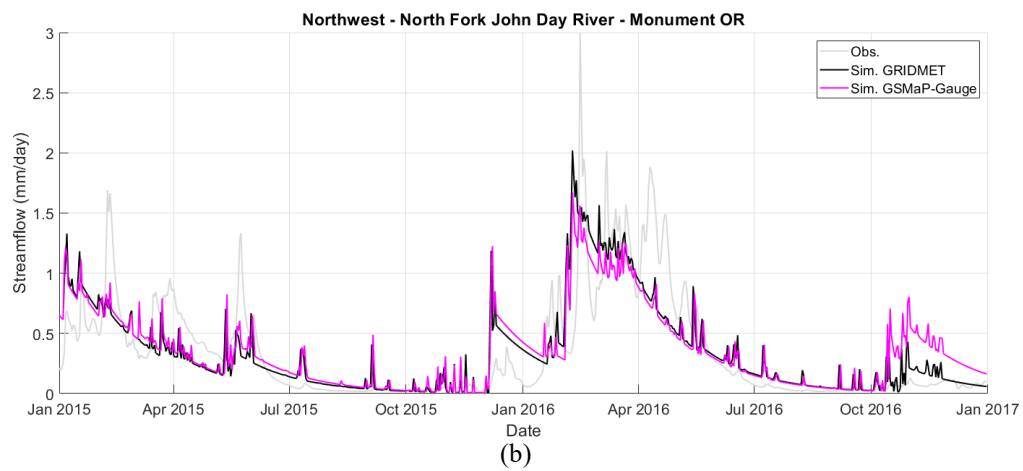
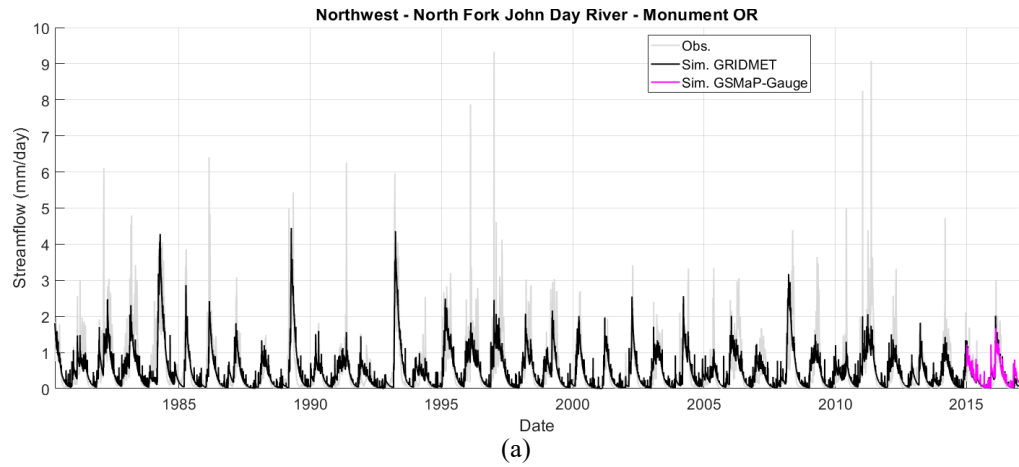
Note: Red values in table above indicate unsatisfactory performance

(d)

Figure 4-37: Year 2015-2016 SAC-SMA performance at Grand River at Lansing, Michigan site with incorporation of JAXA GSMaP-Gauge daily precipitation retrievals

4.7.3 North Fork John Day River at Monument, Oregon

Figure 4-38 summarizes the performance of the calibrated SAC-SMA model at the North Fork John Day River at Monument, Oregon site. With incorporation of GSMP-Gauge data, SAC-SMA model performance was satisfactory.



Performance Metric	Control	GSMaP-Gauge
NSE	0.572	0.551
NRMSE	65.4	67.0
PBIAS	-0.2	4.8

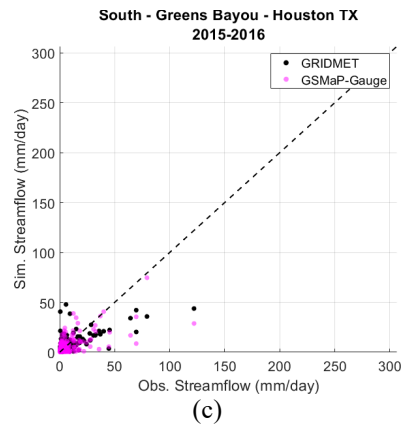
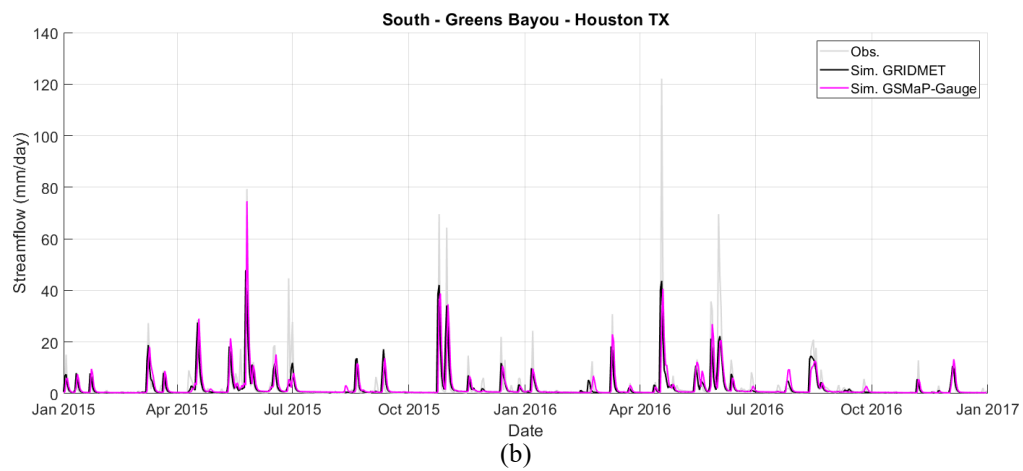
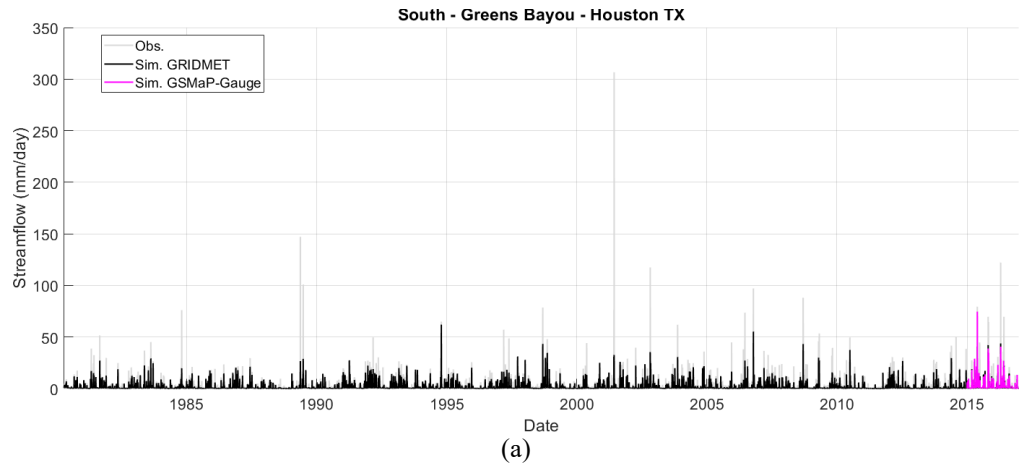
Note: Red values in table above indicate unsatisfactory performance

(d)

Figure 4-38: Year 2015-2016 SAC-SMA performance at North Fork John Day River at Monument, Oregon site with incorporation of JAXA GSMaP-Gauge daily precipitation retrievals

4.7.4 Greens Bayou near Houston, Texas

Figure 4-39 summarizes the performance of the calibrated SAC-SMA model at the Greens Bayou near Houston, Texas site. During the 2015-2016 period, SAC-SMA had satisfactory performance under the Control scenario, but not when daily precipitation data was replaced with GSMaP-Gauge data, due to underestimation of peak flows.



Performance Metric	Control	GSMaP-Gauge
NSE	0.529	0.460
NRMSE	68.6	73.4
PBIAS	-14.3	-11.2

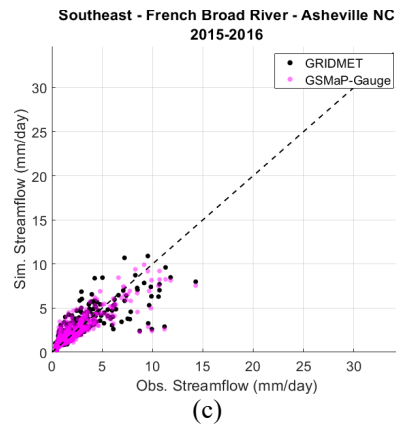
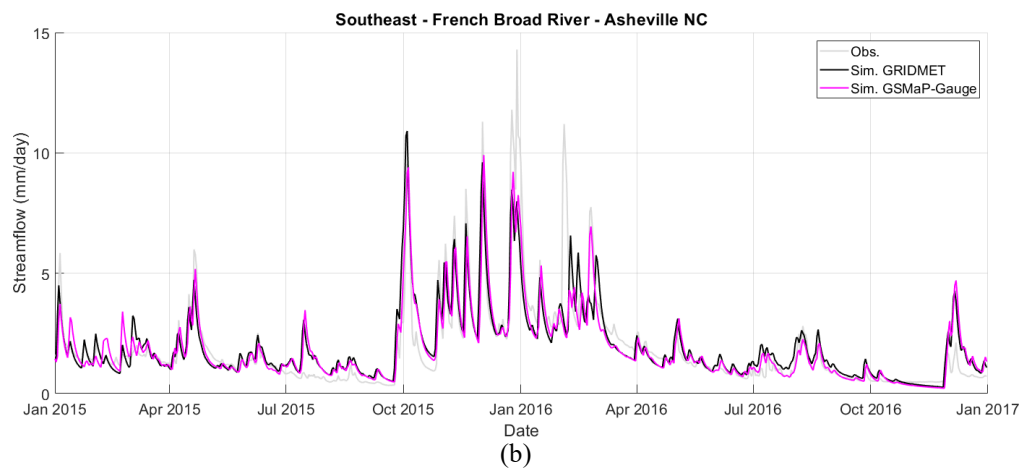
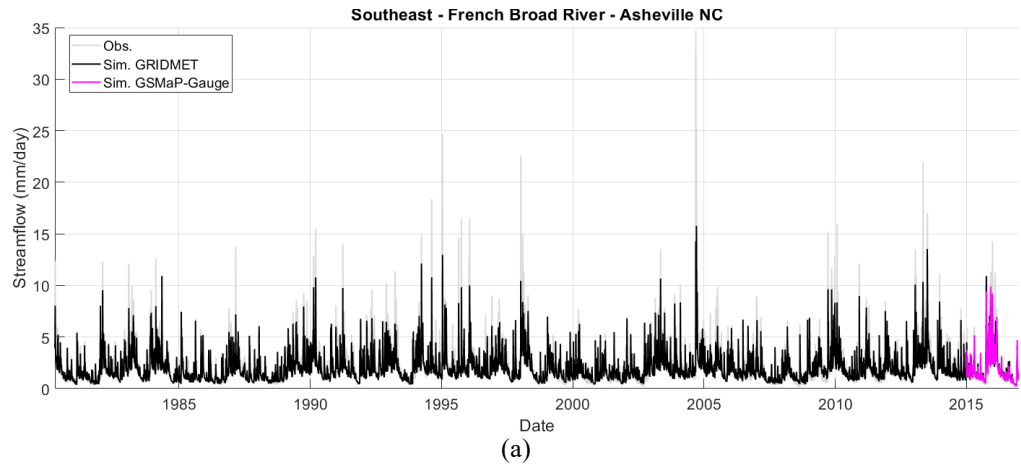
Note: Red values in table above indicate unsatisfactory performance

(d)

Figure 4-39: Year 2015-2016 SAC-SMA performance at Greens Bayou near Houston, Texas site with incorporation of JAXA GSMaP-Gauge daily precipitation retrievals

4.7.5 French Broad River at Asheville, North Carolina

Figure 4-40 summarizes the performance of the calibrated SAC-SMA model at the French Broad River at Asheville, North Carolina site. During the 2015-2016 period, SAC-SMA had satisfactory performance under the Control and GSMaP-Gauge data incorporation scenarios, unlike the GPM IMERG scenario.



Performance Metric	Control	GSMaP-Gauge
NSE	0.701	0.752
NRMSE	54.6	49.7
PBIAS	4.8	0.4

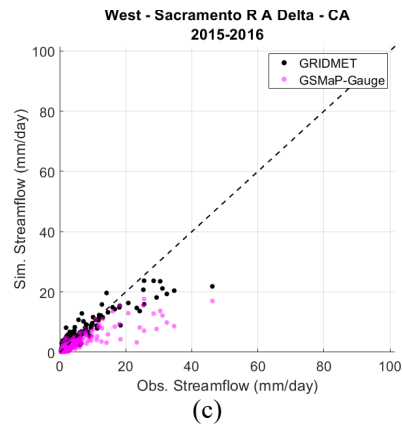
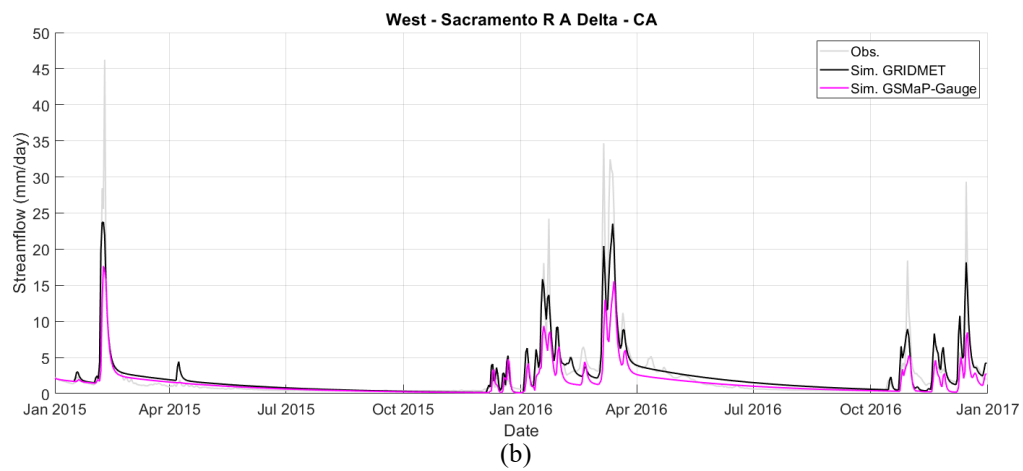
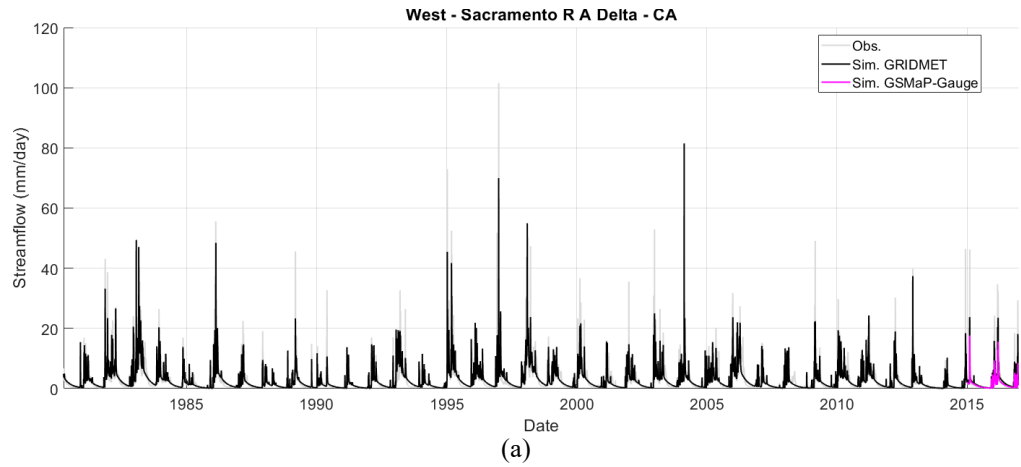
Note: Red values in table above indicate unsatisfactory performance

(d)

Figure 4-40: Year 2015-2016 SAC-SMA performance at French Broad River at Asheville, North Carolina site with incorporation of JAXA GSMaP-Gauge daily precipitation retrievals

4.7.6 Sacramento R.A. Delta, California

Figure 4-41 summarizes the performance of the calibrated SAC-SMA model at the Sacramento R.A. Delta, California site. During the 2015-2016 period, SAC-SMA had satisfactory performance under the Control scenario, but failed according to the PBIAS metric in the GSMaP-Gauge scenario, though model performance was superior to the GPM IMERG data incorporation scenario in which critical precipitation events were missed.



Performance Metric	Control	GSMaP-Gauge
NSE	0.835	0.584
NRMSE	40.5	64.5
PBIAS	5.6	-31.0

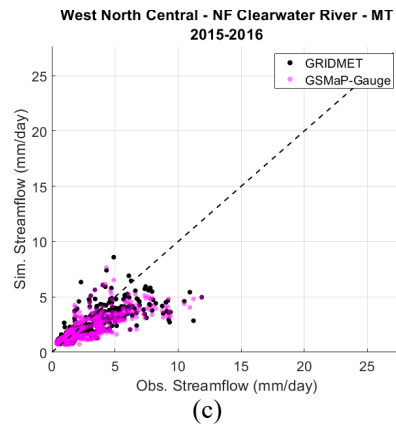
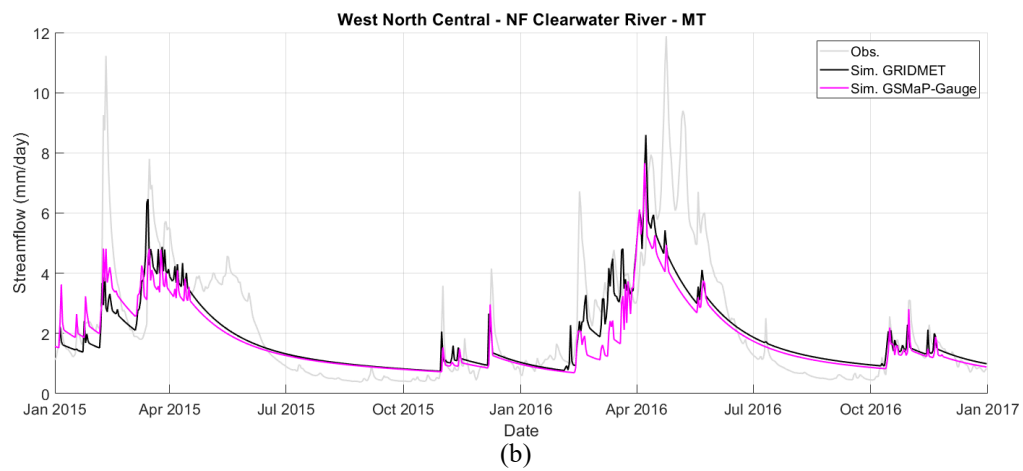
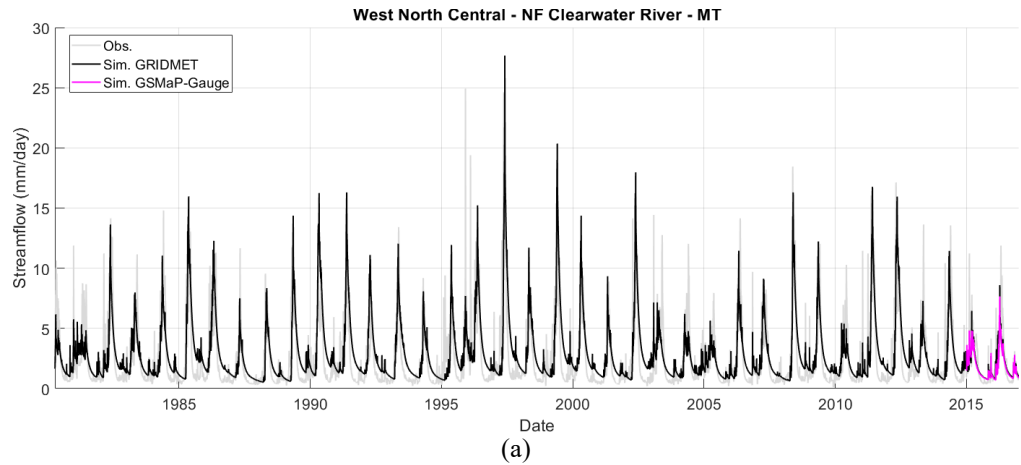
Note: Red values in table above indicate unsatisfactory performance

(d)

Figure 4-41: Year 2015-2016 SAC-SMA performance at Sacramento R.A. Delta, California site with incorporation of JAXA GSMaP-Gauge daily precipitation retrievals

4.7.7 North Fork of Clearwater River near Canyon Ranger Station, Montana

Figure 4-42 summarizes the performance of the calibrated SAC-SMA model at the North Fork of Clearwater River near Canyon Ranger Station, Montana site. During the 2015-2016 period, SAC-SMA had satisfactory performance under the Control and GSMaP-Gauge data incorporation, despite underestimation of streamflows during the spring and summer.



Performance Metric	Control	GSMaP-Gauge
NSE	0.620	0.566
NRMSE	61.6	65.9
PBIAS	-10.5	-17.3

Note: Red values in table above indicate unsatisfactory performance

(d)

Figure 4-42: Year 2015-2016 SAC-SMA performance at North Fork of Clearwater River near Canyon Ranger Station, Montana site with incorporation of JAXA GSMaP-Gauge daily precipitation retrievals

4.8 SAC-SMA calibration using recent remote sensing precipitation retrievals

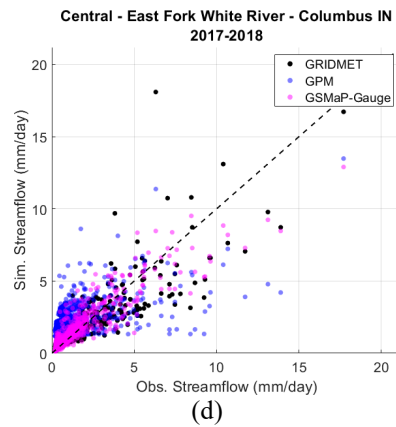
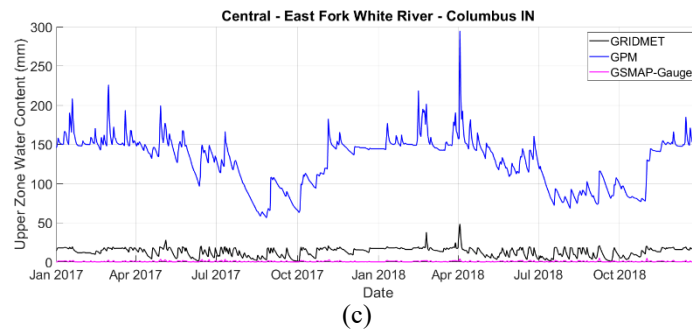
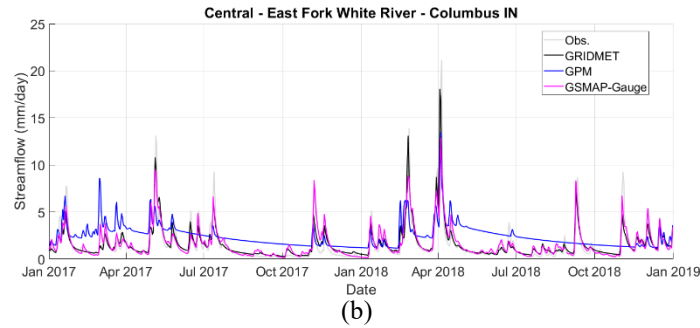
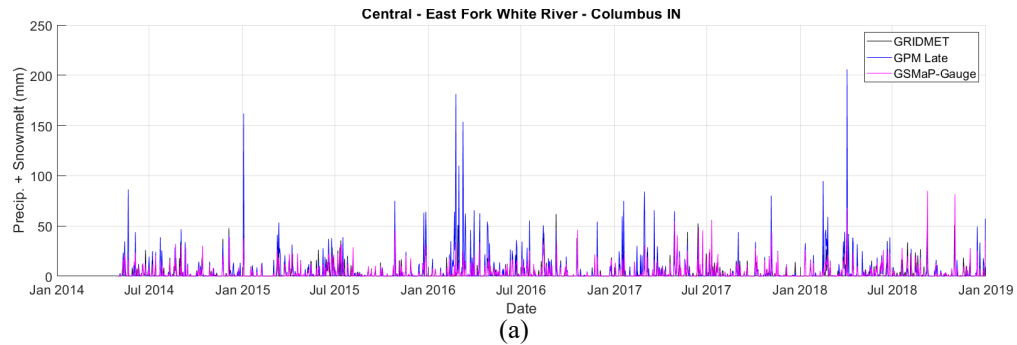
In the previous sections, SAC-SMA was calibrated using long-term (year 1980-2000) reanalysis data from the GRIDMET data product. When SAC-SMA was used to simulate recent streamflows using input of remote sensing precipitation retrievals instead of GRIDMET precipitation estimates, biases in the remote sensing precipitation retrievals, especially in the GPM IMERG Late Release product, oftentimes adversely impacted the SAC-SMA model performance. In the following exercise, SAC-SMA is used to simulate daily streamflows from Jan 2017 to December 2018; however, the SAC-SMA is calibrated using daily remote sensing precipitation retrievals from May 2014 to December 2016 (32 months) instead of GRIDMET precipitation estimates in hopes that this revised calibration procedure would compensate for the biases in the remote sensing precipitation data and allow for more accurate simulation of hydrological flows.

Figure 4-43 through Figure 4-47 illustrate the performance of SAC-SMA when calibrated using recent remote sensing precipitation retrievals. The results generally confirm that the accuracy of SAC-SMA is not only strongly connected to the length of the calibration period, but to the accuracy of the precipitation forcing data set. For the East Fork White River and the Sacramento R.A. Delta watersheds, when calibrated with over 20 years worth of daily GRIDMET precipitation estimates as mentioned previously, SAC-SMA exhibited satisfactory performance (according to the Nash-Sutcliffe, Normalized RMSE, and Percent Bias metrics); however, when calibrated with only 32 months worth of GRIDMET precipitation, SAC-SMA did not perform satisfactorily with the GPM precipitation forcing.

With regard to the use of GPM Late and GSMaP-Gauge precipitation forcing, SAC-SMA calibrated using 32 months worth of GSMaP-Gauge data performed better, often with satisfactory performance at the tested sites, than SAC-SMA calibrated with GPM Late retrievals. Of the five sites tested, GPM-calibrated SAC-SMA only had satisfactory performance at the Greens Bayou watershed, as shown in Figure 4-45, owing to the GPM product's consistency with the rain-gauge derived GRIDMET precipitation data set for that particular watershed.

Table 4-12 and Table 4-13 present some of the SAC-SMA water storage parameters calibrated using 32 months (May 2014 to December 2016) worth of precipitation forcing data from GRIDMET, GPM Late, and GSMaP-Gauge for two of the tested watersheds, East Fork White River and Sacramento R.A. Delta. In the case of the East Fork White River, the stark discrepancy between calibrated water storage parameters between precipitation data sets explains the poor performance of SAC-SMA calibrated with GPM Late data. At this watershed, the GPM product severely overestimated some precipitation events that occurred during the 2014 – 2016 calibration period (refer to Figure 4-43), resulting in the assignment of relatively large capacities for upper and lower soil water storage zones. During the 2017 – 2018 evaluation period, these large storage capacities resulted in a muted streamflow response to precipitation relative to the SAC-SMA simulations calibrated using GRIDMET or GSMaP-Gauge data. For the Sacramento R.A. Delta watershed, the dry bias in the GPM product resulted in the SAC-SMA constructing soil water reservoirs (upper and lower zones) with total capacity about one-third the storage compared to the GRIDMET and half the storage compared to the GSMaP-Gauge calibrations (when lower zone supplemental water capacity is excluded). Results from this

exercise also highlight that even when there is agreement in modeled streamflow between simulations calibrated with different precipitation data products, the SAC-SMA model parameters between these different simulations do not necessarily agree. In summary, this exercise confirms that biases in remote sensing precipitation retrievals have a substantial impact on modeling hydrological flows, and model calibration is not sufficient to mitigate the impact of such errors in precipitation forcing.

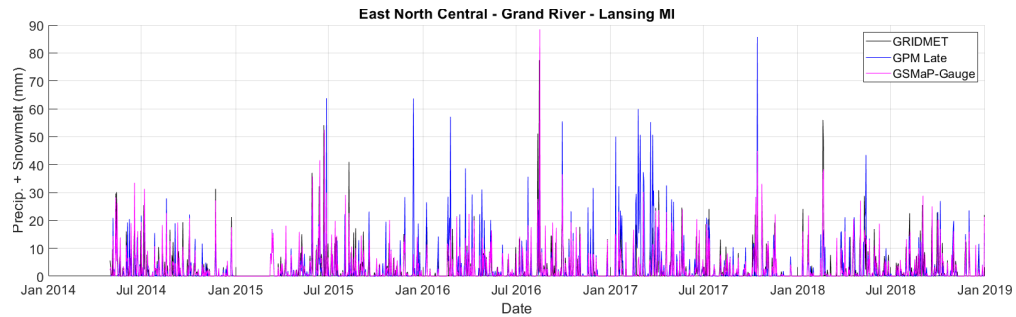


Performance Metric	GRIDMET	GPM	GSMap-Gauge
NSE	0.728	0.113	0.793
NRMSE	52.2	94.1	45.4
PBIAS	2.2	54.8	5.2

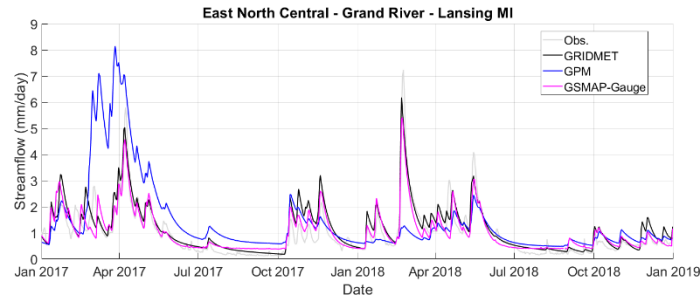
Note: Red values in table above indicate unsatisfactory performance

(e)

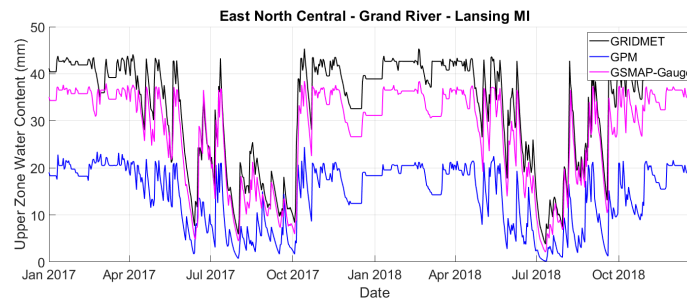
Figure 4-43: Year 2017-2018 SAC-SMA performance at East Fork White River at Columbus, Indiana site with model calibration using daily remote sensing precipitation retrievals. (a) Precipitation time series including snow melt (b) Streamflow time series during 2017-2018 period (c) SAC-SMA normalized upper zone water content (d) Year 2017-2018 scatter plot (e) Performance metrics during the 2017-2018 period.



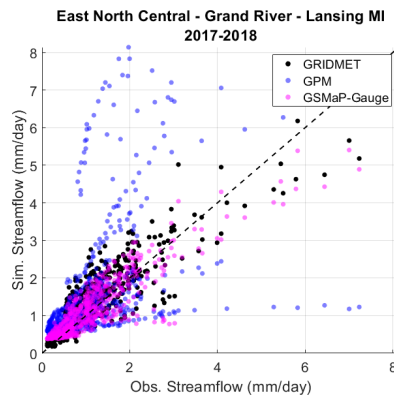
(a)



(b)



(c)



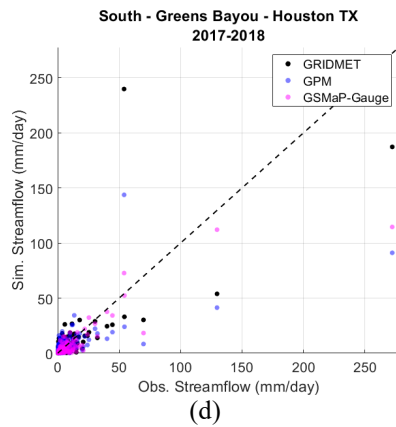
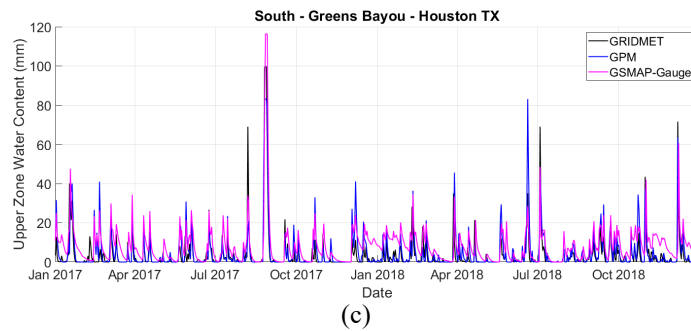
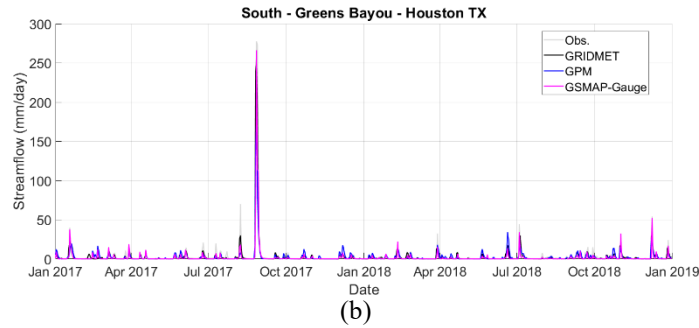
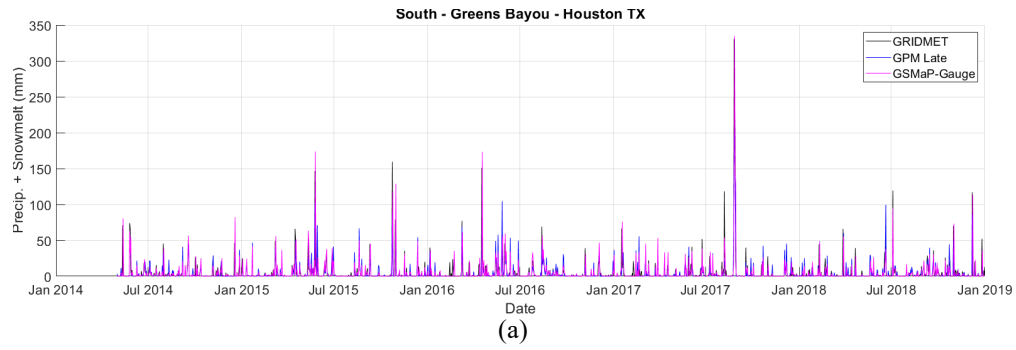
(d)

Performance Metric	GRIDMET	GPM	GSMap-Gauge
NSE	0.758	-1.058	0.800
NRMSE	49.2	143.4	44.6
PBIAS	18.5	46.0	6.8

Note: Red values in table above indicate unsatisfactory performance

(e)

Figure 4-44: Year 2017-2018 SAC-SMA performance at Grand River at Lansing, Michigan site with model calibration using daily remote sensing precipitation retrievals. (a) Precipitation time series including snow melt (b) Streamflow time series during 2017-2018 period (c) SAC-SMA normalized upper zone water content (d) Year 2017-2018 scatter plot (e) Performance metrics during the 2017-2018 period.

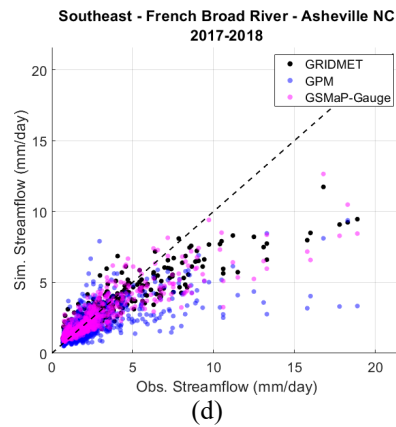
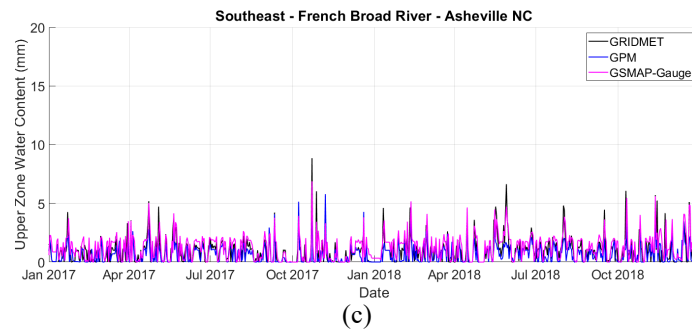
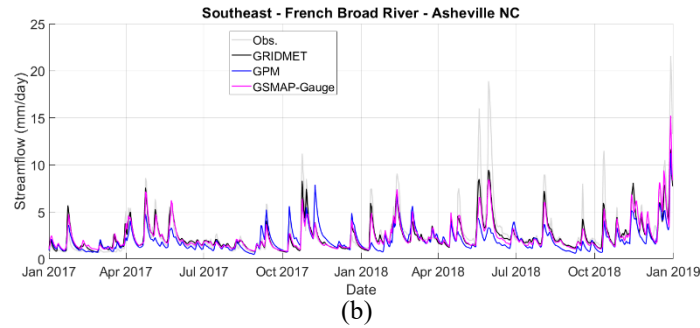
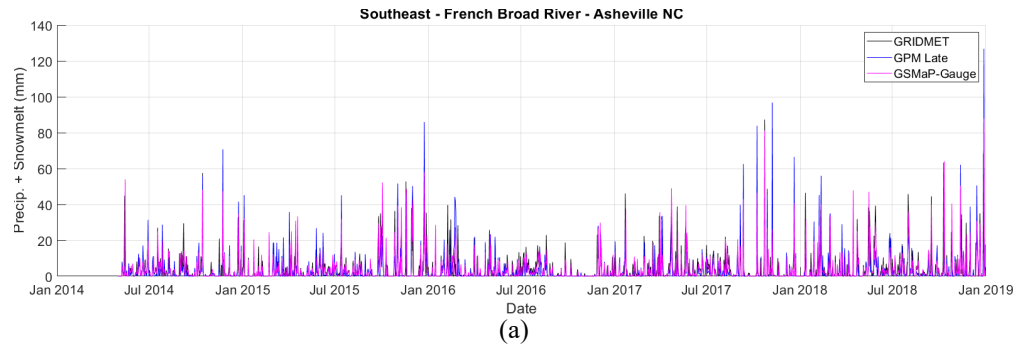


Performance Metric	GRIDMET	GPM	GSMap-Gauge
NSE	0.704	0.640	0.828
NRMSE	54.4	60.0	41.5
PBIAS	-5.3	-13.7	-31.0

Note: *Red* values in table above indicate unsatisfactory performance

(e)

Figure 4-45: Year 2017-2018 SAC-SMA performance at Greens Bayou near Houston, Texas site with model calibration using daily remote sensing precipitation retrievals. (a) Precipitation time series including snow melt (b) Streamflow time series during 2017-2018 period (c) SAC-SMA normalized upper zone water content (d) Year 2017-2018 scatter plot (e) Performance metrics during the 2017-2018 period.

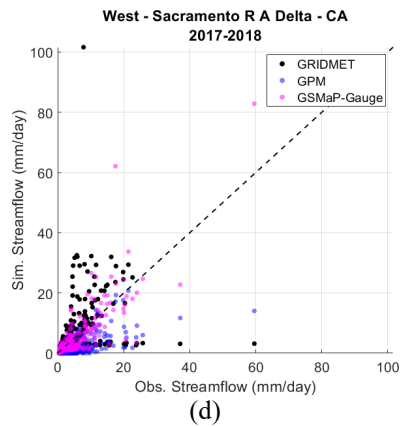
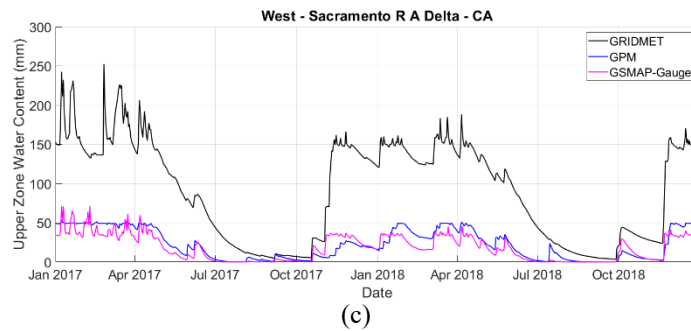
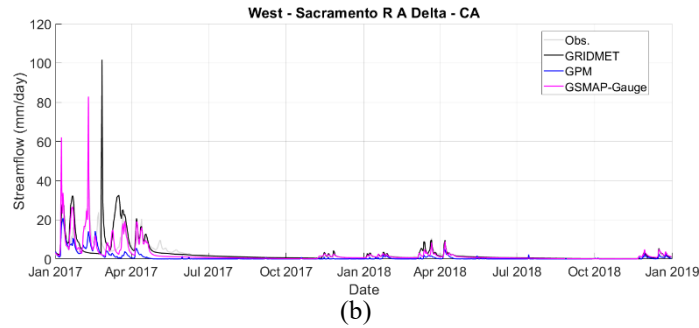
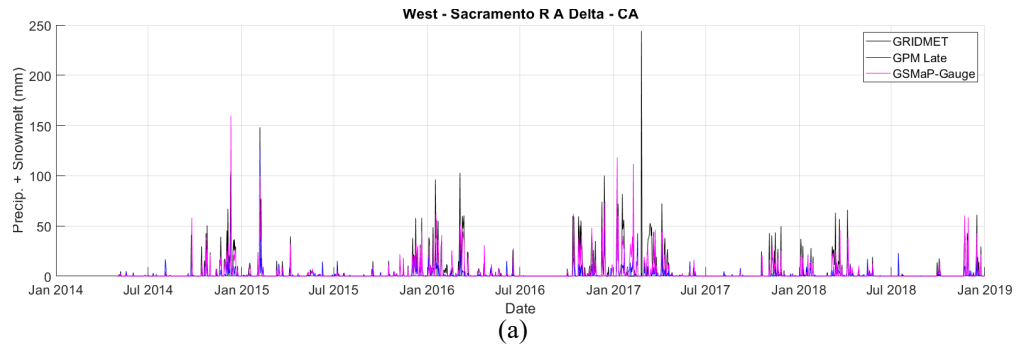


Performance Metric	GRIDMET	GPM	GSMap-Gauge
NSE	0.756	0.384	0.705
NRMSE	49.3	78.4	54.3
PBIAS	-7.8	-23.7	-10.2

Note: Red values in table above indicate unsatisfactory performance

(e)

Figure 4-46: Year 2017-2018 SAC-SMA performance at French Broad River at Asheville, North Carolina site with model calibration using daily remote sensing precipitation retrievals. (a) Precipitation time series including snow melt (b) Streamflow time series during 2017-2018 period (c) SAC-SMA normalized upper zone water content (d) Year 2017-2018 scatter plot (e) Performance metrics during the 2017-2018 period.



Performance Metric	GRIDMET	GPM	GSMap-Gauge
NSE	-0.667	0.328	0.576
NRMSE	129.0	81.9	65.1
PBIAS	16.6	-67.9	-11.2

Note: Red values in table above indicate unsatisfactory performance

(e)

Figure 4-47: Year 2017-2018 SAC-SMA performance at Sacramento R.A. Delta, California site with model calibration using daily remote sensing precipitation retrievals. (a) Precipitation time series including snow melt (b) Streamflow time series during 2017-2018 period (c) SAC-SMA normalized upper zone water content (d) Year 2017-2018 scatter plot (e) Performance metrics during the 2017-2018 period.

Table 4-12: SAC-SMA calibrated water storage parameters (in mm depth units) for the East Fork White River at Columbus, Indiana case study

SAC-SMA Water Storage Parameters (mm)	Definition	GRIDMET	GPM	GSMaP- Gauge
uztwm	Upper zone tension water capacity	18	150	1
uzfwm	Upper zone free water capacity	33	145	99
lztwm	Lower zone tension water capacity	44	500	77
lzfpw	Lower zone free primary free water capacity	23	1000	680
lzfsw	Lower zone supplemental water capacity	61	266	997

Table 4-13: SAC-SMA calibrated water storage parameters (in mm depth units) for the Sacramento R.A. Delta, California case study

SAC-SMA Water Storage Parameters (mm)	Definition	GRIDMET	GPM	GSMaP- Gauge
uztwm	Upper zone tension water capacity	150	49	34
uzfwm	Upper zone free water capacity	102	110	37
lztwm	Lower zone tension water capacity	398	56	205
lzfpw	Lower zone free primary free water capacity	85	21	168
lzfsw	Lower zone supplemental water capacity	340	1000	23

4.9 Summary

In this chapter, the impact of incorporating modern remote sensing and gridded data products covering the gamut of agriculturally and hydrologically relevant variables from atmosphere to root-zone is assessed with regard to hindcasting and near-real-time prediction of crop yield, irrigation demand, assessment of agricultural drought, and monitoring of hydrological flows.

With regard to incorporating SMAP surface soil moisture data into the DSSAT-CSM agricultural simulations, preliminary analysis gave an optimistic outlook for how this new information could improve crop yield simulations. However, in application, biases in remote sensing surface soil moisture retrievals, combined with the coarser than expected spatial resolution of the retrievals (due to post-mission launch sensor failure), showed that incorporation of SMAP L3 Enhanced surface moisture retrievals could not improve or mitigate errors in the DSSAT simulations at the case study sites. Though it is sufficient for atmospheric variables (e.g. incoming solar radiation, air temperature, and precipitation) to have spatial resolutions of 10 km, heterogeneities in surface condition (e.g. type of crop planted, irrigated, non-irrigated, etc.) is an issue that has to be addressed before SMAP retrievals of surface soil moisture can be integrated into the DSSAT crop model. This assessment highlights the need for either remote sensing surface soil moisture retrievals of sub-10km spatial resolution (which may have been possible had the active sensor on the SMAP satellite not failed) or of spatial downscaling of SMAP surface soil moisture retrievals.

As shown in Chapter 3, biases in remote sensing retrievals of daily precipitation would likely adversely impact the accuracy of modeled crop yield, irrigation demand, and

streamflow if such data were incorporated in agricultural and streamflow models. The case studies in this chapter confirm that expectation. Dry and wet biases in remote sensing retrievals of precipitation have a profound impact on crop yield and irrigation demand simulations. As a result of this assessment, remote sensing retrievals of precipitation that are not heavily calibrated with gauge data should not be used in agricultural models nor streamflow models, a finding from this research which casts doubts on the utility of remote sensing precipitation data for near-real-time monitoring of crop state, irrigation planning, and streamflow prediction in ungauged regions.

Remote sensing data aside, integration of multiple high resolution data products available over the continental U.S. can inform analyses of the feasibility of modern agricultural practices at the watershed scale in light of historical climate variability and change. Long-term agricultural simulations driven by modern gridded data products such as GRIDMET, HarvestChoice Global high-resolution soil profile database, USDA NASS Cropland Data Layer, and others, provide insight into the highly non-linear interactions between crop, soil, atmosphere, and climate, and allow for more refined characterizations of agricultural drought (both their occurrence and severity) as exemplified in the case study of year 1980-2016 crop production and irrigation demand in the Apalachicola-Chattahoochee-Flint (ACF) River Basin.

CHAPTER 5

SEASONAL AGRICULTURAL FORECASTS AND CLIMATE CHANGE ASSESSMENTS

5.1 Depth-averaged soil moisture-based historical analog for crop yield and irrigation forecasting – synthetic experiments

In this study, the hypothesis of predicting crop yield and irrigation demand using time series information of regional-scale soil moisture is tested by way of synthetic experiments.

5.1.1 Methodology

In the subsequent case studies, simulated daily 200cm depth averaged soil moisture from the DSSAT model is used to predict end-of-season crop yield and irrigation demand via a historical analog approach outlined as follows:

First for a 100 km by 100 km region, the daily time series of 200cm depth averaged soil moisture is simulated from years 1980 to 2016 using the DSSAT model (with a fallow crop) forced by GRIDMET meteorological data. This time series serves a historical pool of temporally continuous soil moisture data.

Next, for each year from 1980 to 2016, January – June regional-scale simulated depth-averaged soil moisture is compared to the January – June soil moisture time series from the historical pool to determine which years from the historical pool are most similar to the year of interest. The eight years with the lowest RMSE values for January – June simulated

soil moisture are selected as candidates for historical analog years for infilling June – End of Growing Season daily weather for crop yield forecasting.

The DSSAT crop model is then run for a particular crop (i.e. corn) at the local-scale, (e.g. for a single field within the 100 km by 100 km regional domain) using local GRIDMET data from the year of interest for January – June concatenated with daily weather from the historical analog years for the June – End of Growing Season (e.g. November) period. The end result is an ensemble of eight crop yield and irrigation demand predictions for each year from 1980 to 2016 which can be compared to simulated crop yields without using historical analog daily weather data (which represents the “true” or “target” crop yield in these synthetic experiments) to assess predictive skill. This approach is tested for three case study locations as listed in Table 5-1.

Table 5-1: DSSAT-CSM input parameters for crop yield prediction via depth-averaged soil moisture-based historical analog method

Location	DSSAT-CSM Input Parameter			
	Maize cultivar	Planting date	Plant Population [plants/m ² (plants/acre)]	Row Spacing [cm (in)]
Story County, Iowa	PB 8	April 26 th	7.9 (30,000)	76 (30)
San Joaquin County, California*		April 8 th		
Miller County, Georgia**	Jackson Hybrid	March 29 th		

*Simulations include only irrigated crop yields

**Simulations include rainfed and irrigated crop yields

5.1.2 Results

Before assessing skill in this method’s prediction of crop yield and irrigation demand, the skill in using January – June DSSAT simulated soil moisture to predict July – December total precipitation is assessed for each year from 1980 to 2016. Performance of this historical analog approach is assessed in terms of three metrics: (1) Reliability: does the range of historical analog-based estimates encompass the target value? (2) Bias: the

difference between the average of historical analog-based estimates and the target value; and the (3) Standard Deviation of historical analog-based estimates. Figure 5-1 illustrates an ideal scenario in which the ensemble of historical analog-based estimates using the best eight estimates (in red) has reduced bias and reduced spread compared to the ensemble of all possible estimates (in blue), and both ensembles are reliable in that the target value is encompassed.

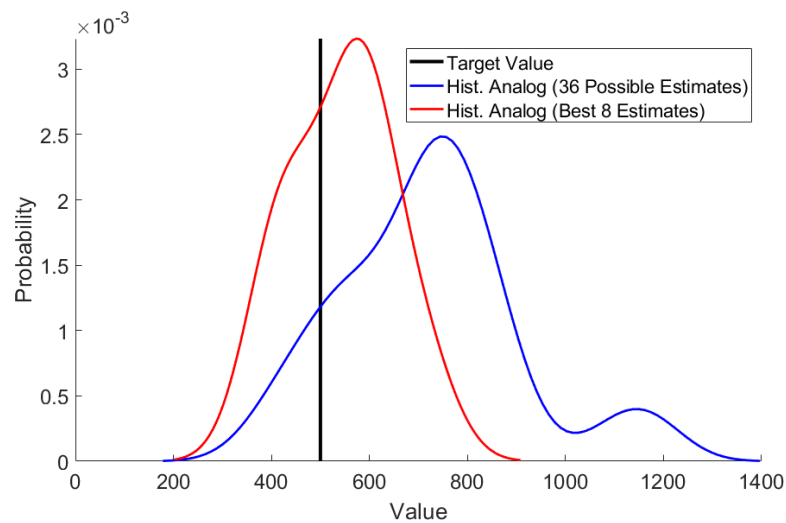


Figure 5-1: Schematic comparing the empirical probability distributions of historical analog-based estimates of a target quantity. The red probability distribution, resultant from the best historical analog based estimates, has reduced bias and reduced spread compared to the control scenario (in blue), while still capturing the target value.

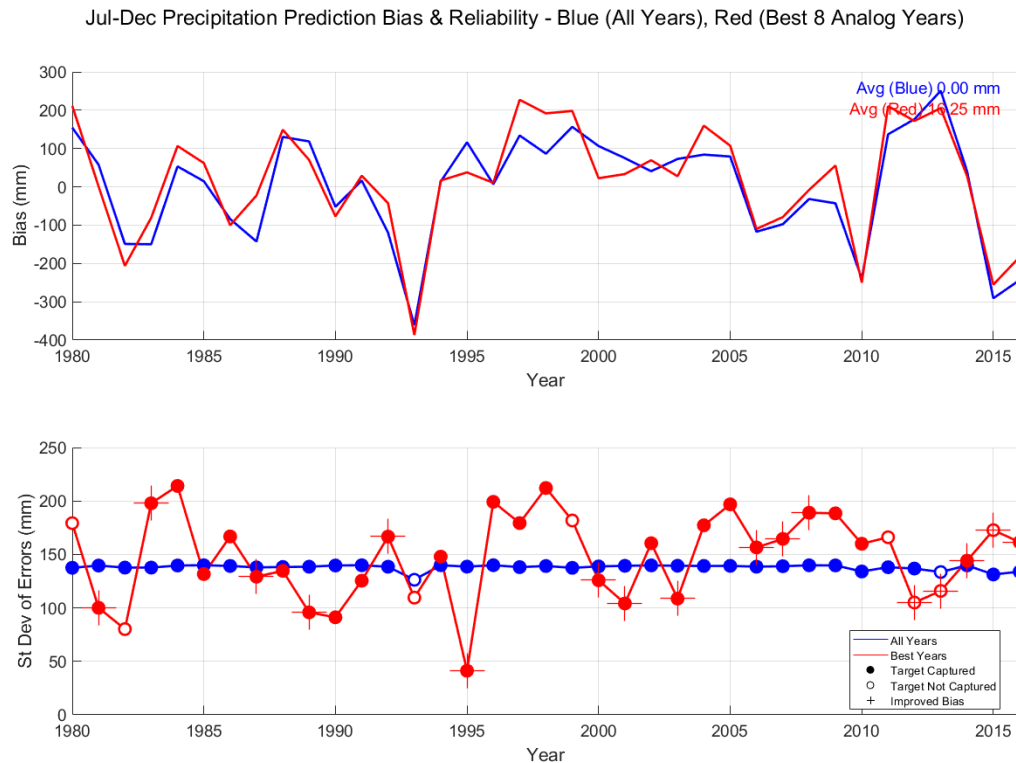


Figure 5-2, Figure 5-3, and Figure 5-4 characterize the bias, reliability, and spread of soil moisture based historical analog forecasts of July – December cumulative precipitation given January – June daily depth averaged soil moisture at the Iowa, Georgia, and California case study locations respectively. The control scenario representing the ensemble of all possible historical analog estimates is presented in blue while the ensemble of the best eight historical analog estimates is presented in red. The upper panels indicate that this application of the historical analog method, when applied over the long term, is not unbiased, as the ensemble of predictions from the top performing eight years tends to overestimate July – December cumulative precipitation on average. For the lower panels, for less than one-third of the years from 1980 – 2015 does this method result in forecasts that are simultaneously reliable, with improved bias, and reduced spread. The lack of skill in predicting July – December cumulative precipitation translates to lack of skill in

forecasting crop yield and irrigation amount as shown in Figure 5-5 through Figure 5-7 for the case study locations.

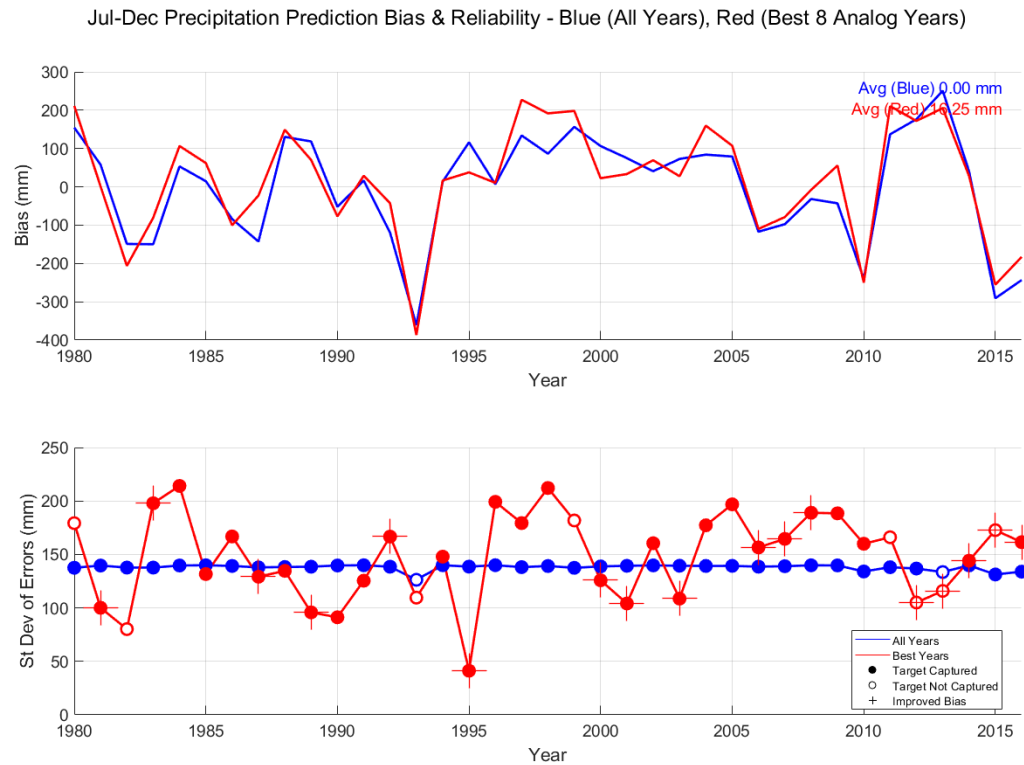


Figure 5-2: Analysis of bias and reliability of soil moisture based historical analog forecasts of July – December cumulative precipitation. Iowa case study site.

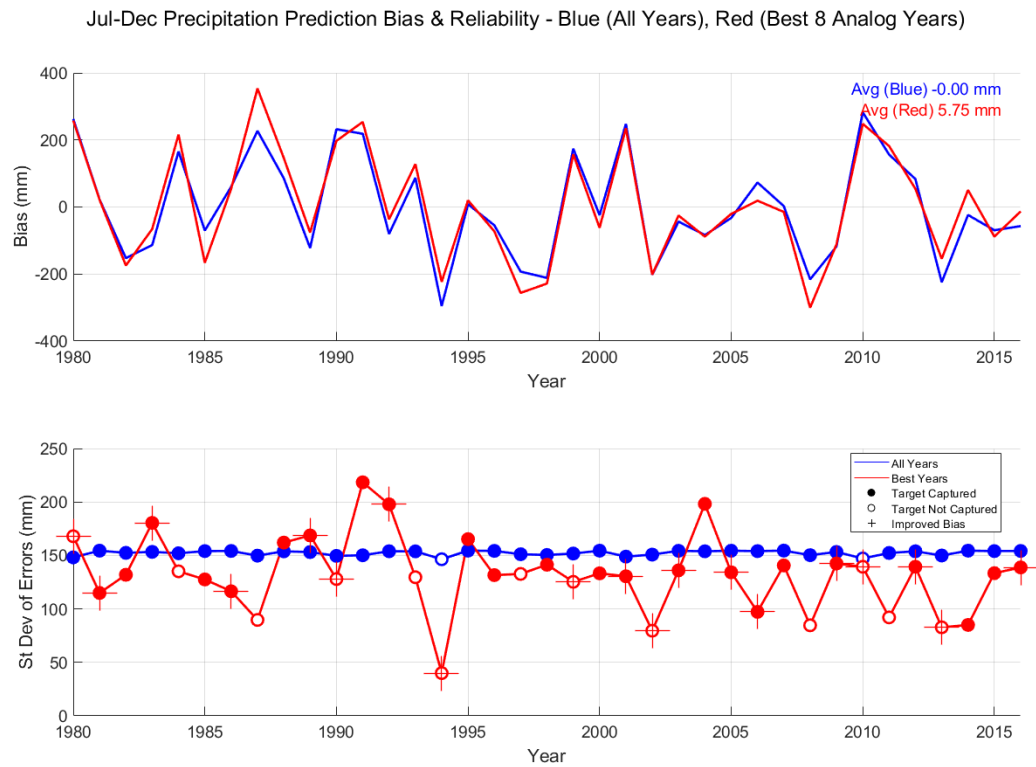


Figure 5-3: Analysis of bias and reliability of soil moisture based historical analog forecasts of July – December cumulative precipitation. Georgia case study site.

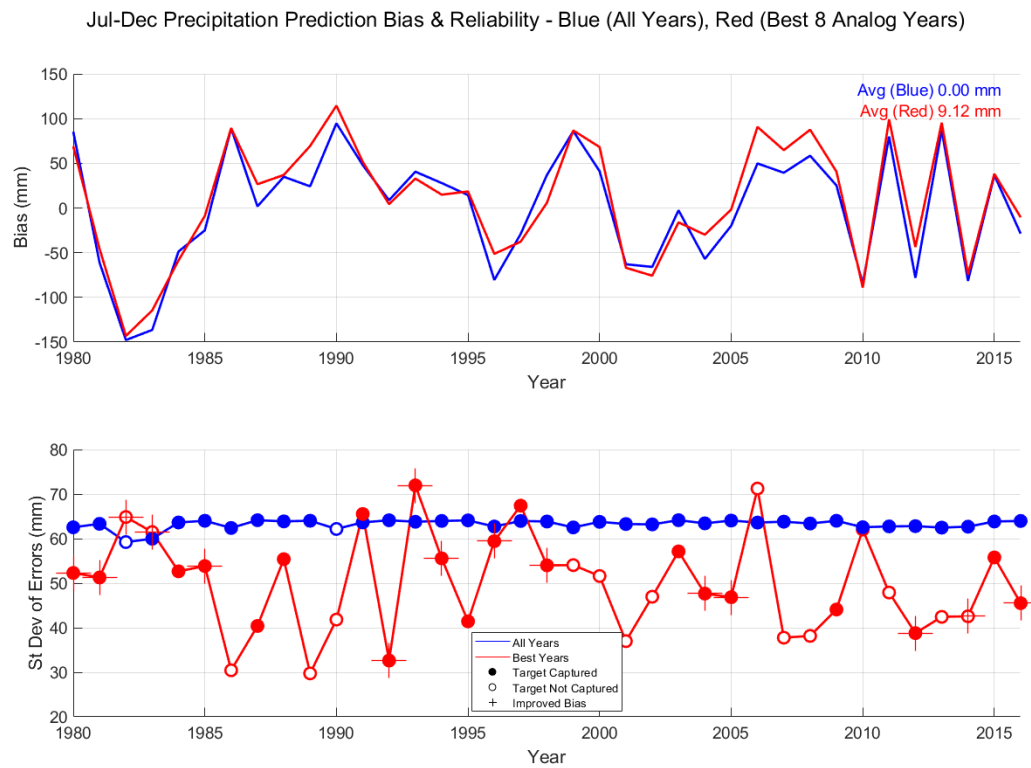


Figure 5-4: Analysis of bias and reliability of soil moisture based historical analog forecasts of July – December cumulative precipitation. California case study site.

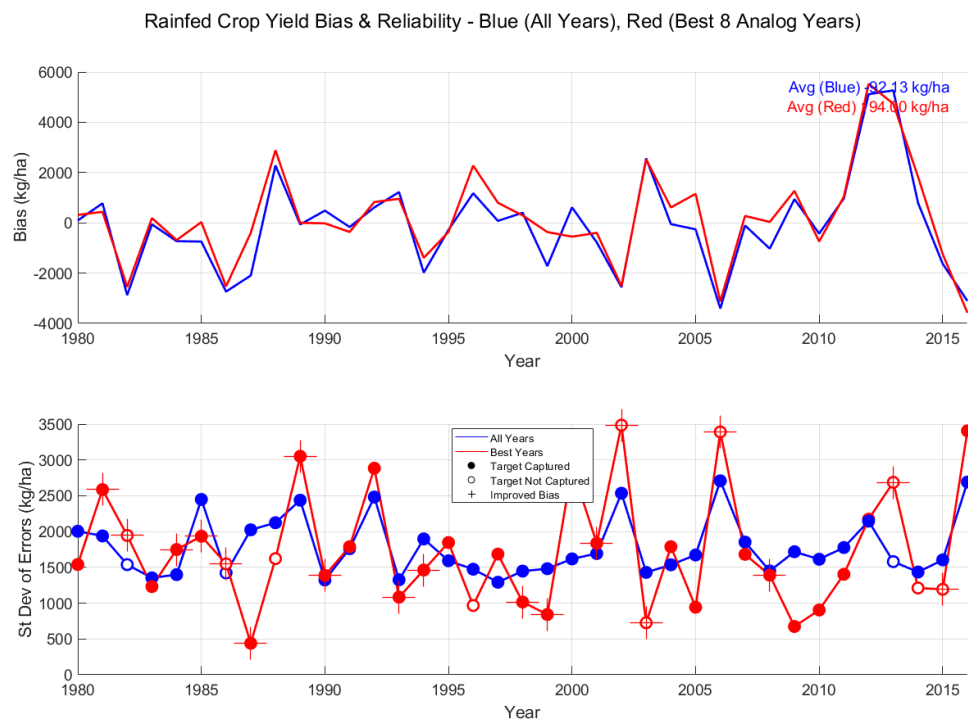


Figure 5-5: Analysis of bias and reliability of soil moisture based historical analog forecasts of rainfed crop yield. Iowa case study site.

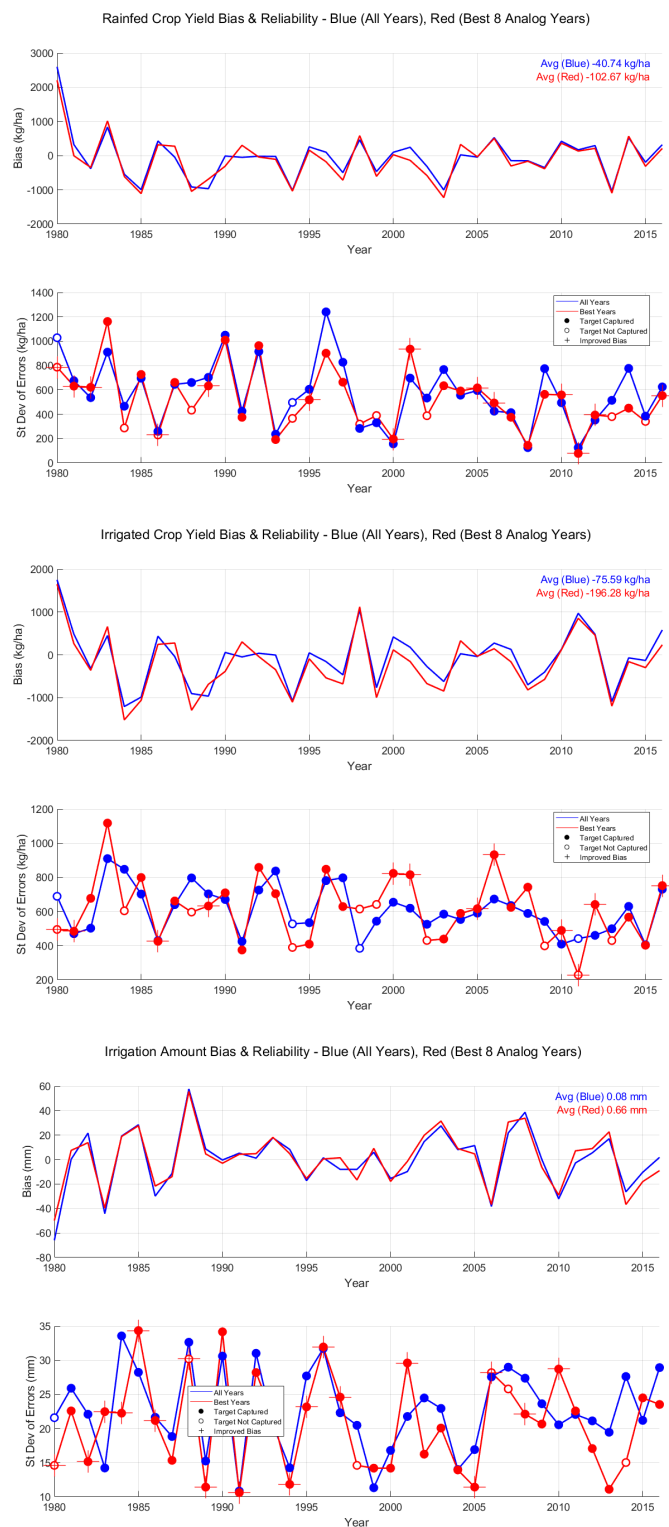


Figure 5-6: Analysis of bias and reliability of soil moisture based historical analog forecasts of rainfed crop yield, irrigated crop yield, and irrigation amount. Georgia case study site.

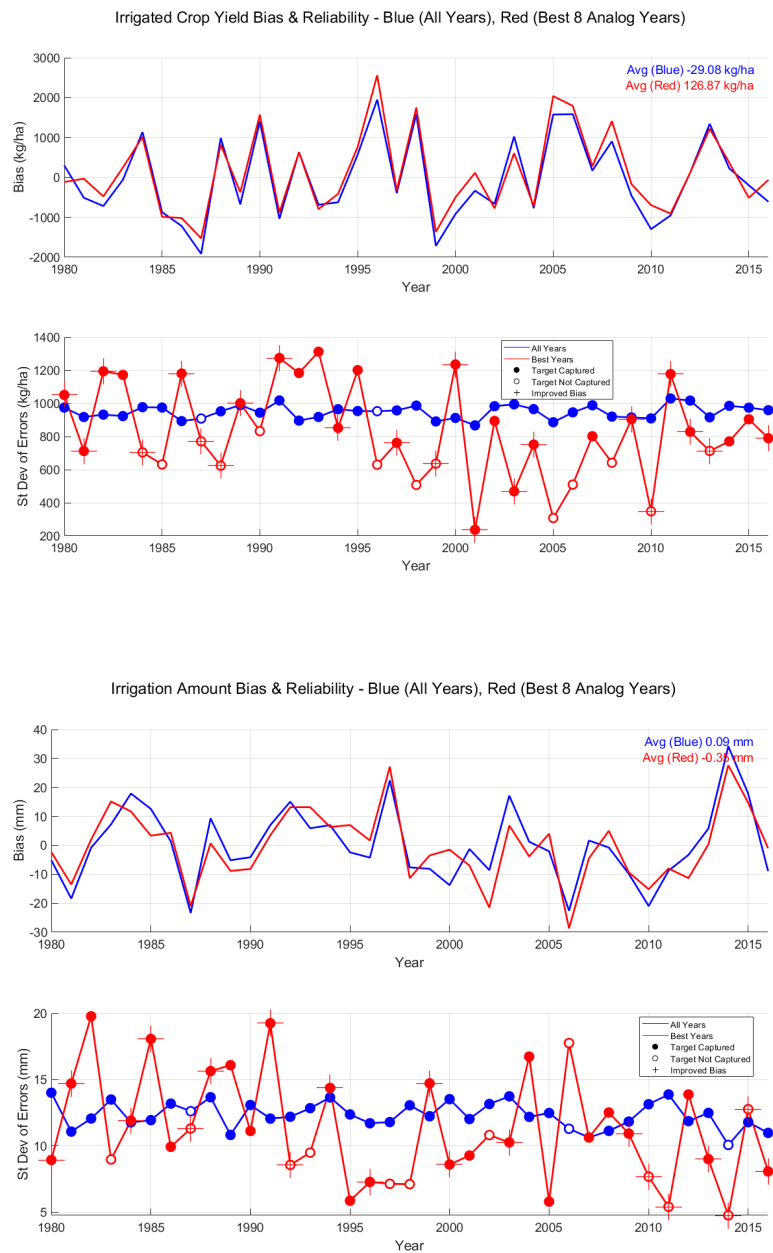


Figure 5-7: Analysis of bias and reliability of soil moisture based historical analog forecasts of irrigated crop yield and irrigation amount. California case study site.

5.2 Comparing DSSAT surface soil moisture to SMAP retrievals

The time series of January to June DSSAT depth-averaged soil moisture did not exhibit skill in predicting crop yield using the historical analog approach tested in the study. This historical analog experiment was repeated using top 5cm soil moisture estimates from DSSAT (instead of depth-averaged soil moisture) and similarly, predictive skill was not shown. These results suggest that remote-sensing surface soil moisture retrievals from SMAP would not have improved the performance of the historical analog approach; however, it is still of interest to assess how consistent SMAP surface soil moisture retrievals are with DSSAT surface soil moisture estimates for a region for which DSSAT has been calibrated.

Using the data from the crop and irrigation hindcasting study for the Apalachicola-Chattahoochee-Flint (ACF) river basin (refer to Section 4.5), Figure 5-8 compares DSSAT simulated surface soil moisture for major crops in ACF Sub-basin #11 (mapped in Figure 5-9) with sub-basin averaged surface soil moisture from the SMAP L3 Enhanced data product. The comparison shows major dry-down and wetting events are captured by both data sets despite some discrepancies. SMAP retrievals are consistent with the more dominant crops in the region, for example, the SMAP surface soil moisture retrievals in June 2016 are in closer agreement with cotton, soybean, and peanut simulated soil moisture than with the simulated soil moisture of the corn crop. For this sub-basin, USDA cropland data shows that corn fields in 2016 represented only six percent of the total sub-basin area, while cotton, soybean, and peanut comprised about 21 percent of the sub-basin as presented in Figure 5-10. It is noted that about 38 percent of the sub-basin area is forest, for which DSSAT surface soil moisture simulations are not available, and it is unlikely that SMAP

retrievals would be reliable over such densely vegetated areas. Nevertheless, the correspondence between SMAP and DSSAT surface soil moisture offers an encouragement that there may be value in SMAP data for agro-hydrological applications.

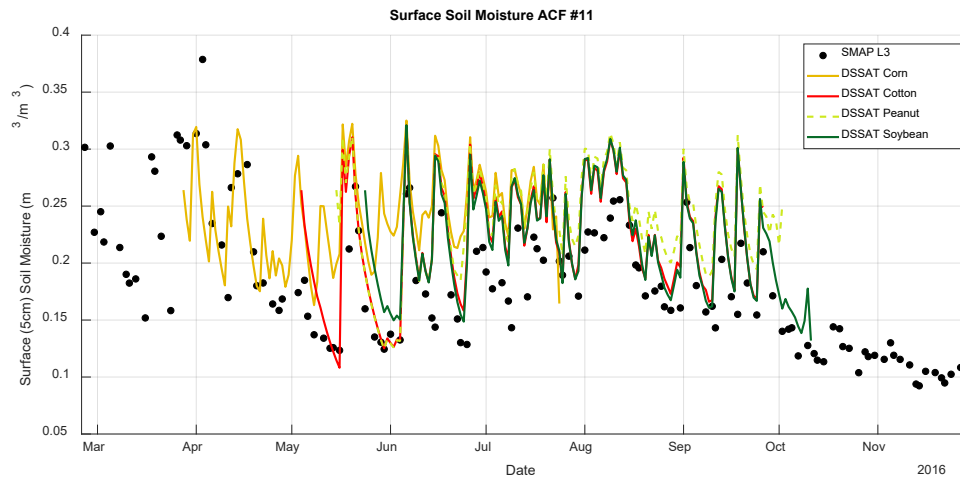


Figure 5-8: Comparison of year 2016 DSSAT surface soil moisture (top 5cm) for major rainfed and irrigated crops in ACF Subbasin #11 and SMAP L3 Enhanced surface soil moisture retrievals

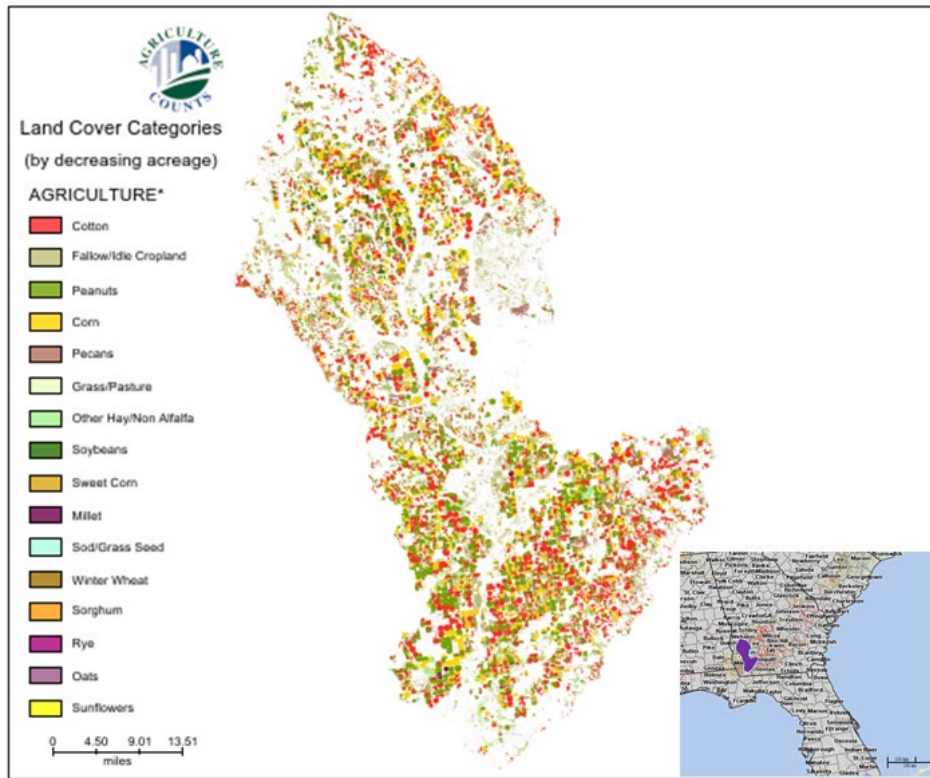


Figure 5-9: Year 2016 USDA Crop Land Layer for ACF Sub-basin #11

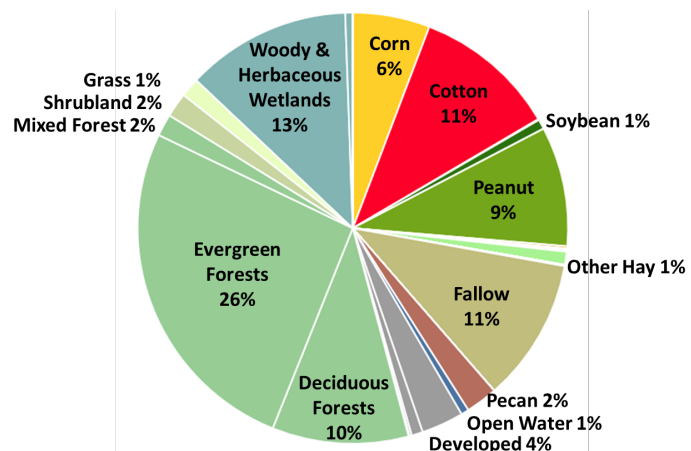


Figure 5-10: Year 2016 USDA Crop Land Data Layer land surface area designations for ACF Sub-basin #11

5.3 GRIDMET-based historical analog for rainfed and irrigated crop yield forecasting

In the following case studies, the same historical analog approach for predicting crop yield and irrigation demand is conducted just as the previous section; however, instead of daily soil moisture data, monthly precipitation data from the GRIDMET data set is used.

5.3.1 Methodology

First for a 100 km by 100 km region, the monthly time series of GRIDMET precipitation is retrieved from years 1980 to 2016. This time series serves a historical pool of temporally continuous monthly precipitation data.

Next, for each year from 1980 to 2016, January – June regional-scale monthly precipitation is compared to the January – June monthly precipitation time series from the historical pool to determine which years from the historical pool are most similar to the year of interest. The eight years with the lowest RMSE values for January – June precipitation are selected as candidates for historical analog years for infilling June – End of Growing Season daily weather for crop yield forecasting.

The DSSAT crop model is then run for a particular crop (i.e. corn) at the local-scale, (e.g. for a single field within the 100 km by 100 km regional domain) using local GRIDMET data from the year of interest for January – June concatenated with daily weather from the historical analog years for the June – End of Growing Season (e.g. November) period. The end result is an ensemble of eight crop yield and irrigation demand predictions for each year from 1980 to 2016 which can be compared to simulated crop yields without using historical analog daily weather data (which represents the “true” or

“target” crop yield in these synthetic experiments) to assess predictive skill. This approach is tested for the Iowa and Georgia case study locations listed previously in Table 5-1.

5.3.2 Results

Similar to the analysis conducted with the depth averaged soil moisture based historical analog method, the skill of the precipitation based historical analog method in forecasting July – December cumulative precipitation given January – June monthly precipitation is assessed in Figure 5-11 and Figure 5-12 for the Iowa and Georgia case study locations respectively. The forecasts of July – December precipitation are not unbiased when this method is applied over the long term, and that similarly there is poor skill in predicting crop yield and irrigation amount as shown in Figure 5-13 and Figure 5-14. Based on these results, it can be assumed that if near-real-time remote sensing precipitation retrievals from GPM IMERG or GSMaP were incorporated into a similar historical analog approach, that the predictive skill in forecasting crop yield and irrigation demand would be even less.

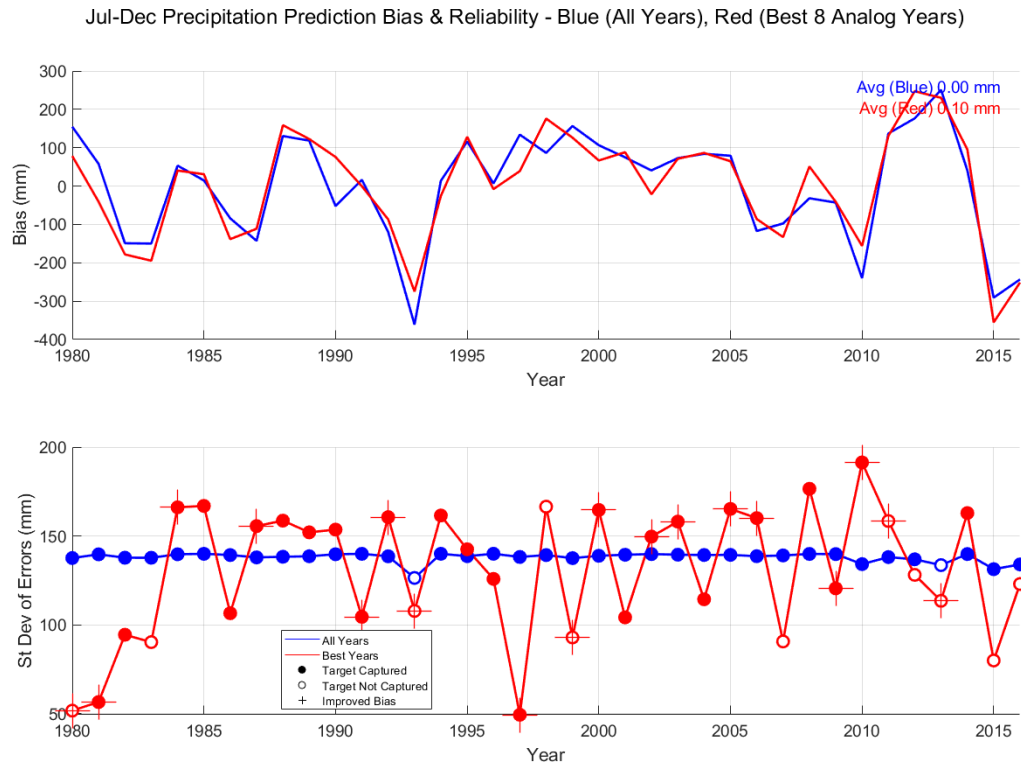


Figure 5-11: Analysis of bias and reliability of monthly precipitation based historical analog forecasts of July – December cumulative precipitation. Iowa case study site.

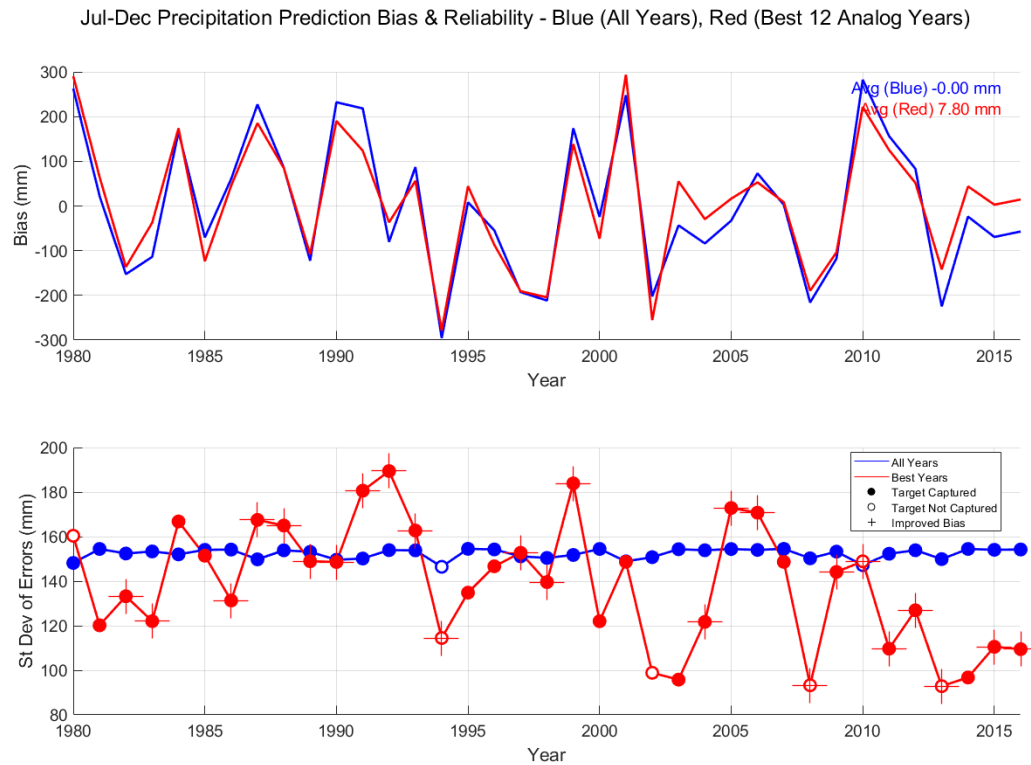


Figure 5-12: Analysis of bias and reliability of monthly precipitation based historical analog forecasts of July – December cumulative precipitation. Georgia case study site.

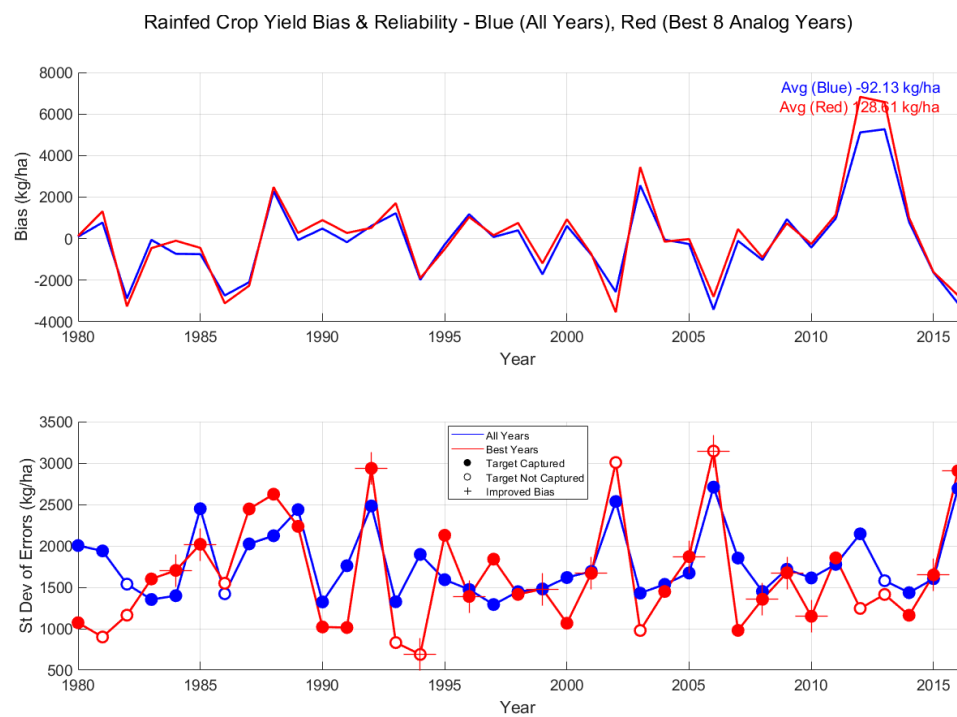


Figure 5-13: Analysis of bias and reliability of monthly precipitation based historical analog forecasts of rainfed crop yield. Iowa case study site.

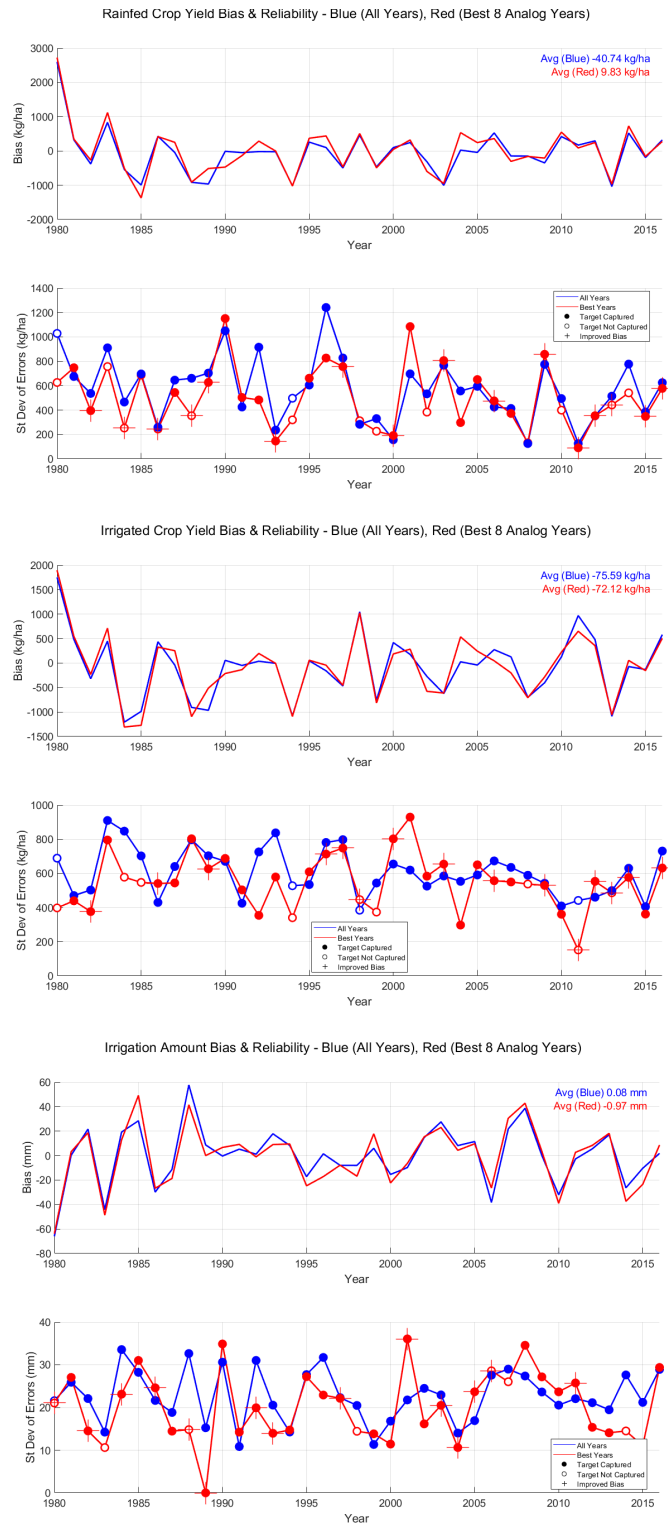


Figure 5-14: Analysis of bias and reliability of monthly precipitation based historical analog forecasts of rainfed crop yield, irrigated crop yield, and irrigation amount. Georgia case study site.

5.4 Assessment of local climate change impacts on crop production and irrigation demand using bias-corrected and downscaled Global Circulation Model (GCM) output

In the following case studies, LOCA bias-corrected and downscaled CMIP5 Global Circulation Model (GCM) outputs are integrated into the DSSAT model for assessment of long-term, localized impacts on crop production and irrigation demand. LOCA downscaled variables include 6 km x 6 km daily estimates of maximum and minimum air temperature and precipitation under two CO₂ emissions scenarios (RCP 4.5 and RCP 8.5) from 32 different climate models. Soil profile data is taken from the Harvest Choice Global High resolution Soil Profile Data set. In this study, rainfed and irrigated corn are modeled from year 2000 to 2095 under all available climate models and emission scenarios for a single 6km pixel in Mitchell County, Georgia and San Joaquin County, California. Table 5-2 lists calibrated input parameters for rainfed and irrigated model runs.

Table 5-2: Calibrated input parameters for LOCA CMIP5 data driven DSSAT-CSM maize simulations.

Site Name	Location		DSSAT-CSM Input Parameter				DSSAT-CSM Automatic-Irrigation Input Parameter	
	Latitude	Longitude	Maize cultivar	Planting date	Plant Popuplation [plants/m ² (plants/acre)]	Row Spacing [cm (in)]	Soil moisture montoring depth [cm (in)]	Available soil moisture threshold (%)
Mitchell County, Georgia	31.2230	-84.1857	PIO 3382	March 29 th	7.9 (30,000)	76 (30)	30 (12)	50
San Joaquin County, California	37.9176	-121.1710	PB 8	April 8 th				70

5.4.1 Generating climate change forecasts of daily solar radiation

The agriculture decision support model used in this study, DSSAT, requires daily input of downwelling surface solar radiation, which is not provided in the LOCA CMIP5 data product. Solar radiation forecasts are instead generated using a basic artificial neural network (ANN) model calibrated from fine resolution GRIDMET data (years 1980 – 2000) at each of the case study sites. The neural network accepts daily input of the following six variables: month of year, daily top of atmosphere (extraterrestrial) solar radiation ($\text{MJ}/\text{m}^2/\text{day}$), maximum air temperature ($^{\circ}\text{C}$), minimum air temperature ($^{\circ}\text{C}$), precipitation (mm), and precipitation from the previous day (mm). Neural network output is daily surface downwelling solar radiation ($\text{MJ}/\text{m}^2/\text{day}$). The network is constructed using the default settings of the MATLAB Deep Learning Toolbox, with six inputs, 10 hidden nodes, and one output node. The training function used to calibrate the network was Bayesian Regularization Backpropagation with the objective function to optimize being Mean Squared Error (MSE). Year 1980 – 2000 daily data from GRIDMET (solar radiation, maximum and minimum air temperatures, and precipitation) was divided into neural network training, validation, and testing data sets using a 70% - 15% - 15% split respectively. Neural network performance for prediction of daily surface solar radiation was additionally assessed in comparison to year 2001 – 2016 surface solar radiation data from GRIDMET.

Figure 5-15 illustrates the performance of the surface solar radiation ANN models developed for Mitchell County, Georgia and San Joaquin County, California case study sites during the year 2001 – 2016 period in relation to the surface solar radiation estimates from the reference GRIDMET data set. The models' agreement with the GRIDMET

reference is excellent, with near or above 90 percent correlation and acceptable scatter. There is a slight underestimation bias, but as will be shown, the bias bias and scatter do not adversely impact analysis of long term trends in crop-yield and irrigation demand from DSSAT simulations that are driven by ANN estimated solar radiation. The Mitchell County site has greater scatter than the San Joaquin County site, and this is attributed to greater cloudiness at the Georgia site. Cloudiness data is not directly incorporated into the ANN (but some information of cloudiness is implicitly included by way of maximum and minimum daily air temperature) and is not available in the LOCA CMIP5 data set. Figure 5-16 and Figure 5-17 present the time series of ANN surface solar radiation output along with the GRIDMET reference for the 2001 – 2016 period.

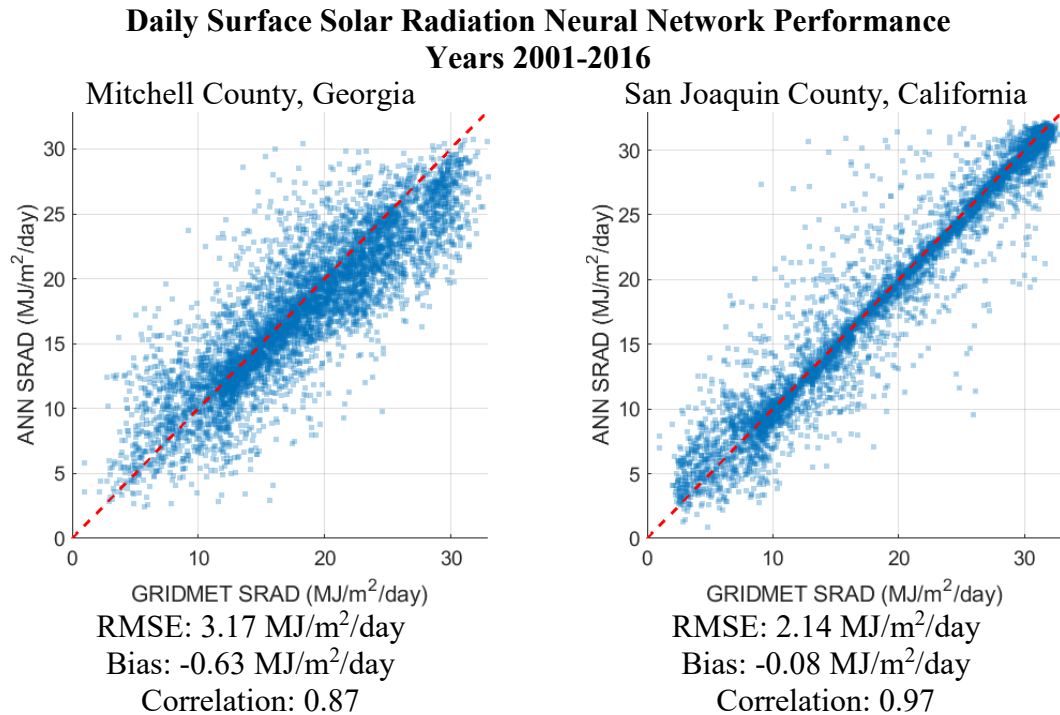


Figure 5-15: Performance of calibrated artificial neural networks (ANN) for estimation of daily surface solar radiation at case study locations during years 2001-2016

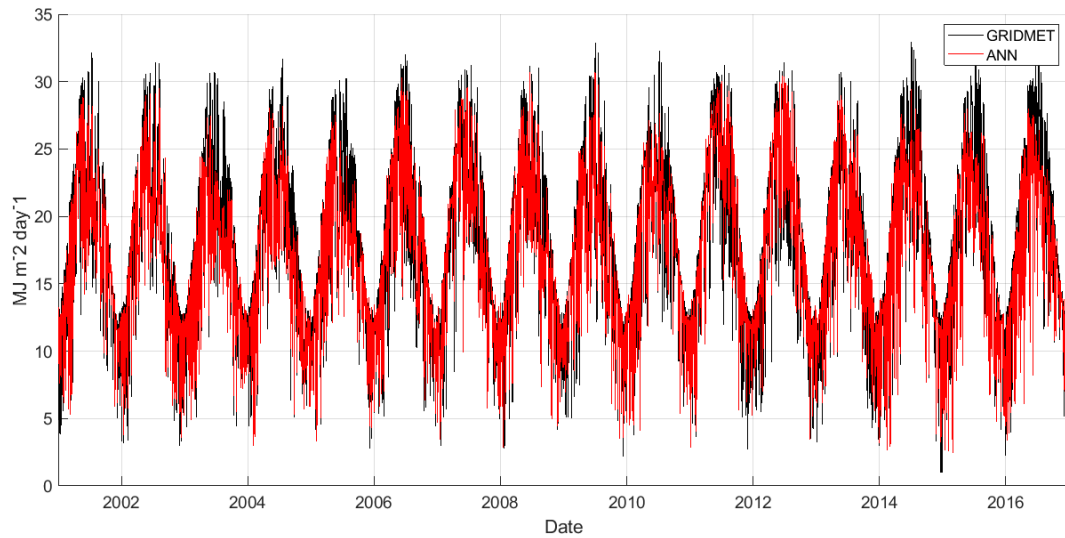


Figure 5-16: Time series of GRIDMET and Artificial Neural Network (ANN) estimated daily surface solar radiation at the Mitchell County, Georgia case study site during years 2001-2016.

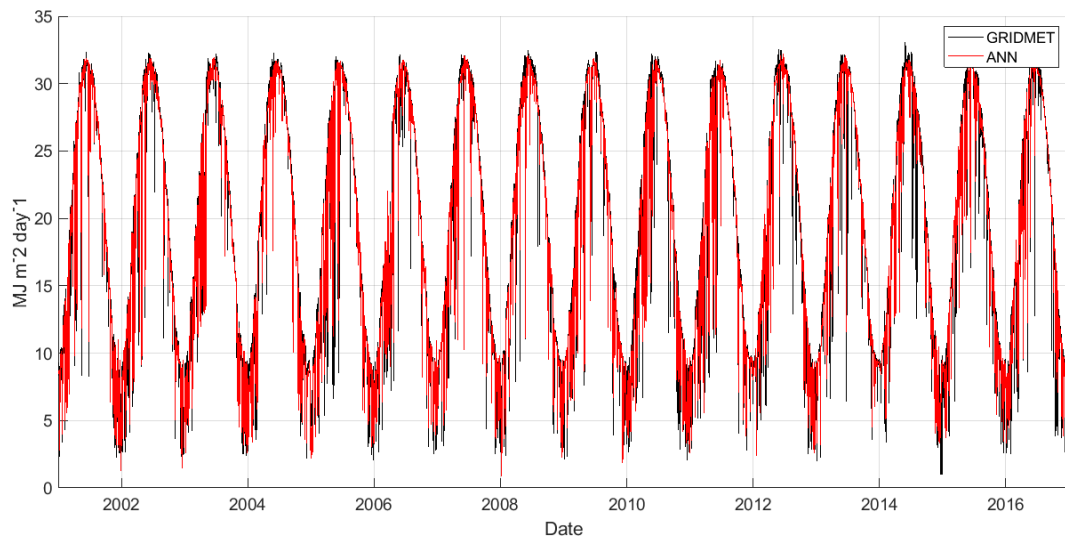


Figure 5-17: Time series of GRIDMET and Artificial Neural Network (ANN) estimated daily surface solar radiation at the San Joaquin County, California case study site during years 2001-2016.

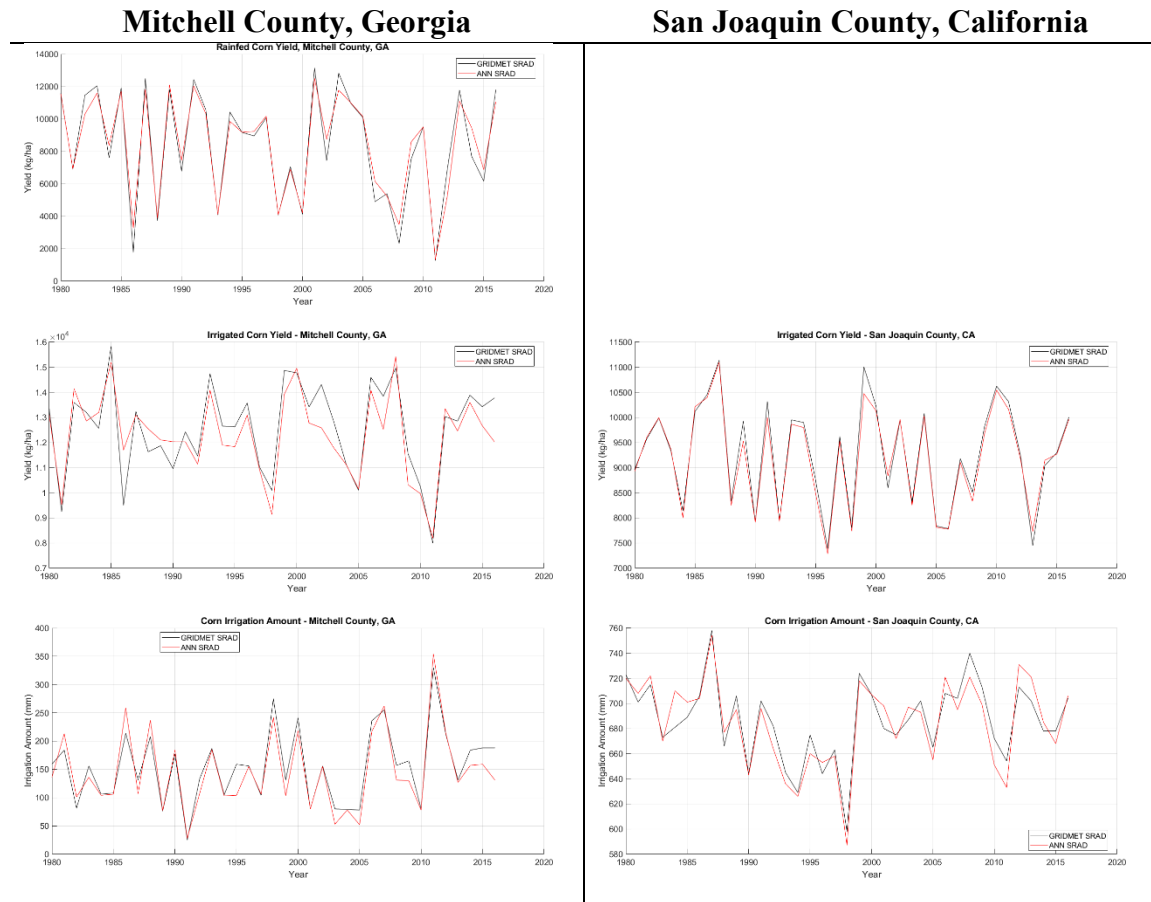
Table 5-3 compares the year 2001-2016 performance of the surface solar radiation ANN model to the commonly used, parsimonious, and seasonally calibrated model of Bristow and Campbell (1984). The Bristow and Campbell model accepts daily input of

extraterrestrial solar radiation and diurnal temperature range (i.e. the difference between daily maximum and minimum air temperatures) and requires calibration of three empirical parameters for each season. Results show that the ANN model has superior (e.g. Mitchell County, GA site) or comparable (e.g. San Joaquin County, CA site) performance to the Bristow and Campbell model.

Table 5-3: Performance of Artificial Neural Network (ANN) model for estimation of surface solar radiation compared to seasonally calibrated Bristow & Campbell (1984) model. Green highlights indicate best performance for the specified metric.

Model	Mitchell County, GA			San Joaquin County, CA		
	RMSE (MJ/m ² /day)	Bias (MJ/m ² /day)	Correlation	RMSE (MJ/m ² /day)	Bias (MJ/m ² /day)	Correlation
Bristow & Campbell	3.51	-0.92	0.85	2.22	-0.03	0.97
ANN	3.17	-0.63	0.87	2.14	-0.08	0.97

Figure 5-18 compares year 1980 – 2016 DSSAT modeled corn yield and irrigation demand at the case study sites, given either GRIDMET or ANN modeled surface solar radiation forcing data. Results confirm the suitability of the ANN modeled surface solar radiation forcing for crop yield and irrigation demand modeling at the case study locations, especially for the purpose of assessing long term trends in local agricultural production and irrigation demand. The ANN model will therefore be used for generating daily surface solar radiation forcing data that corresponds to LOCA downscaled CMIP5 variables, assuming that relationship between ANN model inputs and solar radiation output modeled for the 1980-2000 calibration period will remain valid for the 2000 – 2095 climate change period.



Note: rainfed corn yield was not modeled for the San Joaquin County site.

Figure 5-18: Comparison of DSSAT modeled corn yield and irrigation amount at the Mitchell County, Georgia and San Joaquin County, California case study sites given GRIDMET reference and ANN modeled surface solar radiation forcing data.

5.4.2 Results

Figure 5-19 presents the climate change forecasts of rainfed corn yield, irrigated corn yield, and irrigation demand for the Mitchell County, Georgia case study site. DSSAT simulations were forced with LOCA CMIP5 downscaled data from the 6km x 6km pixel nearest the case study site. In the figure, the uncertainty bars characterize the standard deviation from the mean of crop simulations forced by 32 different GCM models. The green curve represents the RCP 4.5 emissions scenario while the red curve represents the “worst-case” or “business-as-usual” CO₂ emissions scenario. In general, corn crop yield

and irrigation demand forecasts are nearly indistinguishable between the RCP 4.5 and RCP 8.5 scenarios until year 2050, after which the RCP 8.5 scenario reports substantially lower crop yields and more intense irrigation demands than the RCP 4.5 scenario. Under the RCP 4.5 scenario, the mean of modeled rainfed corn yield at the Mitchell County case study site goes from 8,297 kg/ha in year 2000 to 5,211 kg/ha by year 2095, an over 37 percent reduction. Under the RCP 8.5 scenario, year 2095 mean rainfed corn yield is only 2,625 kg/ha, a loss of over 68 percent.

Alarming, regardless of RCP scenario or GCM model, crop yields are forecasted to reduce considerably, even if all water needs of the crop are met (i.e. irrigated crop yield). Under the RCP 4.5 scenario, the mean of modeled irrigated corn yield at the Mitchell County case study site goes from 11,793 kg/ha with 144 mm of irrigation in year 2000 to 8,092 kg/ha with 171 mm of irrigation by year 2095, an over 31 percent reduction in crop yield and 19 percent increase in irrigation demand.

Under the RCP 8.5 scenario, year 2095 mean irrigated corn yield reduces to only 3,779 kg/ha with 189 mm of irrigation, a 68 percent loss in yield and a 31 percent increase in irrigation demand. The finding that even irrigated crop yields are forecasted to fall, despite the absence of water stress (and the abundance of atmospheric CO₂), suggests that temperature rise is responsible for reducing crop yields. As mentioned previously in this dissertation, corn crops have an ideal daily temperature for carbohydrate production, that if surpassed, adversely impacts crop yield, even if no water stress is present. Results suggest that climate change would adversely impact corn's water-use efficiency, in that more water would be required to produce lesser yield.

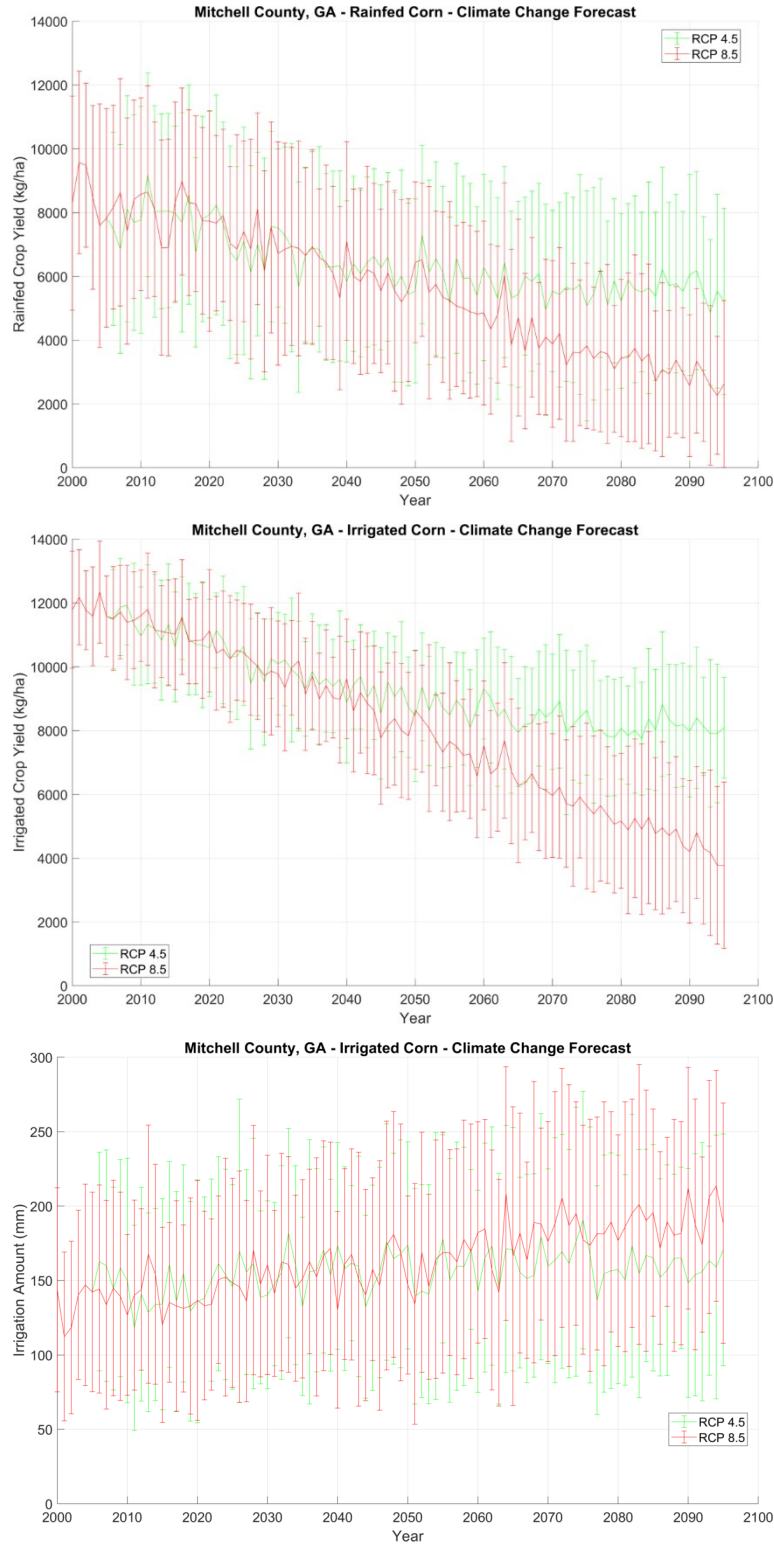


Figure 5-19: Year 2000 – 2095 Mitchell County, Georgia corn crop yield and irrigation demand forecasts from DSSAT model simulations driven by LOCA CMIP5 downscaled data.

Figure 5-20 presents the climate change forecasts of irrigated corn yield and irrigation demand for the San Joaquin County, California case study site. Similar to the Mitchell County site, irrigated corn yield is forecasted to drop substantially by year 2095. Irrigated crop yield goes from 9,239 kg/ha in year 2000 to 6,677 kg/ha by year 2095 under the RCP 4.5 scenario, a 28 percent reduction. Under the RCP 8.5 scenario, irrigated crop yield falls by 48 percent to 4,786 kg/ha by year 2095. However, the mean of modeled irrigation amount remains largely unchanged at approximately 720 mm regardless of RCP scenario; however, the spread of irrigation demand increases more under the RCP 8.5 than the RCP 4.5 scenario.

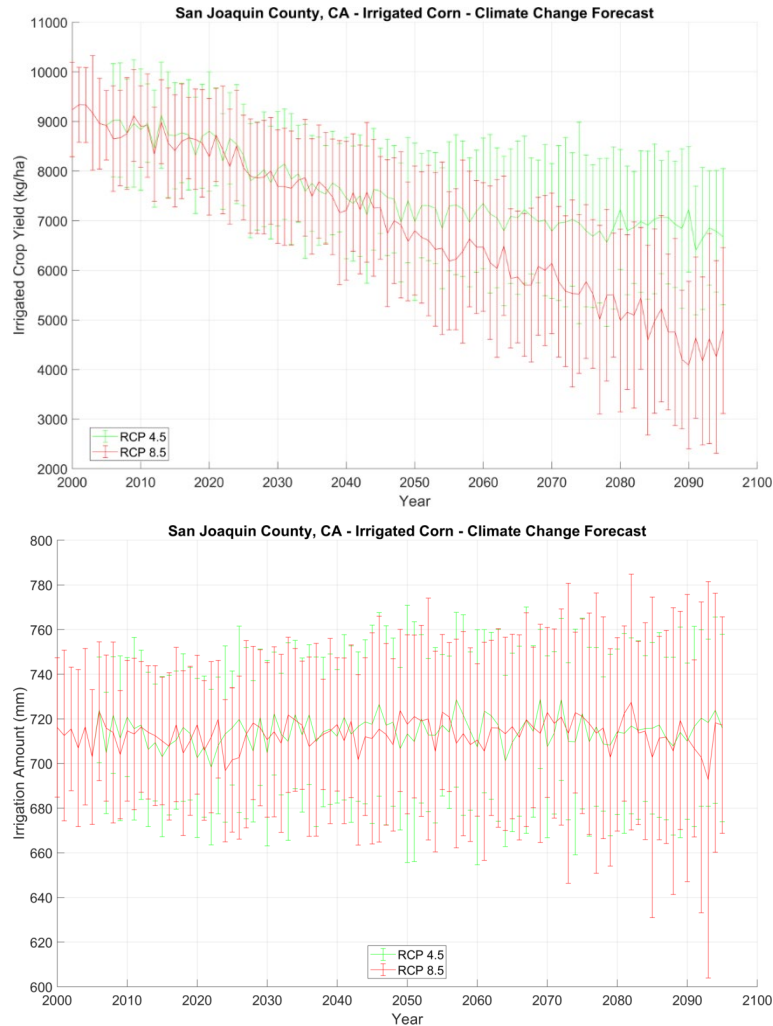


Figure 5-20: Year 2000 – 2095 San Joaquin County, California corn crop yield and irrigation demand forecasts from DSSAT model simulations driven by LOCA CMIP5 downscaled data.

5.5 Summary

In this chapter, the utility of modern remote-sensing and reanalysis gridded data products for seasonal and long-term prediction of crop yield and irrigation demand is assessed. A data-driven historical analog approach involving time series data of SMAP surface soil moisture estimates was assessed to be ineffective for prediction of end-of-season crop yield and irrigation amount. Similarly, the time series of depth averaged soil moisture simulated using the DSSAT model was not effective for prediction of growing

season crop yield or irrigation amount, despite soil moisture being an integrator of precipitation, temperature, and evapotranspiration information. Because reanalysis precipitation data based on rain gauge data showed poor skill in forecasting crop yield and irrigation amount, it can also be assumed that near-real-time remote sensing precipitation retrievals, which can have substantial errors as shown in Chapter 3, would also have poor predictive skill under the historical analog approach tested in this study.

With regard to long-term analysis of climate change impacts on crop yield, this study showed how modern bias-corrected and downscaled GCM data can be combined with other agriculture-relevant gridded data products to quantify climate change impacts on local agricultural production and irrigation demand. The data and methodology adopted in this study can be used to assess the long-term feasibility of current agricultural and irrigation practices.

CHAPTER 6

CONCLUSIONS

6.1 Summary and contributions

This dissertation explores how modern multi-sensor remote sensing and reanalysis gridded data products can provide decision support for crop yield hindcasting and prediction, irrigation planning, agricultural drought assessment, and monitoring of hydrological flows when integrated into state-of-the-science agricultural and hydrological models.

Data products from recently launched remote sensing missions, including NASA SMAP, NASA GPM, JAXA GSMP, along with national and global gridded reanalysis data products such as GRIDMET, Daymet, HarvestChoice Global High Resolution Soil Profile Database, USDA Cropscape Cropland Data Layer, and LOCA downscaled GCM projections, provide relatively fine resolution (spatially and/or temporally) information on a full range of hydrometeorologically relevant parameters and variables from the near surface atmosphere, ground surface, to the bottom of the root-zone. This study assesses how these modern data products can be synergistically incorporated into a popular agricultural decision support model, DSSAT-CSM, and a commonly used rainfall-runoff routing model, Sacramento Soil Moisture Accounting model (SAC-SMA). What follows is a point summary of major findings and contributions from this research in answering the science question: *Can prediction of crop yield, assessment of irrigation demand, and*

monitoring of agricultural drought and hydrological flows be improved by integrating multiple gridded data sets with agricultural and hydrological models?

6.1.1 Quality Assessment of remote sensing retrievals of precipitation over the continental U.S.

- NASA GPM IMERG Version 5 Late Release, JAXA GSMP-Standard and JAXA GSMP-Gauge were assessed in relation to the observation network derived gridded GRIDMET precipitation data set for the various seasons and climate regions of the continental U.S. Generally, satellite retrievals of precipitation overestimate precipitation in relation to the GRIDMET reference, but the nature of the biases vary with season (and implicitly storm-type) and climate region. Despite issues in accurately capturing the magnitude of precipitation events, remote sensing precipitation retrievals appear to capture the occurrence of precipitation events.
- GPM IMERG Version 5 Late Release tends to underestimate precipitation in the western (West and Northwest) climate regions, while overestimating everywhere else. The most severe overestimation is in the winter season, particularly in the Northwest, Northeast, and Central climate regions. Winter time underestimation of precipitation is also apparent in the arid West and Southwest climate regions.
- The JAXA GSMP-Gauge product agrees well with the GRIDMET reference; however, this agreement is due entirely to the incorporation of rain gauge data with the satellite retrievals. This finding highlights the importance of rain gauge calibration of remote sensing precipitation retrievals. The availability, low-

latency, and apparent accuracy of the GSMap-Gauge product as assessed in this study should inspire future versions of the NASA GPM IMERG Late Release data product to more efficiently incorporate rain gauge data. However, results beg the question of how accurate remote sensing retrievals of precipitation are over national and especially global regions which are only scarcely gauged, if at all.

6.1.2 Leveraging SMAP surface soil moisture retrievals to improve accuracy of remote sensing precipitation retrievals

- After identifying dry and wet biases in daily remote sensing precipitation retrievals over the continental U.S., this study investigated whether these biases could be predicted, and thusly removed, given information of daily remote sensing retrievals of surface soil moisture state. Unfortunately, there was no discernable correlation, regardless of climate zone or season, between estimates of surface soil moisture from SMAP and biases in remote sensing retrievals of daily precipitation.

6.1.3 Impact of spatial averaging of high-resolution gridded meteorological data on DSSAT-CSM crop model output

- DSSAT-CSM was originally developed for application at the single field (point-scale). This study aimed to determine the coarsest acceptable spatial resolution for atmospheric weather variables and soil property data for reliable DSSAT mean crop yield and irrigation assessments. While very fine spatial resolution information of daily weather data is ideal (though computationally expensive), results from this study suggest that atmospheric variables and soil property data

of spatial resolution no coarser than ~10km are acceptable for crop yield and irrigation assessments. Thus, it may not be necessary to downscale modern remote sensing precipitation data products for the study purpose (which to date have finest spatial resolution of 10 km), provided that the remote sensing retrievals provide accurate information to begin with.

6.1.4 Hindcasting and near-real-time prediction of crop yield, irrigation demand, and agricultural drought

- Various remote sensing and reanalysis data products (and synergistic combinations of them) were incorporated into the DSSAT-CSM crop model for crop yield prediction and assessment of irrigation demand.
- Dry and wet biases in SMAP L3 Enhanced data product prevented SMAP data from being useful in improving the accuracy of, or reducing the uncertainty in, prediction of crop yield. The failure of the active sensor on the SMAP satellite prevents us from having a truly sub-10km remote sensing characterization of surface soil moisture state. Though it is sufficient for atmospheric variables (e.g. incoming solar radiation, air temperature, and precipitation) to have spatial resolutions of 10 km, heterogeneities in surface condition (e.g. type of crop planted, irrigated, non-irrigated, etc.) is an issue that has to be addressed before SMAP retrievals of surface soil moisture can be integrated into the DSSAT crop model.
- Dry and wet biases in remote sensing retrievals of precipitation have a profound impact on crop yield and irrigation demand simulations. Remote sensing retrievals of precipitation that are not heavily calibrated with gauge data should

not be used in agricultural models, a finding from this research which casts doubts on the utility of remote sensing precipitation data for near-real-time monitoring of crop state and irrigation planning in ungauged regions.

- Integration of multiple high resolution data products can guide critical analyses of the feasibility of modern agricultural practices at the watershed scale in light of climate change. Long-term agricultural simulations driven by modern gridded data products provide insight into the highly non-linear interactions between crop, soil, atmosphere, and climate, and allow for refined characterizations of the occurrence and severity agricultural drought.

6.1.5 Incorporation of remote sensing retrievals of precipitation for near-real-time monitoring of hydrological flows

- Dry and wet biases in remote sensing retrievals of precipitation have a profound impact on streamflow simulations. Remote sensing retrievals of precipitation that are not heavily calibrated with gauge data should not be used in streamflow models, a finding from this research which casts doubts on the utility of remote sensing precipitation data for near-real-time monitoring of streamflow. In order to incorporate remote sensing precipitation data in streamflow models, such data needs to be calibrated with other observational data sets in order for the precipitation data to accurately capture the timing, spatial extent, and magnitude of events.

6.1.6 Use of modern multi-sensor data for seasonal prediction of and climate-change impacts on local crop yield and irrigation demand

- This study investigated a historical data association method for prediction of end-of-season crop yield and irrigation amount.
- Root zone soil moisture estimates did not have skill in predicting end-of-season crop yield via the historical analog method used in this study. It is unclear if there would be skill in this approach provided a longer (e.g., more than 20 years), temporally continuous (e.g., daily) time series of SMAP surface soil moisture retrievals were available. This is because the historical analog approach also failed to show predictive skill when depth-averaged soil moisture (which is more indicative of crop state than surface soil moisture) was used for predicting crop yield and irrigation amounts. Furthermore SMAP-derived root zone soil moisture estimates may have substantial biases.
- Reanalysis estimates of monthly regional precipitation did not, and near-real-time remote sensing precipitation retrievals would not have skill in predicting crop yield and irrigation demand via the historical analog approach tested in this study.
- This study integrated the new LOCA bias-corrected and downscaled CMIP5 Climate Projections into the DSSAT-CSM for assessment of climate change impacts on local-scale crop yield and irrigation demand. According to review of the literature, this is the first study incorporating this data product along with other agriculture-relevant data sets into DSSAT-CSM. Findings from this exercise allowed for evaluation of the long-term feasibility of current agricultural management practices of irrigated corn at the case study sites under multiple projected climate-change scenarios. Incidentally, a simple, but effective

artificial neural network was developed to leverage historical fine resolution weather and solar radiation estimates to predict daily projections of solar radiation which are usually not provided by CMIP5 GCM projections, but are necessary for crop modeling.

6.2 Recommendations for future work

Based on the findings, analyses, and results developed in this thesis, the following topics warrant further investigation:

- Identification of the source of biases in remote sensing retrievals of precipitation and their subsequent correction/removal. Significant dry and wet biases in remote sensing retrievals of precipitation, especially for ungauged regions, seriously hamper the usefulness of such data products in agricultural modeling and streamflow simulation and monitoring. This research identified the existence of these anomalies and quantified them, but it is still not clear what is/are the source(s) of these errors in the raw retrieval algorithms. It is hoped that identification of the causes of dry and wet biases in retrievals would lead to correction and improved accuracy of these vital data products.
- Spatial and temporal downscaling of SMAP surface soil moisture retrievals to 10 km and finer resolution. Even though the SMAP L3 Enhanced data product is posted at ~10 km spatial resolution, the native resolution of the product is still considerably coarser. Sub-10 km heterogeneity in crop plantings suggests potentially substantial differences in surface soil moisture state between different crops planted within a single 10 km SMAP pixel, especially during

stages of crop growth and development that are acutely water-sensitive. Considering that the finest spatial resolution of the USDA Cropscape Crop Land Data Layer is 30 meters, it is of interest to investigate how close to this fine resolution we can reliably downscale SMAP estimates to. Future releases from the SMAP mission do include down to 3 km spatial resolution; however, these proposed products have a long latency and temporal gaps (i.e. 10 - 12 days between retrievals) making them unsuitable for incorporation in near-real-time decision support systems for agriculture.

- While the historical analog approach applied in this study using SMAP surface soil moisture data and/or depth-averaged simulated soil moisture did not demonstrate skill in prediction of precipitation or crop yield, it may be possible that this approach, along with soil moisture time series data, can demonstrate skill in the prediction of streamflow. With streamflow being strongly connected to antecedent soil moisture condition (and to precipitation), such forecasting experiments would be expected to demonstrate predictive skill in accordance with soil moisture persistence characteristics.
- Alternative applications of remote sensing data to support and improve agricultural and hydrologic modeling. Significant biases in remote sensing retrievals and precipitation and surface soil moisture from the GPM, GSMaP, and SMAP missions generally prevent such data products from being directly incorporated into agricultural and streamflow models without correction/pre-processing. However, these data, in spite of biases and errors, may be beneficial through indirect means. For example, remote sensing retrievals of surface soil

moisture, combined with identification of wet days from remote sensing precipitation data can possibly lead to improved modeling of daily solar radiation. Similarly remote sensing data from other missions can be explored to support applications in agricultural planning and modeling of hydrological flows.

REFERENCES

- Abatzoglou, J. T., 2011: Development of gridded surface meteorological data for ecological applications and modelling. *International Journal of Climatology*, **33**, 121-131.
- Anderson, E. A., 1973: National Weather Service River Forecast System Snow Accumulation and Ablation Model, NOAA Tech. Memo. NWS HYDro-17, Silver Spring, MD, 217 pp.
- Andrews, F. T.: Hydromad: Hydrological Model Assessment and Development. [Available online at <http://hydromad.catchment.org>.]
- Andrews, F. T., B. F. W. Croke, and A. J. Jakeman, 2011: An open software environment for hydrological model assessment and development. *Environmental Modelling & Software*, **26**, 1171-1185.
- Baker, J. T., and L. H. Allen, 1993: Contrasting crop species responses to CO₂ and temperature: rice, soybean and citrus. *Vegetatio*, **104**, 239-260.
- Baker, J. T., L. H. Allen, K. J. Boote, P. Jones, and J. W. Jones, 1989: Response of Soybean to Air Temperature and Carbon Dioxide Concentration. *Crop Science*, **29**, 98-105.
- Baldwin, S. A., and M. J. Larson, 2017: An introduction to using Bayesian linear regression with clinical data. *Behaviour Research and Therapy*, **98**, 58-75.
- Behnke, R., S. Vavrus, A. Allstadt, T. Albright, W. E. Thogmartin, and V. C. Radeloff, 2016: Evaluation of downscaled, gridded climate data for the conterminous United States. *Ecological Applications*, **26**, 1338-1351.
- Bracken, C., 2016: Downscaled CMIP3 and CMIP5 Climate Projections - Addendum: Release of Downscaled CMIP5 Climate Projections (LOCA) and Comparison with Preceding Information, U. S. B. o. Reclamation.
- Bristow, K., and G. Campbell, 1984: *On the Relationship Between Incoming Solar Radiation and Daily Maximum and Minimum Temperature*. Vol. 31, 159-166 pp.
- Brumbelow, K., 2001: Improved Methods for Agricultural and Water Resources Planning and Management, Civil Engineering, Georgia Institute of Technology, 379 pp. [Available online at <http://hdl.handle.net/1853/23203>.]
- Brumbelow, K., and A. P. Georgakakos, 2007: Determining crop-water production functions using yield-irrigation gradient algorithms. *Agricultural Water Management*, **87**, 151-161.
- Burnash, R. J. C., 1995: The NWS river Forecast System-Catchment Modeling. *Computer Models of Watershed Hydrology*, V. P. Singh, Ed., Water Resources – Publications, 311–366.

Burnash, R. J. C., R. L. Ferreal, and R. A. McGuire, 1973: *A generalized streamflow Simulation System: Conceptual Modeling for Digital Computers*. U.S. Department of Commerce, National Weather Service and Department of Water Resources.

Chan, S. K., R. Bindlish, P. O'Neill, T. Jackson, E. Njoku, S. Dunbar, J. Chaubell, J. Piepmeier, S. Yueh, D. Entekhabi, A. Colliander, F. Chen, M. H. Cosh, T. Caldwell, J. Walker, A. Berg, H. McNairn, M. Thibeault, J. Martínez-Fernández, F. Uldall, M. Seyfried, D. Bosch, P. Starks, C. Holifield Collins, J. Prueger, R. van der Velde, J. Asanuma, M. Palecki, E. E. Small, M. Zreda, J. Calvet, W. T. Crow, and Y. Kerr, 2018: Development and assessment of the SMAP enhanced passive soil moisture product. *Remote Sensing of Environment*, **204**, 931-941.

Cox, F. R., 1979: Effect of Temperature Treatment on Peanut Vegetative and Fruit Growth. *Peanut Science*, **6**, 14-17.

Daly, C., R. P. Neilson, and D. L. Phillips, 1994: A Statistical-Topographic Model for Mapping Climatological Precipitation over Mountainous Terrain. *Journal of Applied Meteorology*, **33**, 140-158.

Delécolle, R., S. J. Maas, M. Guérif, and F. Baret, 1992: Remote sensing and crop production models: present trends. *ISPRS Journal of Photogrammetry and Remote Sensing*, **47**, 145-161.

Dorigo, W., W. Wagner, C. Albergel, F. Albrecht, G. Balsamo, L. Brocca, D. Chung, M. Ertl, M. Forkel, A. Gruber, E. Haas, P. D. Hamer, M. Hirschi, J. Ikonen, R. de Jeu, R. Kidd, W. Lahoz, Y. Y. Liu, D. Miralles, T. Mistelbauer, N. Nicolai-Shaw, R. Parinussa, C. Pratola, C. Reimer, R. van der Schalie, S. I. Seneviratne, T. Smolander, and P. Lecomte, 2017: ESA CCI Soil Moisture for improved Earth system understanding: State-of-the art and future directions. *Remote Sensing of Environment*, **203**, 185-215.

Efron, B., and R. J. Tibshirani, 1993: *An introduction to the bootstrap*. 2. [print.] with corrections. ed. Chapman & Hall.

El-Sharkawy, M. A., 2011: Overview: Early history of crop growth and photosynthesis modeling. *Biosystems*, **103**, 205-211.

El Sharif, H., J. Wang, and A. P. Georgakakos, 2015: Modeling Regional Crop Yield and Irrigation Demand Using SMAP Type of Soil Moisture Data. *Journal of Hydrometeorology*, **16**, 904-916.

Elster, C., K. Klauenberg, M. Walzel, G. Wübbeler, H. P., M. Cox, C. Matthews, I. Smith, L. Wright, A. Allard, N. Fischer, S. Cowen, S. Ellison, P. Wilson, F. Pennecci, G. Kok, A. van der Veen, and L. Pendrill, 2015: A Guide to Bayesian Inference for Regression Problems, Deliverable of EMRP project NEW04 "Novel mathematical and statistical approaches to uncertainty evaluation", 75 pp.

Entekhabi, D., R. H. Reichle, R. D. Koster, and W. T. Crow, 2010a: Performance Metrics for Soil Moisture Retrievals and Application Requirements. *Journal of Hydrometeorology*, **11**, 832-840.

Entekhabi, D., S. Yueh, P. O'Neill, and K. e. a. Kellogg, 2014: SMAP Handbook JPL Publication JPL 400-1567, J. P. Laboratory, Pasadena, California, 182 pp.

Entekhabi, D., E. G. Njoku, P. E. O'Neill, K. H. Kellogg, W. T. Crow, W. N. Edelstein, J. K. Entin, S. D. Goodman, T. J. Jackson, J. Johnson, J. Kimball, J. R. Piepmeier, R. D. Koster, N. Martin, K.

- C. McDonald, M. Moghaddam, S. Moran, R. Reichle, J. C. Shi, M. W. Spencer, S. W. Thurman, T. Leung, and J. Van Zyl, 2010b: The Soil Moisture Active Passive (SMAP) Mission. *Proceedings of the IEEE*, **98**, 704-716.
- Ewert, F., R. P. Rötter, M. Bindi, H. Webber, M. Trnka, K. C. Kersebaum, J. E. Olesen, M. K. van Ittersum, S. Janssen, M. Rivington, M. A. Semenov, D. Wallach, J. R. Porter, D. Stewart, J. Verhagen, T. Gaiser, T. Palosuo, F. Tao, C. Nendel, P. P. Roggero, L. Bartošová, and S. Asseng, 2014: Crop modelling for integrated assessment of risk to food production from climate change. *Environmental Modelling & Software*.
- Ficklin, D. L., S. M. Robeson, and J. H. Knouft, 2016: Impacts of recent climate change on trends in baseflow and stormflow in United States watersheds. *Geophysical Research Letters*, **43**, 5079-5088.
- Georgakakos, A., P. Fleming, M. Dettinger, C. Peters-Lidard, T. T. C. Richmond, K. Reckhow, K. White, and D. Yates, 2014: Ch. 3: Water Resources. Climate Change Impacts in the United States. *The Third National Climate Assessment*, J. M. Melillo, T. T. C. Richmond, and G. W. Yohe, Eds., U.S. Global Change Research Program.
- Green, T. R., H. Kipka, O. David, and G. S. McMaster, 2018: Where is the USA Corn Belt, and how is it changing? *Science of The Total Environment*, **618**, 1613-1618.
- Gruber, A., W. Arnoud Dorigo, W. Crow, and W. Wagner, 2017: *Triple Collocation-Based Merging of Satellite Soil Moisture Retrievals*. Vol. PP, 1-13 pp.
- Hamon, W. R., 1961: Estimating potential evapotranspiration. *Journal of the Hydraulics Division*, 107-120.
- Han, E., A. Ines, and J. Koo, 2015: Global high-resolution soil profile database for crop modeling applications (Working Paper). HarvestChoice, Washington, D.C., USA. [Available online at <http://ebrary.ifpri.org/cdm/singleitem/collection/p15738coll2/id/129734>.]
- Han, W., Z. Yang, L. Di, and R. Mueller, 2012: CropScape: A Web service based application for exploring and disseminating US conterminous geospatial cropland data products for decision support. *Computers and Electronics in Agriculture*, **84**, 111-123.
- Hengl, T., J. M. de Jesus, R. A. MacMillan, N. H. Batjes, G. B. M. Heuvelink, E. Ribeiro, A. Samuel-Rosa, B. Kempen, J. G. B. Leenaars, M. G. Walsh, and M. R. Gonzalez, 2014: SoilGrids1km — Global Soil Information Based on Automated Mapping. *PLOS ONE*, **9**, e105992.
- Hexem, R. W., and E. O. Heady, 1978: *Water Production Functions for Irrigated Agriculture*. Iowa State Univ. Press.
- Hidalgo, H. G., M. D. Dettinger, and D. R. Cayan, 2008: Downscaling with constructed analogues: Daily precipitation and temperature fields over the United States, C. C. C. Center, 62 pp.
- Hodges, H. F., K. R. Reddy, J. M. McKinion, and V. R. Reddy, 1993: Temperature effects on cotton. *Miss. St. Univ. Exp. Stn. Bull.*

Huxley, P. A., J. Summerfield R, and P. Hughes A, 1976: Growth and development of soyabean cv. TK5 as affected by tropical daylengths, day/night temperatures and nitrogen nutrition. *Annals of Applied Biology*, **82**, 117-133.

Ines, A. V. M., N. N. Das, J. W. Hansen, and E. G. Njoku, 2013: Assimilation of remotely sensed soil moisture and vegetation with a crop simulation model for maize yield prediction. *Remote Sensing of Environment*, **138**, 149-164.

IPCC, 2014: Summary for Policymakers. *Climate Change 2014: Impacts, Adaptation, and Vulnerability. Part A: Global and Sectoral Aspects. Contribution of Working Group II to the Fifth Assessment Report of the Intergovernmental Panel on Climate Change*, C. B. Field, and Coauthors, Eds., Cambridge University Press, 1-32.

JAXA/EORC, 2017: User's Guide for Global Satellite Mapping of Precipitation Microwave-IR Combined Product (GSMaP_MVK), Gauge-calibrated Rainfall Product (GSMaP_Gauge) Version 7, Reanalysis Products (GSMaP_RNL), and Gauge-calibrated Reanalysis Product (GSMaP_Gauge_RNL) Version 6 E. O. R. C.-J. A. E. A. (JAXA/EORC), 8 pp.

JAXA/EORC: GSMaP: Global Satellite Mapping of Precipitation. [Available online at http://sharaku.eorc.jaxa.jp/GSMaP_crest/index.html.]

Jones, J. W., K. J. Boote, W. L. Bartels, G. Baigorría, G. Hoogenboom, and K. Hayhoe, 2012: Iconic Agricultural Crops: Climate Change Impacts on Peanut, Cotton and Corn in Georgia and Florida, Final Project Report Submitted to the Bipartisan Policy Center, F. C. Institute.

Jones, J. W., G. Hoogenboom, C. H. Porter, K. J. Boote, W. D. Batchelor, L. A. Hunt, P. W. Wilkens, U. Singh, A. J. Gijsman, and J. T. Ritchie, 2003: The DSSAT cropping system model. *European Journal of Agronomy*, **18**, 235-265.

Karimi, T., C. O. Stöckle, S. Higgins, and R. Nelson, 2018: Climate change and dryland wheat systems in the US Pacific Northwest. *Agricultural Systems*, **159**, 144-156.

Karl, T. R., and W. J. Koss, 1984: Regional and National Monthly, Seasonal, and Annual Temperature Weighted by Area, 1895-1983, National Climatic Data Center, Asheville, NC, 38 pp.

Kenny, J. F., N. L. Barber, S. S. Hutson, K. S. Linsey, J. K. Lovelace, and M. A. Maupin, 2009: Estimated use of water in the United States in 2005 U.S. Geological Survey Circular 1344, 52 p pp.

Kéry, M., 2010: Chapter 2 - Introduction to the Bayesian Analysis of a Statistical Model. *Introduction to WinBUGS for Ecologists*, Academic Press, 13-28.

Kutz, F. W., J. M. Morgan, J. Monn, and C. P. Petrey, 2012: Geospatial approaches to characterizing agriculture in the Chincoteague Bay Subbasin. *Environmental Monitoring and Assessment*, **184**, 679-692.

Liu, Y. Y., W. A. Dorigo, R. M. Parinussa, R. A. M. de Jeu, W. Wagner, M. F. McCabe, J. P. Evans, and A. I. J. M. van Dijk, 2012: Trend-preserving blending of passive and active microwave soil moisture retrievals. *Remote Sensing of Environment*, **123**, 280-297.

Maas, S. J., 1988: Use of remotely-sensed information in agricultural crop growth models. *Ecological Modelling*, **41**, 247-268.

Menne, M. J., I. Durre, R. S. Vose, B. E. Gleason, and T. G. Houston, 2012: An Overview of the Global Historical Climatology Network-Daily Database. *Journal of Atmospheric and Oceanic Technology*, **29**, 897-910.

Mitchell, K. E., D. Lohmann, P. R. Houser, E. F. Wood, C. Schaake John, A. Robock, B. A. Cosgrove, J. Sheffield, Q. Duan, L. Luo, R. W. Higgins, R. T. Pinker, J. D. Tarpley, D. P. Lettenmaier, C. H. Marshall, J. K. Entin, M. Pan, W. Shi, V. Koren, J. Meng, B. H. Ramsay, and A. A. Bailey, 2004: The multi-institution North American Land Data Assimilation System (NLDAS): Utilizing multiple GCIP products and partners in a continental distributed hydrological modeling system. *Journal of Geophysical Research: Atmospheres*, **109**.

Mo, X., S. Liu, Z. Lin, Y. Xu, Y. Xiang, and T. R. McVicar, 2005: Prediction of crop yield, water consumption and water use efficiency with a SVAT-crop growth model using remotely sensed data on the North China Plain. *Ecological Modelling*, **183**, 301-322.

Moradkhani, H., and S. Sorooshian, 2008: General Review of Rainfall-Runoff Modeling: Model Calibration, Data Assimilation, and Uncertainty Analysis. *Hydrological Modelling and the Water Cycle: Coupling the Atmospheric and Hydrological Models*, S. Sorooshian, K.-L. Hsu, E. Coppola, B. Tomassetti, M. Verdecchia, and G. Visconti, Eds., Springer Berlin Heidelberg, 1-24.

Moriasi, D. N., J. G. Arnold, M. W. Van Liew, R. Bingner, R. D. Harmel, and T. L. Veith, 2007: Model Evaluation Guidelines for Systematic Quantification of Accuracy in Watershed Simulations. *Transactions of the ASABE*, **50**, 885.

Moulin, S., A. Bondeau, and R. Delecolle, 1998: Combining agricultural crop models and satellite observations: From field to regional scales. *International Journal of Remote Sensing*, **19**, 1021-1036.

NASA, 2012: *Global Precipitation Measurement Core Observatory (GPM Brochure)*. 20 pp.

NASA, cited 2015: Precipitation Measurement Missions. [Available online at <http://pmm.nasa.gov/data-access/downloads/gpm>.]

NCDC: U.S. Climate Regions. [Available online at <https://www.ncdc.noaa.gov/monitoring-references/maps/us-climate-regions.php>.]

Nearing, G. S., W. T. Crow, K. R. Thorp, M. S. Moran, R. H. Reichle, and H. V. Gupta, 2012: Assimilating remote sensing observations of leaf area index and soil moisture for wheat yield estimates: An observing system simulation experiment. *Water Resources Research*, **48**, 1-13.

Okamoto, K. i., T. Ushio, T. Iguchi, N. Takahashi, and K. Iwanami, 2005: The global satellite mapping of precipitation (GSMaP) project. *Proceedings. 2005 IEEE International Geoscience and Remote Sensing Symposium, 2005. IGARSS '05.*, 3414-3416.

Pierce, D. W., D. R. Cayan, and B. L. Thrasher, 2014: Statistical Downscaling Using Localized Constructed Analogs (LOCA). *Journal of Hydrometeorology*, **15**, 2558-2585.

Pierce, D. W., D. R. Cayan, E. P. Maurer, J. T. Abatzoglou, and K. C. Hegewisch, 2015: Improved Bias Correction Techniques for Hydrological Simulations of Climate Change. *Journal of Hydrometeorology*, **16**, 2421-2442.

Reddy, K., H. F. Hodges, and V. Reddy, 1992: *Temperature Effects on Cotton Fruit Retention*. Vol. 84.

Severson, K., and K. Johnson, 2011: Drought Spreads Pain From Florida to Arizona. The New York Times, July 12, 2011. [Available online at <https://www.nytimes.com/2011/07/12/us/12drought.html>.]

Sionit, N., B. R. Strain, and E. P. Flint, 1987: INTERACTION OF TEMPERATURE AND CO₂ ENRICHMENT ON SOYBEAN: GROWTH AND DRY MATTER PARTITIONING. *Canadian Journal of Plant Science*, **67**, 59-67.

Thornton, P. E., and S. W. Running, 1999: An improved algorithm for estimating incident daily solar radiation from measurements of temperature, humidity, and precipitation. *Agricultural and Forest Meteorology*, **93**, 211-228.

Thornton, P. E., S. W. Running, and M. A. White, 1997: Generating surfaces of daily meteorological variables over large regions of complex terrain. *Journal of Hydrology*, **190**, 214-251.

Thornton, P. E., H. Hasenauer, and M. A. White, 2000: Simultaneous estimation of daily solar radiation and humidity from observed temperature and precipitation: an application over complex terrain in Austria. *Agricultural and Forest Meteorology*, **104**, 255-271.

Thornton, P. E., M. M. Thornton, B. W. Mayer, N. Wilhelmi, Y. Wei, R. Devarakonda, and R. B. Cook, 2014: Daymet: Daily Surface Weather Data on a 1-km Grid for North America, Version 2. ORNL DAAC, Oak Ridge, Tennessee, USA. Time period: 1980-01-01 to 2016-12-31. Spatial range: Contiguous United States (CONUS). <http://dx.doi.org/10.3334/ORNLDAAAC/1219>. [Available online at <https://daymet.ornl.gov/>.]

Tian, Y., C. D. Peters-Lidard, R. F. Adler, T. Kubota, and T. Ushio, 2009: Evaluation of GSMaP Precipitation Estimates over the Contiguous United States. *Journal of Hydrometeorology*, **11**, 566-574.

USDA NASS, 2015: USDA National Agricultural Statistics Service Cropland Data Layer. USDA-NASS, Washington, DC. USA. [Available online at <https://nassgeodata.gmu.edu/CropScape/>.]

Vara Prasad, P. V., P. Q. Craufurd, and R. J. Summerfield, 2000: Effect of high air and soil temperature on dry matter production, pod yield and yield components of groundnut. *Plant and Soil*, **222**, 231-239.

West, T. O., C. C. Brandt, L. M. Baskaran, C. M. Hellwinckel, R. Mueller, C. J. Bernacchi, V. Bandaru, B. Yang, B. S. Wilson, G. Marland, R. G. Nelson, D. G. D. L. T. Ugarte, and W. M. Post, 2010: Cropland carbon fluxes in the United States: increasing geospatial resolution of inventory-based carbon accounting. *Ecological Applications*, **20**, 1074-1086.

Wood, I. M. W., 1968: The effect of temperature at early flowering on the growth and development of peanuts (<I>Arachis hypogaea</I>). *Australian Journal of Agricultural Research*, **19**, 241-251.

World Bank: Hydrologic Models: Sacramento Soil Moisture Accounting Model (SAC-SMA).
[Available online at http://www.appsolutelydigital.com/ModelPrimer/chapter5_section10.html.]